PROCESSABLE VARIABLE BAND GAP CONJUGATED POLYMERS FOR OPTOELECTRONIC DEVICES

By

EMILIE M. GALAND

A DISSERTATION PRESENTED TO THE GRADUATE SCHOOL
OF THE UNIVERSITY OF FLORIDA IN PARTIAL FULFILLMENT
OF THE REQUIREMENTS FOR THE DEGREE OF
DOCTOR OF PHILOSOPHY

UNIVERSITY OF FLORIDA

2006

ACKNOWLEDGMENTS

Going away from home for such a long time to pursue my Ph.D. studies was the most difficult decision I ever had to make, and I would never have been able to go through this adventure without my parents' support. I was also lucky to share every step of this experience with Thomas Joncheray, who carried out his Ph.D. in polymer chemistry at the same time.

Of course this learning experience would not have been so rich without the guidance of my research advisor Prof. John R. Reynolds. He handled the research group as a businessman, educating us very well for our future industrial careers. I am very grateful for the time he put in reviewing my publications, oral presentations, career launch, and dissertation, and also for his consideration for my well being.

I would like also to acknowledge all the people I collaborated with, and who helped enrich the work presented in this dissertation: Dr. Khalil Abboud for solving X-ray crystal structures, Dr. Tracy McCarley for performing MALDI analyses, Dr. Jeremiah Mwaura for his work on light-emitting diodes, Dr. Young-Gi Kim for his work on solar cells, Dr. Avni Argun for his studies on charge transport, and Prof. Yang Yang and Dr. Vishal Shrotriya from UCLA for performing comparative photovoltaic studies. Thanks go also to the administrative staff, Sara Klossner, Tasha Simmons, Lorraine Williams and Gena Borrero, and to the members of my committee: Prof. Kenneth B. Wagener, Prof. Randolph S. Duran, Prof. Paul H. Holloway and Prof. Ronald K. Castellano.

A special thank you goes to my labmates, Dr. Barry Thompson, Dr. John Sworen, Dr. Florence Courchay, James Leonard, Dr. Christian Nielsen, Trish Hooper, Kate Opper, Nihan Cetinbas, and Pingjie Shi for making our lab such a nice place to work. I specifically want to express my gratitude to Barry and John who taught me a lot about laboratory techniques. John made me crazy with his music but I forgive him because his dancing moves always cheered me

up! Thanks go also to my hood neighbors Flo and James for being my coffee break companions and for making me feel less lonely in front of my columns.

A lot of people spent a couple of hours of their precious time to train me on certain techniques. For that I would like to show my appreciation to Garett Oakley and Genay Jones for helping me with the GPC measurements, Erik Berda and Piotr Matloka for training me on the differential scanning calorimetry and thermo gravimetric analysis instruments, James Leonard for familiarizing me with the unfriendly X-ray software, and Christophe Grenier for helping me with the stubborn computers and printers. The Butler laboratory was the best environment for living a truly "team experience." I want to thank all the members for their contribution to scientific discussions, for being so helpful, and for making this experience so enjoyable.

Thanks go also to the French mafia, Roxane Fabre, Thomas Joncheray, Florence Courchay, Sophie Bernard, Rachid Matmour, Christophe Grenier, Benoit Lauly, Sophie Klein, for their friendship and the get-togethers, which always helped me feel close to home.

Thanks go finally to my Florida tennis team who helped me stay in shape and healthy during that tough time!

TABLE OF CONTENTS

page

LIST OF TABLES

LIST OF FIGURES

Abstract of Dissertation Presented to the Graduate School
of the University of Florida in Partial Fulfillment of the
Requirements for the Degree of Doctor of Philosophy

PROCESSABLE VARIABLE BAND GAP CONJUGATED POLYMERS FOR OPTOELECTRONIC DEVICES

By

Emilie M. Galand

December 2006

Chair: John. R. Reynolds
Major Department: Chemistry

Solution processable variable band gap thienylene-based conjugated polymers were designed for application in various optoelectronic devices. The synthesis of wide band gap regiosymmetric thiophene-dialkoxybenzene and 3,4-ethylenedioxythienyl-dialkoxybenzene polymers was investigated, and organo-soluble isoregic poly(1,4-bis(2-thienyl)-2,5-dialkoxy-benzenes) (PBT-B$(OR)_2$) were successfully synthesized via Yamamoto coupling, with estimated number average molecular weights ranging from 3,000 to 5,000 g mol^{-1}, and a solubility of about 7 mg mL^{-1} in toluene. 1,4-Bis[2-(3,3-dialkyl-(3,4-propylenedioxy)thienyl]-2,5-didodecyloxybenzene derivatives, [BProDOT-R_2-B$(OC_{12}H_{25})_2$)], were prepared by Negishi coupling of the ProDOT and didodecyloxybenzene units in *ca.* 40% yields. They were efficiently electropolymerized to form electroactive films exhibiting redox switching at fairly low potentials (~ +0.1 V vs. Fc/Fc^+). BProDOT-Hex_2-B$(OC_{12}H_{25})_2$ was polymerized via ferric chloride chemical oxidation with an estimated number average molecular weight of 14,600 g mol^{-1}. A solubility of 15 mg mL^{-1} in chloroform was reached, which is attributed to the ProDOT hexyl substituents.

Four analogues of the narrow band-gap poly(3,4-propylenedioxythiophene-dialkyl)-cyano-*p*-phenylene vinylene (PProDOT-R_2:CNPPV) polymer family have been synthesized via

Knoevenagel condensation with number average molecular weights ranging between 9,000 and 24,000 g mol^{-1}. Linear and branched alkoxy substituents were introduced along the polymer backbone yielding organo-soluble materials (15 mg mL^{-1} in chloroform) with improved film quality and variable optical properties.

Conjugated polyelectrolytes were successfully synthesized from the ferric chloride oxidative polymerization of amino-substituted ProDOTs, followed by post-polymerization quaternization of the amino substituents. These materials, well solvated in DMSO, are presently the most fluorescent red-shifted polyelectrolytes ever reported.

The optical, redox, and electronic properties of the polymers were studied by electrochemical and spectroscopic methods. Owing to their solubility properties, the polymers could be processed into homogeneous thin-films by spin-coating or spray-casting, and applied to light-emitting diodes and photovoltaic devices. Particularly when used as electron donors in tandem with the electron acceptor [6, 6]-phenyl C_{61}-butyric acid methyl ester (PCBM) in bulk heterojunction photovoltaic devices, PBT-$B(OR)_2$ polymers exhibited power conversion efficiencies up to ~0.6%. PBProDOT-Hex_2-$B(OC_{12}H_{25})_2$ cathodically switched between orange and highly transmissive gray colors, and the PProDOT-R_2:CNPPV polymers switched between neutral blue/purple states and transmissive gray oxidized and reduced states, which makes them attractive for large area electrochromic displays.

CHAPTER 1
INTRODUCTION

1.1 Conjugated Polymers

1.1.1 Brief History

Although semiconducting conjugated polymers have been known for about 30 years (with the discovery in 1977 by MacDiarmid, Shirakawa, and Heeger, that chemical doping of these materials resulted in increases in electronic conductivity over several orders of magnitude[1,2]), it was only in the early 90s that many developments started to grow both on the fundamental and on the manufacturing levels. In particular, the discovery of light-emitting polymers in 1990, by Richard Friend[3] and his group, in the Cavendish Laboratory at Cambridge University, was a major turning point in the rise of organic electronics. Polymeric materials have the advantage that they are much more easily processed than metals. For instance, they can cover large and flexible surfaces and can be processed from solutions into complex architectures, using techniques such as spin-coating or spray-casting. Most plastics can be deformed reversibly, which is not true for metals. Also the synthetic flexibility of polymers allows easy tailoring of their physical, electronic, and optical properties. All these parameters are the reasons that have motivated the development of syntheses and processing methods of conjugated polymer materials with unique properties, with the goal of applying them in light-emitting diodes, field-effect transistors, photovoltaic cells, and electrochromics. Serious problems such as oxidative stability and device lifetimes have to be overcome for further development in commercial applications, but we may predict that one day, we will all go camping, carrying our flexible LED display with us, surfing the net and watching the TV solar-powered by polymeric materials.

1.1.2 Conjugated Polymers Electronic Properties

The simplest possible form of conjugated polymer is of course polyacetylene $(CH)_n$ whose structure constitutes the core of all conjugated polymers having a conjugated backbone of carbon atoms. The essential structural characteristic of all conjugated polymers is their quasi-infinite π-system, with the electrons that constitute the π-bonds being delocalized over a large number of recurring monomer units. This feature results in materials with directional conductivity, strongest along the axis of the chain. In polyacetylene (PA), delocalization results in two-fold degeneracy in the ground state as illustrated in Figure 1-1a. In aromatic polymers, such as poly(*para*-phenylene) (PPP), the alternating single and double bonds lead to electronic structures of varying energy levels (non-degenerate ground state) (Figure 1-1b).[4] In a polymer, just as in a crystal, the interaction of a polymer unit cell with all its neighbors leads to the formation of electronic bands, the highest occupied electronic levels constitute the HOMO or valence band (VB), and the lowest unoccupied electronic levels constitute the LUMO, or conduction band (CB). It is important to note that the π-system of conjugated polymers is not a strand of atoms with equivalent bond distances between any two neighbouring atoms, as predicted by the Hückel theory (this would give properties of a metal). This simple picture is incorrect because of the Peierls-instability of one-dimensional systems.[4-6] Peierls showed that, due to the coupling between electronic and elastic properties, the polymer develops a structural distortion such as to open a gap in the electronic excitation spectrum. So, conjugated polymers exhibit a band gap due to the Peierls distortion, and they are referred to as semiconductors[7] if their band gap values are below 3 or 4 eV (at higher values, they are insulators). By definition, the band gap is the difference between the VB and the CB. It is equal to the lowest excitation energy, which can be obtained from the onset value at the low energy edge of the optical absorption spectra.

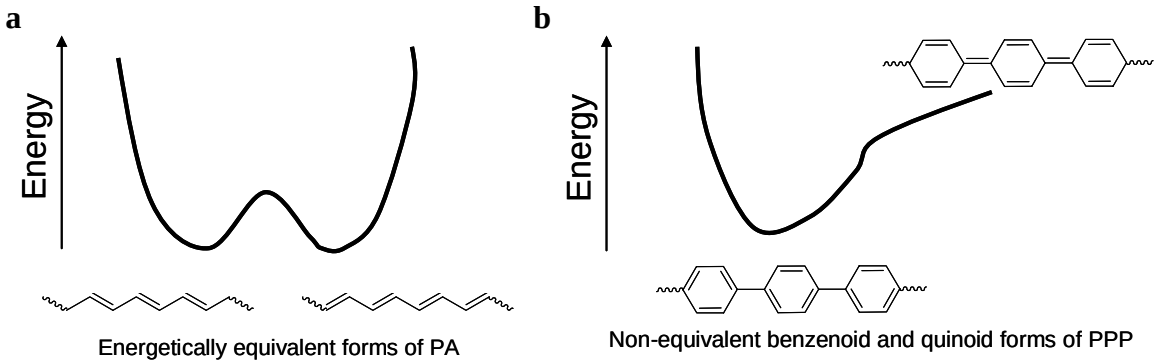

Figure 1-1. Energetic representations of polyacetylene and poly(*para*-phenylene). (a) degenerate PA and (b) non-degenerate PPP. [Modified from Moliton, A.; Hiorns, R. C. *Polym. Int.* **2004**, *53*, 1397-1412].[4]

Being semiconductors with fairly large band gaps, conjugated polymers do not conduct to a significant extent unless charged carriers are created within the conjugated framework[8] (PPP reaches a conductivity of 500 Ω^{-1} cm^{-1} when doped with charged carriers, whereas undoped PPP has a conductivity on the order of 10^{-13} Ω^{-1} cm^{-1}).[4] The charge carriers, either positive (p-type) or negative (n-type), are the products of oxidizing or reducing the polymer respectively. This phenomenon is always accompanied with structural changes localized over a couple of rings (4 to 5 rings for PPP)[9] and this gives rise to new electronic states within the band gap. J. L. Brédas and G. B Street have published a chemist-accessible explanation of these concepts.[10] For the aromatic conjugated polymers, the entity consisting of charge and spin (radical cation or anion) along with an associated geometry distortion is known as a polaron as illustrated in Figure 1-2a. The charge and radical form a bound species, since any increase in the distance between them would necessitate the creation of additional higher energy quinoid units. Upon removal of a second electron, either a separate polaron may form or, if the second electron is removed from the same site as the first, a bipolaron (Figure 1-2b). As the doping level increases, polaron and bipolaron states overlap and form bands, which will, at some point, merge with valence and conduction bands, as illustrated for the p-doping of PPP in Figure 1-3.

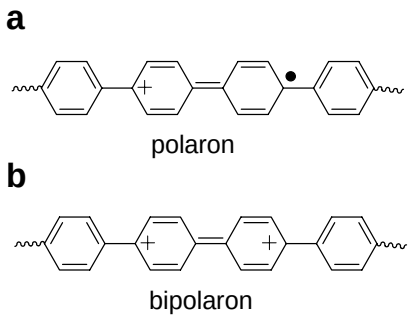

Figure 1-2. Positively charged defects on poly(*para*-phenylene). (a) polaron, (b) bipolaron.

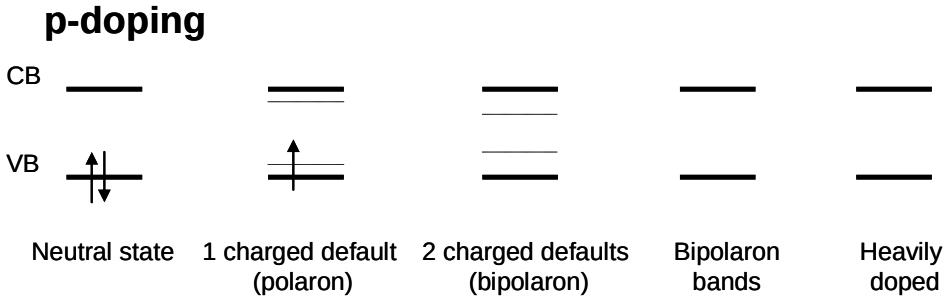

Figure 1-3. Poly(*para*-phenylene) and evolution of energy levels with p-doping. [Modified from Moliton, A.; Hiorns, R. C. *Polym. Int.* **2004**, *53*, 1397-1412].[4]

In PA, the charges which appear upon doping are called solitons. They are termed differently because the charges can propagate along the chain without an increase in distortion energy and can readily separate since the geometric structures that appear on each side of the charges are degenerate in energy (Figure 1-4). Doping dramatically alters the optical spectra of conjugated polymers, with optical transitions occurring between the VB and polaron states, and between polaron states. These transitions have lower energies than interband transitions and a number of colored low band gap conjugated polymers become transparent upon doping.

It is important to note that since the charged defect is simply a boundary between two moieties of equal energy, it can migrate in either direction without affecting the energy of the backbone, provided that there is no significant energy barrier to the process. It is this charge carrier mobility that leads to the high conductivity of these polymers, the conductivity (σ) of a

conducting polymer being related to the number of charge carriers (n) and their mobility (μ). A major challenge is to raise the carrier mobility and the conductivity, which are currently limited by the defects in the polymers. When cast from solution as thin-films, the polymers remain largely a tangle of spaghetti-like strands. Transport along the ideal linear chain can proceed no farther than the length of the fully extended chain; then the charge must hop to another chain. With improved ordering of the polymer chains, however, the conductivity could reach those of even the best metals.

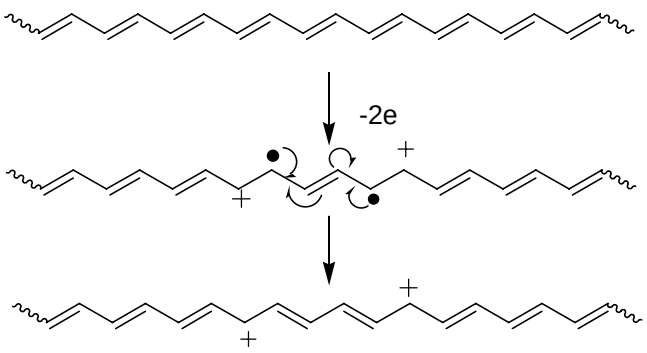

Figure 1-4. Illustration of the formation of two charged solitons on a chain of *trans*-polyacetylene. [Modified from Chance, R. R.; Brédas, J. L.; Silbey, R. *Physical Review B* **1984**, *29*, 4491-4495].[9]

1.2 Band Gap Engineering

The role of conjugated polymers in emerging electronic and display technologies is rapidly expanding, and with it, the need of a variety of polymers with different emissive or absorptive colors, electron or hole affinities, conductivities, and many other properties. Band gap engineering is extensively exploited nowadays for these reasons. It allows varying the optical and electronic properties of a polymer by simple manipulation of the chemical building blocks and the manner in which they are connected. In particular, five parameters influencing the band gaps were established: bond-length alternation, resonance energy, deviation from planarity, inductive effects of the substituents, and interchain coupling in the solid state.[11] Working around

these parameters, researchers have developed various families of conjugated polymers with different band gaps, which are typically classified as low band gap[12] or narrow band gap materials when E_g is less than *ca.* 1.80 eV, and as wide band gap materials for $E_g > 1.80$ eV [recall E (eV) = 1240/λ (nm)]. A description and examples of the way these parameters influence the band gaps are given below as they help in understanding the work presented in this dissertation.

As we discussed before for PA, bond-length alternation is the result of the Peierls effect and is responsible for the non-metallic behavior of neutral PA due to the existence of a band gap. Minimizing the bond-length alternation along a conjugated polymer backbone is consequently an important way to reduce the band gap. In aromatic polymers, the benzenoid structure will prevail over the energetically unfavorable quinoid structure, which results in the existence of what are essentially single bonds between the aromatic rings and hence a large bond-length alternation.[11,13] Making the quinoidal structure more favorable will help increasing the double-bond character of the linkages between aromatic rings and reduce the band gap.[14] For instance, polyisonaphthalene represented in Figure 1-5 (E_g = 1 eV) loses the aromaticity of the thiophene ring when going from the aromatic to the quinoid form, but at the same time its phenylene ring gains aromaticity, which minimizes the overall aromaticity loss and increases the contribution of the quinoid form to the polymer structure compared to polythiophene (E_g = 2 eV).[15]

The donor-acceptor approach has also been particularly developed as a means of reducing bond-length alternation for the building of narrow band gap polymers.[13,16] In that concept, the strong interaction between an electron donor and an electron acceptor increases the double bond character between aromatic rings, and the high-lying HOMO of the donor fragment combined with the low-lying LUMO of the acceptor gives rise to a D-A monomer with an unusually small

HOMO-LUMO separation and to a narrow band-gap upon polymerization (Figure 1-6). By carefully selecting the structures of the donors and acceptors and their respective electron donating and withdrawing strengths, it is possible to manipulate the magnitude of that band gap.[17] As an example, by simply varying the donor strength in the dioxythiophene-cyanovinylene polymer family, Thompson *et al.* gained access to a variety of band gaps as illustrated in Figure 1-7 [recall: EDOT > propylenedioxythiophene (ProDOT) > thiophene for electron donating power].[18]

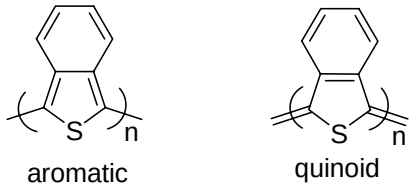

Figure 1-5. Aromatic and quinoid states of polyisonaphthalene. The six-membered ring of polyisothianaphthalene gains aromaticity when the molecule goes from the aromatic to the quinoid state, resulting in a higher contribution of the quinoidal state compared to polythiophene.

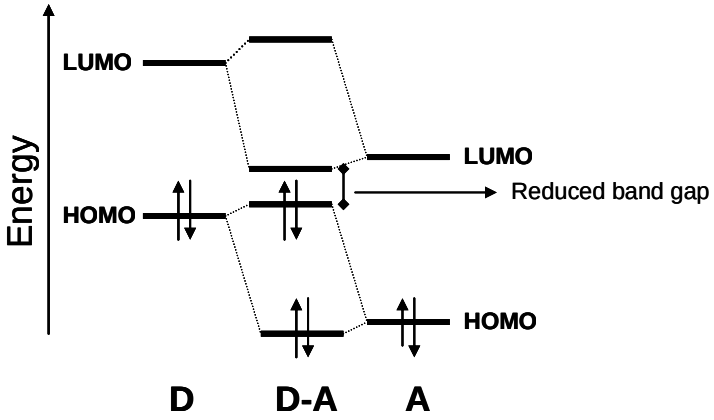

Figure 1-6. Illustration of the donor (D) - acceptor (A) concept. [Modified from van Mullekom, H. A. M.; Vekemans, J. A. J. M.; Havinga, E. E.; Meijer, E. W. *Mater. Sci. Eng.* **2001**, *32*, 1-40].[13] Hybridization of the high-lying HOMO of the donor fragment and the low-lying LUMO of the acceptor fragment yields a D-A unit with an unusually small HOMO-LUMO separation.

Deviation from planarity due to unfavorable intramolecular interactions and interchain interactions will reduce orbital overlap, decrease the π-π stacking and affect the band gap as

well.[8,19,20] Let us take the example of the polythiophene family: polythiophene is highly crystalline and completely insoluble, but as alkyl chains are introduced at the 3- and 4- positions of the thiophene ring for solubility purposes, the steric interactions between adjacent rings generate twisting of the backbone, destroying the conjugation and widening the band gap.[21]

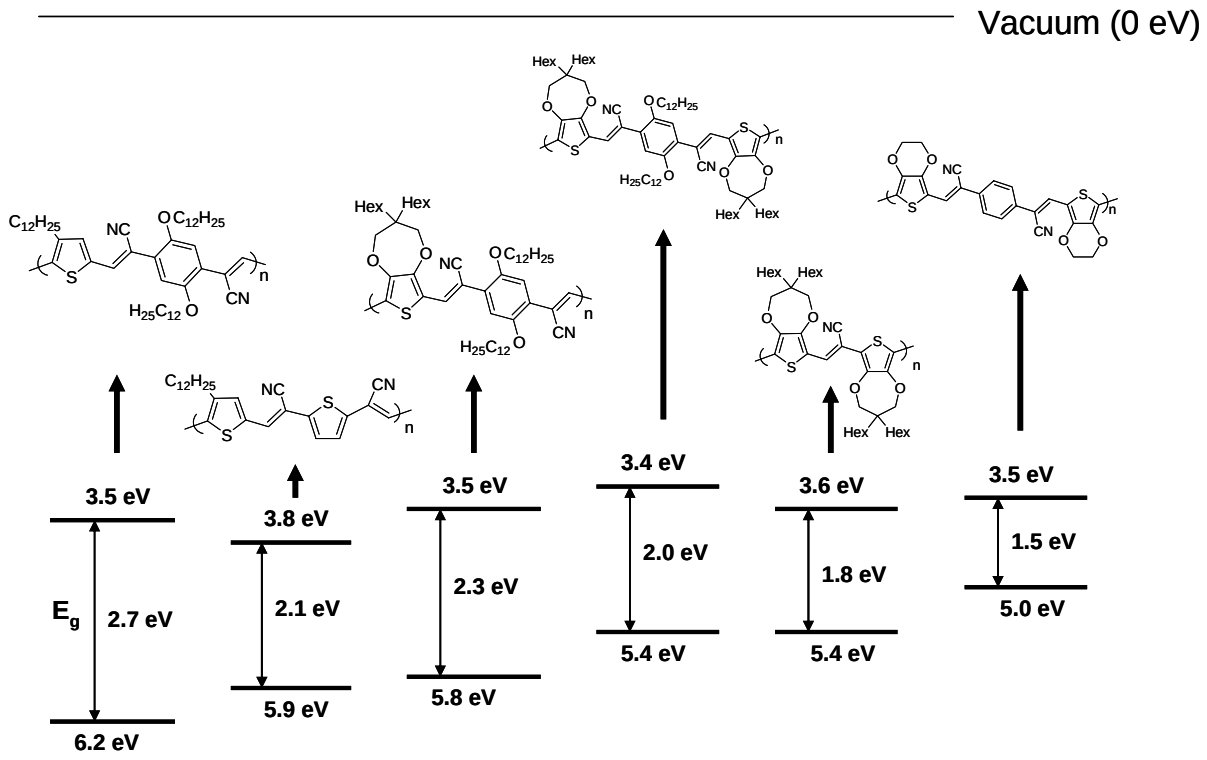

Figure 1-7. Polymer band structures and optical band gaps of the dioxythiophene-cyanovinylene polymer family. [Modified from Thompson, B. C.; Kim, Y.-G.; McCarley, T. D.; Reynolds, J. R. *J. Am. Chem. Soc.* **2006**, *128*, 12714-12725].[18]

Finally, the substitution of the polymer chains with electron rich or electron poor substituents will have an influence on the HOMO and LUMO levels and consequently on the band gap too. A close example to this Ph.D. research is the narrowing of the band gaps in hybrid thienylene-phenylene polymers by replacing alkyl side chains with alkoxy groups due to an increased electron density and reduced steric effect brought by the electron donating oxygen atoms: the onset of the π-π* transition, in solution, of 3 eV for poly(2,5-dihexyl-1,4-bis(2-thienyl)phenylene) is reduced to 2.4 eV for the analogous alkoxy derivatized polymer.[22]

1.3 Polymerization of Thiophene Based Molecules

There are great synthetic advantages working with thiophene based molecules and one of the most important is the variety of polymerization methods available such as oxidative chemical and electrochemical polymerizations, along with metal mediated and solid state polymerizations. General principles, drawbacks, and advantages of the methods covered in this dissertation are given below.

1.3.1 Oxidative Polymerizations

Oxidative polymerizations can be carried out either chemically or electrochemically. The generally accepted mechanism for the oxidative polymerization of heterocycles involves oxidation of the monomer to form a radical cation intermediate. The coupling of two radical cations, or of one radical cation and one neutral monomer followed by rearomatization with the loss of two protons leads first to a dimer unit, and finally to a polymer after repeated coupling. A detailed mechanism can be found in J. A. Irvin's dissertation.[23] Typically, electron-rich monomers are easier to oxidize and allow milder oxidative polymerization conditions, fewer side reactions such as overoxidation and the formation of more stable oxidized polymers.[24] For instance, the oxygen atoms of the ethylenedioxy bridge of EDOT increase the electron density of the thiophene ring and lower its oxidation potential. Indeed, the EDOT oxidation peak is found[25] at +0.88 V vs ferrocene (Fc/Fc^+) while thiophene oxidation was reported[26] around +1.22 V vs Fc/Fc^+ (assuming that the half-wave potential ($E_{1/2}$) of Fc/Fc^+ = 0.38 V vs the saturated calomel electrode (SCE) and $E_{1/2}$ of Ag/Ag^+ = 0.26 V vs SCE).[27] A major drawback in the oxidative polymerization of thiophenes is that it does not link the thiophenes exclusively at the 2- and 5-positions of the thiophene ring. Mislinking of the polymer through the 3- and 4- positions can happen leading to backbone irregularities and crosslinking and consequently to poor electronic properties and solubility problems.[23] This problem can be overcome by substituting the 3- and 4-

positions of the thiophene units, as with EDOT.[28] Regioirregularities can also be found in the oxidative polymerization of unsymmetrical 3-substituted thiophenes due to the lack of regiochemical control over head-to-tail couplings between adjacent thiophene rings.[29] Head-to-head and tail-to-tail couplings can also occur, leading to irregular polymers with sterically driven twisted backbones and poorer packing density. This results in a loss of conjugation, and a poorer orbital overlap and electronic connectivity in three dimensions. Non-oxidative coupling methods[30] with a high degree of regioselectivity (e.g., Rieke method[31] and McCullough methods[32]) have been developed for the synthesis of regioregular polymers. But the most attractive route to achieve a high degree of order, which does not rely on highly controlled polymerization conditions, is the use of symmetrical monomers and will be one of the focuses of the present dissertation.

The advantage of using chemical oxidative methods (in the bulk) over electrochemical methods is the possibility of getting high yields based on monomer. Chemical oxidations are also quite inexpensive relative to metal coupling, usually accomplished with the $FeCl_3$ oxidant. The chain length is usually limited by solubility problems: the oxidized polymers are less soluble than the neutral polymers due to their increased rigidity and can precipitate out of the solution, stopping the progress of the polymerization. This can be reduced by the introduction of flexible substituents on the polymer backbone. As an example, 2,5-dialkoxy-substituted 1,4-bis(2-thienyl)phenylene polymers synthesized via $FeCl_3$ oxidation precipitate out of the chloroform solution when they are substituted with heptoxy groups, but remain in solution with longer hexadecyloxy groups.[22] Reduction to the neutral polymer is accomplished using a strong reducing agent such as hydrazine or ammonium hydroxide. The major drawback of oxidative

chemical polymerization over electropolymerization is that ferric ions coming from the oxidants ($FeCl_3$, $Fe(ClO_4)_3$) are often trapped in the polymer backbone, affecting the device properties.[33]

1.3.2 Metal Mediated Polymerizations

Metal mediated couplings such as Grignard metathesis, Suzuki, and Ni(0) mediated Yamamoto polymerizations are typically used for the polymerization of heterocycles. Grignard Metathesis polymerization developed by the McCullough group[32c] has been used to produce a variety of polythiophenes with high molecular weights and high degree of regioregularity. This method requires the synthesis of the 2,5-dibromo-thiophene derivative, which is then polymerized with a Grignard reagent, such as the readily available and inexpensive methyl magnesium bromide (MeMgBr), and catalytic amounts of $Ni(dppp)Cl_2$ as illustrated for the synthesis of disubstituted PProDOTs[34] in Figure 1-8. It proceeds via an unusual quasi-living chain-growth mechanism, which allows the synthesis of polymers with predetermined molecular weights and narrow molecular weight distributions.[35] GriM is fast, easy, can be carried out on large scales, and does not require cryogenic temperatures. The use of GriM for the polymerization of monomers made of other kinds of heterocycles than substituted thiophenes has rarely been reported and it is consequently difficult to determine how efficient that method would be on such molecules. The closest example to the present research is the synthesis of high molecular weight electron rich poly(3,4-ethylenedioxythiophene)-2,5-didodecyloxybenzene (LPEB) via GriM.[36]

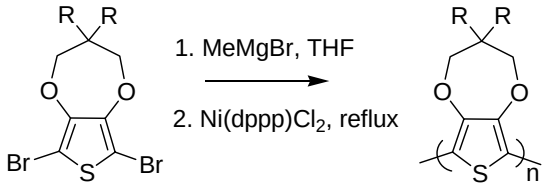

Figure 1-8. GriM polymerization of disubstituted PProDOTs.

The Yamamoto Coupling, using zerovalent bis(1,5-cyclooctadiene)nickel reagent ($Ni(COD)_2$) is a powerful synthetic method to couple electron poor aromatic rings, and more interesting in that research, to couple electron rich aromatic rings which are more reluctant to metal oxidative addition and consequently to most metal mediated coupling reactions. For instance, it has been effective for the polymerization of electron rich carbazoles with molecular weigths around 100,000 g. mol^{-1} (mechanism of the polymerization shown below in Figure 1-9).[37] The mechanism involves the insertion of Ni(0) into the C-X bond of a halogenated heterocycle, disproportionation between two of the resulting derivatives and reductive elimination of the Ni(II) compound.[38] Addition of the Ni(0) reagent is done slowly in order to avoid the formation of the less stable dinickel-substituted complex (Figure 1-9), which would result in the termination of the propagation of the polymer chain due to hydrolysis or decomposition. Each coupling is followed by the irreversible conversion of Ni(0) to $Ni(II)X_2$ and for this reason, the polymerization requires stoichiometric amounts of the expensive bis(1,5-cyclooctadiene)nickel(0) [$Ni(COD)_2$] reagent. Another drawback is that even if the Yamamoto coupling has been used for the polymerization of thiophene-based molecules, it always led to relatively small molecular weights making it quite challenging for the synthesis of our polymers.[39] Finally, it is important to note first that the use of $Ni(COD)_2$ requires expensive equipment since it has to be stored cold (otherwise it decomposes quickly) and in an oxygen free atmosphere, and second that it is often trapped[40] in the polymers.

1.3.3 Solid State Polymerization

Solid state polymerization of polythiophenes was reported for the first time by Meng *et al.* in 2003.[41] They found by chance, that 2,5-dibromo-3,4-ethylenedioxythiophene (DBEDOT) polymerizes spontaneously, without the addition of catalyst. This was discovered after a sample of DBEDOT transformed into a highly conductive black material (up to 80 S cm^{-1}) after two

years of storage at room temperature. The reaction takes place in air, vacuum, or light, heating decreases the reaction time, and elemental bromine is released during the reaction as illustrated by the mechanism in Figure 1-10.[41] The resulting polymer is doped with bromine and can be reduced to its neutral form after dedoping with hydrazine. It was suggested that short intermolecular Hal•••Hal contacts are required in order for the reaction to take place. Indeed, DBEDOT which has short Hal•••Hal intermolecular contacts of 3.45 and 3.50 Å is much more reactive than 2,5-diiodo-3,4-ethylenedioxythiophene (DIEDOT), which has an intermolecular Hal•••Hal contact of 3.73 Å. These Hal•••Hal intermolecular contacts are smaller than the sum of van der Waals radii (3.7 Å for Br•••Br and 4.0 Å for I•••I).

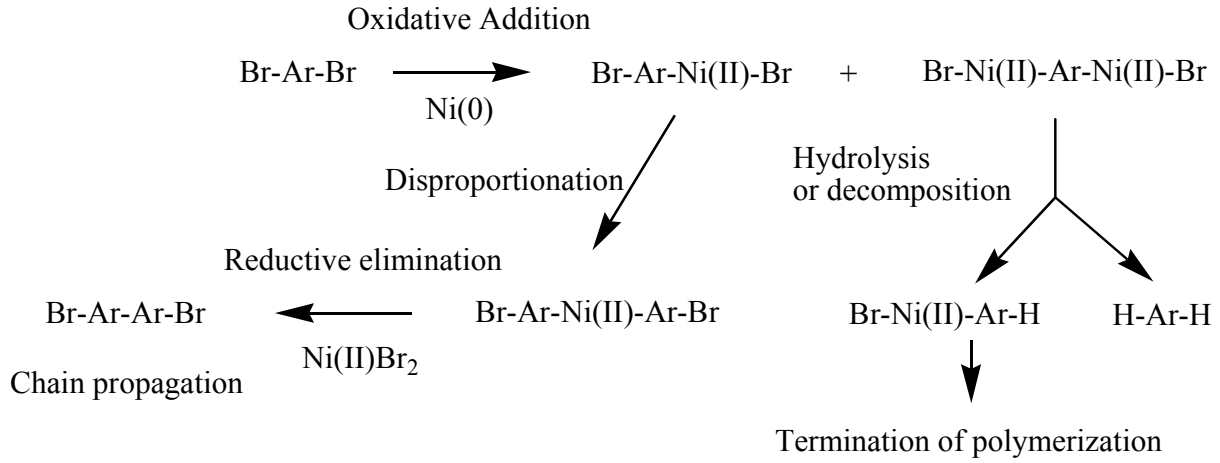

Figure 1-9. Mechanism of aryl (Ar) polymerization via Yamamoto coupling and of the polymer chain degradation/termination occurring during the polymerization. [Mechanism modified from Zhang, Z.-B.; Fujiki, M.; Tang, H.-Z.; Motonaga, M.; Torimitsu, K. *Macromolecules* **2002**, *35*, 1988-1990].[37]

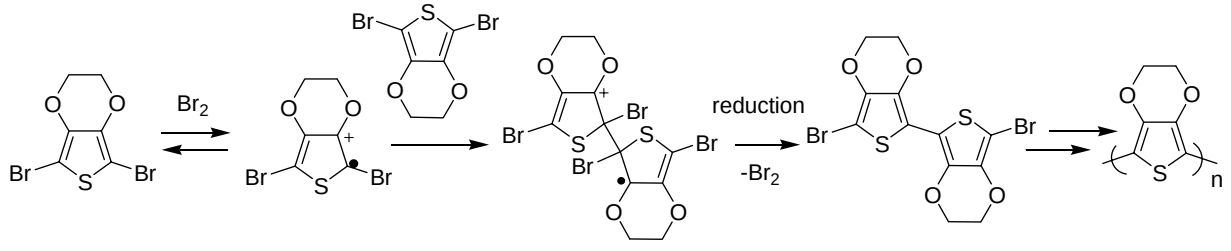

Figure 1-10. Mechanism of the solid state polymerization of DBEDOT.

1.3.4 Knoevenagel Polymerization

The Knoevenagel condensation involves the nucleophilic addition of a carbanion to a carbonyl group (aldehyde or ketone) in the presence of a base, followed by an elimination reaction in which a molecule of water is lost as illustrated in Figure 1-11.[42] The Knoevenagel polycondensation has proven very efficient for the synthesis of donor-acceptor type polymers,[43] and especially of narrow band gap polymers,[18,43] with the combination of electron poor diacetonitrile monomers and electron rich dialdehyde monomers. Usually these condensations are accomplished in THF/alcohol mixtures (e.g., THF/*t*-butanol or THF/2-propanol) as reaction media and with *t*-butoxide (*t*-BuOK) or tetrabutylammonium hydroxide (Bu_4NOH) strong bases.[17,43,44] Crosslinking of the polymer by Thorpe-Ziegler and/or Michael side reactions of the cyano or vinylene groups can be avoided by the use of one equivalent of base per cyano group.[42,43] Previous work reported by our group on the synthesis of thiophene-cyanovinylene polymers has also shown that the use of *t*-BuOK is preferred over Bu_4NOH.[43] The polymerizations proceeded gradually with *t*-BuOK and led to processable materials, whereas the use of Bu_4NOH led to the rapid formation of black insoluble precipitates. These observations have been used as support for the work on the ProDOT:cyanovinylene polymers presented in this dissertation.

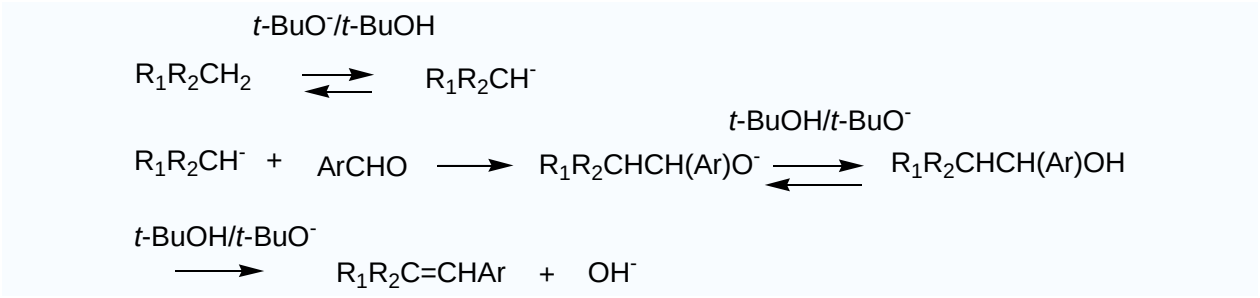

Figure 1-11. Illustration of the Knoevenagel condensation steps.

1.4 3,4-Alkylenedioxythiophene Based Polymers, from Thiophene to EDOT to ProDOT

Improvement of the properties and capabilities of basic conjugated polymers such as polythiophenes became of great importance in the mid 80s for the organic electronics community. More specifically, the quest for specific electronic and optical properties led to diverse structural modifications of the thiophene polymer building unit, and to the very interesting EDOT molecule. As discussed in the section on oxidative polymerizations of thiophene based molecules, the ethylenedioxy bridge of EDOT prevents parasite reactions at the 3- and 4- positions of thiophene, conferring a high reactivity to the free 2- and 5- positions, which gives rise to highly regular conjugated backbones upon polymerization. The electron donating oxygen atoms of the ethylenedioxy-bridge bring also an increased electron density, which increases the HOMO level and lowers the oxidation potential of the EDOT based molecules compared to their thiophene counterparts. This effect occurs without introducing unfavorable steric interactions between adjacent side chains, as found with regular long alkoxy substituents. Also, the ethylenedioxy-bridge is too strained for a high level of conjugation with the thiophene ring favoring its reactivity towards oxidative polymerization.[45,46]

These properties have been widely exploited for improving the properties of conjugated polymers, such as milder oxidative polymerization conditions and the formation of more stable polymers. The most obvious and popular example is of course PEDOT which has a low oxidation potential, is electrochromic (deep blue neutral state and highly transmissive oxidized state), is highly conductive and highly stable, and which is being used as a charge injecting layer in light emitting devices, as a component in electrochromic displays, and even as electrodes in field effect transistors and photovoltaic cells.[47,48] But a variety of copolymers which use EDOT as a building block,[49] like the thienylene-phenylene family, also benefit from its properties. This is illustrated for example by poly[1,4-bis[2-(3,4-ethylenedioxy-thienyl)]-2,5-dialkoxybenzenes]

(PBEDOT-B(OR)$_2$)[46] which exhibit band gap values between 1.75 eV and 2.0 eV, and polymer half wave potentials as low as -0.4 V versus Fc/Fc$^+$, whereas poly[1,4-bis(2-thienyl)]-2,5-dialkoxybenzenes][50] exhibit band gaps around 2.1 eV and minimum polymer half wave potentials of 0.15 V vs Fc/Fc$^+$. The properties of EDOT have also been exploited for improving the electron donating power of the donor moiety in donor-acceptor systems based on thiophene blocks and for building narrower band gap materials. This is illustrated in Figure 1-12 for different combinations of thiophene and EDOT donor moieties with cyanovinylene acceptor moieties.[17] In that example, it is clearly seen that as the EDOT content increases, the band gap diminishes.

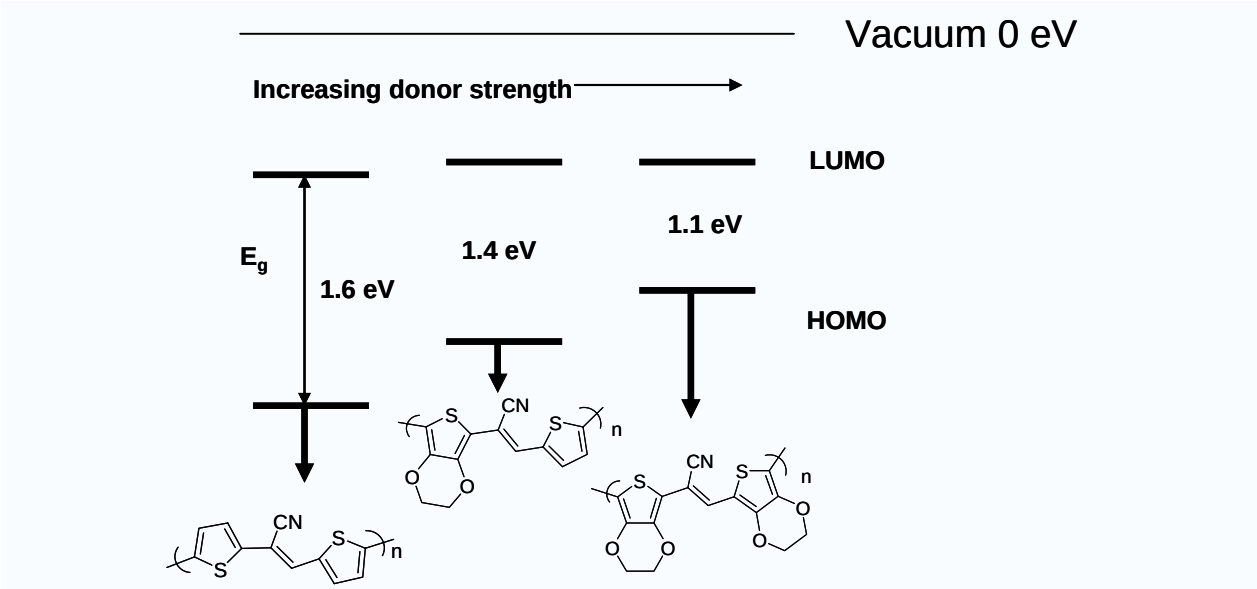

Figure 1-12. Effect of increasing donor strength in a donor-acceptor-donor configuration. [Modified from Thomas, C. A.; Zong, K.; Abboud, K. A.; Steel, P. J.; Reynolds, J. R. *J. Am. Chem. Soc.* **2004**, *126*, 16440-16450].[17]

With the recent emergence of soft and flexible plastic devices for use in solar cells, electrochromic devices, or light-emitting diodes (LEDs), it became particularly important to synthesize neutral soluble conjugated polymers, which can be processed directly from solution into thin-films, for instance by spray-casting or spin-coating. For that purpose, intense work has

been done in the substitution of thiophene with solubilizing substituents,[45,51] and ProDOT has emerged as the best compromise between the synthetic flexibility of thiophene and the electronic properties of EDOT. First, similar to EDOT based monomers, the oxygen atoms of the propylenedioxy bridge of ProDOT increase the electron density of the thiophene ring and lower its oxidation potential (ProDOT oxidation peak reported around +0.98 V *vs.* Fc/Fc^{+}).[52] The effect of the electron donating oxygens on the oxidation potential is a bit less for ProDOT than for EDOT due to its twisting conformation, which diminishes the overlap between the oxygen lone pairs and the aromatic thiophene ring. Second, various kinds of substituents (linear or branched, alkyl or alkoxy chains, etc.) can be introduced easily on the ProDOT ring which allows derivatization, chemical polymerization, and inducing solubility of the polymers in organic solvents.[53,54] Mishra *et al.* reported the synthesis of a hydroxyl substituted ProDOT, in a single step, from commercially available starting materials, which led to the preparation of a variety of electroactive derivatives.[55] Also ProDOT can be disubstituted on the central carbon of the propylene bridge without disturbing the C_2 symmetry. This was used by Reeves *et al.* who made a recent impact in the field of soft electronics with the development of regiosymmetric spray-coatable electrochromic ProDOT polymers, prepared via Grignard metathesis.[34] This is a great advantage compared to EDOT which has been mostly unsymmetrically substituted (except in the case of PheDOT[56,57]) due to the poor yields and tedious synthesis encountered during the functionalization process. Researchers are now taking advantage of the electron rich properties, synthetic flexibility and easy derivatization of the ProDOT molecules and are working on the design of a variety of soluble hybrid conjugated polymers containing ProDOT to have access to a broader range of electronic and optical properties. For instance, Thompson *et al.* recently reported the building of a soluble narrow band gap polymer using the donor-acceptor approach,

with a substituted ProDOT derivative as the donor unit and a cyanophenylene derivative as the acceptor unit as illustrated in Figure 1-13.[18,43,58]

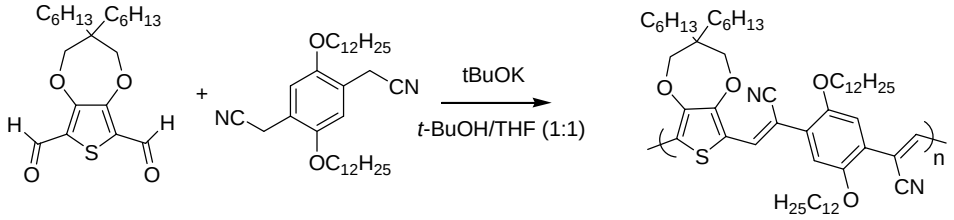

Figure 1-13. Synthesis of poly(3,4-propylenedioxythiophene-dihexyl)-cyano-*p*-phenylene-vinylene.

1.5 Applications

A variety of parameters need to be considered for application of conjugated polymers in semiconductor devices and only those which can be manipulated by synthetic chemists are described below for each application. The properties which are of interest in these applications (Light-Emitting Diodes (LEDs), solar cells, and electrochromic devices) are of course the ability to synthesize soluble polymers in high bulk yields for obtaining solution-processable or film-forming polymers, and the ability to produce large quantities. This can be accomplished by introducing flexible side chains on the polymer backbone. For instance, the solubility of the branched PProDOT($CH_2OEtHx)_2$ (M_n = 47,000 g mol^{-1}) is about four times more important (57 mg mL^{-1}) than the solubility of PProDOT($Hx)_2$ (13 mg mL^{-1}, M_n = 38,000 g mol^{-1}) in toluene.[34]

In polymer LEDs, light emission results from the formation of excitons in the polymeric layer, which will emit light upon relaxation to the ground state. These excitons form by the meeting of electrons and holes injected by varying work function electrodes. The color of the emitted light is dependent on the band gap of the material, and consequently a wide range of band gaps are needed for PLED applications: this is where band gap engineering intervenes.[59] Band gap engineering has to be done keeping in mind that the backbone structure and

conformation play an important role on the luminescence efficiency. Indeed, once an exciton is formed, strong intermolecular interactions between polymer chains form weakly emissive interchain species (ground-state aggregates or excimers) which lead to a spectral red-shift and reduced quantum yields.[20] One extensively used method to prevent this photoluminescence quenching phenomenon is to introduce bulky side groups to separate the backbones from each other.[60] But for effective charge injection and transport in LEDs, high carrier density and mobilities are also required, and consequently a high degree of π-interactions and packing.[61] All these parameters have to be taken into consideration by the chemist and carefully balanced.

In electrochromic devices, we obviously need an electrochromic material which possesses the ability to reversibly change color by altering its redox state.[62] Intrinsically, all conjugated polymers have the potential to be electrochromic. This phenomenon is the result of the change of conjugation which occurs upon oxidation or reduction of the polymer (interconversion between the quinoid and the aromatic states and apparition of lower energy transitions due to the formation of polarons and bipolarons as detailed earlier). The HOMO level of the polymer controls the oxidation potential, and the LUMO level controls the reduction potential. As an example, PEDOT is a great electrochromic material which switches between an opaque blue color in the undoped state and a transmissive sky blue color in the oxidized state.[63] A variety of colors are needed in order to be able to develop a variety of applications, and this can be realized by fine-tuning of the band gap (as explained earlier).[64-66] The materials should also be stable while switching between their oxidized and reduced states (or neutral states) with a certain lifetime.

A large number of reviews are available on polymer photovoltaics and there is no need here to go over an extensive summary of the principles, and of all the parameters which need to be

improved in order to attain solar efficiencies approaching 10%.[43,67-69] Provided below is a summary of the most important points which have to be considered by a synthetic chemist. In organic solar cells, upon photoexcitation, an exciton is created (electron-hole pair) in the polymer layer, and a current is created from the splitting of this bound exciton, and the collection of the holes at a high work function electrode, and of electrons at a low work function electrode. The exciton-splitting process occurs only at interfaces (at the junction between the electrode and the conducting polymer or at the interface between polymers of differing electron affinities). The lifetime of an exciton is short and only excitons that are formed within about 4-20 nm of the junction have a chance to reach it.[67] Conjugated polymer bulk heterojunctions (interpenetrating networks of electron-accepting and electron-donating polymers) sandwiched between two varying work function electrodes are currently the best answer to that problem, and particularly those using a solubilized form of C_{60} such as (6,6)-phenyl C_{61}-butyric acid methyl ester (PCBM) as the acceptor layer. The photoinduced charge transfer in these blends happens on an ultrafast timescale of up to 45 femtoseconds, which is much faster than the recombination process, which happens in a microsecond regime (100 ns-10 ms).[70-72]

One of the main tasks of the synthetic chemist now is to find the "ideal" electron-donating polymer. The best materials available right now are poly(3-hexylthiophene) (P3HT),[73-75] poly(2-methoxy-5-(2'-ethylhexoloxy)-1,4-phenylenevinylene) (MEH-PPV),[76] and poly(2-methoxy-5-(3',7'-dimethyloctyloxy)-*p*-phenylenevinylene) (MDMO-PPV),[77] all contain side chains that make them soluble in common organic solvents. But there is a mismatch between the absorption spectrum of these materials and the solar spectrum. While the photon flux of the AM1.5 solar spectrum peaks around 700 nm (1.8 eV), P3HT, MEH-PPV and MDMO-PPV absorb strongly over the 350-650 nm wavelength range (3.5-1.9 eV). As a result, a film of P3HT

(240 nm thick) absorbs only about 21% of the sun's photons.[67] Taking this information into consideration, a synthetic chemist should specifically look at the synthesis of a polymer[43] 1) exhibiting a band-gap capable of strongly absorbing sunlight ($E_g < 1.8$ eV),[68,74] 2) being resistant to oxidation and consequently having a fairly low lying HOMO (about 5.2 eV or lower,[78] assuming that the energy level of the Saturated Calomel Electrode (SCE) is 4.7 eV below the vacuum level[79]), and 3) having a LUMO offset of about 0.3-0.4 eV relative to the PCBM for effective charge transfer (above 3.8 eV).[80] It is important to note that the HOMO and LUMO energy levels are negative values because they are under the vacuum level which is considered as the zero level. Consequently a HOMO level located at 5.4 eV is considered as lower than 5.2 eV. Great improvement of the solar efficiency has also been observed upon increasing the degree of order of the polymers. P3HT annealed above its glass transition temperature shows enhanced crystallization and a dramatic increase in the hole mobility, which when applied in solar cells facilitates charge transport to the electrodes and increases the solar efficiency.[71,73,75,81] So for application in photovoltaics, a synthetic chemist should also consider the ordering capabilities of its polymers. An interesting path was taken recently by Hou *et al.*: to benefit from the ordering properties of P3HT and to get band gaps approaching 1.8 eV, they have built two-dimensional conjugated polythiophenes with bi(thienylenevinylene) side chains. They were able to lower the band gap by 0.2 eV compared to P3HT and they reached solar efficiencies of 3.18%, whereas they obtained efficiencies of 2.41% with P3HT using the same conditions.[82]

1.6 Study Overview

This work focuses on the design and synthesis of new processable conjugated polymers for optoelectronic devices such as electrochromic devices, solar cells, and light-emitting diodes. Two terms define the main lines of this project: processability and design. Processability was one of our priorities in order to be able to use the polymers on large and flexible surfaces. Design of

the polymer structure was a way to induce processability and to manipulate the optical and electronic properties in order to target specific applications. Both narrow and wide band gap polymers were synthesized in order to cover a broad range of applications.

Chapter 2 describes briefly the techniques employed for the work presented in this dissertation. In chapter 3, the synthesis of wide band gap polymers of the thienylene-phenylene family has been investigated, including the already known thiophene-dialkoxybenzene and EDOT-dialkoxybenzene derivatives, as well as a novel ProDOT-dialkoxybenzene derivative. The newly developed ProDOT-phenylene materials were electropolymerized in order to quickly look at their redox and electronic properties. For all the derivatives, various chemical polymerizations were studied (Yamamoto coupling, ferric chloride oxidative coupling, GriM), as well as solid state polymerizations, in order to develop methods for synthesizing the polymers in high bulk yields. Flexible linear alkyl and alkoxy substituents were grafted onto the monomers to induce solubility of the derived polymers in organic solvents. In chapter 4, narrow band gap polymers were prepared by Knoevenagel condensation of electron rich 3,4-propylenedioxythiophenes and electron poor cyanovinylenes. A variety of substituents were introduced on the backbones of the polymers to induce solubility in organic solvents (linear and branched alkoxy-substituents), and their effects on the optical and electronic properties were studied. Chapter 5 describes the synthesis of wide band gap amino-substituted PProDOTs for developing a new type of conjugated polyelectrolyte.

Along with the synthetic details and molecular characterizations, a complete characterization of the polymers by electrochemical, optical and photophysical methods is given in chapters 3-5 in order to evaluate their optical and electronic properties, and their potential in certain optoelectronic applications. Structural studies such as X-ray analyses and DSC

measurements are also detailed in chapters 3 and 4 for a quick look at some of the materials ordering properties. These studies have led to the incorporation of the materials into devices by other members of the Reynolds group and this thesis will briefly outline the results at the end of Chapters 3-5.

CHAPTER 2
EXPERIMENTAL

Molecular and structural analyses as well as electrochemical and spectroscopic methods were used in this work for developing a deeper understanding of the newly synthesized materials potential. The techniques are extensively described in the Reynolds group dissertations,[23,43,83-85] and only an overview of the points of interest and of the general experimental conditions employed will be given. More specific details can be found at the end of Chapters 3-5.

2.1 General Synthetic Methods

All chemicals were purchased from Acros or Aldrich Chemicals and used as received unless stated otherwise. The monomer structure and purity were determined by ^{1}H-NMR and ^{13}C-NMR spectroscopy, elemental analysis, high-resolution mass spectrometry (HRMS), as well as infra-red (IR) spectroscopy and single crystal X-ray analysis when applicable. Melting point measurements were also performed on solids for complete characterization. ^{1}H-NMR and ^{13}C-NMR were recorded on Varian-VXR 300 MHz, Gemini 300 MHz, and Mercury 300 MHz spectrometers. Elemental analyses were performed by Robertson Microanalytical Laboratories, Inc. or the University of Florida, Department of Chemistry spectroscopic services. High-resolution mass spectrometry was performed by the spectroscopic services at the Department of Chemistry of the University of Florida with a Finnigan MAT 96Q mass spectrometer. IR measurements were accomplished with a Spectrum One Perkin Elmer FT-IR spectrometer. Single crystals X-ray measurements were accomplished at the Center for X-ray Crystallography in the University of Florida Chemistry Department by Dr. Khalil A. Abboud. Single crystals were obtained either by the slow cooling recrystallization method (single solvent or two solvents method), or in a closed vial, by diffusion of a poor solvent into a smaller vial containing the compound dissolved in a small amount of good solvent. Data were collected at 173 K on a

Siemens SMART PLATFORM equipped with a CCD area detector and a graphite monochromator utilizing MoK_α radiation (λ = 0.71073 Å). Cell parameters were refined using up to 8192 reflections. A full sphere of data (1850 frames) was collected using the ω-scan method (0.3° frame width). The first 50 frames were re-measured at the end of data collection to monitor instrument and crystal stability (maximum correction on I was < 1 %). Absorption corrections by integration were applied based on measured indexed crystal faces. The structure was solved by the Direct Methods in *SHELXTL6 (2000,* Bruker-AXS, Madison, Wisconsin) and refined using full-matrix least squares.

All polymers were purified by precipitation followed by Soxhlet extraction as described in Chapters 3-5. Characterization was accomplished by ^{1}H-NMR, elemental analysis, matrix assisted laser desorption ionization time of flight mass spectrometry (MALDI-TOF MS), and infra-red spectroscopy when applicable. ^{1}H-NMR was recorded on Inova 500 MHz and Mercury 300 MHz. MALDI-TOF MS was performed by Dr. Tracy D. McCarley with a Bruker ProFLEX III instrument at Louisiana State University. Methylene chloride or chloroform were used as solvents, and terthiophene, dithranol, or 2-(-4-hydroxyphenylazo)benzoic acid (HABA) as matrix. Polymer molecular weights were estimated by gel permeation chromatography (GPC). GPC was performed on two 300 x 7.5 mm Polymer Laboratories PLGel 5 μM mixed-C columns with Waters Associates liquid chromatography 2996 photodiode array detector. All molecular weights are relative to polystyrene standards (Polymer Laboratories; Amherst, MA). The polymer solutions were prepared in tetrahydrofuran (THF) or chloroform ($CHCl_3$) and a constant flow rate of 1 mL min^{-1} was used. Polymer thermal stability was assessed by thermogravimetric analysis (TGA). TGA measurements were performed on a Perkin-Elmer TGA 7 instrument under nitrogen at heating rates of 20°C min^{-1} from 50°C to 900°C. The ordering properties were

also characterized by differential scanning calorimetry (DSC). DSC scans were run under nitrogen on a DuPont 951 instrument or on a TA Instruments DSC Q1000, using sample weights of ~ 4 mg.

2.2 Electrochemical Methods

2.2.1 Introduction

Electrochemistry is an important tool in the field of conjugated polymers for having an idea of a monomer's ability to polymerize (the lower the oxidation potential, the easier it is to oxidatively polymerize the monomer) and for determining the resultant polymer's redox and electronic properties. From the onsets of oxidation and reduction potentials, the HOMO and LUMO levels of a polymer can be estimated. This is usually accomplished by cyclic voltammetry (CV) or differential pulse voltammetry (DPV). Since all electrochemical measurements reported in this dissertation will be referenced[86] versus Fc/Fc^+, the conversion to the HOMO and LUMO energies was accomplished by adding 5.1 eV to the onsets of oxidation and reduction of the polymer respectively (assuming that Fc/Fc^+ is at 5.1 eV below the vacuum level).[27]

2.2.2 Electrochemical Set-Up

Electrochemistry was performed using a three-electrode cell with a platinum (Pt) wire or a Pt flag as the counter electrode, a silver wire pseudo-reference electrode calibrated using a 5 mM solution of Fc/Fc^+ in 0.1 M electrolyte solution, and a platinum (or gold) button (0.02 cm^2) or ITO coated glass slide (7 × 50 × 0.7 mm, 5-15 Ω) as the working electrode. The ITO electrodes were purchased from Delta Technologies, Ltd. Characterization of the polymer films was performed in 0.1 M electrolyte solution. An EG&G Princeton Applied Research Model 273 potentiostat was used under the control Corrware II software from Scribner and Associates. The electrolyte solutions were prepared from tetrabutylammonium perchlorate (TBAP) or

tetrabutylammonium hexafluorophosphate ($TBAPF_6$) electrolytes dissolved in freshly distilled acetonitrile (ACN), methylene chloride (CH_2Cl_2), or propylene carbonate (PC). The experiments were performed under an argon blanket.

For electrochemical analysis, the polymers were either electrodeposited onto the working electrodes, or synthesized chemically and deposited by drop-casting or spray-casting from 3-10 mg mL^{-1} chloroform or toluene solutions. The electrodeposition was accomplished either by repeated scanning or by holding the potential of the working electrode near the monomer's oxidation peak (previously determined by CV) in a 10 mM monomer solution. The electrodeposited polymer films were rinsed with the solvent used in the electrolyte preparation and in which films are not soluble. Cyclic voltammograms or differential pulse voltammograms were recorded after breaking in the polymer film with about 10 CV cycles for getting reproducible results.

2.2.3 CV/DPV

The principles of CV have been extensively developed in dissertations from J. A. Irvin and C. A. Thomas.[23,83] In CV, we measure the current created at the working electrode when the potential is linearly cycled from a starting potential to a final potential and back to the starting potential. In polymer electrochemistry,[79] the polymer is adhered to the electrode and charge transfer occurs by hopping (Figure 2-1). If the polymer is well adhered to the electrode, the peak current will increase linearly as function of the scan rate.[85] In the case of reversible systems and if the rate of reaction of the adsorbed species is much greater than of species in solution (situation mostly encountered in our labs), the peak current can be expressed as shown in Equation 2-1.

$$i_p = -n^2 F^2 \nu A \Gamma_{O,i} / (4RT) \quad \text{Equation (2-1)}$$

with n the number of electrons, A the electrode area (in cm^2), $\Gamma_{O,i}$ the surface concentration of adsorbed O (in mol cm^{-2}) before the experiment begins, ν the scan rate (in V/s), and F Faradays constant (96,485 C mol^{-1}). For such systems, the anodic wave on scan reversal is the mirror image of the cathodic wave reflected across the potential axis and $E_p \approx E_{1/2,}$ and the curve i = f(E) is totally symmetrical if hopping faster than ν (same charge before and after peak). But in reality, inhomogeneity of film, charge transport, structural and resistive changes in the film, fast scan rate compared to hopping, and differences in adsorption strength of O and R give rise to asymmetry.

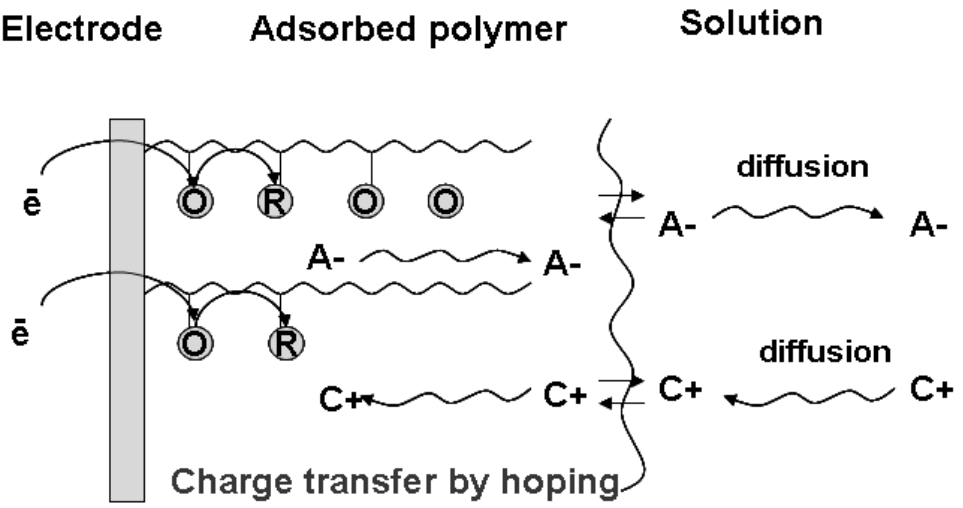

Figure 2-1. Charge transport by hopping in polymer adsorbed to the electrode. Electron injection into the film results in the reduction of O to R and the entry (or expulsion) of counterions (A- or C+).

In DPV,[79,83,87,88] the potential is pulsed and each pulse has a certain amplitude (between 10-100 mV) as illustrated in Figure 2-2. After each pulse the potential returns to a value slightly higher than prior to the pulse (step size usually between 1-2 mV), which gives a staircase shape. The current is measured just prior to application of the pulse and at the end of the pulse and the difference between the two currents is plotted as a function of the base potential. The duration of the pulse (step time) usually varies between 5-20 ms. Longer step times allow more time for the

current to decay, and consequently a smaller difference in the sampled currents and a higher sensitivity. For a reversible system, the peak potential is about the same on the forward and reverse scans and corresponds to $E_{1/2}$. With increasing irreversibility, E_p moves away from $E_{1/2}$ at the same time that peak width increases and its height diminishes. It is important to note that when doing DPV measurements on a polymer, the calibration of the pseudo reference silver wire has to be done by DPV.

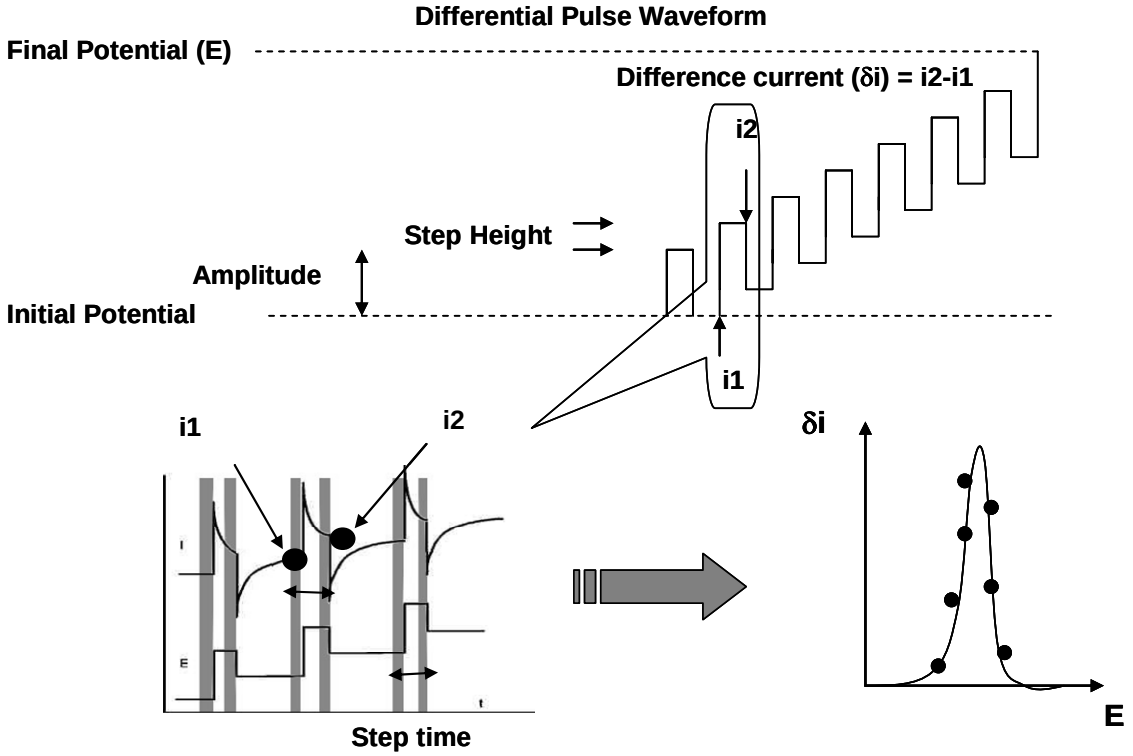

Figure 2-2. Differential pulse waveform. In DPV, the potential is pulsed and the current is measured just prior to application of the pulse (i_1) and at the end of the applied pulse (i_2). The difference between the two currents (δi) is plotted as a function of the base potential.

The advantage of using DPV over CV is that the major component of the current difference measured is the faradaic current, which flows due to an oxidation or reduction at the electrode surface. The capacitive or charging current component, due to electrical charging of the electrode double layer, is largely eliminated. This renders the peaks more symmetrical and increases the

signal to noise ratio compared to the CV method. Consequently, the onsets of oxidation and reduction are more defined, as will be the HOMO and LUMO levels.

2.3 Optical and Spectroscopic Methods

Analysis of a conjugated polymer's interaction with light is essential for evaluating the polymer's potential in optoelectronic applications. This interaction can vary depending on the polymer's conformation, and consequently it is usually evaluated in the solid state and in solution (in good and bad solvents), and at various temperatures, by UV-Vis-nIR absorption or emission measurements, and studies of color switching upon doping.

2.3.1 Absorption Spectra and Molar Absorptivities

Measurement of the UV-Vis absorption of a polymer solution is a basic spectroscopic method rich with information. A comparison between the absorption spectra of a polymer solution and its monomer solution will tell if the polymerization took place. Indeed, in a polymer, the increased degree of conjugation will induce a red-shift of the absorption maximum. Also, by recording the absorption spectra of polymer chains of different lengths, using a GPC equipped with a photodiode-array detector, it is possible to determine the minimum chain length necessary to obtain optimum optical properties. A polymer's extinction coefficient, extracted from the absorption maxima of three polymer solutions of different concentrations, will bring information on how efficiently a polymer absorbs light, which is of particular importance for application in solar cells. Finally, the UV-Vis absorption of polymer solutions gives information on how well a polymer is solvated in specific solvents, and this will be discussed below in the solvatochromic section. Absorption spectra were obtained using a Varian Cary 500 Scan UV-vis-nIR spectrophotometer and quartz crystal cells (1 cm x 1 cm x 5.5 cm, Starna Cells, Inc.).

2.3.2 Solvatochromism/Thermochromism

The term solvatochromism is used to describe the change in position and sometimes intensity of a UV-Vis absorption spectrum following a change in polarity of the solvent in which the polymer is dissolved. A change of the UV-Vis absorption spectrum upon a temperature change is called thermochromism,[89,90] and upon the addition of ions[89,91] is called ionochromism. In all three cases, chromism is induced by a conformational change of the conjugated backbone driven by both intrachain steric hindrance and interchain interactions (attractive interactions, π-π interactions, excitons, etc.) that accompany the formation (or disruption) of small aggregates.[92] The conformational change leads to a modification of the effective conjugation length, which induces optical shifts in the UV-Vis absorption spectra of conjugated polymers. A planarization of the polymer backbone always leads to a red-shift of the absorption, but the direction of the shift caused by aggregation depends on the details of the molecular packing. Also, polymer backbone planarity usually causes "fine structure" or shoulders to appear on the main π-π* absorption peak. Disordered polymers have a great number of different, but similar energetic states (due to their conformational freedom) and therefore usually have broad UV-Vis spectra. However a fixing of the molecular conformation through planarization leads to a decrease of the number of energetic states, allowing the fine vibronic structures to be resolved as additional peaks or shoulders.

Specifically, in solvatochromic studies, going from a "good" solvent to a more poorly solvating solvent will induce aggregation and more delocalized assemblies, and create a red-shift of the absorption spectrum.[93] A "good" solvent is assumed to disrupt the conjugation upon side-chain disordering and twisting of the backbone, and to affect the effective conjugation length. This phenomenon has been observed for a variety of polythiophene derivatives. For instance, the

absorption of poly(1,4-(2,5-dialkoxyphenylene)-2,5-thiophene) shifts from 468 nm to 495 nm upon decreasing the quality of the solvent.[93] Solvatochromic studies are an important tool for selecting the solvents best suited for dissolving the selected polymers, which might be helpful for optimum polymer characterization and device preparation. In thermochromism, it is heating which is either assumed to disrupt the conjugation and create disorder, or to break the aggregates and isolate the polymer chains.[57] Polymers exhibiting solvatochromic or thermochromic properties have the potential of being applied in sensors or smart materials.[94]

For the solvatochromic study, the same experimental set up as for the absorption experiments described in the above section was employed. It was accomplished by first dissolving the polymer in a good solvent and then progressively adding a poor solvent, while maintaining a constant polymer concentration. A constant concentration was maintained using the following procedure (Figure 2-3): a polymer solution of known concentration was prepared in the "good solvent". Then equal volumes of that solution were poured into a couple of graduated flasks, and the flasks were filled up to the same maximum with different volumes of "good" solvent and "poor" solvent.

The spectral changes which occurred upon heating could not be recorded with the UV-Vis-nIR spectrophotometer because the temperature needed to observe thermochromism was too high (however pictures of the color changes were taken and reported).

2.3.3 Photoluminescence Spectra and Fluorescence Quantum Efficiencies

The luminescence properties of conjugated polymers are of considerable interest because of their potential applications as the emissive materials in LEDs. A useful figure is the photoluminescence (PL) quantum yield (Φ), defined as the number of photons emitted in photoluminescence per absorbed photon. It is easily measured by a synthetic chemist for polymer solutions, and allows making a first selection of polymers which might have a potential in LEDs.

Measurements of Φ on thin-film solids are more representative but not as straightforward;[95,96] they were accomplished in this work by Dr. J. Mwaura. The PL quantum yield of a polymer solution is much higher than Φ of polymer thin-films coated from the same solution. This is due to the formation of less emissive interchain species which quenches the fluorescence in the solid state. PL quantum yields are determined using the comparative method of Williams *et al.* which involves the use of well characterized standard samples with known Φ values.[97] The standard must be chosen such that its excitation wavelength is found at a slightly lower value than the absorption maximum of the polymer solution. The absorption values of the polymer and standard solutions should not exceed 0.1 at the excitation wavelength (in 10 mm fluorescence cuvettes) in order to avoid self-absorption.[98] The PL quantum yield of a polymer solution is calculated according to Equation 2-2, where the subscript R refers to the standard (or reference) and A is the absorbance of the solution, E is the integrated emission area across the band and η is the refractive index of the solution.

$$\Phi = \Phi_R \times \frac{\left(1-10^{A_R}\right)}{\left(1-10^{A}\right)} \times \frac{E}{E_R} \times \frac{\eta^2}{\eta_R^2} \qquad \text{Equation (2-2)}$$

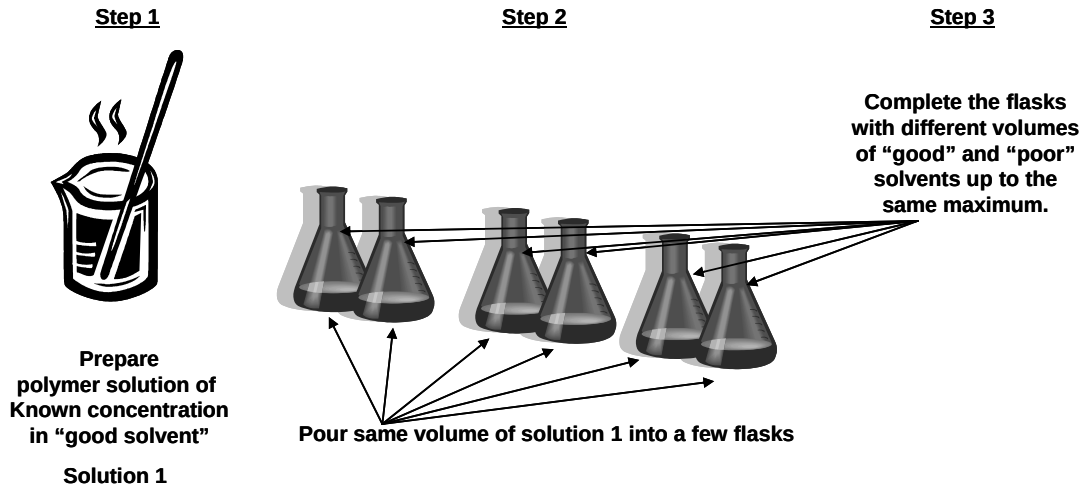

Figure 2-3. Example of the procedure used to maintain a constant polymer concentration in flasks containing varying amounts of good and poor solvents.

The photoluminescence spectra of the polymer solutions were registered on a Jobin Yvon Fluorolog-3 spectrofluorimeter in right-angle mode. Solution quantum efficiency measurements were carried out using a Spex F-112 photon counting fluorimeter, relative to oxazine 1 in ethanol ($\Phi = 0.11$),[99] coumarin 6 in ethanol ($\Phi = 0.78$),[100] or cresyl violet perchlorate in ethanol ($\Phi = 0.54$),[101] with the optical density of the solution kept below A = 0.1.

2.3.4 Spectroelectrochemistry

Spectroelectrochemical measurements were performed in order to define the optical band gaps of the polymers and observe their electrochromic behavior. The optical band gap is determined from the low-energy absorption edge (onset of the π-π^* transition) of the neutral absorption spectrum of the polymer thin-film. The electrochromic behavior is observed by recording the spectral changes upon oxidation and reduction of the polymer thin-film. The polymer films were prepared either by spray-casting polymer solutions (5-10 mg mL^{-1} in chloroform) onto ITO coated glass using an air brush (Testor Corps) at 12 psi, or by using electropolymerization as described previously. Characterization of the polymer films was performed in 0.1 M electrolyte solution using the electrochemical set-up described previously, with a Pt wire as the counter electrode in order to avoid blocking the incident light. The absorption spectra were recorded using a Varian Cary 500 Scan UV-vis-nIR spectrophotometer for bench top experiments or a Stellarnet diode-array Vis-nIR spectrophotometer with fiber-optic capabilities for dry-box studies.

2.3.5 Colorimetry

Colorimetry measurements are useful to give a quantitative description of the color states that an electrochromic polymer thin-film can reach as it is oxidized or reduced. Three attributes are used to describe colors: the hue (dominant wavelength), the saturation (level of white and/or black), and the luminance (the brightness of the transmitted light). Two color systems were

specifically used in this dissertation to give a quantitative representation of these attributes: the 1931 *Yxy* and the 1976 *L*a*b* systems, both established by the Commission Internationale de l'Eclairage (CIE) (detailed information can be found in the referenced citations). [64,102]

In the CIE 1931 *Yxy* color space, *Y* represents the luminance, and *x* and *y* represent the hue and saturation. The luminance is usually presented as a percentage relative to the background luminance, and called "relative luminance". The two-dimensional *xy* diagram is known as the chromaticity diagram (illustration in Figure 2-4). It has the shape of a horseshoe, with the wavelengths of visible light found on the surrounding line, and the shortest and longest wavelengths being connected by a straight line. Every color is contained in the horseshoe and the location of a point on the *xy* diagram gives information on the hue and saturation of the color. The *xy* chromaticity diagram is particularly useful to track the color states of a polymer for different doping levels. The CIE *L*a*b** space is more commonly used in industry, with *L** representing the luminance and *a** and *b** being related to the hue and saturation.

Polymer thin-films were deposited by spray-casting onto ITO coated glass as for the spectroelectrochemical studies. Colorimetric measurements were obtained with a Minolta CS-100 Chroma Meter using the electrochemical set-up described previously, with a Pt wire as the counter electrode. The sample was illuminated from behind with a D50 (5000K) light source in a light booth designed to exclude external light.

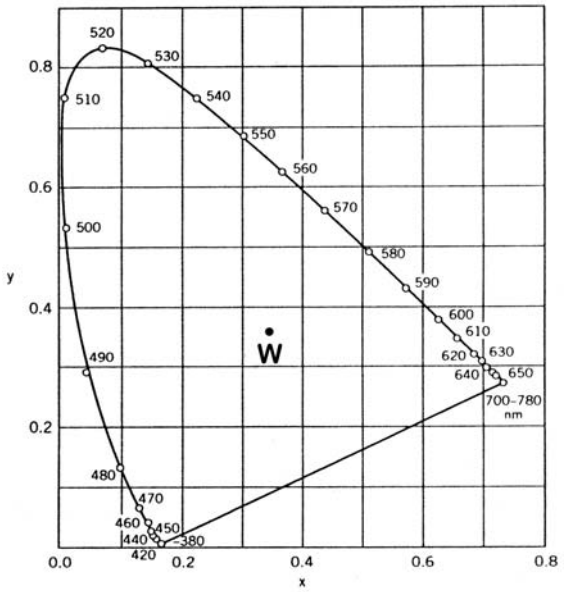

Figure 2-4. CIE 1931 *xy* chromaticity diagram. [Modified from Thompson, B. C.; Schottland, P.; Zong, K.; Reynolds, J. R. *Chem. Mater*. **2000**, *12*, 1563-1571].[64]

CHAPTER 3
WIDE BAND GAP BIS-HETEROCYCLE-PHENYLENE POLYMERS

3.1 Introduction

Thiophene-phenylene based copolymers have been extensively studied for their interesting electrical and optical properties such as redox electroactivity and electrochromism, reactivity to chemical sensing, charge transport and light emission.[22,24,36,46,50,103-110] In addition, the various coupling reactions available for heterocycles, and the variety of methods for the polymerization of thiophene based monomers render them fairly easy to synthesize. Phenylene rings are particularly convenient to derivatize with variable substituents, and the subsequent polymerization of thiophene-phenylene monomers yields materials with controllable band gaps and solubilities.[22,46,50] As described in the general Introduction, simply replacing the phenylene alkyl substituents with alkoxy groups can reduce considerably the band gap due to the electron donating effect and reduced steric effect brought by the oxygens.[22]

The regiosymmetric poly(1,4-bis(2-thienyl)-2,5-dialkoxyphenylene)s are particularly interesting members of that family (Figure 3-1). Their synthesis was originally accomplished by J. Ruiz *et al.*[22,111] from the catalytic oxidation of bis-thiophene-dialkoxybenzene monomers with ferric chloride. Low molecular weight materials were obtained (~ 2,000-3,800 g mol^{-1}), and it was revealed that these polymers showed an X-ray diffraction pattern that indicated a high crystalline content relative to analogous polymers being unsymmetrically substituted. These polymers have a band gap only slightly larger than P3HT (2.1 eV vs. 1.9 eV) and based on their ability to give polymer films with a high degree of order, they are of interest for use in solar cells.[50] A synthetically interesting aspect about these regiosymmetric polymers is their ability to achieve a high degree of order without having to prepare unsymmetrical monomers (which are

usually more challenging to synthesize), or having to rely on highly controlled polymerization conditions.

Regiosymmetric poly[1,4-bis(2-(3,4-ethylenedioxy)thienyl)-2,5-dialkoxybenzene]s, illustrated in Figure 3-1, can also be found in the literature.[46,105] The ethylenedioxy bridge between the 3- and 4-positions of the thiophene gave access to smaller band gaps (~ 1.7-2.0 eV) than the ones obtained for their thiophene analogs due to the electron donating effect of the oxygens atoms of EDOT, as explained earlier. This makes these derivatives also of interest for photovoltaics, but their synthesis needs to be further investigated for improving their solution properties and molecular weights, and a study of their ordering properties has to be accomplished too. Indeed, the derivatives which have been reported have been synthesized either by electrochemical methods, which do not allow easy characterization, processing, and synthesis of the polymers in high bulk yields, or by chemical polymerizations, which have led to low molecular weight materials (4,000 g mol^{-1} via ferric-chloride-mediated polymerization, and 2,900 g mol^{-1} via Ullman coupling) with poor film properties.[23,46] In addition, the derivatives prepared by oxidative polymerization with $FeCl_3$ were poorly soluble, and difficult to characterize and to process, but it could not be determined if this insolubility was the result of crosslinking through the phenylenes or if it was intrinsic to the molecules.

The chemical synthesis of these regiosymmetric thiophene-phenylene (PBT-$B(OR)_2$) and EDOT-phenylene polymers (PBEDOT-$B(OR)_2$) has been revisited (section 3.3) in order to obtain polymers with higher molecular weights than the ones previously reported, while being able to analyze and process the materials easily for application in soft, and flexible, photovoltaic and electrochomic devices. The monomer syntheses and characterizations are described in section 3.2. The redox, spectroelectrochemical, and electrochromic properties of the polymers

have been studied, and the results are detailed in sections 3.4 and 3.5. Application of PBT-$B(OR)_2$ in photovoltaic devices has been investigated by members of the group and is detailed in section 3.7.

The work was finalized by the addition of a new member to the regiosymmetric thienylene-phenylene family. This member contains ProDOT as the thienylene moiety, which allows taking advantage of its electron donating ability and of its easy derivatization. This type of molecule was targeted in order to improve the solubility and processability of the thienylene-phenylene polymer family. In particular, we report here the synthesis of methyl substituted (R = Me) and hexyl (R = Hex) substituted poly[1,4-bis[2-(3,4-propylenedioxythienyl)]-2,5-didodecyloxybenzene] [PBProDOT-R_2-$B(OC_{12}H_{25})_2$], with the methyl substituted molecule studied for comparison with the more soluble hexyl derivatized molecule (Figure 3-1). The monomer syntheses and characterizations are described in section 3.2. Both polymers were prepared by electropolymerization, and the BProDOT-Hex_2-$B(OC_{12}H_{25})_2$ monomer was also polymerized by chemical oxidation using ferric chloride to yield a polymer highly soluble in organic solvents as described in section 3.3. PBProDOT-Hex_2-$B(OC_{12}H_{25})_2$ exhibits interesting electrochromic and solvatochromic properties, which are reported in sections 3.4, 3.5, and 3.6. Preliminary investigations utilizing this polymer as an emitter in LEDs, and as a hole transport layer in solar cells, have been accomplished by Reynolds group members and a brief overview of the results is included in section 3.7.

3.2 Monomer Syntheses and Characterizations

It was decided to synthesize the regiosymmetric PBT-$B(OR)_2$, PBEDOT-$B(OR)_2$, and PBProDOT-R_2-$B(OC_{12}H_{25})_2$ from the corresponding symmetrical bis-thienylene-dialkoxybenzene monomers (from their dibrominated version in most cases). The benzenes were substituted with long and flexible heptoxy and/or dodecyloxy chains to induce solubility.

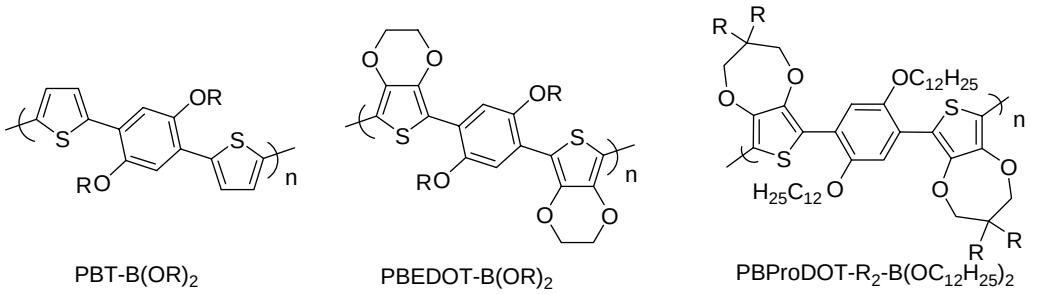

Figure 3-1. Targeted thienylene-phenylene polymers.

3.2.1 Bis-thiophene-dialkoxybenzenes

1,4-Dibromo-2,5-dialkoxybenzene was prepared according to the literature by Williamson etherification of 1,4-dibromo-2,5-dihydroxybenzene with the corresponding alkyl halide.[22] The synthesis of the dibrominated 1,4-bis(2-thienyl)-2,5-diheptoxybenzene (Br_2-BT-B(OC_7H_{15})$_2$), and 1,4-bis(2-thienyl)-2,5-didodecyloxybenzene (Br_2-BT-B($OC_{12}H_{25}$)$_2$) monomers started by the deprotonation of thiophene with *n*-butyllithium, and further reaction with trimethylstannyl chloride to give 2-(trimethylstannyl)thiophene (Th-Sn(CH_3)$_3$) as illustrated in Figure 3-2. 1,4-Bis(2-thienyl)-2,5-dialkoxybenzene (BT-B(OR)$_2$) was obtained by the Stille coupling of 1,4-dibromo-2,5-dialkoxybenzene with Th-Sn(CH_3)$_3$. There is significant literature precedent for the preparation of this type of molecule via Negishi coupling instead.[22,50,103,104] However, Stille coupling was chosen because it allows isolating, purifying, characterizing, and storing Th-Sn(CH_3)$_3$. Finally, the Br_2-BT-B(OR)$_2$ monomers were prepared by bromination of BT-B(OR)$_2$ with *N*-bromosuccinimide (NBS). Yellow needles were obtained after purification by recrystallization (72% and 86% yields for R = C_7H_{15} and R = $C_{12}H_{25}$, respectively).

The monomers were fully characterized by ^{1}H-NMR, ^{13}C-NMR, HRMS, elemental analysis, melting point determination, and UV-Vis spectroscopy. They both exhibit an absorption maximum at 376 nm (Figure 3-14), and extinction coefficients of 37,600 M^{-1} cm^{-1} for Br_2-BT-B(OC_7H_{15})$_2$ and of 27,160 M^{-1} cm^{-1} for Br_2-BT-B($OC_{12}H_{25}$)$_2$.

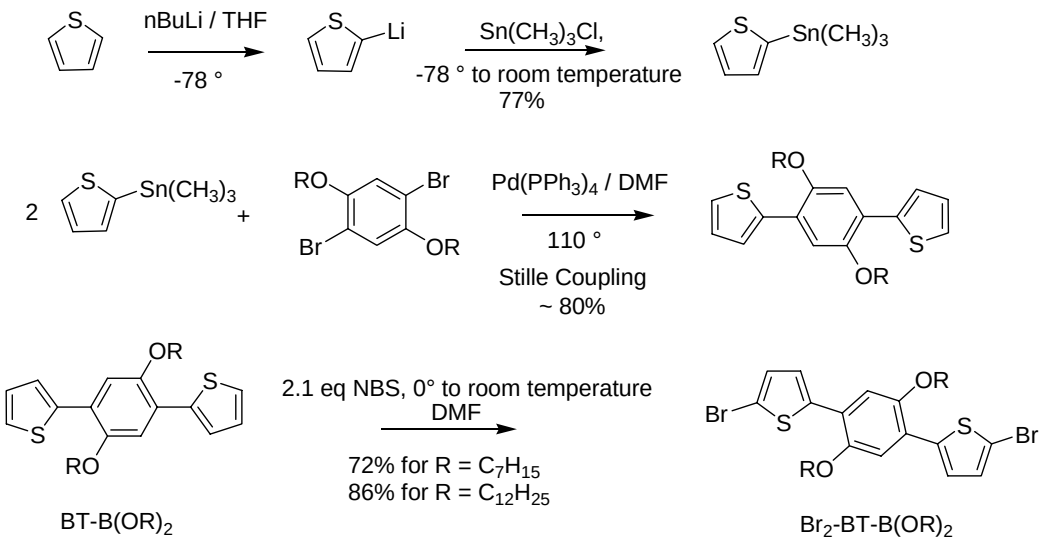

Figure 3-2. Bis-thiophene-dialkoxybenzene monomer synthesis.

Crystals of Br_2-BT-B(OC_7H_{15})$_2$ were grown by slow diffusion of ethanol into a vial containing a xylene solution of the monomer. Figure 3-3a shows the molecular structure of the monomer, while Figure 3-3b shows the packing mode of the material as well as the crystalline unit (obtained by single crystal X-ray diffraction studies). Br_2-BT-B(OC_7H_{15})$_2$ crystallizes in the monoclinic space group C2/c with the alkoxy chains and phenyl rings being coplanar. As illustrated in Figure 3-3c, the molecules have a relatively small dihedral angle of 20.8˚ between the central phenylene and thiophene rings, which allows efficient stacking of adjacent molecules with a good cofacial arrangement and an interchain distance of 5.79 Å. The intermolecular distance is a very important parameter for application of organic materials to devices requiring high carrier mobility. Small distances are necessary for strong intermolecular overlap of the π-atomic orbitals and charge transfer by hopping.[112] Materials such as thiophene oligomers or P3HT are of high interest because they exhibit small interchain distances (in the order of 3.8 Å for P3HT).[113] The 5.79 Å interchain value found for Br_2-BT-B(OC_7H_{15})$_2$ would not be great if extended to the polymer. Br_2-BT-B($OC_{12}H_{25}$)$_2$ crystals were not of sufficient size for single-crystal structure analysis.

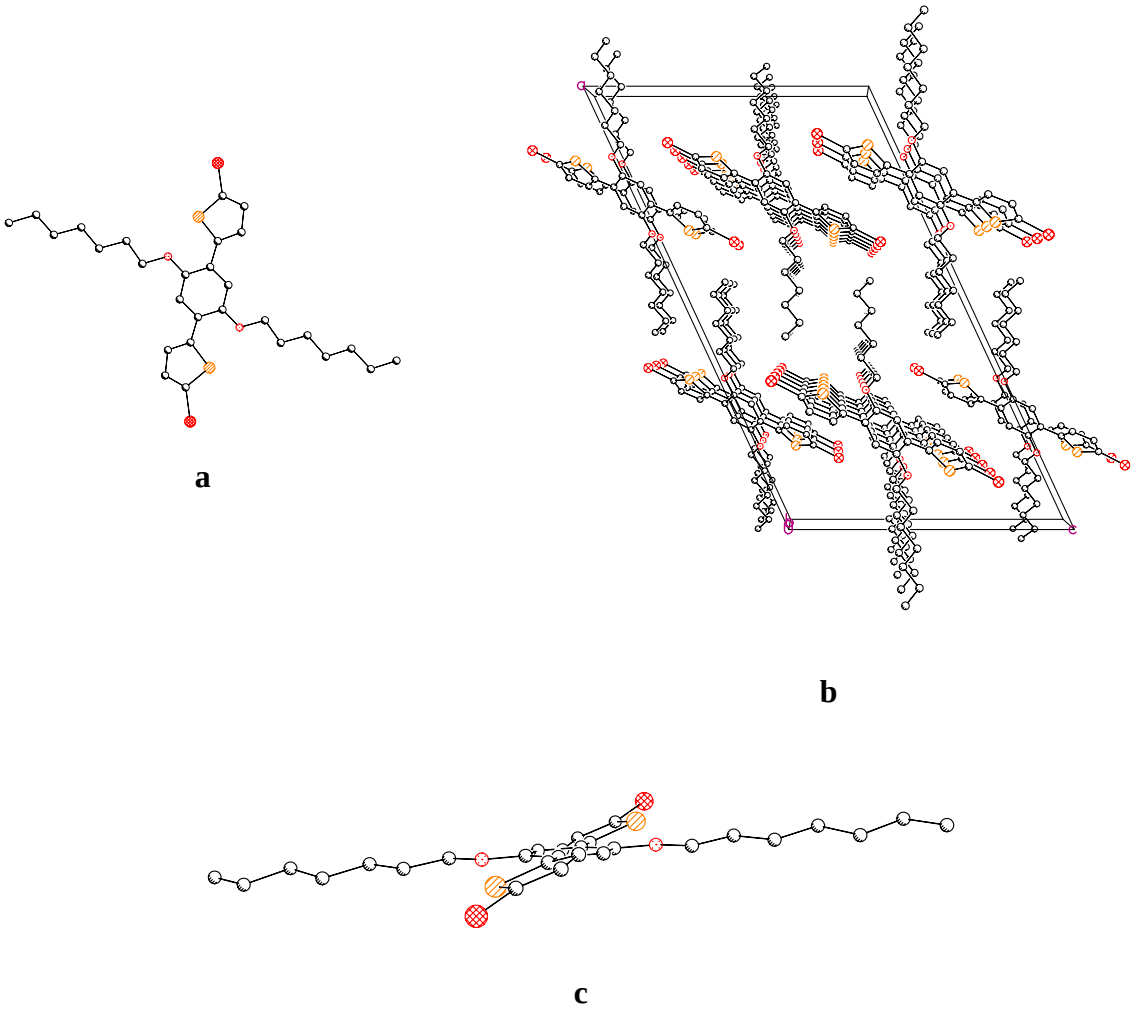

Figure 3-3. Single crystals X-ray analysis of Br_2-BT-B(OC_7H_{13})$_2$. (a) Molecular structure, (b) packing mode, (c) Side view.

3.2.2 Bis-EDOT-dialkoxybenzenes

The synthesis of 1,4-bis[2-(5-bromo-3,4-ethylenedioxy)thienyl]-2,5-diheptoxybenzene [Br_2-BEDOT-B(OC_7H_{15})$_2$], and of 1,4-bis[2-(5-bromo-3,4-ethylenedioxy)thienyl]-2,5-didodecyl-oxybenzene [Br_2-BEDOT-B($OC_{12}H_{25}$)$_2$] monomers started by the deprotonation of EDOT with *n*-butyllithium, and further reaction with trimethylstannyl chloride to give 2-trimethyltin-3,4-ethylenedioxythiophene (EDOT-Sn(CH_3)$_3$) as illustrated in Figure 3-4. 1,4-Bis[2-(3,4-ethylenedioxy)thienyl]-2,5-dialkoxybenzene (BEDOT-B(OR)$_2$) was obtained by Stille coupling

of 1,4-dibromo-2,5-dialkoxybenzene with EDOT-$Sn(CH_3)_3$. As for the thiophene derivatives, the Stille route was chosen over the Negishi coupling previously reported for these molecules,[46] because of the possibility to isolate, purify, and store EDOT-$Sn(CH_3)_3$. The monomer precursors BEDOT-$B(OR)_2$ were obtained in 70-80% yields after purification by recrystallization. Their bromination was accomplished by addition of NBS in DMF at -78°C, followed by progressive warming of the solution to 0°C. This step was particularly challenging as oxidation problems arose easily. The electron donating power of EDOT considerably decreases the oxidation potential of BEDOT-$B(OR)_2$ molecules compared to their thiophene counterparts (~ 0.35 V vs Fc/Fc^+ for 1,4-bis[2-(3,4-ethylenedioxy)thienyl]-2,5-diheptoxybenzene[46] versus 0.55 V for 1,4-bis(2-thienyl)-2,5-diheptoxybenzene[50]), making them more sensitive to oxidation.[23] Attempts in THF from -78°C to 0°C, led to black insoluble tars, probably resulting from the formation of oxidized polymer. The use of DMF at low temperatures allowed milder oxidative conditions and successful bromination.[114] The reaction was stopped by addition of a solution of ammonium hydroxide, which reduced the crude product, and quenched unreacted NBS and the hydrogen bromide released.[115] For purification, a combination of flash column chromatography on silica gel and of repeated recrystallizations was needed, in order to isolate the dibrominated monomer from its monobrominated version. Also a fast solvent flow was required for the column chromatography otherwise the monomers polymerized on the silica gel. Indeed, when slow elution was used, no monomer could be extracted from the column. Instead, an orange-pink material, highly fluorescent under UV light, was recovered after dumping the contents of the column in a beaker containing hydrazine and removing the silica gel by filtration. A toluene solution of that material was analyzed by UV-Vis spectroscopy and an absorption maximum of 455 nm was determined in the case of Br_2-BEDOT-$B(OC_7H_{15})_2$, which provides evidence that

some coupling occurred (the absorption maxima of the monomer are at 376 nm and 398 nm). The monomers were obtained in 40% and 57% yields for Br_2-BEDOT-B(OC_7H_{15})$_2$ and Br_2-BEDOT-B($OC_{12}H_{25}$)$_2$, respectively.

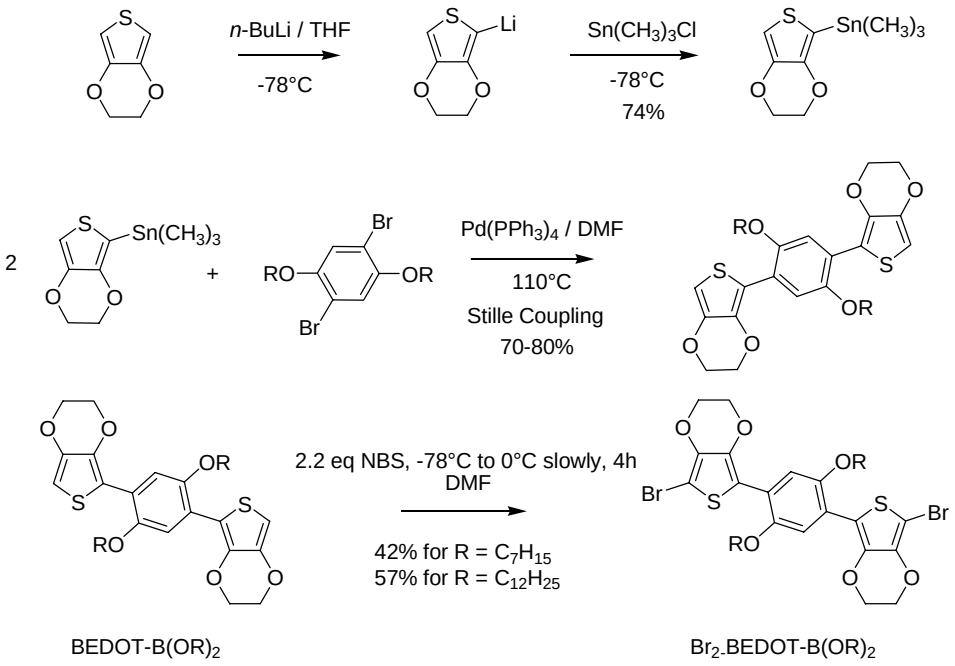

Figure 3-4. Bis-EDOT-dialkoxybenzene monomer synthesis.

The monomers were fully characterized by ^{1}H-NMR, ^{13}C-NMR, HRMS, elemental analysis, melting point determination, and single crystal X-ray studies. For X-ray analysis, the crystals of Br_2-BEDOT-B($OC_{12}H_{25}$)$_2$ were grown from a methanol/THF mixture (1/1) and the crystals of Br_2-BEDOT-B(OC_7H_{15})$_2$ from an ethanol/THF mixture (3/1). Figure 3-5a shows the molecular structure of Br_2-BEDOT-B(OC_7H_{15})$_2$, while Figure 3-5b shows its packing mode. Br_2-BEDOT-B(OC_7H_{15})$_2$ crystallizes in the monoclinic space group P2(1)/n with the alkoxy chains and phenyl rings being coplanar. The dihedral angle between the central phenylene and EDOT rings is very small (6.1°), which renders the molecules almost planar. This quasi-planarity helps the molecules pack close to one another with a small interchain distance of 3.7 Å. Molecular planarity is a desirable feature since less energy is required to stabilize the bipolaron state upon

polymer oxidation. Figure 3-6a shows the molecular structure of Br_2-BEDOT-B($OC_{12}H_{25}$)$_2$, and Figure 3-6b shows its packing mode. Br_2-BEDOT-B($OC_{12}H_{25}$)$_2$ crystallizes in the monoclinic space group C2/c with the alkoxy chains and phenyl rings being also coplanar. The dihedral angle between the central phenylene and EDOT rings is even smaller than the one found for Br_2-BEDOT-B(OC_7H_{15})$_2$ (1.7°) and this extremely small deviation from planarity, illustrated in Figure 3-6c, gives rise to closer π-stacking with an interchain distance of 3.5 Å. We noticed that the cofacial arrangement is not as great as what was observed for Br_2-BT-B(OC_7H_{15})$_2$. The tight packing observed for the Br_2-BEDOT-B(OR)$_2$ monomers particularly motivates the development of oligomeric or polymeric derivatives of these molecules, where a possible extension of these properties would lead to materials with high charge mobility.

3.2.3 Bis-ProDOT-dialkoxybenzenes

The monomers BProDOT-Me_2-B($OC_{12}H_{25}$)$_2$ and BProDOT-Hex_2-B($OC_{12}H_{25}$)$_2$ were synthesized from 1,4-dibromo-2,5-didodecyloxybenzene and the corresponding substituted ProDOT unit by Negishi coupling. The substituted ProDOT derivatives were synthesized by transetherification of 3,4-dimethoxythiophene and the dialkyl-substituted propane-1,3-diols as previously reported (Figure 3-7).[34] The synthesis of 3,4-dimethoxythiophene was accomplished using the synthetic route shown in Figure 3-7. It started with the tetrabromination of thiophene followed by debromination of the 2 and 5 positions of the thiophene ring with zinc dust in glacial acetic acid.[116] Ullman type coupling between sodium methoxide and 3,4-dibromothiophene in the presence of copper oxide (CuO) afforded 3,4-dimethoxythiophene.[117] The ProDOT derivatives were lithiated with one equivalent of *n*-butyllithium and reacted with anhydrous zinc chloride ($ZnCl_2$) (Figure 3-8). Coupling with 1,4-dibromo-2,5-didodecyloxybenzene was first attempted using tetrakis(triphenylphosphine) palladium (0) [Pd(PPh_3)$_4$] as the catalyst, as

previously reported for EDOT and thiophene derivatives,[22,46] but was limited possibly by unfavorable steric interactions between the heterocycles. However, the Negishi coupling was more successful using a different catalyst system made of commercially available $Pd(0)_2(dba)_3$ and tri-*t*-butylphosphine ligands [P(*t*-Bu)$_3$] which has been proven very efficient for coupling sterically demanding molecules.[118] Both monomers were obtained in decent yields (*ca.* 40 %) after purification by column chromatography, and were characterized by UV-Vis, ^{1}H-NMR, ^{13}C-NMR, melting point determination, elemental analysis, and HRMS. As expected, the monomer containing long and flexible hexyl chains on the ProDOT unit melts at a lower temperature (45˚-46˚C) than the methyl substituted monomer (80˚-82˚C). BProDOT-Me_2-B($OC_{12}H_{25}$)$_2$ and BProDOT-Hex_2-B($OC_{12}H_{25}$)$_2$ exhibit similar absorption maxima in toluene at 354 nm and 356 nm respectively, with extinction coefficients of 16,430 M^{-1} cm^{-1} for the former and of 15,640 M^{-1} cm^{-1} for the latter. Replacement of the methyl groups by the longer hexyl chains on ProDOT does not lead to any observable change in the monomer's optical properties.

Suitable crystals for an X-ray diffraction study of BProDOT-Me_2-B($OC_{12}H_{25}$)$_2$ were obtained by slow cooling recrystallization from a hexanes/ethyl acetate mixture (5/1 ratio). BProDOT-Me_2-B($OC_{12}H_{25}$)$_2$ crystallizes in the triclinic P-1 space group. The molecular structure is shown in Figure 3-9a and the packing mode in Figures 3-9b and 3-9c. The molecules, which are located on inversion centers, are nearly planar with a dihedral angle of 6.6˚ between the central phenyl and thiophene rings. The molecules stack with a close to perfect cofacial arrangement with a small interchain distance of 3.679 Å as evident in Figure 3-9c**.** If extended to the polymers (or oligomers), these two features would greatly favor inter-chain transport. BProDOT-Hex_2-B($OC_{12}H_{25}$)$_2$ crystals were not of sufficient size for single-crystal structure analysis.

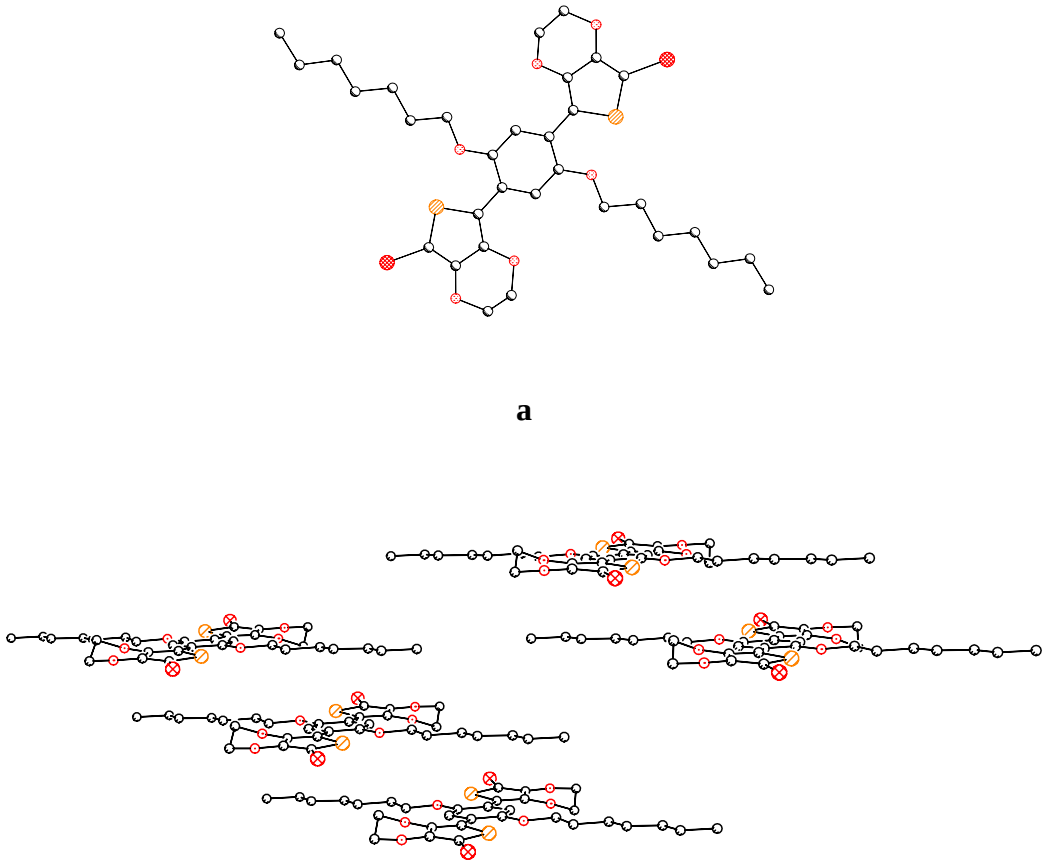

a

b

Figure 3-5. Single crystals X-ray analysis of Br_2-BEDOT-B(OC_7H_{13})$_2$. (a) Molecular structure, (b) packing mode.

3.3 Polymer Syntheses and Characterizations

3.3.1 Polymerization Attempts via GriM

As described in the general Introduction, GriM has been used by Wang *et al.* for the preparation of the electron rich poly[(3,4-ethylenedioxythiophene)-2,5-didodecyloxybenzene] (LPEB), whose repeat unit structure is similar to the molecules studied in this report (Figure 3-10).[36] This polymer was synthesized at high molecular weights (~ 30,000 g mol^{-1}) with a low polydispersity of 1.30.

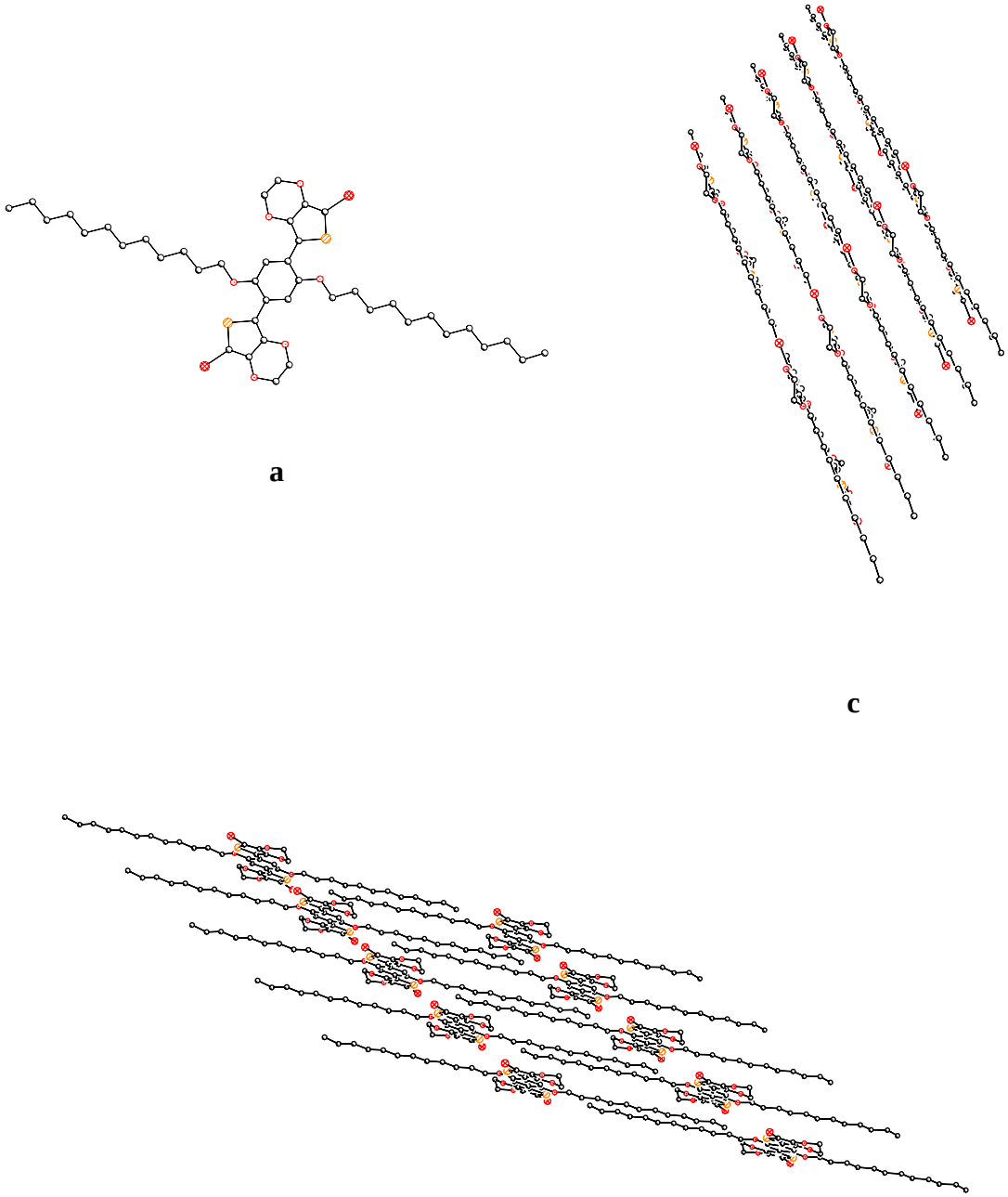

Figure 3-6. Single crystals X-ray analysis of Br_2-BEDOT-$B(OC_{12}H_{25})_2$. (a) Molecular structure, (b) packing mode, (c) quasi-planar arrangement of adjacent Br_2-BEDOT-$B(OC_{12}H_{25})_2$ molecules.

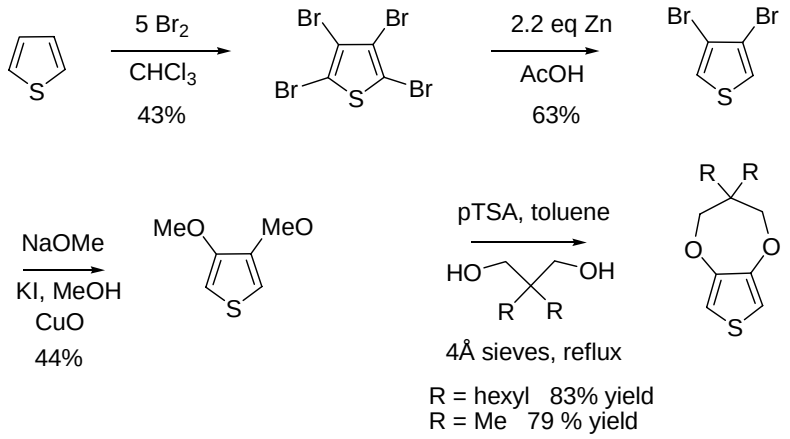

Figure 3-7. Synthesis of methyl- and hexyl-substituted ProDOTs.

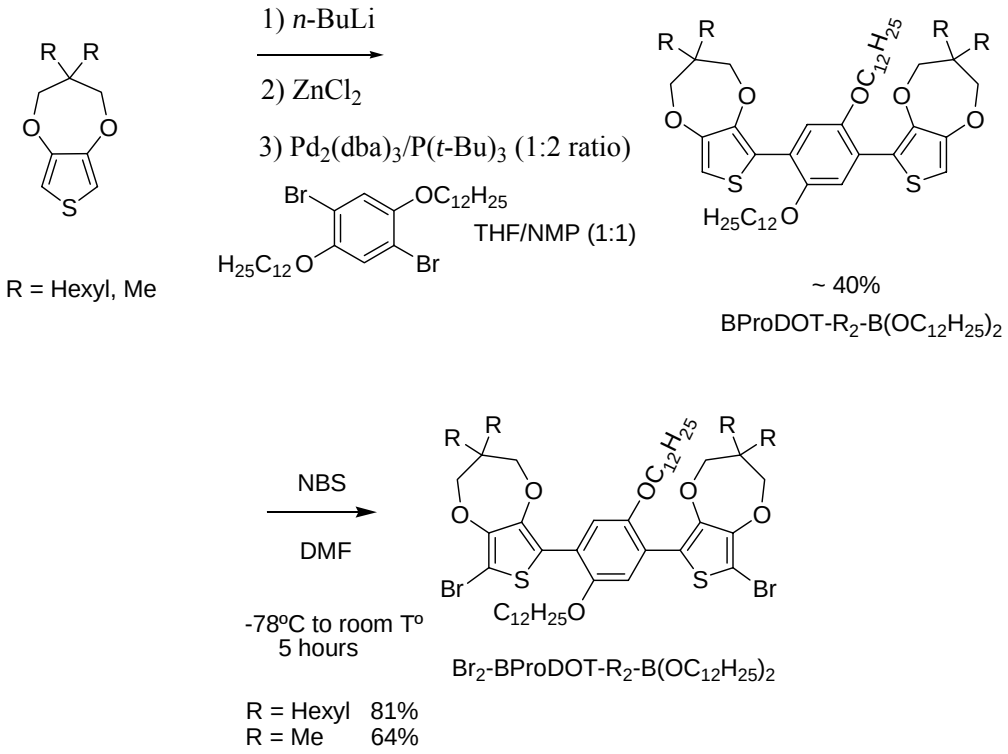

Figure 3-8. Synthesis of BProDOT-R_2-dialkoxyphenylene and Br_2-BProDOT-R_2-dialkoxyphenylene monomers.

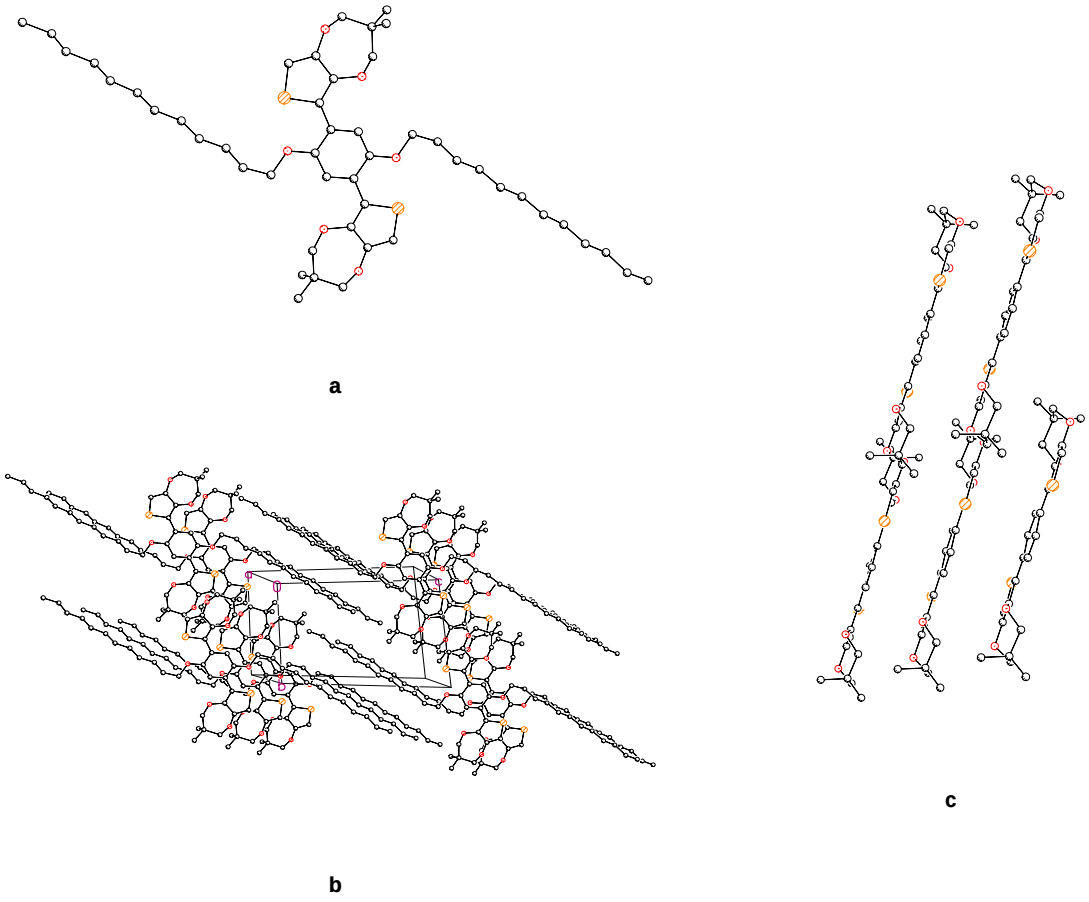

Figure 3-9. Single crystals X-ray analysis of BProDOT-Me_2-B($OC_{12}H_{25}$)$_2$. (a) Molecular structure, (b) packing mode, (c) π-stacking of BProDOT-Me_2-B($OC_{12}H_{25}$)$_2$ illustrated without the phenylene side chains ($OC_{12}H_{25}$).

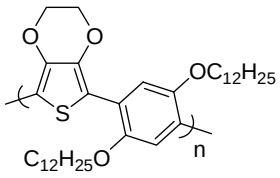

LPEB

Figure 3-10. Structure of LPEB.

It was decided to attempt the same conditions as the ones used by Wang *et al.* to polymerize the dibromo-thienylene-phenylene monomers (Br_2-BT-B(OR)$_2$, Br_2-BEDOT-B(OR)$_2$, and Br_2-BProDOT-R_2-B($OC_{12}H_{25}$)$_2$), as illustrated in Figure 3-11. The monomers were treated with methylmagnesium bromide (MeMgBr) at reflux, and then Ni(dppp)Cl_2 was added

for coupling the bromomagnesio intermediates. Unfortunately, no polymer was formed, and in all cases the monomers were recovered in ~ 90% yields after work up. In order to check if the metalation of the thienyl bromide occurred, the bromomagnesio intermediates were quenched with deionized water. This method had been used by Wang *et al.* in their work on LPEB for proving that the metalation was occurring at the bromo-EDOT site. In our case, no thiophene protons were observed proving that the metalation did not take place. The Grignard reagent MeMgBr was switched for the less stable and more reactive *t*-butyl magnesium chloride, but the reaction failed again. One explanation could be that the three ring symmetrical system does not provide enough reactivity to the aryl-Br sites. Another explanation could be that with the addition of an extra heterocycle the system has become too electron rich to allow metalation of the bromo-aryl site. It had been reported that extremely limited lithiation of BEDOT-B$(OR)_2$ could be accomplished after addition of *n*-BuLi or *sec*-BuLi, due to the too strong electron donating power of the molecules, and this example supports the second explanation.[23] There is very little literature precedent on the polymerization via GriM of multiple ring systems, and consequently it is difficult to give a definitive explanation for the failure encountered here.

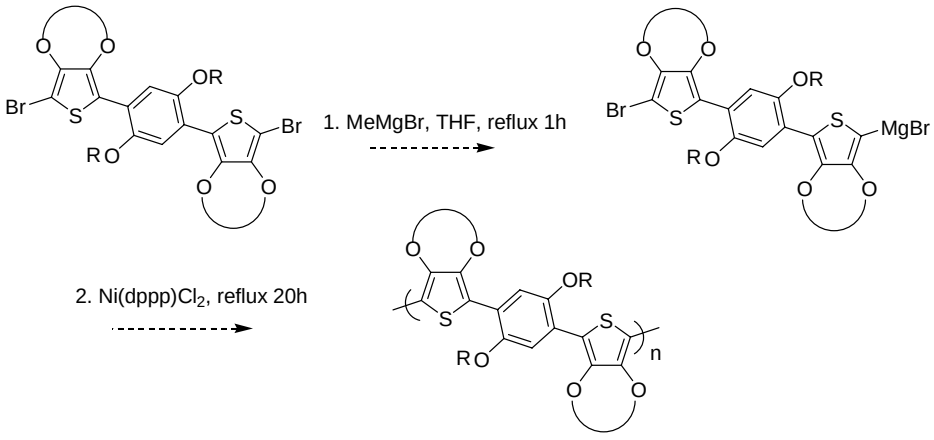

Figure 3-11. GriM route for the polymerization of the dibromo-thienylene-phenylene monomers.

3.3.2 Polymerization via Yamamoto Coupling

3.3.2.1 Poly(bis-thiophene-dialkoxybenzene)s

The polymerization of the Br_2-BT-$B(OR)_2$ monomers has been carried out via Yamamoto coupling according to the synthetic route shown in Figure 3-12. The zerovalent nickel reagent, $Ni(COD)_2$, was mixed with 1,5-cyclooctadiene (COD), a molar equivalent of 2,2′-bipyridyl (Bpy), and DMF at 60 ºC, and this mixture was added dropwise to the DMF monomer solution. The solution color changed from yellow to dark red and the red polymers precipitated out of the solution. The polymers were purified by Soxhlet extraction with methanol followed by hexanes, to remove unreacted monomer, inorganic impurities, and low molecular weight polymer. Final extraction with toluene afforded red solids in 55% yield for PBT-$B(OC_7H_{15})_2$ and 40 % yield for PBT-$B(OC_{12}H_{25})_2$ after solvent evaporation. These materials exhibit a solubility of about 7 mg mL^{-1} in toluene.

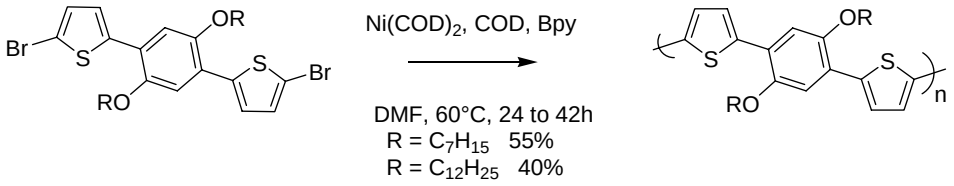

Figure 3-12. Polymerization of Br_2-BT-$B(OR)_2$ monomers via Yamamoto coupling.

The polymers were characterized by ^{1}H-NMR, GPC, MALDI, and elemental analysis. The results of the molecular weight (MW) analysis performed by GPC (polystyrene standards, THF as mobile phase, 40°C) are summarized in Table 3-1. Number average molecular weights of ~ 5,000 g mol^{-1} and of ~ 3,000 g mol^{-1} were estimated for PBT-$B(OC_7H_{15})_2$ and PBT-$B(OC_{12}H_{25})_2$, respectively, which correspond to polymers of about 17 to 29 rings. The low polydispersity (1.30) is explained by the Soxhlet extraction with hexanes which removed the low molecular weight material. The low molecular weights may be explained by the electron donating-ability of the system, which as the molecular weight increased, deactivated more and more the bromo-

thiophene reactive sites and rendered the oxidative addition of the Ni(0) complex more difficult. The decrease in solubility, observed as the polymer chains were getting bigger (the polymers were precipitating out of the solution), could have stopped the coupling process too. For improving the solubility, the polymerization has also been attempted in mixtures of DMF and toluene (1/2), but higher molecular weights could not be reached.

Table 3-1. GPC estimated molecular weights of the PBT-B$(OR)_2$ polymers (polystyrene standards, THF as mobile phase, 40°C).

Polymers	M_n (g mol^{-1})	M_w (g mol^{-1})	PDI	Average number of rings
PBT-B$(OC_7H_{15})_2$	4,960	6,340	1.3	29
PBT-B$(OC_{12}H_{25})_2$	2,945	3,950	1.3	17

As structure proof, the polymers were characterized by MALDI-MS using a terthiophene matrix. The MALDI spectra are displayed in Figure 3-13 and show that the spacing between the peaks corresponds to ~ 468 amu for PBT-B$(OC_7H_{15})_2$, and to ~ 609 amu for PBT-B$(OC_{12}H_{25})_2$, which correlates well with the calculated molecular weights of the repeat units (n) of the polymers. The different series in the MALDI spectra show that there is a variety of end-groups: H/H, H/Br, Br/Br. A predominance of H/H end groups over H/Br or Br/Br end-groups at low molecular weights could have explained why a large degree of polymerization could not be reached. However a comparison between the peak intensities shows that there seems to be no preference for one type of end-group over the other. This comforts us in our assumption that solubility and electron density are the most probable parameters limiting the growing of the polymer chains.

Figure 3-14 shows the solution UV-Vis absorbance of the polymers in toluene. The solutions are orange (photograph in Figure 3-14), and the absorption maxima are found at 469 nm for PBT-B$(OC_7H_{15})_2$, and at 463 nm for PBT-B$(OC_{12}H_{25})_2$. Figure 3-14 also shows the UV-

Vis absorbance of the monomers, which is blue-shifted compared to the UV-Vis absorption of the polymers due to the lower degree of conjugation.

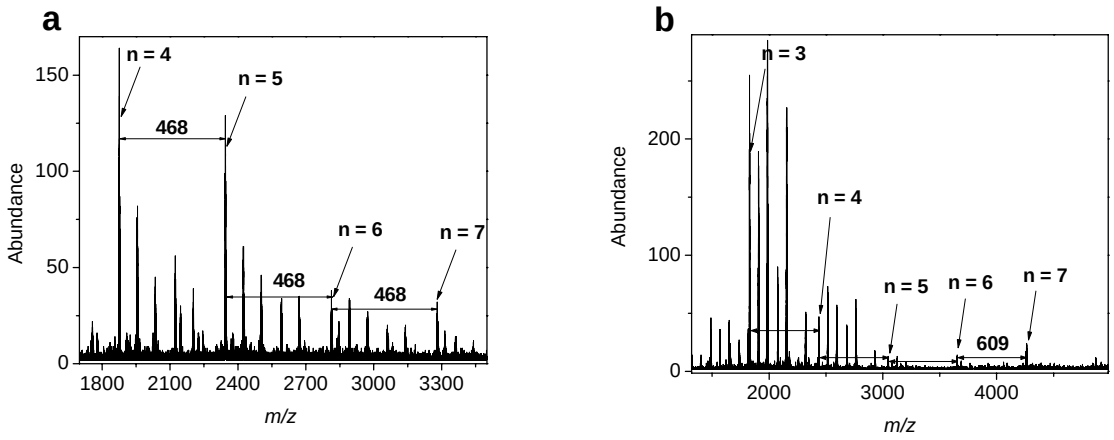

Figure 3-13. MALDI-MS of BT-B(OR)$_2$ polymers. (a) PBT-B(OC_7H_{15})$_2$, (b) PBT-B($OC_{12}H_{25}$)$_2$. Terthiophene was used as the matrix.

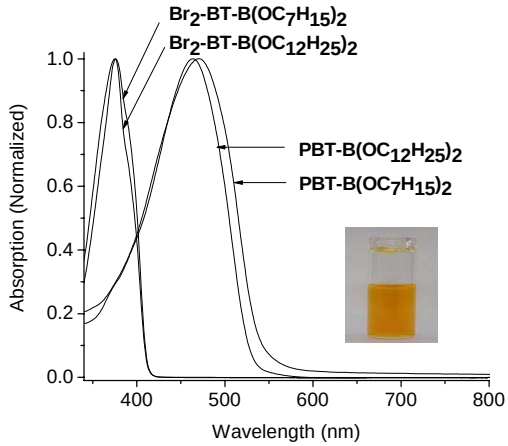

Figure 3-14. Solution UV-Vis absorbance of Br_2-BT-B(OR)$_2$ monomers, and PBT-B(OR)$_2$ polymers in toluene.

The ordering properties of the polymers were studied by DSC as illustrated by the second DSC scans displayed in Figures 3-15a and 3-15b. The symmetrically derivatized polymers exhibited two endothermic transitions and one exothermic transition. The first endothermic

transition (T_{m1}), observed at -39°C for PBT-B(OC_7H_{15})$_2$ and at -41°C and PBT-B($OC_{12}H_{25}$)$_2$, has been attributed to the melting of the side chains. Previous ordering studies done by the Reynolds group on this type of molecule (synthesized via $FeCl_3$) have shown that the highest transition (T_{m2}) can be attributed to an isotropic melt of the polymer backbone, and the first exothermic transition (T_{c1}) to their crystallization.[22] The melting temperature T_{m2} was lower for PBT-B($OC_{12}H_{25}$)$_2$ (134°C) than for PBT-B(OC_7H_{15})$_2$ (190°C), probably due to the molecular weight differences. These DSC results confirmed the semicrystalline nature of the polymers.

The thermal stability of the polymers was studied by TGA both in air and in a nitrogen atmosphere using a 20°C min^{-1} temperature ramp from 50°C to 900°C. The thermograms displayed in Figure 3-16 show that the polymers exhibit a high thermal stability, losing less than 5% weight in air at 335°C for PBT-B(OC_7H_{15})$_2$, and at 322°C for PBT-B($OC_{12}H_{25}$)$_2$. A similar behavior was observed under nitrogen, with a loss of less than 5% weight at 352°C for PBT-B(OC_7H_{15})$_2$, and at 323°C for PBT-B($OC_{12}H_{25}$)$_2$. A drastic degradation process occurred from these temperatures up to ~ 650°C for PBT-B(OC_7H_{15})$_2$, and up to ~ 750°C PBT-B($OC_{12}H_{25}$)$_2$. Above 850°C, less than 7% of PBT-B($OC_{12}H_{25}$)$_2$ and less than 15% of PBT-B(OC_7H_{15})$_2$ remained.

3.3.2.2 Poly(bis-alkylenedioxythiophene-dialkoxybenzene)s

The polymerizations of the Br_2-BEDOT-B(OR)$_2$ and Br_2-BProDOT-R_2-B($OC_{12}H_{25}$)$_2$ monomers have also been carried out via Yamamoto coupling using the same conditions as those employed for PBT-B(OR)$_2$. Unfortunately, a maximum of 3 repeat units for PBEDOT-B($OC_{12}H_{25}$)$_2$ (M_n = 1,792, M_w = 2,497, DPI = 1.40) and of 4 repeat units for PBProDOT-R_2-B($OC_{12}H_{25}$)$_2$ [PBProDOT-Me_2-B($OC_{12}H_{25}$)$_2$: M_n = 3,394, M_w = 6,119, PDI = 1.80; PBProDOT-Hex_2-B($OC_{12}H_{25}$)$_2$: M_n = 1,859, M_w = 2,525, PDI = 1.36] were coupled. Even though the size of the PBEDOT-B($OC_{12}H_{25}$)$_2$ oligomers was small, the material was difficult to solubilize.

According to the work previously reported on these types of molecules,[46] and the work presented in this dissertation, it is clear that these PBEDOT-B($OC_{12}H_{25}$)$_2$ molecules are likely not the best candidates for the production of highly processable films for optoelectronic devices. It was consequently decided to stop further synthetic work on them. However, the solubility and processing expectations were quite good for PBProDOT-R_2-B($OC_{12}H_{25}$)$_2$, and it was decided to continue investigating other synthetic pathways and to study more deeply their electronic properties.

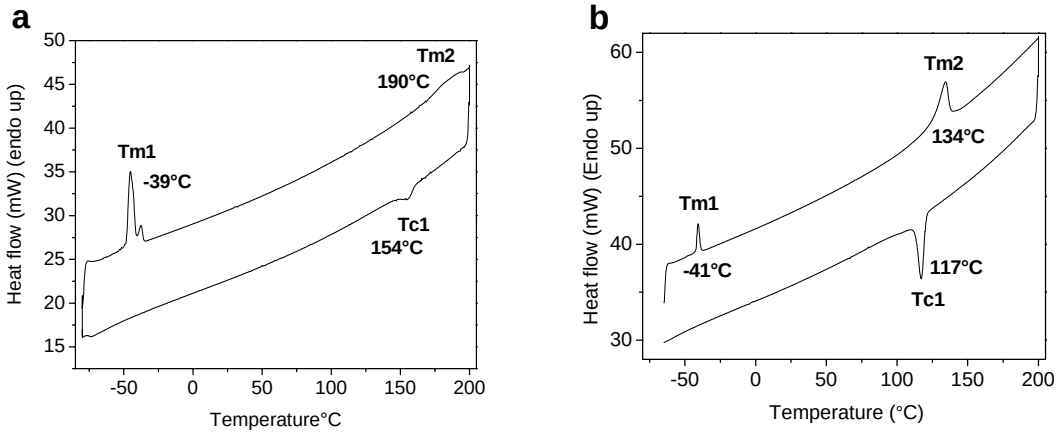

Figure 3-15. DSC thermograms (second scans) of PBT-B(OR)$_2$ polymers. (a) PBT-B(OC_7H_{15})$_2$, and (b) PBT-B($OC_{12}H_{25}$)$_2$. The temperature was cycled between -80°C and 200°C at 10°C min^{-1}.

3.3.3 Solid State Polymerization Attempts

It was hypothesized that a solid state polymerization, following the same process as the one discovered for the spontaneous polymerization of Br_2-EDOT, could happen for the dibromo-thienylene-phenylene monomers (as detailed in the general introduction).[41] Crystals of Br_2-BEDOT-B(OC_7H_{15})$_2$ were progressively heated for 2 days up to 150°C, and then from 150°C to 180°C, in a sublimation apparatus under vacuum, in order to prepare a polymer film on a glass

substrate in situ (Figure 3-17). No sublimation occurred and as the temperature was increased, the crystals became darker and finally melted into a black gum once the melting temperature was reached. Once cold, this black insoluble material looked like charcoal and was extremely friable. It was stirred overnight in a mixture of ACN and hydrazine monohydrate, then filtered and washed with neat ACN. No color change occurred upon addition of hydrazine and the material could not be dissolved in organic solvents. It also did not show any conductivity after being doped with iodine, and it was finally deduced that this material was probably the result of degradation, not polymerization.

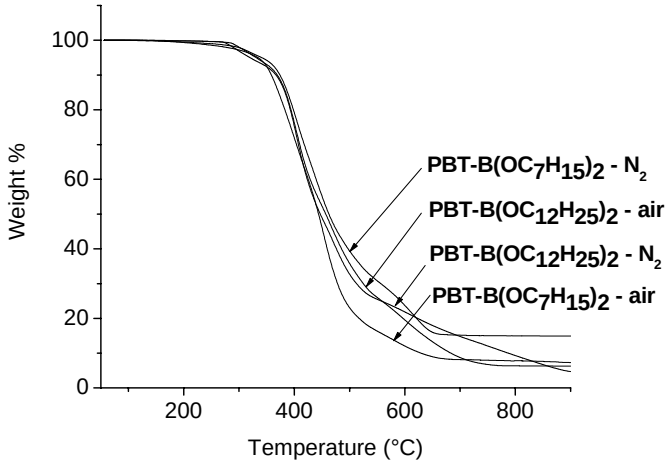

Figure 3-16. Thermogravimetric analysis of the PBT-B$(OR)_2$ polymers. Measurements performed both in air and in a nitrogen atmosphere, using a 20°C min^{-1} temperature ramp from 50°C to 900°C.

Before pursuing further experiments, it was decided to first examine the bromine distances in the Br_2-BEDOT-B$(OC_7H_{15})_2$ crystal structure. The smallest bromine distance found between adjacent molecules in the same row, represented by a dashed line in Figure 3-18, had a value of 5.38 Å (7.54Å between bromines on facing rings), bigger than the sum of the van der Waals radii. These distances were even bigger for Br_2-BEDOT-B$(OC_{12}H_{25})_2$ (10.64 Å in the same row, and 7.76 Å between facing rings) and Br_2-BT-B$(OC_7H_{15})_2$ (10.16 Å in the same row and 5.79 Å

between facing rings), and it was deduced that further investigation on the solid state polymerization of these molecules would not likely give a successful polymerization.

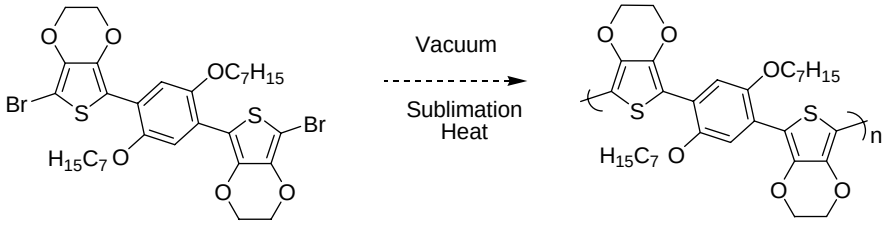

Figure 3-17. Attempt in the solid state polymerization of Br_2-BEDOT-B(OC_7H_{15})$_2$.

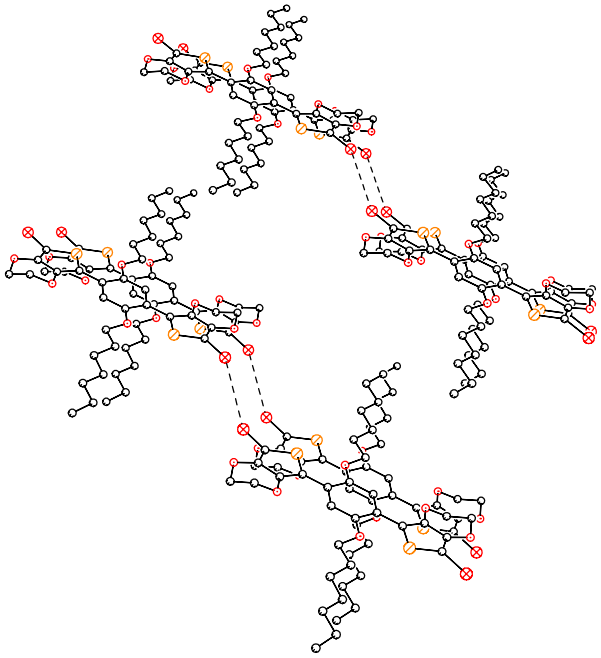

Figure 3-18. Crystal packing of Br_2-BEDOT-B(OC_7H_{15})$_2$ illustrating the intermolecular distances between bromine atoms.

3.3.4 Electropolymerization

The electropolymerization of the BEDOT-B(OR)$_2$ and BT-B(OR)$_2$ families is already well documented and was consequently not investigated in this work.[46,50,105] In order to develop an understanding of the redox properties of polymer films of the new BProDOT-R_2-B($OC_{12}H_{25}$)$_2$

family, the two BProDOT-R_2-B($OC_{12}H_{25}$)$_2$ monomers have been electrochemically polymerized on a platinum button electrode. The electrodeposition was accomplished using an ACN/dichloromethane (CH_2Cl_2) (5/3) solution, with 0.1 M TBAP and saturated in monomer (0.01 M). Dichloromethane was required due to the poor solubility of the monomers in ACN. However, too much CH_2Cl_2 hindered polymer formation and deposition on the electrode and only the use of monomer saturated solutions helped to circumvent that problem. The repeated scanning electropolymerizations of BProDOT-Me_2-B($OC_{12}H_{25}$)$_2$ and of BProDOT-Hex_2-B($OC_{12}H_{25}$)$_2$ are shown in Figures 3-19a and 3-19b respectively. During the first anodic scan, a single peak is observed which corresponds to irreversible monomer oxidation and formation of cation radicals. The peaks of monomer oxidation ($E_{p,m}$) are observed at +0.55 V for BProDOT-Me_2-B($OC_{12}H_{25}$)$_2$ and at +0.52 V for BProDOT-Hex_2-B($OC_{12}H_{25}$)$_2$ vs Fc/Fc^+. With repeated potential scanning, a polymer film grows onto the electrode surface in both cases. Cathodic and anodic redox processes are observed during polymer reduction and oxidation, and both increase in intensity with repeated scanning indicative of a successful effective electroactive polymer film deposition. The oxidation potential of the polymer also increases with film thickness due to the increase in polymer resistance. For spectroelectrochemical studies, a polymer thin-film of PBProDOT-Me_2-B($OC_{12}H_{25}$)$_2$ was also potentiostatically deposited onto an ITO-coated glass electrode at +0.5 V for 50 s, using the same electrolyte and concentration as used for the electropolymerization on Pt button.

3.3.5 Oxidative Polymerization via Ferric Chloride

As described in the Introduction (section 3.1), the oxidative chemical polymerizations of the BEDOT-B(OR)$_2$ and BT-B(OR)$_2$ families via $FeCl_3$ has been previously reported. Low molecular weight materials resulted, with particularly poor processing properties in the case of PBEDOT-B(OR)$_2$. It was hypothesized that the low oxidation potential of BProDOT-Hex_2-

$B(OC_{12}H_{25})_2$, as well as its solubility inducing hexyl- and dodecyloxy-substituents, would confer the material favorable conditions for being polymerized via oxidative polymerization. Consequently, the chemical polymerization of BProDOT-Hex_2-$B(OC_{12}H_{25})_2$ was carried out by addition of a ferric chloride slurry ($FeCl_3$, 3 equiv.) in chloroform to a chloroform solution of the monomer over a 2 hour period. The polymerization was carried out overnight at room temperature and the oxidized polymer was then precipitated in cold methanol, collected, dissolved in chloroform, and stirred for 6 hours with about 10 mL of hydrazine monohydrate to reduce the polymer into its neutral form. The neutral polymer was precipitated one more time into cold methanol, filtered through a cellulose thimble, and purified by Soxhlet extraction with methanol as the refluxing solvent to remove unreacted monomer and inorganic impurities. Final extraction with chloroform afforded a red solid in 92 % yield after solvent evaporation. The polymer was soluble in common organic solvents such as THF, dichloromethane, chloroform and toluene.

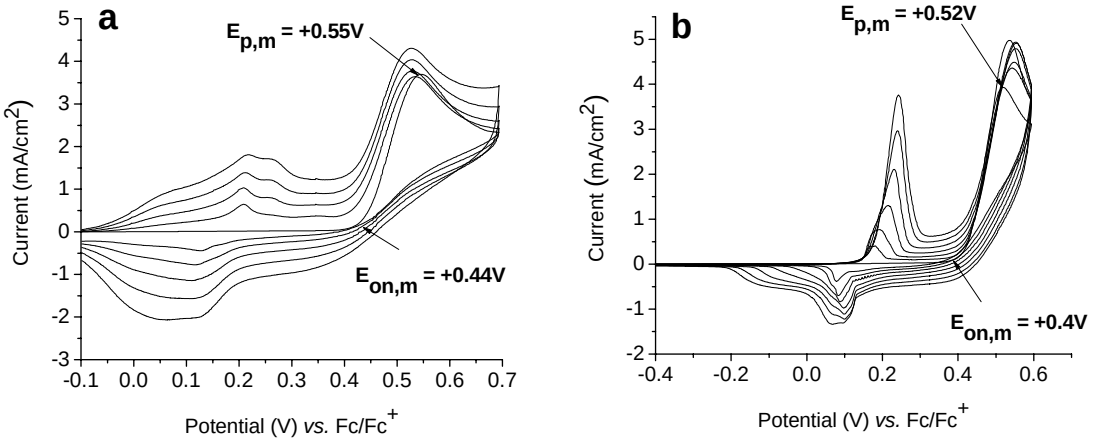

Figure 3-19. Repeated potential scanning electropolymerization of BProDOT-R_2-$B(OC_{12}H_{25})_2$ monomers. (a) BProDOT-Me_2-$B(OC_{12}H_{25})_2$ and (b) BProDOT-Hex_2-$B(OC_{12}H_{25})_2$, 0.01 M saturated solution of 0.1 M TBAP in ACN/CH_2Cl_2 (5/3) at a scan rate of 50 mV s^{-1}.

The ^{1}H-NMR spectra of the material obtained after polymerization was compared to the ^{1}H-NMR spectrum of the BProDOT-Hex_2-B($OC_{12}H_{25}$)$_2$ monomer (Figure 3-20). As expected, the methylene protons at 0.88, 1.27, 1.39, and 1.82 ppm give splitting patterns in the monomer spectrum. They are found at about the same frequency for the polymer (the peak at 1.82 ppm is shifted slightly down-field) but do not resolve. The alkoxy methylene protons at 3.90, 3.91, and 3.99 ppm give also splitting patterns in the monomer but overlap into a broad multiplet at 3.96-4.06 ppm in the polymer. The signal of the phenylene proton (a) is shifted down-field in the polymer by 0.11 ppm. The signal of the ProDOT proton end groups (6.45 ppm, (b)) disappeared as expected for polymerization to a substantial degree.

As structure proof, the polymer was characterized by MALDI mass spectrometry using a terthiophene matrix. Proton end groups were observed and the spacing between the peaks corresponds to ~1090 amu, which corresponds to the calculated molecular weight of the repeat unit of the polymer. Iron and chlorine were efficiently removed as demonstrated by elemental analysis, which shows the presence of only one iron per 47 sulfurs, and of one chlorine per 40 sulfurs. Molecular weight (MW) analysis performed by GPC (polystyrene standards, THF as mobile phase) gave a number average molecular weight of 14,600 g mol^{-1} and a weight average molecular weight of 23,000 g mol^{-1} with a polydispersity index of 1.6. As illustrated in Figure 3-21, polymer elution was monitored with an in-line photodiode array detector to record the UV-Vis absorption of selected fractions of the polymer. Spectra were recorded at various times which allowed monitoring the electronic spectra as a function of molecular weight. For fractions with MW higher than polystyrene equivalents of 25,000 g mol^{-1}, the optimum optical conditions are attained and the absorption maximum is at 573 nm. The narrow MW seen in the gel permeation chromatogram indicates that the polymer does not contain low MW oligomers

(Appendix B). Interestingly, the absorption spectrum of the polymer in THF is red shifted compared to the absorption spectrum in toluene (*vide post*). Therefore THF is not as good a solvent as toluene for this polymer and induces conformational changes to a more planar and rigid structure. More details on the solvent effect will be given in the solvatochromism section (section 3.6).

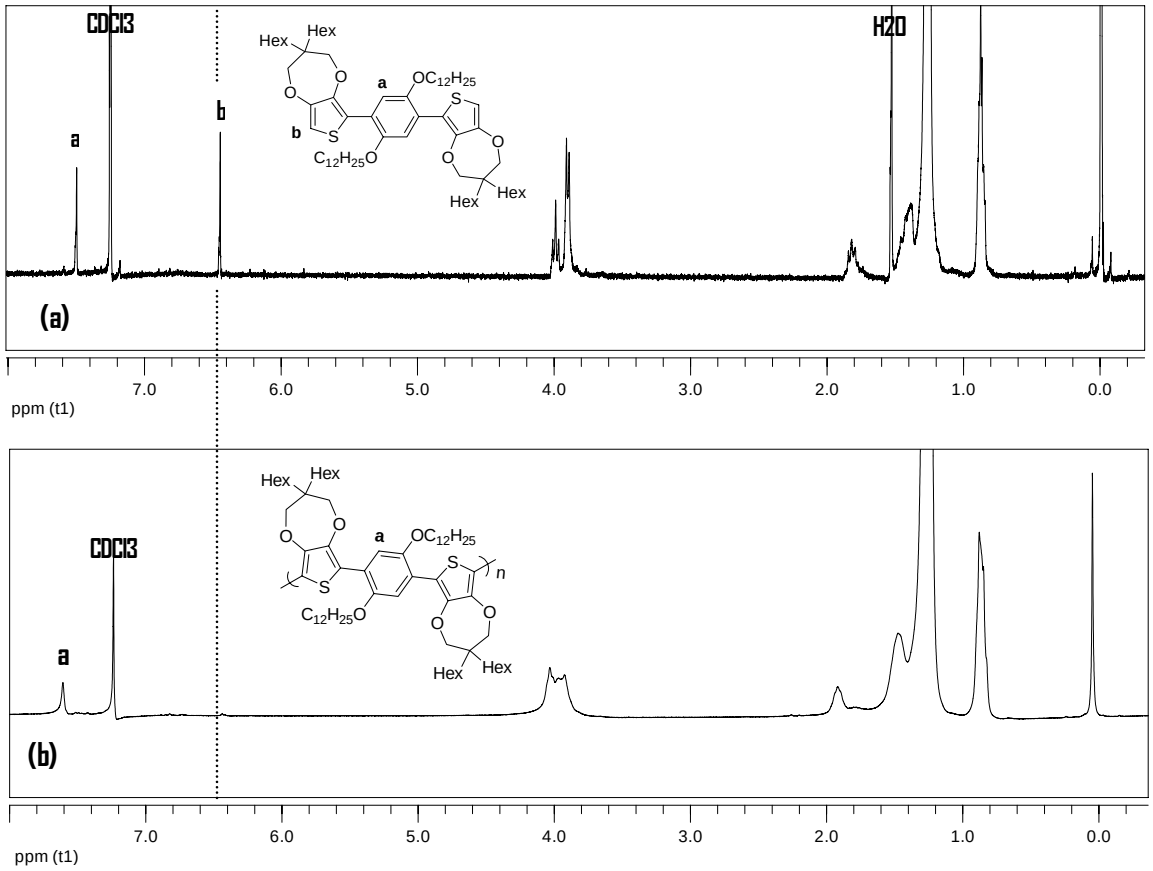

Figure 3-20. ^{1}H-NMR spectra. (a) ^{1}H-NMR($CDCl_3$) spectrum of BProDOT-Hex_2-B($OC_{12}H_{25}$)$_2$, (b) ^{1}H-NMR($CDCl_3$) spectrum of PBProDOT-Hex_2-B($OC_{12}H_{25}$)$_2$.

The thermal stability of PBProDOT-Hex_2-B($OC_{12}H_{25}$)$_2$ was studied by TGA in a nitrogen atmosphere using a 20°C min^{-1} temperature ramp from 50°C to 900°C. The thermogram displayed in Figure 3-22 shows that the polymer exhibits a high thermal stability, having lost less than 5% weight at 357°C. Between that temperature and 450°C, a drastic degradation process occurred, leading to a ~ 70% weight loss, which matches with the side chain degradation. Above

450°C, the degradation became more progressive, and probably corresponds to the polymer backbone degradation. At 900°C, less than 7% of the polymer remained.

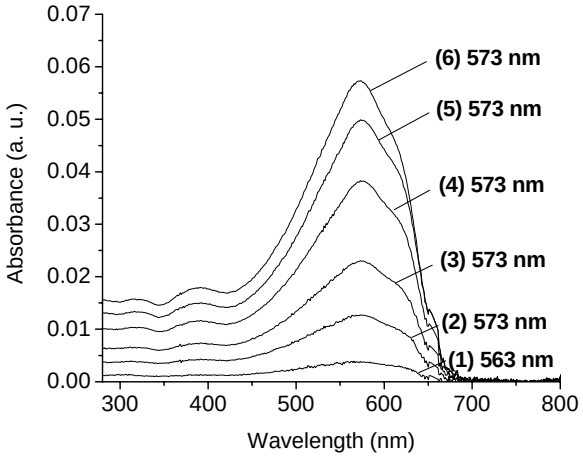

Figure 3-21. Absorption spectra for molecular weight fractions of PBProDOT-Hex_2-$B(OC_{12}H_{25})_2$. Molecular weights are reported in g mol^{-1} vs. peak values for polystyrene. (1) 18,900, (2) 25,000, (3) 30,350, (4) 38,400, (5) 46,700, (6) 61,500.

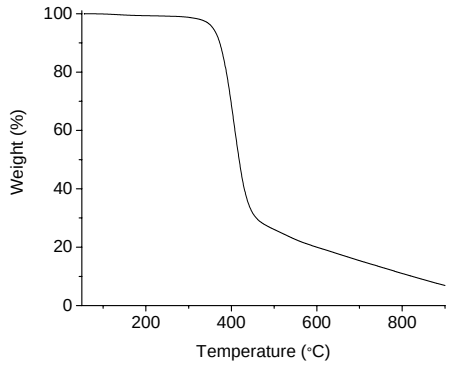

Figure 3-22. Thermogravimetric analysis of the PBProDOT-Hex_2-$B(OC_{12}H_{25})_2$ in a nitrogen atmosphere. A 20°C min^{-1} temperature ramp from 50°C to 900°C was used.

3.4 Polymer Electrochemistry and Spectroelectrochemistry

3.4.1 PBT-$B(OR)_2$

The redox properties of the PBT-$B(OR)_2$ polymers were studied by electrochemistry. The polymers were deposited on Pt button electrodes by drop-casting from 3 mg mL^{-1} toluene

solutions, and cyclic voltammograms were recorded in 0.1 M TBAP/PC. An onset of oxidation ($E_{onset,ox}$) of +0.25 V vs Fc/Fc^+ and a $E_{1/2}$ of +0.29 V were determined for PBT-B(OC_7H_{15})$_2$ (Figure 3-23a). According to these results, the polymer has a HOMO energy of about 5.3-5.4 eV (as detailed in Chapter 2). Figure 3-23b shows the cyclic voltammograms of PBT-B($OC_{12}H_{25}$)$_2$ at different scan rates. The voltammograms are broad and not well defined, and consequently it was not possible to determine $E_{1/2}$. The onset of polymer oxidation was found around +0.35 V, slightly more positive than the value found for the heptoxy analog. This locates the HOMO level at about 5.4-5.5 eV. These two PBT-B(OR)$_2$ derivatives fulfill the energy requirements for stability to oxidation since their HOMO levels are lower than 5.2 eV (general Introduction).

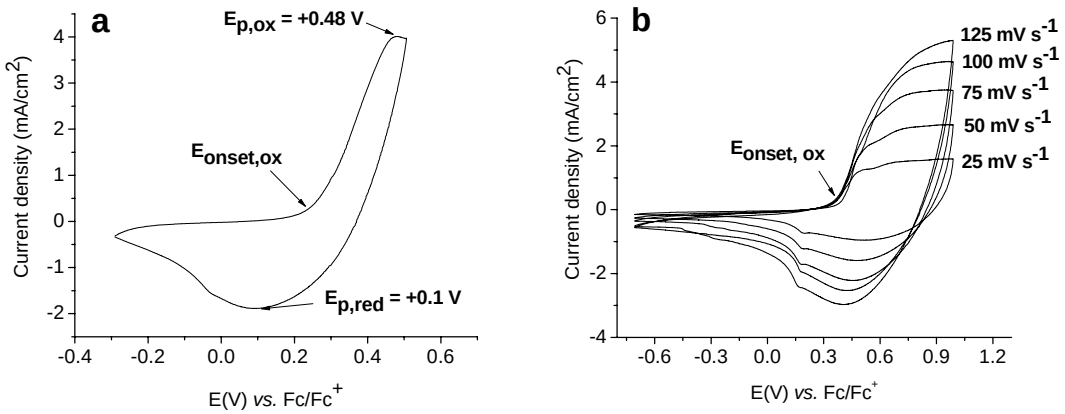

Figure 3-23. PBT-B(OR)$_2$ cyclic voltammetry. (a) CV of PBT-B(OC_7H_{15})$_2$ at 100 mV s^{-1}, (b) CV and scan rate dependence of PBT-B($OC_{12}H_{25}$)$_2$. The polymers were deposited by drop-casting from 3 mg mL^{-1} toluene solutions, and the measurements were accomplished in 0.1 M TBAP in PC.

Spectroelectrochemical studies were accomplished in order to finalize the estimation of the position of the HOMO and LUMO energies, and to observe the polymer spectral changes upon oxidation. Polymer thin-films were spray-cast onto ITO coated glass plates from 3 mg mL^{-1} toluene solutions, and UV-Vis-nIR spectra were recorded in the neutral state and then at higher

oxidizing potentials. Figure 3-24 shows the spectral changes of PBT-B(OC_7H_{15})$_2$ and photographs of the polymer film in the neutral and oxidized states, and Figure 3-25 shows the spectral changes of PBT-B($OC_{12}H_{25}$)$_2$. Both polymers are orange in the neutral state with absorption maxima at 447 nm for PBT-B(OC_7H_{15})$_2$, and at 454 nm for PBT-B($OC_{12}H_{25}$)$_2$. Once the oxidation potentials reached ~ 0.21 V for PBT-B(OC_7H_{15})$_2$, and ~ 0.30-0.35 V for PBT-B($OC_{12}H_{25}$)$_2$, spectral changes started to occur, such as the progressive disappearance of the π-π^* transition of the neutral state, and the formation of polaron transitions in the 600-800 nm region, and of bipolaron transitions in the near-IR region. For each polymer, the starting point of these changes correlates well with the onset of oxidation determined by electrochemistry. Once completely oxidized, PBT-B(OC_7H_{15})$_2$ exhibits a new absorption maximum in the visible region at 738 nm, and its film color changes to blue. Similar color changes were observed for PBT-B($OC_{12}H_{25}$)$_2$, which exhibits an absorption maximum in the visible at 662 nm in the oxidized state. Both polymers exhibit an absorption onset in the neutral state at 590 nm, corresponding to an optical band gap of approximately 2.1 eV. The LUMO energies of the polymers were deduced by adding this band gap value to the HOMO energies estimated by electrochemistry: 3.2-3.3 eV for PBT-B(OC_7H_{15})$_2$ and 3.3-3.4 eV for PBT-B($OC_{12}H_{25}$)$_2$. Consequently the polymers fulfill the energy requirements for transferring charges to PCBM (LUMO offsets >0.4 eV relative to PCBM) as explained in the general Introduction.

3.4.2 PBProDOT-R_2-B($OC_{12}H_{25}$)$_2$

The polymer films of PBProDOT-R_2-B($OC_{12}H_{25}$)$_2$ electrodeposited on Pt button (section 3.3.4) were rinsed with a monomer free solution of ACN/CH_2Cl_2 (5/3) in which the films are not soluble, and cyclic voltammograms were further recorded with scan rate values ranging from 25 to 250 mV s^{-1} (Figures 3-26a and 3-26b). Linear relationships were observed between the current

and the scan rate, indicating that the films are electrode supported and electroactive. The redox processes for the BProDOT-Me_2-$B(OC_{12}H_{25})_2$ system are broad and overlap well as expected for a nicely electroactive polymer, with the peak oxidation ($E_{p,ox}$) and reduction ($E_{p,red}$) potentials around +0.25 V and -0.01 V respectively, at 100 mV s^{-1}. However, $E_{p,ox}$ and $E_{p,red}$ for PBProDOT-Hex_2-$B(OC_{12}H_{25})_2$ (+0.16 V and -0.04 V respectively, at 100 mV s^{-1}) are highly separated as the longer and bulkier chains on the hexyl substituted ProDOT inhibit the fast movement of counter ions. The electrochemical results are summarized in Table 3-2. Both molecules have similar electrochemical values, with half wave potentials around +0.05-0.1 V, which shows that functionalizing the ProDOT unit with long solubilizing hexyl chains has little influence on the electronic properties. These potentials are lower than the values measured for the analogous 1,4-bis(2-thienyl)-2,5-diheptoxybenzene polymer which exhibits[50] an $E_{1/2}$ value of +0.36 V vs Fc/Fc^+, showing the effect of the electron donating oxygens of the ProDOT unit on the polymer oxidation potential. A lower $E_{1/2}$ of -0.40 V vs Fc/Fc^+ has been reported for the analogous 1,4-bis(3,4-ethylenedioxythienyl)-2,5-didodecyloxybenzene polymer due to the stronger electron donating effect of EDOT.[46]

Comparative cyclic voltammetry studies have been done on the chemically synthesized PBProDOT-Hex_2-$B(OC_{12}H_{25})_2$. A film of that polymer was deposited by drop-casting on a Pt button electrode from a 10 mg mL^{-1} chloroform solution, and cyclic voltammograms were recorded for different scan rates in 0.1 M TBAP/PC electrolyte as illustrated in Figure 3-27 and compared to the electrochemically synthesized films. The polymer exhibits an $E_{1/2}$ of +0.23 V at 100 mV s^{-1}, which is a bit higher than the value obtained for the electropolymerized film, but not surprisingly different due to the different morphologies one would expect to form for the two film preparation methods. A HOMO energy of about 5.3-5.4 eV was deduced from the onset of

oxidation at ~ +0.25 V, which is similar to what was determined for the PBT-B$(OR)_2$ derivatives. A linear relationship is found between the peak current and the scan rate indicating that the polymer is electroactive and bound to the electrode.

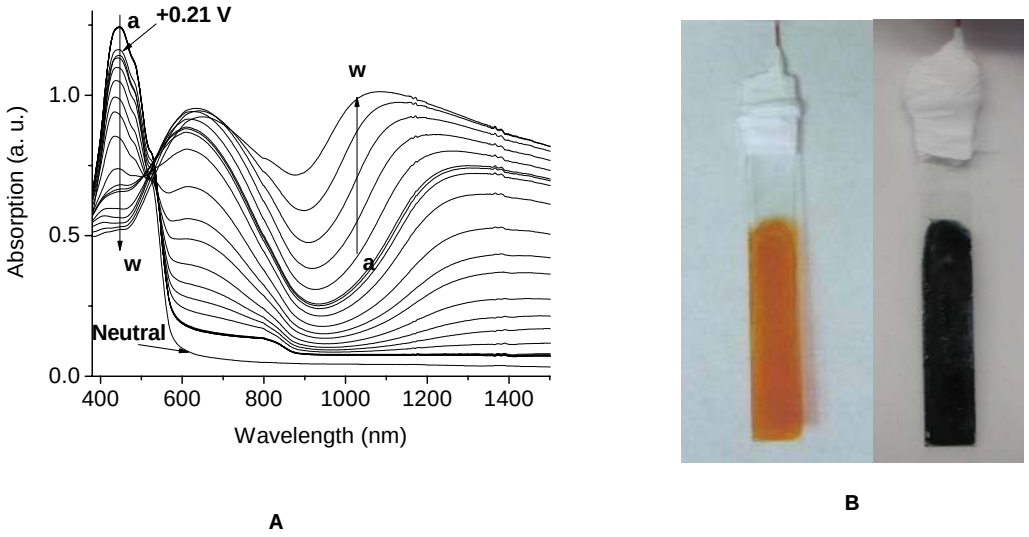

Figure 3-24. Spectroelectrochemical analysis of PBT-B$(OC_7H_{15})_2$ spray-cast onto ITO coated glass. (A) U.V.-Vis.-n.I.R. spectra taken in the neutral state and at potentials of (a) -0.49 V, (b) -0.39V, (c) -0.29 V, (d) -0.19 V, (e) -0.09 V, (f) +0.01 V, (g) +0.11 V, (h) +0.21 V, (i) +0.22 V, (j) +0.23 V, (k) +0.24 V, (l) +0.25 V, (m) +0.26 V, (n) +0.27 V, (o) +0.28 V, (p) +0.29 V, (q) +0.30 V, (r) +0.31 V, (s) +0.41 V, (t) +0.51 V, (u) +0.61 V, (v) +0.71 V, (w) +0.81 V vs Fc/Fc^+ in 0.1 M TBAP/PC; (B) Film colors in the neutral and oxidized states.

Table 3-2. Electrochemical results for BProDOT-R_2-B$(OC_{12}H_{25})_2$ monomers and polymers.

	$E_{on,m}$ (V)[a]	$E_{p,m}$ (V)	$E_{p,ox}$ (V)[b]	$E_{p,red}$ (V)[b]	$E_{1/2}$ (V)[b]	E_g (eV)
BProDOT-Me_2-B$(OC_{12}H_{25})_2$	0.44	0.55	0.25	-0.01	0.12	2.1
BProDOT-Hex_2-B$(OC_{12}H_{25})_2$	0.4	0.52	0.16	-0.04	0.06	2.1

Note: All potentials reported vs Fc/Fc^+
[a]$E_{on,m}$: onset of monomer oxidation**;** [b]Scan rate = 100 mV s^{-1}.

The chemically prepared PBProDOT-Hex_2-B$(OC_{12}H_{25})_2$ was studied by spectroelectrochemistry after film deposition by spray-casting onto ITO coated glass from a 10 mg mL^{-1} chloroform solution. A highly homogeneous film was obtained and dried under

vacuum. The spectra were recorded in 0.1 M TBAP in PC in the neutral state, and stepping the potential from -0.02 V to +0.78 V every 0.05 V as shown in Figure 3-28.

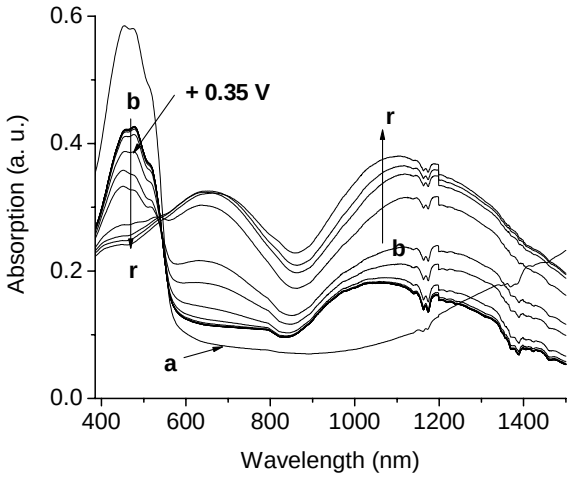

Figure 3-25. Spectroelectrochemical analysis of PBT-B($OC_{12}H_{25}$)$_2$ spray-cast onto ITO coated glass. U.V.-Vis.-n.I.R. spectra taken (a) in the neutral state and at potentials of (b) -0.55 V, (c) -0.45 V, (d) -0.35 V, (e) -0.25 V, (f) -0.15V, (g) -0.05 V, (h) +0.05 V, (i) +0.15 V, (j) +0.20 V, (k) +0.25 V, (l) +0.30 V, (m) +0.35 V, (n) +0.40 V, (o) +0.45 V, (p) +0.50 V, (q) +0.55 V, (r) +0.65 V vs Fc/Fc^+ in 0.1 M TBAP/PC.

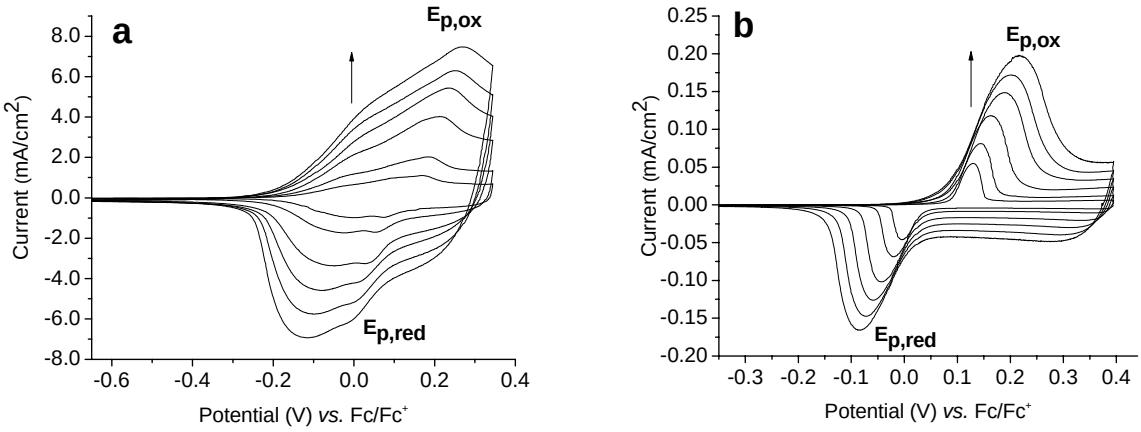

Figure 3-26. PBProDOT-R_2-B($OC_{12}H_{25}$)$_2$ cyclic voltammograms. (a) CV of PBProDOT-Me_2-B($OC_{12}H_{25}$)$_2$, and (b) CV of PBProDOT-Hex_2-B($OC_{12}H_{25}$)$_2$. Polymers electrodeposited on Pt button and measurements accomplished in 0.1 M TBAP in ACN/CH_2Cl_2 (5/3) at scan rates of 25, 50, 100, 150, 200, and 250 mV s^{-1}.

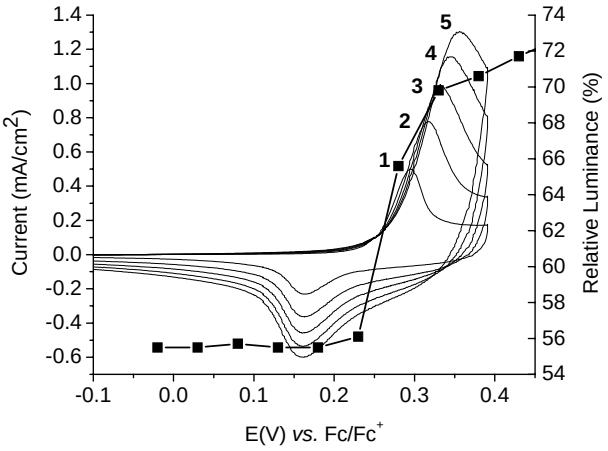

Figure 3-27. Cyclic voltammograms of PBProDOT-Hex_2-$B(OC_{12}H_{25})_2$ as function of scan rate. (1) 100, (2) 150, (3) 200, (4) 250 mV s^{-1}. Polymer deposited by drop-casting on Pt button electrode, in 0.1 M TBAP/PC electrolyte. The CV are superimposed with % relative luminance versus applied potential (▪) for PBProDOT-Hex_2-$B(OC_{12}H_{25})_2$.

The polymer exhibits an orange-red color in the neutral state with two absorption maxima at 544 nm and 507 nm (Figure 3-28a) which can be attributed to vibronic coupling. Upon oxidation, the π-π* transition of the neutral state disappears and, as soon as the potential reaches about +0.3 V a polaron transition appears in the 600-800 nm region with a maximum absorption at 738 nm, changing the film color to light blue (Figure 3-28i). Upon further increase in potential, this transition progressively disappears and bipolaron transitions are observed (1500 nm peaks) (Figure 3-28, i-r), and the polymer film becomes highly transmissive with a light gray color. This demonstrates the potential utility of this polymer in electrochromic applications. Polymer overoxidation and decomposition seemed occurring above +0.9 V. An optical band gap of 2.1 eV was determined from the onset of absorption of the neutral polymer.

For comparison, a thin-film of PBProDOT-Me_2-$B(OC_{12}H_{25})_2$ was potentiostatically deposited onto an ITO-coated glass electrode (electropolymerization section). After washing with a CH_2Cl_2/ACN (3/5) solution, the orange polymer film was placed in a 0.1 M TBAP/PC electrolyte solution and various absorption spectra were recorded in the neutral state, and at

stepped potentials sequentially from -0.28 V to +0.42 V oxidizing the polymer progressively (Figure 3-29). Overoxidation seemed to occur at higher potentials and the polymer film started to fall off the ITO electrode. As with PBProDOT-Hex_2-$B(OC_{12}H_{25})_2$, PBProDOT-Me_2-$B(OC_{12}H_{25})_2$ exhibits an optical band gap of 2.1 eV and a similar color change during redox switching, supporting our previous statement that the hexyl chains introduce little or no change in the optical properties. Surprisingly, the two PBProDOT-R_2-$B(OC_{12}H_{25})_2$ polymers exhibit the same band gaps as the recently studied poly(1,4-bis(2-thienyl)-2,5-diheptoxybenzene).[50] This result brings out the subtleties of the effect of side chains on the optical properties of π-conjugated polymers. In this instance, the thiophene linked polymers may be packing in an even more regular manner in the solid state than the polymers studied here.

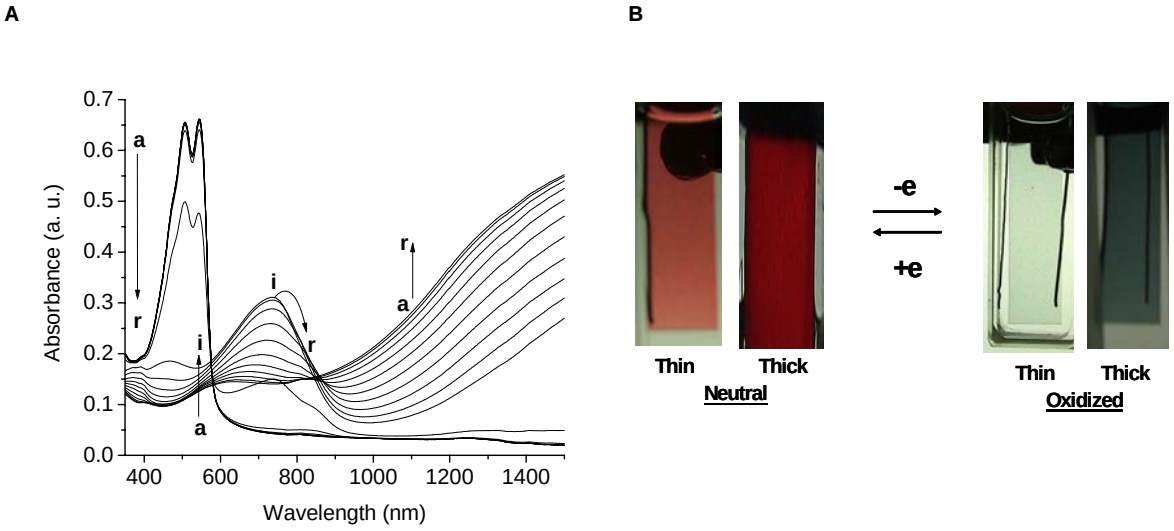

Figure 3-28. Spectroelectrochemical analysis of PBProDOT-Hex_2-$B(OC_{12}H_{25})_2$ spray-cast onto ITO coated glass. (A) U.V.-Vis.-n.I.R. spectra taken (a) in the neutral state and at potentials of (b) -0.02 V, (c) +0.03 V, (d) +0.08 V, (e) +0.13 V, (f) +0.18 V, (g) +0.23 V, (h) +0.28 V, (i) +0.33 V, (j) +0.38 V, (k) +0.43 V, (l) +0.48 V, (m) +0.53 V, (n) +0.58 V, (o) +0.63 V, (p) +0.68 V, (q) +0.73 V, (r) +0.78 V vs Fc/Fc^+ in 0.1 M TBAP/PC; (B) the film colors are displayed for thin and thick films.

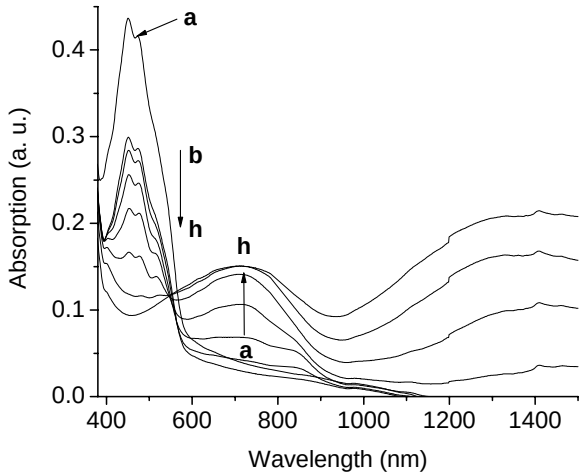

Figure 3-29. Spectroelectrochemical analysis of PBProDOT-Me_2-$B(OC_{12}H_{25})_2$ electro-polymerized on ITO coated glass. U.V.-Vis.-NIR. spectra taken (a) in the neutral state and at potentials of (b) -0.28 V, (c) -0.08 V, (d) +0.02 V, (e) +0.12 V, (f) +0.22 V, (g) +0.32 V, (h) +0.42 V, vs Fc/Fc^+ in 0.1 M TBAP/PC.

3.5 Colorimetry

3.5.1 PBT-$B(OR)_2$

Thin-films of PBT-$B(OC_7H_{15})_2$ and PBT-$B(OC_{12}H_{25})_2$ were deposited on ITO by spray-casting from 3 mg mL^{-1} toluene solutions, and were analyzed by in-situ colorimetric analysis. The relative luminance was measured as the neutral polymers were progressively oxidized. In the small 0.45-0.5 V potential window, the relative luminance of PBT-$B(OC_7H_{15})_2$ changed from 30% to 2.5% upon oxidation. There was also a considerable relative luminance change for PBT-$B(OC_{12}H_{25})_2$ (from 70% to 30%) between 0.45 and 0.55 V.

The L*a*b* values of films of about 0.2 μm in thickness were also determined to allow color matching. For PBT-$B(OC_7H_{15})_2$: L = 61; a = 50; b = 87 for the orange color (neutral state) and L = 24; a = -5; b = -23 for the blue color (doped state). For PBT-$B(OC_{12}H_{25})_2$: L = 86; a = 22; b = 68 for the orange color (neutral state) and L = 73; a = -6; b = -7 for the blue color (doped state).

The available color states of these polymers were tracked using the *xy* chromaticity diagrams shown in Figures 3-30a and 3-30b (as detailed in Chapter 2).[119] As the potential was increased and the polymers were doped, the *x* and *y* coordinates decreased. The abrupt color changes observed in the luminance experiments, can also be clearly seen on the *xy* chromaticity diagram by large changes in the *xy* coordinates between similar potential ranges (0.45-0.6 V for PBT-B(OC_7H_{15})$_2$ and 0.49-0.54 V for PBT-B($OC_{12}H_{25}$)$_2$) .

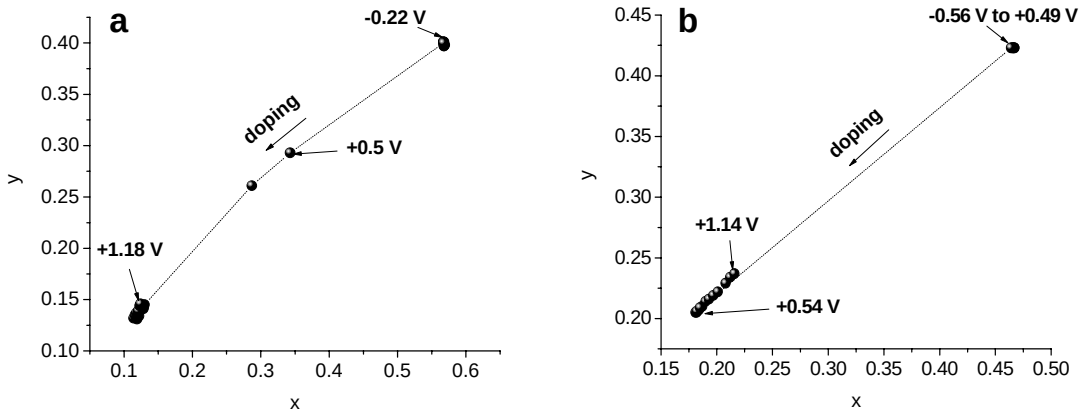

Figure 3-30. CIE 1931 *xy* chromaticity diagrams of PBT-B(OR)$_2$ polymers. Circles linked by a dashed line represent the color track for thin-films of (a) PBT-B(OC_7H_{15})$_2$, and (b) PBT-B($OC_{12}H_{25}$)$_2$, which go from orange to blue. The potential was increased in 0.05 V steps.

3.5.2 PBProDOT-R_2-B($OC_{12}H_{25}$)$_2$

A thin-film of the chemically synthesized PBProDOT-Hex_2-B($OC_{12}H_{25}$)$_2$ was deposited onto ITO by spray-casting from a 10 mg mL^{-1} chloroform solution and was also analyzed by in-situ colorimetric analysis. The relative luminance was measured as the neutral polymer was progressively oxidized and the results are superimposed in Figure 3-27 onto the cyclic voltammogram to compare the optical changes along with the material oxidation. Optical changes started occurring at +0.23 V vs Fc/Fc^+, which corresponds to the polymer's onset of

oxidation. At this potential, there was a sharp increase in the luminance which went from 55 % to 70 % in less than 0.1 V. Finally, upon further oxidation the luminance reached saturation at +0.6 V.

The L*a*b* values of the thin-film colors in the neutral and oxidized states were also determined. In the red-orange neutral state, L = 79, a = 40, b = 14, and in the fully oxidized light gray state, L = 90, a = -1 and b = -3 for a spray-cast film of about 0.2 μm in thickness. The available color states that PBProDOT-Hex_2-$B(OC_{12}H_{25})_2$ has to offer were also tracked using the *xy* chromaticity diagram shown in Figure 3-31. As the potential was increased and the polymer was doped the x coordinate decreased and the y coordinate decreased after an initial increase. The abrupt color change which occurred at +0.23 V and was observed on the luminance spectrum in Figure 3-27, can also be clearly seen on the *xy* chromaticity diagram by a large change in the *xy* coordinates at that potential. Note that for clarity, this chromaticity diagram is a 25 x magnification of the region of interest of the full *xy* chromaticity diagram displayed in Chapter 2. A few differences were observed for thicker films, such as a more pronounced blue color in the oxidized state (photograph in Figure 3-28), a lower luminance value (around 30 %) characteristic of a more opaque film, and no difference in the luminance values between the neutral and the fully oxidized states.

3.6 Solvatochromism, Thermochromism, and Ionochromism

While heating (about 60°C) 0.1 M TBAP in CH_2Cl_2/ACN solutions of the BProDOT-R_2-$B(OC_{12}H_{25})_2$ monomers, a reversible color change was surprisingly observed (from yellow to red as seen in Figure 3-32). This phenomenon was interestingly not seen without the presence of the electrolyte. It was deduced that upon the increase in temperature, the backbone of the three rings system twisted and gained a certain conformation (in this case more planar due to the red-shift),

which favored the coordination of the ions coming from the electrolyte and the locking of that position. These observations motivated the solvatochromic study of PBProDOT-Hex_2-$B(OC_{12}H_{25})_2$.

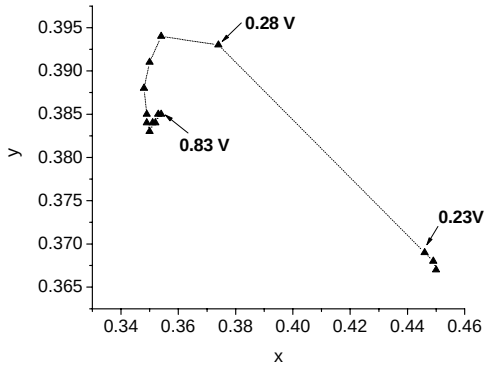

Figure 3-31. CIE 1931 *xy* chromaticity diagram of a thin-film of PBProDOT-Hex_2-$B(OC_{12}H_{25})_2$. Triangles linked by a dashed line represent the color track for the polymer film which goes from orange to light gray. The potential was increased in 0.05 V steps.

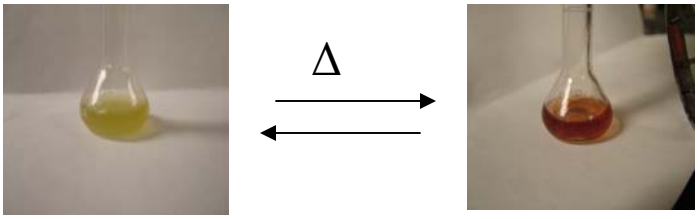

Figure 3-32. Thermochromic changes observed for a 0.1 M TBAP in CH_2Cl_2/ACN solution of the BProDOT-Me_2-$B(OC_{12}H_{25})_2$ monomers.

At room temperature, a 1.36 x 10^{-5} mol L^{-1} toluene solution of the chemically synthesized PBProDOT-Hex_2-$B(OC_{12}H_{25})_2$ was yellow and exhibited an absorption maximum at 478 nm as illustrated in Figure 3-33. The resolution of the fine structure was not as well defined as it was in the film absorption spectrum (Figure 3-28), and the solution absorption was blue-shifted compared to the film absorption where the maximum was observed at 544 nm. This was expected since solvated polymer chains are more disordered in solution and consequently have a lower conjugation length.

Upon addition of methanol, while maintaining a constant polymer concentration (1.36 x 10^{-5} mol L^{-1}), the solution became more red and showed an absorption maximum at 503 nm, with a vibronic side band at 541 nm. In pure toluene, the polymer was highly solvated and poorly ordered. Upon addition of methanol, the polymer exhibited more extensive conjugation as could be deduced from the shift of the absorption maximum to longer wavelengths. According to the literature, the energy difference of 0.18 eV (1460 cm^{-1}) from the main peak to the vibronic peak is consistent with a C=C stretching mode which would be expected to couple strongly to the electronic structure.[120] This is an additional evidence for the presence of more ordered molecules in the presence of poorly solvating solvents.

The combined ionic and thermochromic properties observed for the BProDOT-R_2-$B(OC_{12}H_{25})_2$ monomers were also checked on the polymers. PBProDOT-Hex_2-$B(OC_{12}H_{25})_2$ was dissolved in a CH_2Cl_2/ACN solution containing TBAP. As methanol, acetonitrile behaves as a poor solvent for the polymer and turned the polymer solution into a deep red color, making it impossible to check for ionochromic/thermochromic effects. Another attempt was performed on a pure methylene chloride polymer solution containing TBAP. Upon heating, no color change could be observed suggesting that the chromic phenomenon probably resulted from the simultaneous action of temperature, ions, and poor solvent. This was verified by heating a methylene chloride monomer solution containing TBAP, and indeed, no color change could be observed this time.

3.7 Application to Devices

3.7.1 Photovoltaic Devices

3.7.1.1 PBT-$B(OR)_2$

Bulk heterojunction solar cells using the PBT-$B(OR)_2$ polymers as the electron donors and PCBM as the electron acceptor (device structure ITO/PEDOT-PSS/PBT-$B(OR)_2$:PCBM/LiF/Al)

were prepared by Dr. Young-Gi Kim in order to evaluate for the first time the photovoltaic properties of such materials. Blends containing 1:4 (w/w) of each polymer with PCBM were spin-coated from 1,2-dichlorobenzene solutions into ~ 45 nm thick photoactive layers. Figure 3-34a shows the i-V characteristics of the PBT-B($OC_{12}H_{25}$)$_2$ based device under AM 1.5 illumination for a calibrated solar simulator with an intensity of 100 mW cm^{-2}, and Table 3-3 summarizes the photovoltaic results. The PBT-B(OC_7H_{15})$_2$/PCBM device exhibited the best performance with a power conversion efficiency (η) of ~ 0.6%, a short circuit current (I_{sc}) of 2.49 mA cm^{-2}, an open circuit voltage (V_{oc}) of 0.74 V, and a fill factor (FF) of 32%.

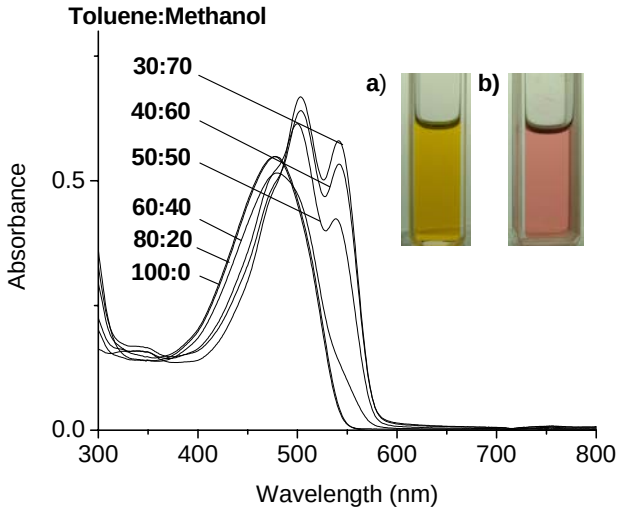

Figure 3-33. UV-vis absorption spectra of PBProDOT-Hex_2-B($OC_{12}H_{25}$)$_2$ in toluene/methanol mixtures. Pictures: solutions (a) in toluene, (b) in a mixture of toluene and methanol.

Incident photon to current efficiency measurements (IPCE) match the polymer absorption spectra near the absorption maxima of the polymers, indicating that the polymers are effective photoexcited electron donors that contribute mainly to the photocurrent in the device (Figure 3-34b). Both polymers exhibit IPCEs of ~ 16% at 410 nm. Consequently, PBT-B(OC_7H_{15})$_2$ and PBT-B($OC_{12}H_{25}$)$_2$ showed their potential for use in organic photovoltaic devices, harvesting

incident light of the mid-range energy. It would be interesting to combine these polymers with lower or higher band gap polymers in order to absorb over a broader spectral range and to improve the photovoltaic efficiencies…but for that physicists have to take over that project now!

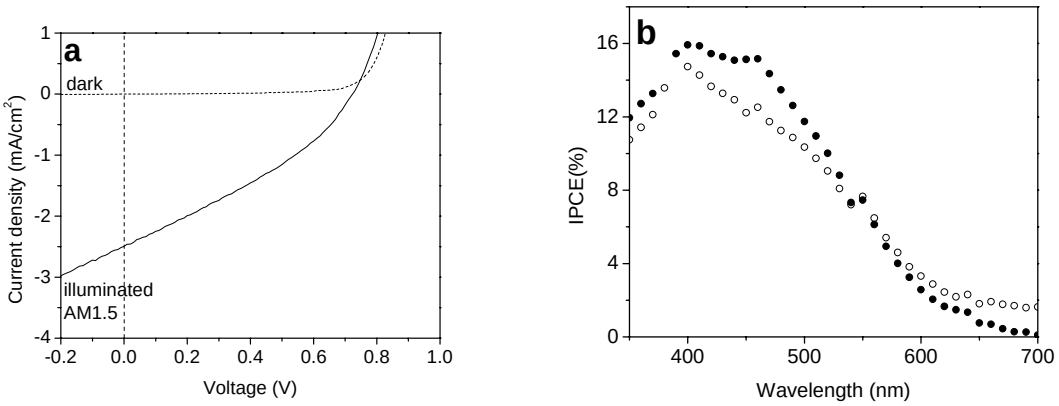

Figure 3-34. Photovoltaic results of solar cells made of a 1/4 blend (w/w) of PBT-B$(OR)_2$/PCBM. (a) Current voltage characteristic for PBT-B$(OC_{12}H_{25})_2$ under AM1.5 conditions (100 mW cm^{-2}). (b) IPCE results for PBT-B$(OC_{12}H_{25})_2$ (●) and PBT-B$(OC_7H_{15})_2$ (○).

Table 3-3. Summarized photovoltaic characteristics of PBT-B$(OR)_2$/PCBM based solar cells.

Photosensitizer	η (%)	FF	V_{oc} (V)	I_{sc} (mA cm^{-2})
PBT-B$(OC_7H_{15})_2$	0.59	0.32	0.74	2.49
PBT-B$(OC_{12}H_{25})_2$	0.48	0.39	0.76	1.59

3.7.1.2 PBProDOT-Hex$_2$-B$(OC_{12}H_{25})_2$

Bulk heterojunction solar cells using PBProDOT-Hex$_2$-B$(OC_{12}H_{25})_2$ as the electron donor and PCBM as the electron acceptor have also been prepared by the group of Prof. Yang Yang at the University of California (UCLA), using the same conditions as the ones used for PBT-B$(OR)_2$ (see section above). The device exhibited a power conversion efficiency of 0.22%, a short circuit current of 0.98 mA cm^{-2}, an open circuit voltage of 0.55 V, and a fill factor of 41% (see i-V characteristic of the device in Figure 3-35). The polymer's photovoltaic properties are not as great as the ones determined for PBT-B$(OR)_2$. This might be due to poorer hole transport

properties, probably resulting from a less regular packing in the solid state (as it had been already suggested from the band gap results, see section 3.4.2).

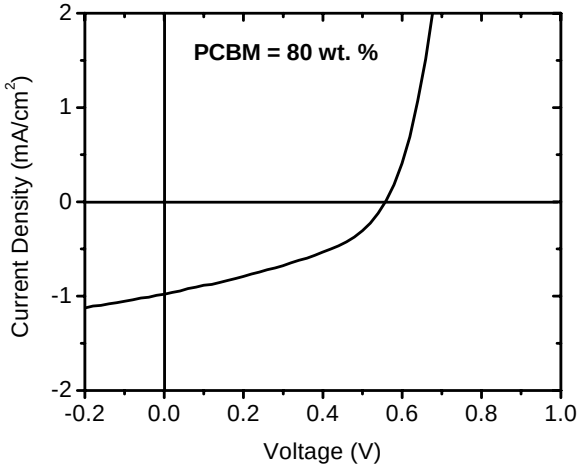

Figure 3-35. Current voltage characteristic of a solar cell made of a 1/4 blend (w/w) of PBProDOT-Hex$_2$-B(OC$_{12}$H$_{25}$)$_2$ /PCBM under AM1.5 conditions (100 mW cm^{-2}).

3.7.2 LEDs

The chemically synthesized PBProDOT-Hex$_2$-B(OC$_{12}$H$_{25}$)$_2$ exhibits a yellow-orange fluorescence in toluene with an evaluated quantum efficiency of 54 % (against Coumarin 6 standard; Φ = 0.78).[100] The emission spectrum illustrated in Figure 3-36 exhibits two well-defined vibronic bands at 539 nm and 582 nm, and one poorly resolved band at approximately 630 nm in toluene. For a spin-coated film, the emission spectrum has a similar shape although it is red shifted due to a more organized conformation (Figure 3-36). The vibronic bands are seen at 571, 617 and 679 nm (Photoluminescence Quantum Efficiency (PLQE) = 3.5 ± 2 %).

Dr. J. Mwaura investigated the potential of this polymer in LEDs. For that study, devices of the following architecture were prepared: ITO/PEDOT-PSS (40 nm)/PBProDOT-Hex$_2$-B(OC$_{12}$H$_{25}$)$_2$ (50 nm)/Ca (5 nm)/Al (200 nm). As shown in Figure 3-36, the device exhibits a broad emission dominated by a peak at λ_{max} = 570 nm. The electroluminescence (EL) spectrum

is similar to the photoluminescence (PL) spectrum of the solid film, indicating that the electroluminescence results from a singlet π,π* exciton with the same structure as that produced by photoexcitation. The absence of red-shifting on the EL spectrum relative to the PL spectrum suggests that the electroluminescence is dominated by the non-aggregated polymer chains, with the interchain aggregates contributing to little or no emission.

On the device characteristics illustrated in Figure 3-37, it can be seen that the PBProDOT-Hex_2-$B(OC_{12}H_{25})_2$ device turns on at 6 V. The EL intensity increases with voltage, peaking at 13 V, and decreasing at higher voltages, possibly due to device breakdown. At 13 V, the device emits the highest luminance at ~ 240 cd m^{-2} and a current density of 1100 mA cm^{-2}. Figure 3-37 shows the external electron-to-photon quantum efficiency (EQE) of the PBProDOT-Hex_2-$B(OC_{12}H_{25})_2$ EL device as a function of applied voltage. The efficiency increases after turn on, peaking at 8 V at ~ 0.03 %, after which it steadily decreases as the applied voltage and current density increase. These low EQE show that the polymer is not likely effective for development in LED applications.

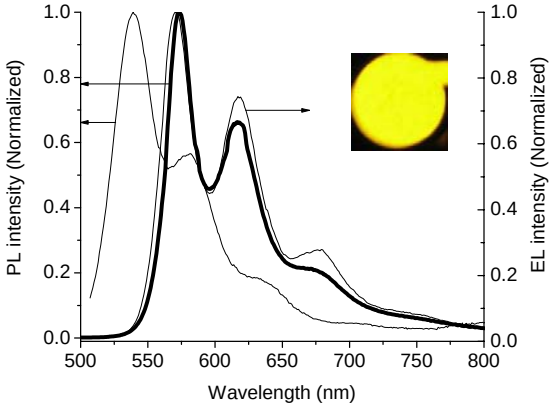

Figure 3-36. Photoluminescence emission spectrum of PBProDOT-Hex_2-$B(OC_{12}H_{25})_2$ in toluene solution and in thin-film (bold line) superimposed with electroluminescence spectrum of an EL device with the following configuration: ITO/PEDOT-PSS/PBProDOT-Hex_2-$B(OC_{12}H_{25})_2$/Ca/Al. The inset picture represents the light emission of the EL device.

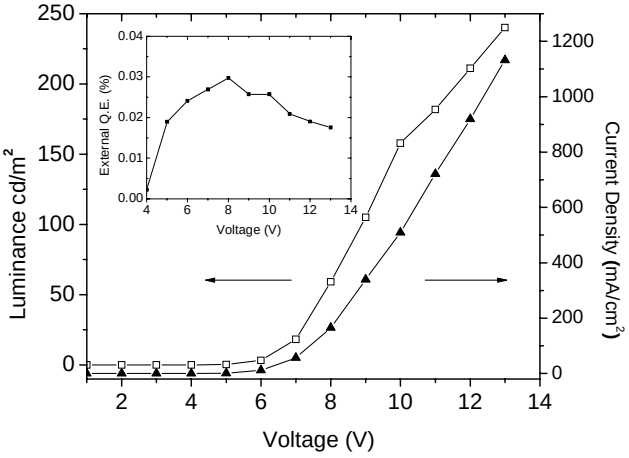

Figure 3-37. LED properties of an ITO/PEDOT-PSS/PBProDOT-Hex$_2$-B(OC$_{12}$H$_{25}$)$_2$/Ca/Al device. Luminance spectrum (□) and current density (▲). Left top inset: External quantum efficiency.

3.8 Conclusions and Perspective

The packing properties (small interchain distances, or cofacial arrangements of the rings of adjacent layers) of the regiosymmetric Br$_2$-BT-B(OR)$_2$ and Br$_2$-BEDOT-B(OR)$_2$ monomers, revealed that these materials might be interesting building blocks for producing hole transporting materials (oligomers or polymers) for organic electronic devices requiring high charge transport, like photovoltaics. This idea was supported also by previously reported studies on the ordering properties of PBT-B(OR)$_2$, which have shown the propensity of these materials to crystallize.[22] For that reason, their chemical polymerization has been revisited with the goal of obtaining higher molecular weight materials than the one previously reported, with good processability. Yamamoto coupling via Ni(COD)$_2$ proved to be the most effective method among the methods which have been attempted in this work (GriM, solid state polymerization) or in the literature, for getting the monomers to couple between each other. However the molecular weights stayed limited, especially in the case of PBEDOT-B(OR)$_2$. This is due in part to its too powerful electron donating properties which diminish the reactivity of the growing chains to the Ni

oxidative addition. It is also due to its poor solubility probably resulting from its propensity to aggregate as suggested by the tight packing observed in the X-ray crystal structures of the monomers. Polymers of reasonable size, processability, and film homogeneity, were obtained in the case of PBT-B$(OR)_2$, and it was decided to investigate the electronic, electrochromic, and photovoltaic properties of this material only. DSC studies confirmed the semi-crystalline nature of this regiosymmetric polymer, and comforted us in our idea to built photovoltaics with this material. The electrochemical and spectroelectrochemical studies attested the PBT-B$(OR)_2$ polymers ability to harvest incident light in the mid-visible energy range (E_g of 2.1 eV), stability to oxidation, and capacity to transfer charges to PCBM. When applied as the hole transporting layer in bulk heterojunction photovoltaic devices with PCBM as the acceptor, they effectively produced photocurrent, and power conversion efficiencies up to 0.6% were reached. These results are of valuable importance and should not be compared to the 5% efficiencies that have been obtained for P3HT:PCBM devices, since such performances are the results of years of optimization from various research groups.[73-75] There are only a few examples of polymers which have been successfully employed in solar cells and most of them have never reached 1% efficiencies.[121] Apart from their photovoltaic properties, these materials exhibit nice electrochromic properties, switching between deep orange and blue colors, in the neutral and oxidized states, respectively.

In order to overcome the solubility limitations of PBEDOT-B$(OR)_2$ and to make a similarly electron rich material, we decided to replace the EDOT moiety of this regiosymmetric member by alkyl (Me or hexyl) -substituted ProDOT heterocycles, the methyl substituted derivative being studied for comparison. Due to their novelty, these materials were first electropolymerized before investigating their chemical polymerization, in order to get a quick

look at their redox and electronic properties. The PBProDOT-R_2-B($OC_{12}H_{25}$)$_2$ polymers exhibit band gaps of 2.1 eV, quite close to their thiophene counterparts likely due to a less regular packing in the solid state. This in turn compensates the electron donating effect of the oxygen substituents appended to the thiophene ring and gives rise to films having a similar orange color in the neutral state.[103] Conversely, as the polymer was progressively oxidized a different behavior was observed for PBProDOT-Hex_2-B($OC_{12}H_{25}$)$_2$ and a highly transmissive state was reached while the thiophene analogues retain a deeper blue color.[50,103] A chemical synthesis was developed for this polymer, giving rise to a highly soluble material that can be processed by spray-casting or spin-coating techniques. These interesting solubility and color switching properties open the door to electrochromic applications using large or flexible surfaces such as electrochromic displays or smart windows. Unfortunately maximum power conversion efficiencies of 0.22% were reached, and these poorer photovoltaic properties compared to PBT-B(OR)$_2$, might be the result of a less regular packing of PBProDOT-Hex_2-B($OC_{12}H_{25}$)$_2$ in the solid state. However, the particularly tight crystalline packing and the close to perfect cofacial arrangement of adjacent molecules of the three ring BProDOT-Me_2-B($OC_{12}H_{25}$)$_2$ system could motivate the development of oligomers of this type for electronic applications requiring high charge carrier mobility.

3.9 Experimental

1,4-Dibromo-2,5-diheptoxybenzene (1a).[22] Freshly recrystallized 1,4-dibromo-2,5-dihydroxybenzene (13.19 g, 4.90×10^{-2} mol) was dissolved in EtOH (75 mL) under argon to give a slightly pink solution. A 75 mL solution of KOH (7.01 g, 1.25×10^{-1} mol) in EtOH was slowly added and the solution color turned brown. The solution mixture was stirred at room temperature for 2 h. Then 1-bromoheptane (22.45 g, 1.25×10^{-1} mol) was dissolved in EtOH (20 mL) and this solution was added dropwise to the reaction mixture forming a beige

precipitate. This solution was heated at 65-70°C for 18 h. It was cooled to room temperature and deionized water was added yielding a pink precipitate. The precipitate was filtered on a Büchner funnel and a slightly pink solid was collected and dried under vacuum. This solid was purified by recrystallization from ethanol/benzene (3/1) to give 17.58 g (77%) of white crystals [mp = 56-58°C (lit.[22] mp = 59-60°C)]. ^{1}H-NMR ($CDCl_3$, ppm): δ = 7.08 (s, 1H), 3.94 (t, 2H), 1.80 (p, 2H), 1.48 (m, 2H), 1.31 (m, 6H), 0.89 (t, 3H). ^{13}C-NMR ($CDCl_3$, ppm): δ = 150.45, 118.94, 111.50, 70.67, 31.94, 29.36, 29.15, 26.11, 22.76, 14.21. Anal. Calcd for $C_{20}H_{32}Br_2O_2$: C, 51.74, H, 6.95. Found: C, 52.01, H, 7.26.

1,4-Dibromo-2,5-didodecyloxybenzene (1b).[22] 1,4-Dibromo-2,5-didodecyloxybenzene was prepared according to the procedure described for 1,4-dibromo-2,5-diheptoxybenzene utilizing freshly recrystallized 1,4-dibromo-2,5-dihydroxybenzene (11.27 g, 4.20×10^{-2} mol), KOH (1.01×10^{-1} mol), and 1-bromododecane (1.01×10^{-1} mol). Recrystallization from ethanol/benzene (3/1) gave 23.89 g (94%) of white crystals [mp = 75-77°C (lit.[22] mp = 77-79°C)]. ^{1}H-NMR ($CDCl_3$, ppm): δ = 7.09 (s, 1H), 3.95 (t, 2H), 1.81 (p, 2H), 1.48 (m, 2H), 1.29 (m, 16H), 0.89 (t, 3H).

2-(Trimethylstannyl)thiophene [Th-Sn(CH_3)$_3$].[122] Thiophene was dried over calcium hydride overnight and then purified by distillation under reduced pressure (bp = 30-35°C at 130 torr). Thiophene (4.38 g, 5.20×10^{-2} mol) was dissolved in anhydrous THF (35 mL) under argon. The solution was cooled to -78°C and butyllithium (21.90 mL, 2.50 M in hexanes, 5.50×10^{-2} mol) was added dropwise via an addition funnel. The clear solution was stirred for 1 h and became slightly pink. Trimethylstannyl chloride (54.70 mL, 1 M in THF, 5.50×10^{-2} mol) was then added dropwise and the solution turned slightly yellow. The mixture was allowed to warm to room temperature with stirring overnight and the color turned brown. Deionized water was

added (30 mL) and the mixture was extracted with diethyl ether. The organic phase was washed with brine, dried over magnesium sulfate ($MgSO_4$) and filtered through a Büchner funnel. The solvent was evaporated and a brown oil was collected. This oil was purified by distillation (bp = 93-97°C at 25 mmHg) and 9.90 g (77%) of a white solid were obtained and dried under vacuum. ^{1}H-NMR ($CDCl_3$, ppm): δ = 7.65 (d, 1H), 7.24 (m, 2H), 0.37 (s, 9H).

2-(Trimethylsilyl)-3,4-ethylenedioxythiophene [EDOT($SnCH_3$)$_3$].[36] A solution of 3,4-ethylenedioxythiophene (EDOT) in THF was dried overnight over potassium. A solution of EDOT (7.50 g, 5.28×10^{-2} mol) in anhydrous THF (50 mL) was cooled at -78°C under argon and *n*-butyllithium (2.5 M in hexanes, 5.81×10^{-2} mol) was added dropwise via addition funnel. The mixture was stirred at -78°C for 1 h and then warmed up to 0°C for 30 min, changing the clear solution to an orange color. The solution was cooled back to -78°C and trimethylstannyl chloride (1 M in THF, 5.28×10^{-2} mol) was added dropwise thanks to an addition funnel. The orange solution was warmed to room temperature and stirred overnight. Deionized water was added to the solution and the mixture was extracted with ether. The organic phase was washed with Brine and dried over $MgSO_4$. After filtration through a Büchner funnel, the solvent was evaporated and a brown oil was obtained and purified by distillation under vacuum (bp = 110°C at 0.4 mmHg). After cooling, 11.93 g of white-clear solid (74%) were collected. ^{1}H-NMR ($CDCl_3$, ppm): δ = 6.56 (s, 1H), 6.30 (s, 2H), 4.16 (m, 4H), 0.35 (s, 9H).

1,4-Bis(2-thienyl)-2,5-diheptoxybenzene [BT-B(OC_7H_{15})$_2$].[22] Th-Sn(CH_3)$_3$ (9.28 g, 3.76×10^{-2} mol) and 1,4-dibromo-2,5-diheptoxybenzene (8.69 g, 1.87×10^{-2} mol) were dissolved in anhydrous DMF (200 mL) under argon at 80°C. Argon was bubbled into the reaction mixture for 20 min. Then, Pd(PPh_3)$_4$ catalyst (1.68 g, 1.50×10^{-3} mol) was added quickly and the orange solution was warmed to 120°C and stirred overnight giving rise to a green-black mixture. It was

then cooled to room temperature and poured into deionized water (500 mL). The mixture was extracted with diethyl ether; the organic phase was collected, washed with brine and dried over $MgSO_4$. An orange organic solution was obtained after filtration on a Büchner funnel. The solvent was evaporated and a yellow solid was collected and placed under vacuum. After recrystallization from ethanol/benzene (3/1), 7.17 g (81%) of yellow crystals were obtained [mp = 76-77ºC (lit.[22] mp = 77-78ºC)]. ^{1}HNMR ($CDCl_3$, ppm): δ = 7.54 (d, 1H), 7.34 (d, 1H), 7.26 (s, 1H), 7.10 (dd, 1H), 4.08 (t, 2H), 1.90 (p, 2H), 1.52 (m, 2H), 1.32 (m, 6H), 0.90 (t, 3H).

1,4-Bis(2-thienyl)-2,5-didodecyloxybenzene [BT-B($OC_{12}H_{25}$)$_2$].[22] BT-B($OC_{12}H_{25}$)$_2$ was prepared according to the procedure described for BT-B(OC_7H_{15})$_2$ utilizing Th-Sn(CH_3)$_3$ (9.80 g, 3.97×10^{-2} mol) 1,4-dibromo-2,5-didodecyloxybenzene (11.86 g, 1.96×10^{-2} mol), anhydrous DMF (300 mL) and Pd(PPh_3)$_4$ (9.06×10^{-1} g, 7.80×10^{-4} mol). The yellow solid was dried under vacuum and recrystallized from ethanol/benzene (3/1) to give 9.35 g (78%) of thin yellow crystals [mp = 77-78ºC (lit.[22] mp = 77-78ºC)]. ^{1}H-NMR ($CDCl_3$, ppm): δ = 7.54 (d, 1H), 7.33 (d, 1H), 7.26 (s, 1H), 7.09 (dd, 1H), 4.08 (t, 2H), 1.90 (p, 2H), 1.52 (m, 2H), 1.27 (m, 16H), 0.88 (t, 3H).

1,4-Bis[2-(3,4-ethylenedioxy)thienyl]-2,5-diheptoxybenzene [BEDOT-B(OC_7H_{15})$_2$]. EDOT($SnCH_3$)$_3$ (6.00 g, 1.96×10^{-2} mol) and 1,4-dibromo-2,5-diheptoxybenzene (4.54 g, 9.70×10^{-3} mol) were dissolved in anhydrous DMF (300 mL). The solution was heated at 80ºC to dissolve everything. Argon was bubbled into the solution for 15 min and Pd(PPh_3)$_4$ (5.04×10^{-3} g, 4.36×10^{-4} mol) was quickly added. The reaction was stirred at 120ºC overnight and the yellow-orange solution turned black. The solution was cooled to room temperature and poured into deionized water. The mixture was extracted with diethyl ether and the organic phase was washed with brine, dried over $MgSO_4$ and filtered on a Büchner funnel. The solvent was

evaporated and a yellow solid was collected and dried under vacuum. After recrystallization from ethanol/benzene (3/1), 4.62 g of yellow crystals (81%) were obtained [mp = 84-87ºC (lit.[46] mp = 85-87ºC)]. ^{1}H-NMR ($CDCl_3$, ppm): δ = 7.68 (s, 1H), 6.37 (s, 1H), 4.28 (m, 4H), 4.04 (t, 2H), 1.88 (p, 2H), 1.52 (m, 2H), 1.32 (m, 6H), 0.89 (t, 3H).

1,4-Bis[2-(3,4-ethylenedioxy)thienyl]-2,5-didodecyloxybenzene [BEDOT-B($OC_{12}H_{25}$)$_2$]. BEDOT-B($OC_{12}H_{25}$)$_2$ was prepared according to the procedure described for BEDOT-B(OC_7H_{15})$_2$ utilizing EDOT($SnCH_3$)$_3$ (10.83 g, 3.56×10^{-2} mol), 1,4-dibromo-2,5-didodecyloxybenzene, (10.73 g, 1.78×10^{-2} mol), anhydrous DMF (300 mL) and $Pd(PPh_3)_4$ (0.82 g, 7.10×10^{-4} mol). After recrystallization from ethanol/benzene (3/1), 9.12 g (71%) of yellow-orange crystals were collected [mp = 92-96ºC (lit.[46] mp = 92-95ºC)]. ^{1}H-NMR ($CDCl_3$, ppm): δ = 7.68 (s, 1H), 6.37 (s, 1H), 4.28 (m, 4H), 4.04 (t, 2H), 1.88 (p, 2H), 1.52 (m, 2H), 1.27 (m, 16H), 0.89 (t, 3H).

1,4-Bis(2-(5-bromo)thienyl)-2,5-diheptoxybenzene [Br_2-BT-B(OC_7H_{15})$_2$]. BT-B(OC_7H_{15})$_2$ (2.07 g, 4.40×10^{-3} mol) was dissolved in anhydrous DMF (125 mL) under argon and the yellow slurry was cooled to 0ºC. Freshly recrystallized N-bromosuccinimide (NBS) (1.66 g, 9.38×10^{-3} mol) was added in small portions. The reaction was left at 0ºC for 3 h. Then it was warmed at room temperature and stirred overnight. Deionized water (300 mL) was added to the yellow slurry and the mixture was extracted with diethyl ether. The organic phase was washed with brine, dried over $MgSO_4$ and filtered through a Büchner funnel. The solvent was evaporated and a yellow solid was collected and dried under vacuum. Pure crystals, 1.99 g (72%) were obtained by recrystallizations from ethanol/benzene (3/1) and ethanol/THF (3/1) [mp = 104-105ºC]. ^{1}H-NMR ($CDCl_3$, ppm): δ = 7.25 (d, 1H), 7.16 (s, 1H), 7.04 (d, 1H), 4.07 (t, 2H), 1.91 (p, 2H), 1.52 (m, 2H), 1.34 (m, 6H), 0.91 (t, 3H). ^{13}C-NMR ($CDCl_3$): δ =

149.30, 140.70, 129.50, 124.80, 122.80, 113.40, 111.60, 70.06, 31.98, 29.53, 29.27, 26.39, 22.85, 14.35. Anal. Calcd for $C_{28}H_{36}Br_2O_2S_2$: C, 53.51, H, 5.77. Found: C, 53.64, H, 5.77. HRMS $C_{28}H_{36}Br_2O_2S_2$: calcd, 626.0523; obsd, 626.0524.

1,4-Bis(2-(5-bromo)thienyl)-2,5-didodecyloxybenzene [Br_2-BT-B($OC_{12}H_{25}$)$_2$]. Br_2-BT-B($OC_{12}H_{25}$)$_2$ was prepared according to the procedure described for Br_2-BT-B(OC_7H_{15})$_2$ utilizing BT-B($OC_{12}H_{25}$)$_2$ (8.86 g, 1.45×10^{-2} mol), anhydrous DMF (350 mL) and freshly recrystallized NBS (5.39 g, 3.05×10^{-2} mol). After successive recrystallizations from ethanol/benzene (2/1), ethanol/THF (2/1), and methanol/THF (2/1), 9.54 g (86%) of pure yellow crystals were obtained [mp = 101-103ºC]. ^{1}H-NMR ($CDCl_3$, ppm): δ = 7.25 (d, 1H), 7.17 (s, 1H), 7.04 (d, 1H), 4.08 (t, 2H), 1.92 (p, 2H), 1.52 (m, 2H), 1.27 (m, 16H), 0.89 (t, 3H). ^{13}C-NMR ($CDCl_3$): δ = 149.20, 140.60, 129.49, 124.80, 122.80, 113.20, 111.61, 70.06, 32.17, 29.92, 29.89, 29.84, 29.80, 29.61, 26.44, 22.94, 14.40. Anal. Calcd for $C_{38}H_{56}Br_2O_2S_2$: C, 59.37, H, 7.34. Found: C, 59.67, H, 7.54. HRMS $C_{38}H_{56}Br_2O_2S_2$: calcd, 766.2088; obsd, 766.2098.

1,4-Bis[2-(5-bromo-3,4-ethylenedioxy)thienyl]-2,5-diheptoxybenzene [Br_2-BEDOT-B(OC_7H_{15})$_2$]. BEDOT-B(OC_7H_{15})$_2$ (1.00 g, 1.70×10^{-3} mol) was dissolved in anhydrous DMF (75 mL) and the solution was cooled at -78ºC under argon. Freshly recrystallized and dry NBS (0.75 g, 4.24×10^{-3} mol) was added in small portions to the yellow slurry. The temperature was raised slowly to 0ºC as the slurry turned from yellow to green to blue. After 4 h, NH_4OH (10 mL) was quickly added changing the solution color to yellow and the mixture was stirred an extra 10 min. Deionized water was then added to the solution and the mixture was extracted with diethyl ether. The organic phase was washed with brine, dried over $MgSO_4$ and filtered through a Büchner funnel. The solvent was evaporated and a yellow solid was collected and dried under vacuum. The solid was purified by column chromatography on silica gel using CH_2Cl_2/hexane

(1/1) at a fast flow rate. The compound polymerizes on the column if the elution is too slow. The solid was finally purified by recrystallization in methanol/THF (3/1) to give 0.56 g (42%) of yellow crystals [mp = 162-163ºC]. ^{1}H-NMR ($CDCl_3$, ppm): δ = 7.70 (s, 1H), 4.33 (m, 4H), 4.05 (t, 2H), 1.90 (p, 2H), 1.52 (m, 2H), 1.34 (m, 6H), 0.91 (t, 3H). ^{13}C-NMR ($CDCl_3$): δ = 148.57, 139.30, 137.86, 120.41, 113.74, 112.68, 88.20, 69.91, 64.78, 64.72, 31.77, 29.26, 29.07, 26.21, 22.62, 14.11. Anal. Calcd for $C_{32}H_{40}Br_2O_6S_2$: C, 51.62, H, 5.41. Found: C, 51.82, H, 5.59. HRMS $C_{32}H_{40}Br_2O_6S_2$: calcd, 744.0633; obsd, 744.0629.

1,4-Bis[2-(5-bromo-3,4-ethylenedioxy)thienyl]-2,5-didodecyloxybenzene [Br_2-BEDOT-B($OC_{12}H_{25}$)$_2$]. Br_2-BEDOT-B($OC_{12}H_{25}$)$_2$ was prepared according to the procedure described for Br_2-BEDOT-B(OC_7H_{15})$_2$ utilizing BEDOT-B($OC_{12}H_{25}$)$_2$ (2.58 g, 3.55×10^{-3} mol), anhydrous DMF (250 mL) and freshly recrystallized NBS (1.57 g, 8.88×10^{-3} mol). After purification by column chromatography on silica gel with methylene chloride/hexanes (1/2), followed by recrystallization from methanol/THF (1/1), 1.80 g (57%) of yellow crystals were obtained [mp = 126-127ºC]. ^{1}H-NMR ($CDCl_3$, ppm): δ = 7.70 (s, 1H), 4.33 (m, 4H), 4.05 (t, 2H), 1.90 (p, 2H), 1.52 (m, 2H), 1.27 (m, 16H), 0.88 (t, 3H). ^{13}C-NMR ($CDCl_3$): δ = 148.81, 139.56, 138.09, 120.66, 113.99, 112.95, 88.43, 70.16, 65.01, 64.95, 32.15, 29.91, 29.87, 29.66, 29.59, 29.50, 26.50, 22.92, 14.30. Anal. Calcd for $C_{42}H_{60}Br_2O_6S_2$: C, 57.01, H, 6.83. Found: C, 56.62, H, 6.94. HRMS $C_{42}H_{60}Br_2O_6S_2$: calcd, 882.2198; obsd, 882.2199.

Poly(1,4-bis(2-thienyl)-2,5-diheptoxybenzene) [PBT-B(OC_7H_{15})$_2$]. $Ni(COD)_2$ (1.04 g, 3.78×10^{-3} mol) and Bpy (4.95×10^{-1} g, 3.17×10^{-3} mol) were combined in a Schlenk flask under argon and dissolved in anhydrous DMF (30 mL). A solution of 1,5-cyclooctadiene (0.39 mL, 3.12×10^{-3} mol) was quickly added via a syringe. The purple solution was warmed to 60°C for 40 min and slowly added to a 50 mL solution of Br_2-BT-B(OC_7H_{15})$_2$ (1.98 g, 3.15×10^{-3}

mol) in anhydrous DMF. The color turned immediately red. The reaction was maintained at 60°C for 48 h in the dark. The solution was cooled to room temperature and poured into methanol (1 L) yielding a red precipitate which was filtered through a Soxhlet thimble. The precipitate was purified by Soxhlet extraction for 24 h with methanol and 30 h with hexanes. The polymer was fractionated with toluene. The toluene was evaporated under reduced pressure to afford 0.82 g (55%) of red solid. ^{1}H-NMR ($CDCl_3$, ppm): δ = 7.50 (Th-H), 7.21 (Ar-H), 7.05 (Th-H), 4.15 (OCH_2), 1.95 (OCH_2CH_2), 1.32 (CH_2), 0.90 (CH_3). GPC analysis: M_n = 4,960, M_w = 6,340, PDI = 1.28.

Poly(1,4-bis(2-thienyl)-2,5-didodecyloxybenzene) [PBT-B($OC_{12}H_{25}$)$_2$]. PBT-B($OC_{12}H_{25}$) was prepared according to the procedure described for PBT-B(OC_7H_{15})$_2$ utilizing Ni(COD)$_2$ (8.61×10^{-2} g, 3.13×10^{-3} mol), Bpy (4.90×10^{-1} g, 3.14×10^{-3} mol), anhydrous DMF (50 mL), 1,5-cyclooctadiene (0.32 mL, 2.62×10^{-3} mol) and Br_2-BT-B($OC_{12}H_{25}$)$_2$ (2.00 g, 2.60×10^{-3} mol). The polymerization solution was stirred at 60°C for 24 h. A red solid (6.36×10^{-1} g, 40%) was recovered after Soxhlet extraction in toluene. ^{1}H-NMR ($CDCl_3$, ppm): δ = 7.50 (Th-H), 7.21 (Ar-H), 7.05 (Th-H), 4.13 (OCH_2), 1.96 (OCH_2CH_2), 1.27 (CH_2), 0.87 (CH_3). GPC analysis: M_n = 2,945, M_w = 3,950, PDI = 1.34.

2,3,4,5-Tetrabromothiophene (3). Thiophene (80.00 g, 9.52×10^{-2} mol) and chloroform (35 mL) were combined in a 2L 3-neck flask equipped with a reflux condenser and an addition funnel and vented to an empty 3-neck round bottom flask connected to a scrubber charged with a saturated sodium hydroxide solution and sodium bisulfite. The reaction mixture was cooled at 0°C with an ice bath and bromine (125 mL, 4.76 mol) was added slowly over a five hours period. The flask was warmed at room temperature and stirred for 12 hours. A solution of ammonium hydroxide was added slowly to the solid mixture and the solid pieces were broken via spatula.

Chloroform was added and the solution heated at 60°C for about 30 min to dissolve the solid. Then, the solution was transferred to a separatory funnel and extracted with chloroform. The chloroform layer was collected and dried over magnesium sulfate. After filtration through a Büchner funnel, the solution was placed in the fridge and 162.80 g (43%) of white crystals were collected, filtered through a Büchner funnel, washed with cold chloroform and dried under vacuum. ^{13}C-NMR ($CDCl_3$, ppm): δ 116.9, 110.3.

3,4-Dibromothiophene (4).[116] 2,3,4,5-Tetrabromothiophene (162.80 g, 4.07×10^{-1} mol) was dissolved in glacial acetic acid (163 mL) in a 500 mL 3-neck round bottom flask equipped with a condenser. Zinc powder (58.60 g, 8.96×10^{-1} mol) was added in small portions and the reaction mixture was refluxed overnight under nitrogen. Then the solution was cooled to room temperature, poured into deionized water and extracted with diethyl ether. The ether layer was collected and dried over magnesium sulfate. After filtration through a Büchner funnel, the solvent was evaporated and a yellow oil was collected. The oil was purified by distillation under reduced pressure and 61.08 g (63%) of 3,4-dibromothiophene were obtained [bp: 110°C at 17 mmHg (lit.[123] 94-95°C, 12 mmHg)]. ^{1}H-NMR ($CDCl_3$, ppm): δ 7.30 (s, 2H); ^{13}C-NMR ($CDCl_3$, ppm): δ 123.8, 113.9.

3,4-Dimethoxythiophene (5).[124] A solution of sodium methoxide was prepared by refluxing for 2 h under nitrogen anhydrous methanol (250 mL) with sodium (20.00 g, 8.69×10^{-1} mol) in a 500 mL 3-neck round bottom flask equipped with a condenser. Then 3,4-dibromothiophene (51.30 g, 2.14×10^{-1} mol) was added as well as cupper oxide (17.00 g, 2.14×10^{-1} mol) and potassium iodide (0.35 g, 2.14×10^{-3} mol). Every two days of reflux, another amount of potassium iodide (0.35 g, 2.14×10^{-3} mol) was added to the purple slurry. The reaction was kept under reflux for six days total. Then, the mixture was cooled to room

temperature, poured into deionized water and extracted with diethyl ether. The ether layer was washed with brine, dried over $MgSO_4$, and after filtration through a Büchner funnel the solvent was evaporated to give a pink oil. The oil was purified under reduced pressure and 27.28 g (89%) of clear oil were collected [bp: 98°C at 11 mmHg (lit.[125] 110°C at 17 mmHg)]. ^{1}H-NMR ($CDCl_3$, ppm): δ 6.21 (s, 1H), 3.87 (s, 3H); ^{13}C-NMR ($CDCl_3$, ppm): δ 148.01, 96.45, 57.80.

3,3-Dimethyl-3,4-dihydro-2H-thieno[3,4-b][1,4]dioxepine [ProDOT-Me$_2$].[126] To a 500 mL three-necked flask equipped with a Soxhlet extractor containing a cellulose thimble with 4 Å molecular sieves was added 3,4-dimethoxythiophene (5.94 g, 4.12×10^{-2} mol), 2,2-dimethyl-1,3-propanediol (8.58 g, 8.25×10^{-3} mol), *p*-toluenesulfonic acid monohydrate (0.78 g, 4.12×10^{-3} mol) and freshly distilled toluene (300 mL) under nitrogen. The solution was refluxed overnight. Then it was cooled at room temperature and washed with deionized water. The toluene fraction was washed with Brine and dried over $MgSO_4$. After filtration through a Büchner funnel, the toluene was evaporated to give a yellow-brown solid. The solid was purified by column chromatography on silica gel with 2:3 methylene chloride/hexanes as eluent to yield 6.01 g (79%) of white product [mp = 42-43ºC (lit.[126] mp = 49-51ºC)]. ^{1}H-NMR ($CDCl_3$, ppm): δ 6.48 (s, 1H), 3.74 (s, 2H), 1.04 (s, 3H); ^{13}C-NMR ($CDCl_3$, ppm): δ 150.22, 105.70, 80.30, 39.09, 21.89.

3,3-Dihexyl-3,4-dihydro-2H-thieno[3,4-b][1,4]dioxepine [ProDOT-Hx$_2$].[54] ProDOT-Hex_2 was prepared according to the procedure described for ProDOT-Me_2 utilizing 3,4-dimethoxythiophene (5.00 g, 3.47×10^{-2} mol), 2,2-dihexyl-1,3-propanediol (16.94 g, 6.94×10^{-2} mol), *p*-toluenesulfonic acid monohydrate (0.66 g, 3.47×10^{-3} mol) and freshly distilled toluene (300 mL) under nitrogen. The brown oil was purified by column chromatography (2:3, methylene chloride, hexanes) to give 9.33 g (83%) of product as a yellow oil. ^{1}H-NMR ($CDCl_3$): δ 6.43 (s, 2H), 3.85 (s, 4H), 0.98-1.40 (20H, m), 0.89 (m, 6H).

1,4-Bis[3,3-dimethyl-3,4-dihydro-2H-thieno[3,4-b][1,4]dioxepin-6-yl]-2,5-didodecyl-oxybenzene [BProDOT-Me_2-B($OC_{12}H_{25}$)$_2$]. ProDOT-Me_2 (5.00 g, 2.7 x 10^{-2} mol) was dissolved in anhydrous THF (150 mL) in a 1L 3-neck round bottom flask equipped with a condenser under nitrogen. The solution was cooled to -78°C and *n*-BuLi (2.90 x 10^{-2} mol) was added dropwise via syringe and the solution stirred for 1 hour at -78°C. Zinc chloride in THF (3.10 x 10^{-2} mol) was added dropwise via syringe and the solution was warmed to room temperature followed by addition via cannula of anhydrous NMP (200 mL). Then, 1,4-dibromo-2,5-didodecyloxybenzene (5.48 g, 9.00 × 10^{-3} mol), $Pd_2(dba)_3$ (0.33 g, 3.60 × 10^{-4} mol) and $P(tBu)_3$ (0.146 g, 7.20 × 10^{-4} mol) were dissolved in a mixture of anhydrous THF (100 mL) and anhydrous NMP (50 mL) in a Schlenk flask. This purple solution was transferred via cannula to the solution containing the zinc chloride derivative of ProDOT-Me_2 and the mixture was heated at 100°C for 12 h. The light brown solution was cooled to room temperature and poured into deionized water (500 mL). The mixture was extracted with ethyl ether, the ether layer was washed with brine and dried over magnesium sulfate. After filtration through a Büchner funnel, the solvent was evaporated and a light brown solid collected. This solid was purified by column chromatography (1:1, benzene, hexanes) followed by recrystallization (1:5, ethyl acetate, hexanes) to give 3.02 g (42%) of yellow crystals [mp: 80-82°C]. ^{1}H-NMR ($CDCl_3$): δ 7.49 (s, 1H), 6.53 (s, 1H), 4.01 (t, 2H), 3.81 (s, 2H), 3.79 (s, 2H), 1.84 (p, 2H), 1.47 (m, 2H), 1.27 (m, 16H), 1.07 (s, 6H), 0.88 (t, 3H); ^{13}C-NMR ($CDCl_3$): δ 149.9, 149.5, 146.8, 121.8, 118.7, 114.9, 104.9, 80.3, 80.1, 70.0, 39.1, 32.1, 29.9, 29.8, 29.7, 29.6, 29.5, 26.4, 22.9, 22.0, 14.3. HRMS: calcd for $C_{48}H_{74}O_6S_2$: 810.4927. Found: 810.4928. Anal. Calcd for $C_{48}H_{74}O_6S_2$: C, 71.07; H, 9.19. Found: C, 71.16, H, 9.38.

1,4-Bis[3,3-dihexyl-3,4-dihydro-2H-thieno[3,4-b][1,4]dioxepin-6-yl]-2,5-didodecyloxy-benzene [BProDOT-Hex$_2$-B(OC$_{12}$H$_{25}$)$_2$]. ProDOT-Hex$_2$ (6.34 g, 2.0 x 10^{-2} mol) was dissolved in anhydrous THF (100 mL) in a 500 mL 3-neck round bottom flask equipped with a condenser under nitrogen. The solution was cooled to -78˚C and *n*-BuLi (2.10 x 10^{-2} mol) was added dropwise via syringe and the solution stirred for 1 hour at -78˚C. Zinc chloride in THF (2.30 x 10^{-2} mol) was added dropwise via syringe and the solution was warmed to room temperature followed by addition via cannula of anhydrous NMP (100 mL). 1,4-Dibromo-2,5-didodecyloxybenzene (4.83 g, 8.00 × 10^{-3} mol), $Pd_2(dba)_3$ (0.293 g, 3.20 × 10^{-4} mol) and P(*t*-Bu)$_3$ (0.129 g, 6.40 × 10^{-4} mol) were dissolved in anhydrous THF (100 mL) and anhydrous NMP (100 mL) in a Schlenk flask. This purple solution was transferred via cannula to the solution containing the zinc chloride derivative of ProDOT-Hex$_2$ and the mixture was heated at 100˚C for 12 hours. The light brown solution was cooled to room temperature and poured into deionized water (300 mL). The mixture was extracted with ethyl ether, the ether layer was washed with brine and dried over magnesium sulfate. After filtration through a Büchner funnel, the solvent was evaporated and a yellow oil collected. This oil was purified by column chromatography (1:3, benzene, hexanes) and dried under vacuum to give 3.82 g (44%) of a yellow solid [mp: 45-46°C]. ^{1}H-NMR ($CDCl_3$): δ 7.50 (s, 1H), 6.45 (s, 1H), 3.99 (t, 2H), 3.90 (s, 2H), 3.91 (s, 2H), 1.82 (p, 2H), 1.39 (m, 4H), 1.27 (m, 34H), 0.88 (m, 9H); ^{13}C-NMR ($CDCl_3$): δ 149.6, 149.3, 146.5, 121.6, 117.8, 114.7, 104.1, 69.9, 43.9, 32.3, 32.1, 32.0, 30.4, 29.9, 29.9, 29.8, 29.7, 29.6, 26.4, 23.1, 22.9, 22.8, 14.3, 14.2. HRMS: calcd for $C_{68}H_{114}O_6S_2$: 1090.8057. Found: 1090.8070. Anal. Calcd for $C_{68}H_{114}O_6S_2$: C, 74.81; H, 10.52. Found: C, 74.62, H, 10.64.

Poly[1,4-Bis[3,3-dihexyl-3,4-dihydro-2H-thieno[3,4-b][1,4]dioxepin-6-yl]-2,5-didodecyloxybenzene] [PBProDOT-Hex$_2$-B(OC$_{12}$H$_{25}$)$_2$]. BProDOT-Hex$_2$-B(OC$_{12}$H$_{25}$)$_2$ (8.03 ×

10^{-1} g, 7.30 x 10^{-4} mol) was dissolved in chloroform (15 mL) under nitrogen. A slurry of iron chloride (3.58 × 10^{-1} g, 2.2 x 10^{-3} mol) in chloroform (15 mL) was added dropwise to the monomer solution over a 2 hour period. With addition of oxidant, the yellow solution turned dark purple. The mixture was stirred overnight at room temperature and then precipitated into methanol (500 mL). The precipitate was filtered through a Soxhlet thimble and redissolved in chloroform (250 mL) where it was stirred for 6 h with excess hydrazine monohydrate (10 mL). The solution was concentrated by evaporation and the polymer solution poured into methanol (400 mL) where a red precipitate formed. The precipitate was filtered through a Soxhlet thimble, purified via Soxhlet extraction for 18h with methanol and extracted for 8h with chloroform. The solvent was evaporated from the chloroform fraction and a red solid collected (0.74 g, 92%). ^{1}H-NMR ($CDCl_3$, ppm): δ = 7.61 (b, 1H), 3.96-4.06 (b, 6H), 1.92 (b, 2H), 1.0-1.50 (bm, 38H), 0.88 (bm, 9H). GPC analysis: M_n = 14,600, M_w = 22,990, PDI = 1.57. Anal. Calcd for $C_{68}H_{112}O_6S_2$: C, 74.94; H, 10.35; S, 5.88. Found: C, 70.90; H, 10.59; S, 4.73; Cl, 0.13; Fe, 0.22.

8,8'-(2,5-bis(dodecyloxy)-1,4-phenylene)bis(6-bromo-3,3-dimethyl-3,4-dihydro-*2H*-thieno[3,4-*b*][1,4]dioxepine) [Br_2-BProDOT-Me_2-B($OC_{12}H_{25}$)$_2$]. BProDOT-Me_2-B($OC_{12}H_{25}$)$_2$ (2.32 g, 2.86 x 10^{-3} mol) was dissolved in anhydrous DMF (250 mL) in a 500 mL three necked flask under nitrogen, and the solution was cooled at -78°C. NBS was quickly added to the yellow slurry and the mixture was progressively warmed to room temperature. After 5 h, the reaction was stopped by addition of a solution of ammonium hydroxide to the green slurry. The mixture was extracted with diethyl ether and the organic layer was dried over $MgSO_4$. After filtration through a Büchner funnel the solvent was evaporated and a bright yellow solid was collected. The crude product was purified by column chromatography on silica gel with hexanes/ methylene chloride (1:1) followed by recrystallization from hexanes/ethyl acetate (5:1) yielding

1.76 g (64%) of pure white crystals [mp: 110-111°C]. ^{1}H-NMR ($CDCl_3$): δ 7.56 (s, 1H), 4.02 (t, 2H), 3.87 (s, 2H), 3.83 (s, 2H), 1.83 (p, 2H), 1.47 (m, 2H), 1.27 (m, 16H), 1.08 (s, 6H), 0.88 (t, 3H). ^{13}C-NMR ($CDCl_3$): δ 149.16, 147.75, 145.95, 121.14, 118.24, 114.05, 94.22, 80.39, 80.31, 70.01, 39.17, 32.14, 29.91, 29.87, 29.84, 29.65, 29.58, 29.43, 26.44, 22.91, 21.96, 14.34. HRMS: calcd for $C_{48}H_{72}Br_2O_6S_2$: 966.3137. Found: 966.3181. Anal. Calcd for $C_{48}H_{72}Br_2O_6S_2$: C, 59.49; H, 7.49. Found: C, 59.62, H, 7.77.

8,8'-(2,5-bis(dodecyloxy)-1,4-phenylene)bis(6-bromo-3,3-dihexyl-3,4-dihydro-*2H*-thieno[3,4-*b*][1,4]dioxepine) [Br_2-BProDOT-Hex_2-$B(OC_{12}H_{25})_2$]. Br_2-BProDOT-Hex_2-$B(OC_{12}H_{25})_2$ was prepared according to the procedure described for Br_2-BProDOT-Me_2-$B(OC_{12}H_{25})_2$ utilizing BProDOT-Hex_2-$B(OC_{12}H_{25})_2$ (0.58 g, 5.32×10^{-4} mol), NBS (0.24 g, 1.33×10^{-3} mol) and anhydrous DMF (50 mL). The crude product was purified by column chromatography on silica gel with hexanes/ CH_2Cl_2 (2:1) followed by hexanes/CH_2Cl_2 (7:1) yielding 0.54 g (81%) of slightly yellow crystals. Mp: 75-77°C. ^{1}H-NMR ($CDCl_3$): δ 7.58 (s, 1H), 4.02 (t, 2H), 3.98 (s, 2H), 3.94 (s, 2H), 1.87 (p, 2H), 1.44 (m, 6H), 1.27 (m, 32H), 0.90 (m, 9H). ^{13}C-NMR ($CDCl_3$): δ 148.99, 147.46, 145.75, 121.02, 117.37, 113.88, 93.32, 69.92, 44.05, 32.21, 32.15, 31.99, 30.37, 29.94, 29.88, 29.86, 29.69, 29.60, 26.46, 26.46, 23.07, 22.92, 22.88, 14.34, 14.29. HRMS: calcd for $C_{68}H_{112}Br_2O_6S_2$: 1246.6267. Found: 1246.632. Anal. Calcd for $C_{68}H_{112}Br_2O_6S_2$: C, 65.36; H, 9.03. Found: C, 65.64, H, 9.36.

CHAPTER 4
NARROW BAND-GAP CYANOVINYLENE POLYMERS

4.1 Introduction

As discussed in the general Introduction, organic soluble narrow band-gap polymers are particularly desirable for photovoltaics due to their spectral absorption which matches the solar terrestrial radiation.[127-130] They are also needed for deep red and near-IR emitting devices,[127] for applications using n- and p-type conductors,[131] and for electrochromic devices especially due to their potentially multicolored states.[132,133]

The donor-acceptor approach (D-A) described earlier is one of the most effective ways of building a narrow band-gap polymer, and in particular significant effort has been applied to the combination of electron rich heterocycles with highly electron demanding cyano-substituted aryl units.[13,134,135] Recently our group described the synthesis of narrow band-gap cyanovinylene-dioxythiophene polymers and the concepts for building an ideal light absorbing material for effective charge transfer to PCBM (see general Introduction).[18,43,58] In that study, it was demonstrated that PProDOT-Hex_2:CNPPV is a promising candidate of the cyanovinylene-dioxythiophene family for photovoltaic devices. It is a strongly absorbing photoexcitable donor for PCBM, and exhibits good solubility in organic solvents, an optical band gap of 1.7 eV, a HOMO level of 5.7 eV, and a LUMO level of 3.5 eV. However, initial observations have shown that spin-coated films of the polymer blended with poly(2-methoxy-5-(2'-ethyl-hexyloxy)-1,4-phenylene vinylene) (MEH-PPV) and with the acceptor PCBM, have a discontinuous surface which becomes rougher as the contents of PProDOT-Hex_2:CNPPV increase, probably due to an aggregated polymer morphology. Photovoltaic efficiencies of 0.1-0.2 % have been measured, suggesting the need of further polymer structural optimization. In parallel with the photovoltaic study, it has also been observed that this polymer provides appealing electrochromic properties,

switching between deep blue neutral state and colorless transmissive reduced and oxidized states. Finally, it is important to note that this polymer is synthesized by Knoevenagel polymerization and does not involve the use of transition metal catalysts. Catalysts impurities are often trapped in the polymer and are responsible for photoluminescence quenching, electrical shorts or preferred conduction paths in thin-film devices leading to decreased performance.[136]

In pursuit of enhanced processing for photovoltaics and to further investigate the electrochromic capabilities of propylenedioxythiophene:cyanovinylene (ProDOT:cyanovinylene) polymers, we decided to synthesize analogues of PProDOT-Hex_2:CNPPV and study a variety of side chains as shown in Figure 4-1. The effects of the side chains on the optical and electronic properties, solubility, and film forming ability were studied. Specifically, we report on the substitution of the ProDOT moieties with alkoxy chains to attain higher solubility and greater processability relative to the alkyl substituted PProDOT-Hex_2:CNPPV polymer.[58] The first polymer, PProDOT-$OHex_2$:CNPV-DDO**,** was fully substituted with linear alkoxy substituents: linear dodecyloxy chains on the phenylene ring and linear hexyloxy chains on the ProDOT ring as illustrated in Figure 4-1. Disorder inducing branches were introduced on the ProDOT moiety of the second polymer, PProDOT-$OEtHex_2$:CNPV-DDO, this material being also substituted with linear dodecyloxy substituents on the phenylene ring but with 2-ethyl hexyloxy chains on the ProDOT ring. The branching location was changed on the third and fourth polymers by using linear hexyloxy chains on the ProDOT ring and unsymmetrically substituting the phenylene ring with methyloxy groups and 2-ethylhexyloxy (PProDOT-$OHex_2$:CNPV-MEH)) or 3,7-dimethyloctyloxy groups (PProDOTOHex_2:CNPV-MDMO). Also, with PProDOT-$OHex_2$:CNPV-MEH and PProDOT-$OHex_2$:CNPV-MDMO we considered substitution

mimicking those in MEH-PPV and MDMO-PPV, the most efficient polymers to date for organic solar cells [along with P3HT].[76,77]

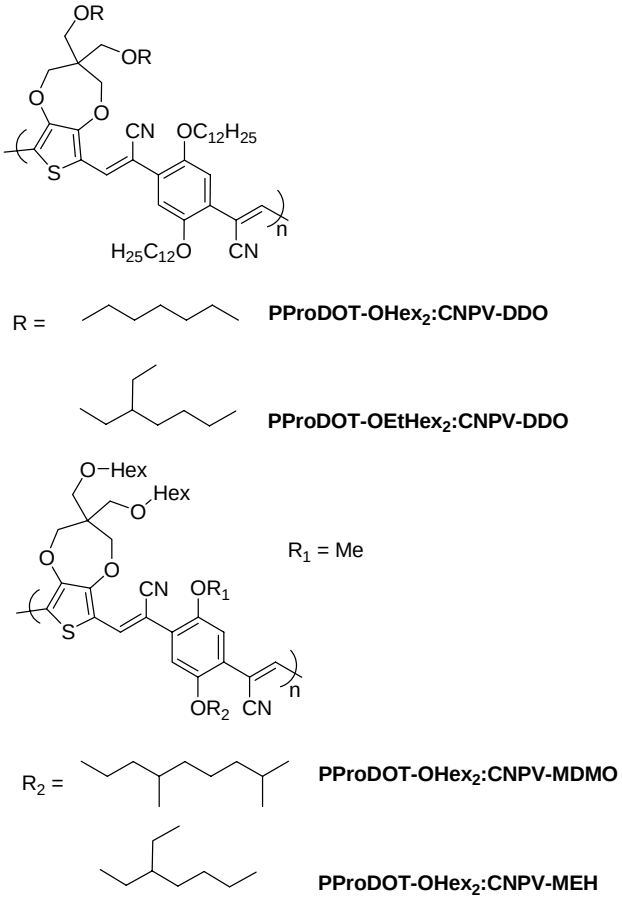

Figure 4-1. Family of ProDOT:cyanovinylene polymers synthesized via the Knoevenagel methodology.

Molecular and macromolecular characterization was accomplished by a combination of NMR and IR spectroscopy, MALDI mass spectrometry and GPC. The details of these characterizations will be described in section 4.2 along with the synthesis of the monomers and polymers. Section 4.3 will give a brief analysis of the ordering properties. A study of the spectroelectrochemical, redox, and electrochromic properties will be given in sections 4.4 and 4.5. An exploration of the polymers light emitting capacities, and light harvesting properties in bulk heterojunction polymer/PCBM solar cells is included in section 4.6.

4.2 Monomer and Polymer Synthesis and Characterization

Knoevenagel condensation is the polymerization method of choice for the synthesis of the propylenedioxythiophene:cyanovinylene polymer family. Previous work done on this type of polymer has shown that dialdehyde-functionalized thiophenes are far more accessible than diacetonitrile-functionalized thiophenes.[43] Consequently the polymers were built from the coupling of an electron donating ProDOT-dialdehyde moiety with and electron withdrawing phenylene-diacetonitrile moiety.

The synthesis of the acetonitrile monomers **1** has been already deeply investigated, and it was deduced that the best synthetic pathway consists of alkylation of commercial hydroquinone or *p*-methoxyphenol, bromomethylation, and cyanide substitution (Figure 4-2). All these steps have been previously reported in the literature.[137-139] The ProDOT moieties were derivatized with linear and branched alkoxy-chains using nucleophilic substitution of the corresponding alcohols on the key ProDOT($CH_2Br)_2$ precursor previously synthesized by our group[34] (Figure 4-3). The synthesis of the dialdehyde monomers **2** was accomplished by lithiation of the ProDOT derivative with *n*-butyllithium, followed by addition of excess DMF. According to previous work done by the Reynolds group, this is the most effective method available for the formylation of ProDOT rings.[43] The monomer structures and purity were verified by ^{1}H-NMR, ^{13}C-NMR, elemental analysis, HRMS, along with melting point analysis and IR spectroscopy when applicable.

The polymerization was accomplished by Knoevenagel condensation of the acetonitrile and aldehyde monomers in a 1:1 mixture of *t*-BuOH/THF with one equivalent of *t*-BuOK per cyano group as shown in Figure 4-4. After a 2 h reflux, the polymers were precipitated into methanol and filtered into a cellulose extraction thimble. The thimble was placed in a Soxhlet apparatus and methanol was refluxed over the thimble for 24 h to remove any unreacted

monomer and base. Final extraction with chloroform afforded blue or purple solids in yields ranging between 40 and 80% after solvent evaporation (Table 4-1).

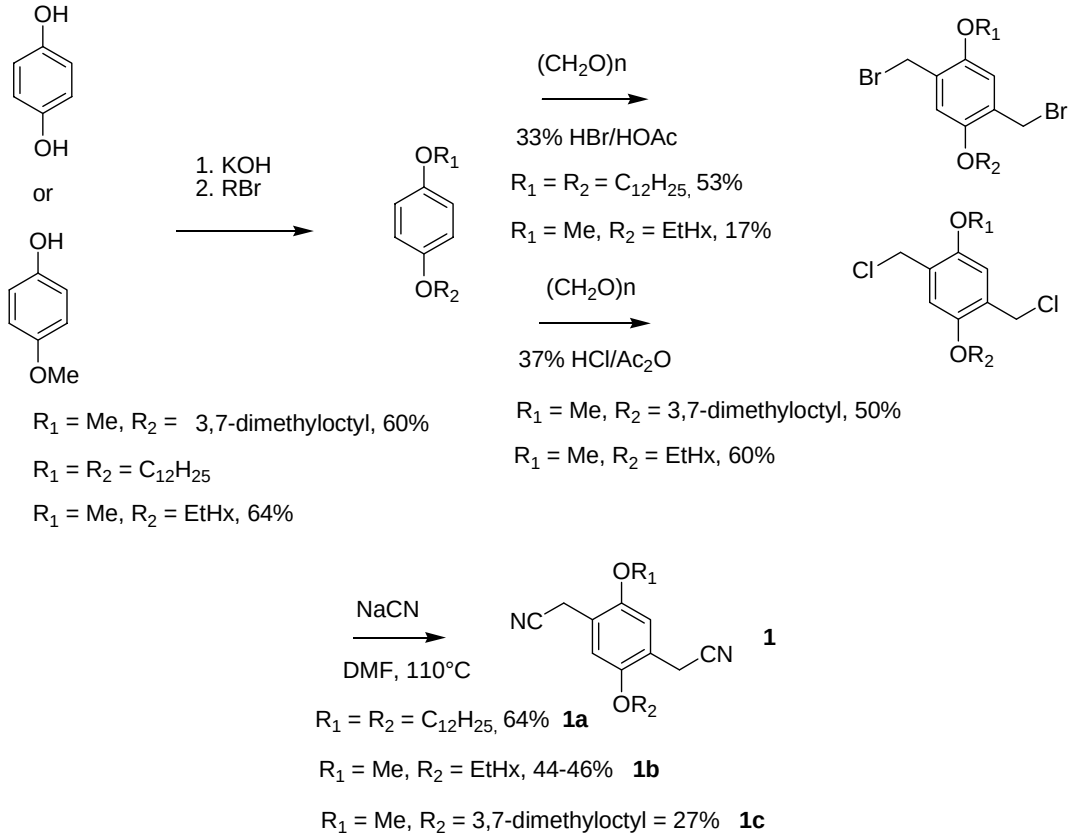

Figure 4-2. Synthesis of the phenylene-diacetonitrile acceptor monomers.

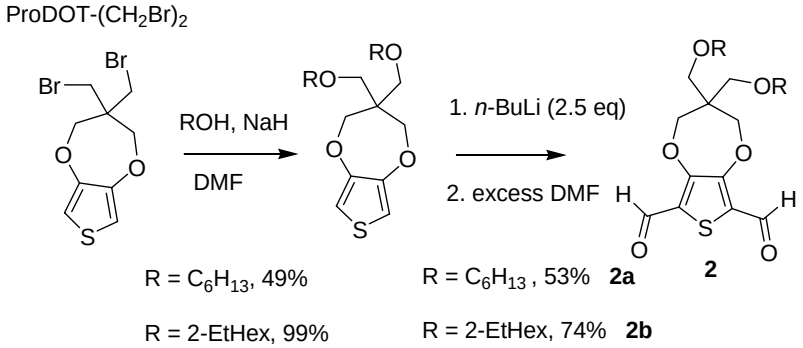

Figure 4-3. Synthesis of the ProDOT-dialdehyde monomers.

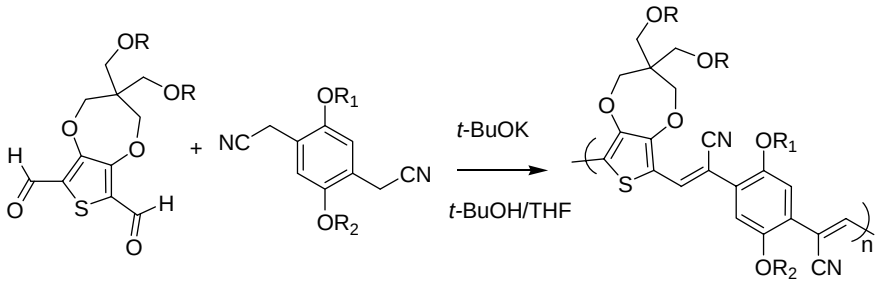

Figure 4-4. Synthesis of the ProDOT:cyanovinylene family of polymers via Knoevenagel polymerization.

Table 4-1. GPC estimated molecular weights of the ProDOT:cyanovinylene polymers (polystyrene standards, THF as mobile phase) and yields of the Knoevenagel polymerizations.

	M_n (g mol^{-1})	M_w (g mol^{-1})	PDI	Average number of rings	Yield (%)
PProDOT-OEtHex$_2$:CNPV-DDO	10,300	14,800	1.4	20	61
PProDOT-OHex$_2$:CNPV-DDO	13,000	17,500	1.3	28	77
PProDOT-OHex$_2$:CNPV-MEH	23,700	31,100	1.3	66	45
PProDOT-OHex$_2$:CNPV-MDMO	8,700	11,400	1.3	22	41

The polymers are highly soluble in common organic solvents such as hexanes, chloroform, methylene chloride and tetrahydrofuran. ^{1}H-NMR, IR, and MALDI-MS support the proposed structures of the polymers. End-groups were not visible by ^{1}H-NMR. Residual nitrile IR stretching bands at ~ 2250 cm^{-1} corresponding to the monomers were not observed, while bands were observed at ~ 2204-2206 cm^{-1} indicating the presence of conjugated cyanovinylene linkages (Figure 4-5). MALDI analyses, performed in reflectron mode with a HABA matrix, confirmed the polymer structure, with a spacing between the peaks corresponding interestingly to the molecular weight of two repeat units, and residual masses of 18 Da. This phenomenon has already been observed for PProDOT-Hex$_2$:CNPPV[18,43] and, as illustrated by the results of Figure 4-6, only even-numbered chains are seen in the MALDI spectra. This effect has been observed in polycondensation reactions and has been explained by the cyclization of the polymer chains due to strong electronic interactions (e. g. π-π, donor-acceptor and dipole-dipole interactions)

enforcing a parallel and coplanar alignment of the growing chains, inducing a hair-pin conformation.[140,141] Based on the observed *m/z* values for the polymers and the mass accuracy of our instrument, we are able to identify the oligomers as linear species and rule out the possibility that they are cyclic. In fact, the observed residual mass of 18 Da, presumably H_2O, is consistent with end groups of a phenylene unit with a single free acetonitrile and a ProDOT unit with a single free aldehyde.

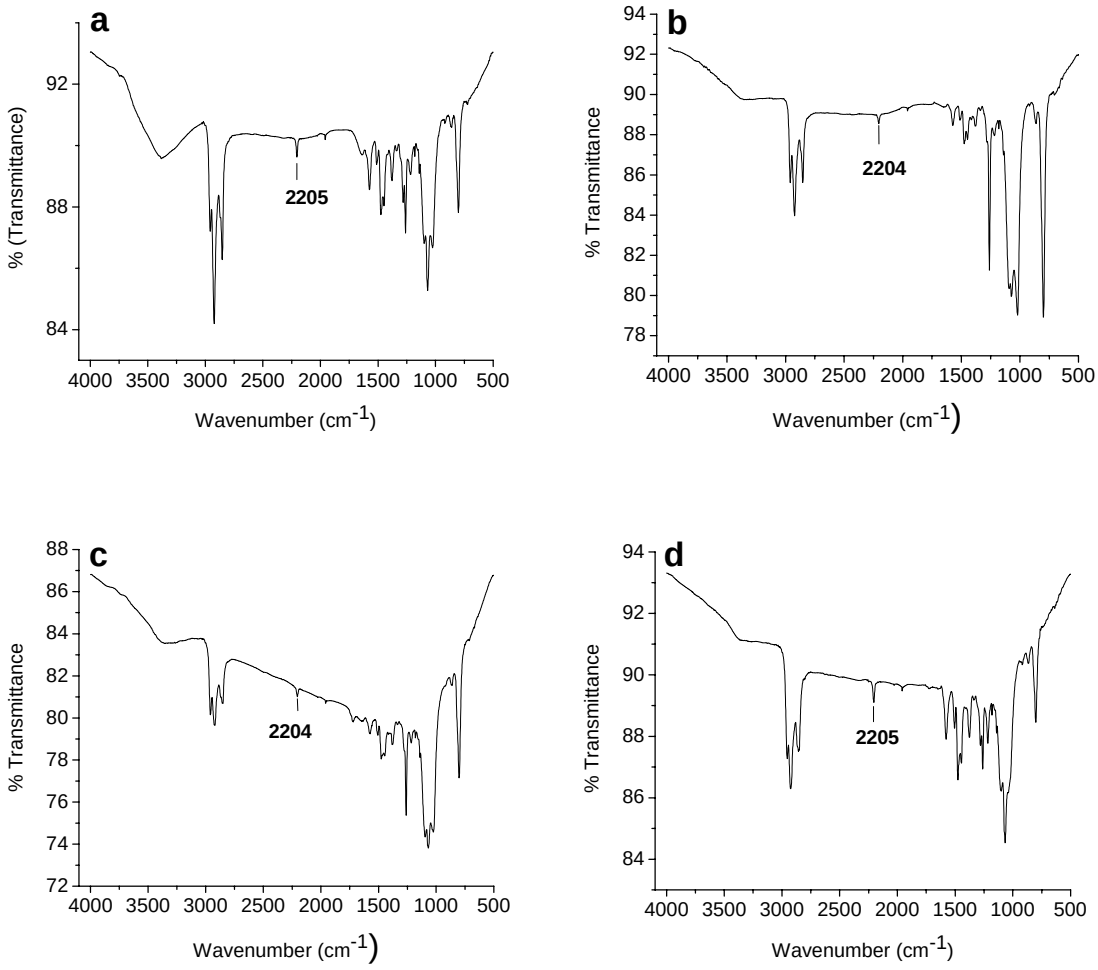

Figure 4-5. IR spectra of ProDOT:cyanovinylene polymers. (a) PProDOT-OEtHex$_2$:CNPV-DDO, (b) PProDOT-OHex$_2$:CNPV-DDO, (c) PProDOT-OHex$_2$:CNPV-MEH, (d) PProDOT-OHex$_2$:CNPV-MDMO.

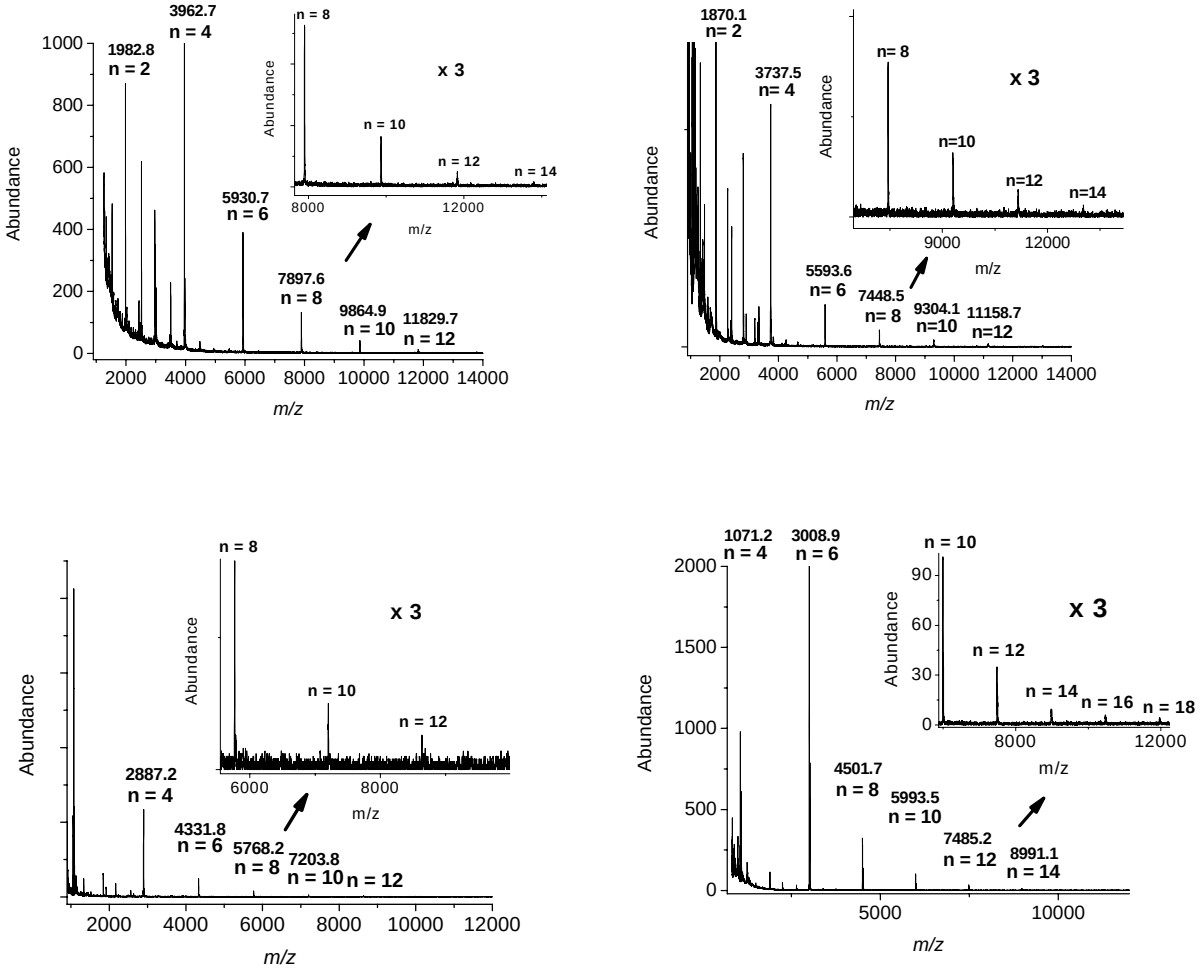

Figure 4-6. MALDI-MS of ProDOT:cyanovinylene polymers. (a) PProDOT-OEtHex$_2$:CNPV-DDO, (b) PProDOT-OHex$_2$:CNPV-DDO, (c) PProDOT-OHex$_2$:CNPV-MEH, (d) PProDOT-OHex$_2$:CNPV-MDMO. It illustrates that the dominant spacing pattern corresponds to two repeat units. HABA was used as the matrix. The inset is a 3 x magnification of the high *m/z* region.

Molecular weight analyses performed by GPC (polystyrene standards, THF as mobile phase) gave number average molecular weights ranging from 9,000 to 24,000 g mol^{-1} which corresponds to an average number of rings ranging from 20 to 66 per chain (Table 4-1). The use of stoichiometric proportions of acetonitrile and aldehyde monomers is a necessity in this A-A + B-B polycondensation. This is made difficult by the aldehyde monomers **2** being sticky oils, which makes accurate weighing difficult. This may explain the variations in the molecular

weights obtained and we suppose that near stoichiometric conditions were reached for the synthesis of PProDOT-OHex$_2$:CNPV-MEH, which exhibits the highest molecular weight of about 24,000 g mol^{-1}. MALDI analysis confirmed the presence of chains up to 12-18 repeat units (Figure 4-6), though no conclusion can be given on the average molecular weights using this method since it is more difficult for high molecular weight mass components to undergo the desorption/ionization process, "fly" in the mass spectrometer, and be detected.[142-144]

As illustrated in Figure 4-7, chromatographic polymer elution during GPC analysis was monitored with an in-line photodiode array detector to record the UV-Vis absorption of selected fractions of the polymers. Spectra were recorded at various elution times which allowed monitoring polymer absorption as a function of molecular weight relative to the polystyrene standards. The polymers exhibit a broad absorption in the 500-700 nm visible region. For PProDOT-OEtHex$_2$:CNPV-DDO we begin reaching the polymer limit when the molecular weight reaches about 12,000 g mol^{-1} (Figure 4-7-1d). Below that molecular weight, the absorption spectra exhibit maxima centered in the 530-580 nm region and a broad shoulder around 620 nm; above 12,000 g mol^{-1} the shoulder becomes more defined giving rise to a second absorption maximum undergoing small changes from 617 nm to 627 nm as the chain size further increases. For PProDOT-OHex$_2$:CNPV-DDO, PProDOT-OHex$_2$:CNPV-MEH and PProDOT-OHex$_2$:CNPV-MDMO the polymer limits were reached after about 15,000 g mol^{-1}, 20,000 g mol^{-1} and 12,000 g mol^{-1} respectively, since little variations in the absorption maxima were observed at higher molecular weights. The comparison between these results and the number average molecular weights summarized in Table 4-1 supports that our polymers have desirable degrees of polymerization and dispersity.

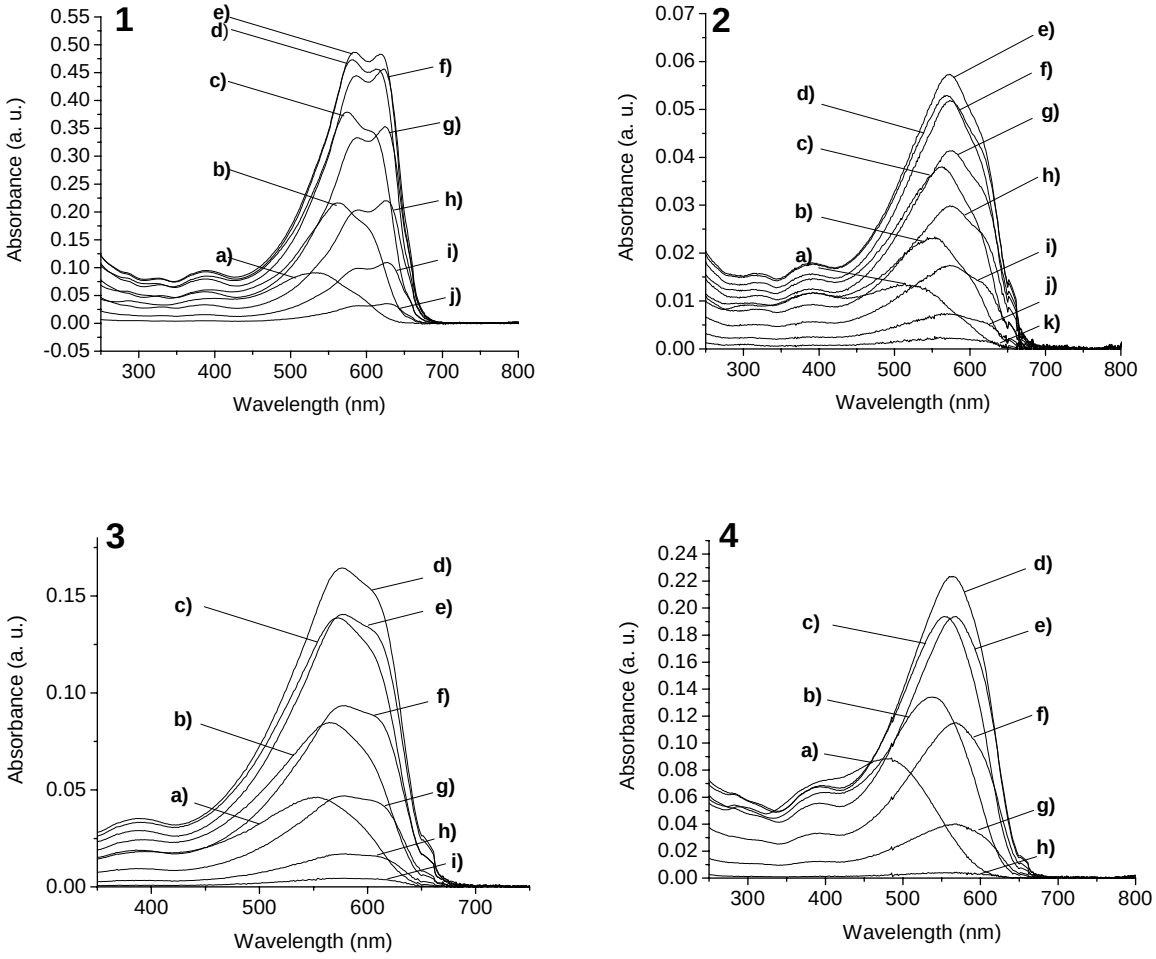

Figure 4-7. Absorption spectra for molecular weight fractions of the ProDOT:cyanovinylene polymers. 1) PProDOT-OEtHex$_2$:CNPV-DDO, 2) PProDOT-OHex$_2$:CNPV-DDO, 3) PProDOT-OHex$_2$:CNPV-MEH, 4) PProDOT-Hex$_2$:CNPV-MDMO. Absorption maxima (λ_{max}) and molecular weights in g mol^{-1} vs polystyrene are reported. 1) (a) 534.1 nm, 5,000, (b) 562.1 nm, 6,500, (c) 574.3 nm, 8,900, (d) 581 nm and 612 nm, 12,200, (e) 582.8 nm and 617.1 nm, 15,100, (f) 623.2 nm, 20,000, (g) 624.4 nm, 27,000, (h) 626.8 nm, 36,000, (i) 626.8 nm, 49,300, (j) 626.8 nm, 69,500. 2) (a) 513.4 nm, 6,000, (b) 553.6 nm, 8,000, (c) 563.3 nm, 10,600, (d) 569.4 nm, 14,800, (e) 573.1 nm, 18,800, (f) 573.1 nm, 23,900, (g) 573.1 nm, 28,900, (h) 573.1 nm, 34,500, (i) 573.1 nm, 42,400, (j) 573.1 nm, 53,800, (k) 573.1 nm, 67,200. 3) (a) 554 nm, 10,100, (b) 565 nm, 14,000, (c) 573 nm, 20,200, (d) 577 nm, 30,100, (e) 579 nm, 38,200, (f) 579 nm, 50,500, (g) 579 nm, 69,300, (h) 579 nm, 95,600, (i) 579 nm, 132,700. 4) (a) 485.4 nm, 4,000, (b) 539 nm, 6,200, (c) 554 nm, 8,600, (d) 564.5 nm, 12,200, (e) 567 nm, 16,200, (f) 567 nm, 22,700, (g) 567 nm, 31,900, (h) 567 nm, 47,900.

The thermal stability of the polymers was studied by thermogravimetric analysis (TGA) in a nitrogen atmosphere using a 20°C min^{-1} temperature ramp from 50°C to 900°C. The thermograms show that the polymers exhibit a high thermal stability losing less than 2-3% weight at 300°C followed by a drastic degradation process at about 370°C. Above 800°C less than 20% of material remains (Figure 4-8).

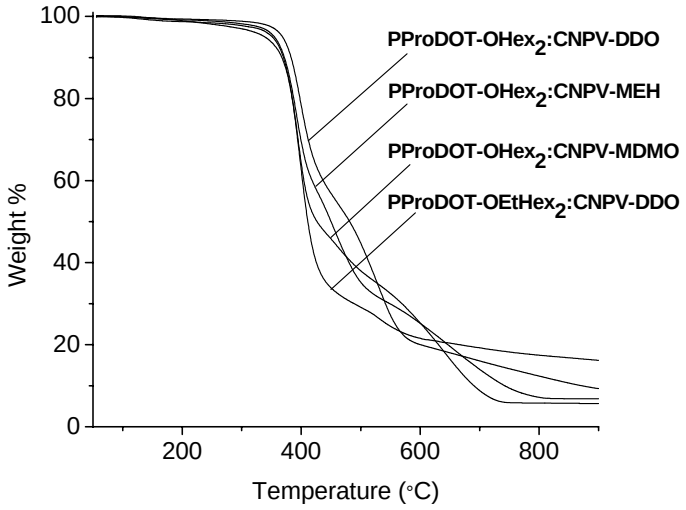

Figure 4-8. Thermogravimetric analysis of the ProDOT:cyanovinylene polymers. Measurements performed in a nitrogen atmosphere using a 20°C min^{-1} temperature ramp from 50°C to 900°C.

Figure 4-9 shows the solution UV-Vis absorbance and photoluminescence of the polymers in toluene. They absorb over a broad spectral range (*ca.* 500-700 nm), with absorption coefficients[67] around 25,000 M^{-1} cm^{-1}. The polymer substituted with linear chains on the phenylene and ProDOT rings (PProDOT-$OHex_2$:CNPV-DDO, Figure 4-9b) exhibits an absorption maximum at 619 nm and the polymer solution is deep blue. As we introduce branches on the ProDOT ring (PProDOT-$OEtHex_2$:CNPV-DDO, Figure 4-9a) the absorption maximum slightly shifts to 617 nm, while it drastically falls to 606 nm (PProDOT-$OHex_2$:CNPV-MEH, Figure 4-9c) as branches are introduced on the phenylene moiety, and the solution color becomes

more red as demonstrated in the photographs in Figure 4-9. A λ_{max} of 567 nm is observed for PProDOT-OHex$_2$:CNPV-MDMO as the vibronic coupling which yields splitting in the spectrum is reduced. Unsymmetrical branching on the phenylene ring induces a large influence on the polymer disorder and conjugation, shifting the absorption to the blue region, transmitting more red light and giving the solution a purple appearance, whereas branching on the ProDOT unit seems to have no significant influence. The polymers emit in the red and near-infrared region with emission maxima decreasing from 658 nm for the more ordered polymer (Figure 4-9b) to 643 nm for the least ordered polymer (Figure 4-9d), as illustrated for PProDOT-OHex$_2$:CNPV-MEH in the photograph in Figure 4-9c. The fluorescence quantum efficiency of the polymers was estimated around 12% (Oxazine 1 standard; $\Phi = 0.11$).

4.3 Ordering Properties

While heating 1,2-dichlorobenzene solutions of the polymers, it was noted that they undergo a reversible thermochromic transition: when heated, the color of the polymer solution changed from blue (or purple) to red, returning to blue when it was cooled to room temperature as illustrated in the photographs in Figure 4-10. This thermochromic behavior can either be related to a more twisted backbone conformation at higher temperature, or to the breaking of aggregates (or both).[57] Looking at the spectral changes and vibronic features would have helped being more specific, but these parameters could not be studied since the spectroscopic equipment available at the time did not support the high temperatures necessary to observe the full thermochromic changes (UV-Vis spectrometer equipped with a water heating system supporting 95°C maximum). For PProDOT-OHex$_2$:CNPV-DDO a purple tint started appearing around 85°C, but the distinct change from a deep blue color to a red solution happened between 100°C and 130°C.

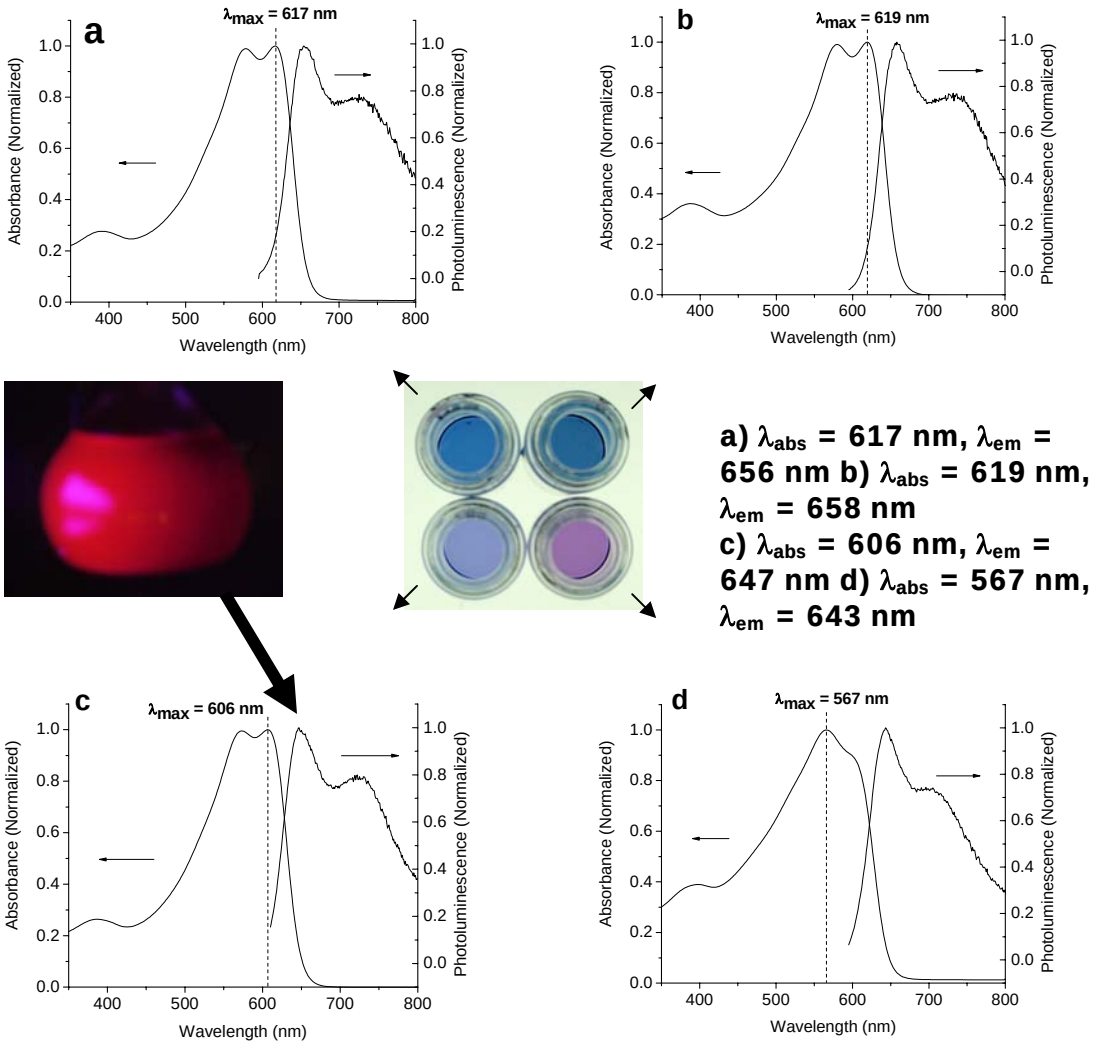

Figure 4-9. Solution UV-Vis absorbance and photoluminescence of ProDOT:cyanovinylene polymers in toluene. (a) PProDOT-OEtHex$_2$:CNPV-DDO, (b) PProDOT-OHex$_2$:CNPV-DDO, (c) PProDOT-OHex$_2$:CNPV-MEH, (d) PProDOT-OHex$_2$:CNPV-MDMO. The photograph in the center illustrates the colors of toluene solutions of the different polymers and the left photograph illustrates the photoluminescence of PProDOT-OHex$_2$:CNPV-MEH irradiated by UV light.

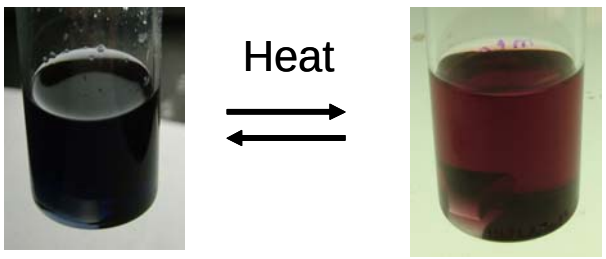

Figure 4-10. Thermochromic behavior of PProDOT-OHex$_2$:CNPV-DDO in 1,2-dichlorobenzene.

DSC was employed to study the ordering properties of the polymers and the DSC curves of the second scans are displayed in Figure 4-11. For reproducibility purposes, the first DSC scans were discarded because they are dependent of the heating and cooling procedures applied to the sample before analysis (thermal history effect). All polymers showed about the same behavior at low temperatures. First, they exhibited a glass transition (T_g) around -125°C, which can be clearly seen on the DSC scan of PProDOT-OEtHex$_2$:CNPV-DDO (Figure 4-11a), but was very difficult to detect for the other polymers. Figures 4-11c.1 and 4-11d.1 are magnifications of the T_g observed on the first scans of PProDOT-OHex$_2$:CNPV-MEH and PProDOT-OHex$_2$:CNPV-DDO, respectively. By comparing the DSC curves of the first (Figures 4-11c.1 and 4-11d.1) and second scans (Figure 4-11c and 4-11d) of these polymers, it is clearly seen that as further DSC scans were accomplished, the T_g (and Tc_1) became more and more difficult to detect because of the higher degree of ordering gained during the first scans. After the T_g, as the temperature was increased, the side chains of the polymers gained in mobility and finally reached a temperature where they had enough energy to crystallize as was observed by the exothermic transition (T_{c1}) around -90°C. Then two endothermic transitions corresponding to the melting of the side chains (T_{m1} and T_{m2}) were observed around -48°C and -38°C respectively. The temperature was increased up to 250°C and no other transitions could be observed for the polymers except for PProDOT-OEtHex$_2$:CNPV-DDO, which exhibited an endothermic transition corresponding to the melting of the backbone at 180°C. The polymers were cooled back to -150°C, and a first exothermic transition was observed for PProDOT-OEtHex$_2$:CNPV-DDO at 147°C corresponding to the backbone crystallization (T_{c2}). A second exothermic transition was observed for all polymers at temperatures ranging between -70°C to -90°C, depending on the polymer, and corresponding to the crystallization of the side chains (T_{c3} for PProDOT-

OEtHex$_2$:CNPV-DDO and Tc$_2$ for the other polymers). From the backbone melting and crystallization peaks observed for PProDOT-OEtHex$_2$:CNPV-DDO it can be concluded that this polymer has a more semicrystalline nature than the other polymers, which are amorphous.

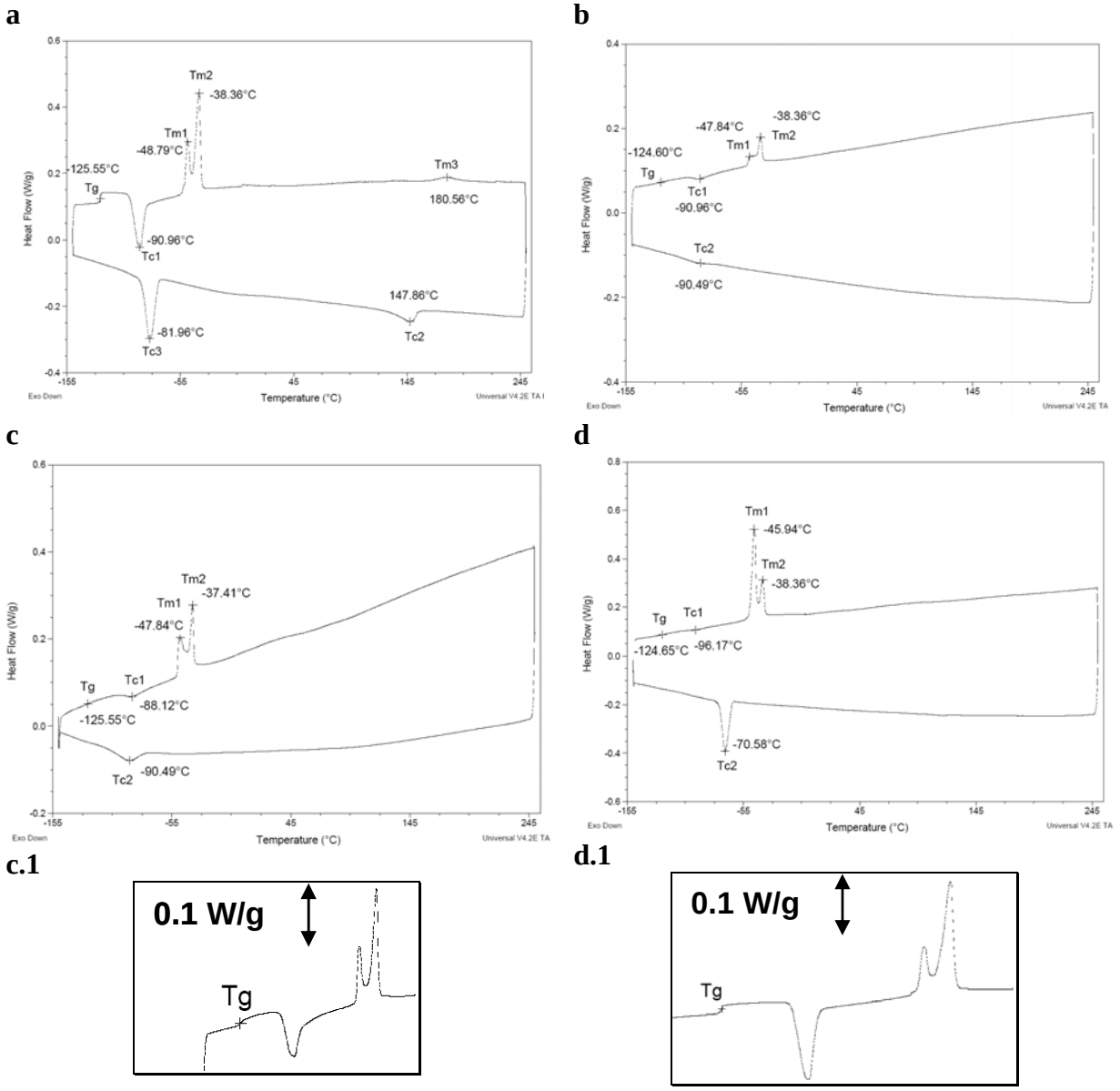

Figure 4-11. DSC curves of ProDOT:cyanovinylene polymers. (a) PProDOT-OEtHex$_2$:CNPV-DDO, (b) PProDOT-OHex$_2$:CNPV-MDMO, (c) PProDOT-OHex$_2$:CNPV-MEH, (d) PProDOT-OHex$_2$:CNPV-DDO, and low temperature magnification of the first scans at of (c.1) PProDOT-OHex$_2$:CNPV-MEH and (d.1) PProDOT-OHex$_2$:CNPV-DDO. Heating and cooling rates were 10°C min^{-1}.

4.4 Polymer Electrochemistry and Spectroelectrochemistry

For photovoltaic, electrochromic, or LED applications it is necessary to have a good understanding of the redox properties of the polymers and to be able to estimate the HOMO and LUMO levels. Towards that end, cyclic voltammetry and differential pulse voltammetry were employed. Polymer films were deposited by drop casting on a Pt button electrode from a 5 mg mL^{-1} chloroform solution, and the voltammograms were recorded in 0.1 M $TBAPF_6$/ACN electrolyte. The measurements were performed in an oxygen and water free environment in an argon-filled glovebox due to the instability of the reduced form of the polymers.[78] The oxidation and reduction processes were addressed separately as cycling over the full potential range resulted in rapid polymer degradation. Multiple cycling was used to break in the polymers, and the measurements were taken once the electrochemical response became constant.

Figures 4-12 and 4-13 show respectively the CV and DPV results obtained for the polymers. The polymers exhibit onsets of oxidation ranging from 0.6 V to 0.8 V vs Fc/Fc^+ and onsets of reduction ranging from -1.4 V to -1.6 V as detailed in Table 4-2. The differences between the oxidation and reduction potentials yield electrochemical band-gaps varying between 2.0 and 2.4 eV, with the band-gaps obtained by DPV being slightly smaller than those obtained by CV. This is not surprising since the onsets of oxidation measured by DPV are generally more defined than those obtained by CV. Indeed, DPV measures a current difference and the major component of that difference is the faradaic current. The capacitive component due to the charging of the electrode double layer is largely eliminated in comparison with CV measurements. DPV also avoids pre-peaks that are observed for instance on the CV spectrum of PProDOT-$OHex_2$:CNPV-MDMO (Figure 4-12d) and which are attributed to trapped charges in the polymer film.[17] The polymer HOMO and LUMO energies were estimated from the onsets of oxidation and reduction respectively. The polymers are relatively stable to oxidation with low

lying HOMO levels varying between 5.7 and 5.9 eV. These low HOMO values allow the polymers to be easily handled in air without encountering undesired oxidation. This is a useful property as we consider use of these materials in optoelectronic devices. With LUMO levels around 3.5-3.7 eV the polymers are also good candidates for charge transfer to C_{60}-based acceptors (0.5-0.7 eV LUMO offsets with LUMO of PCBM being at 4.2 eV). These results are in accordance with those previously reported on the PProDOT-Hex_2:CNPPV analogue.[18,43,58]

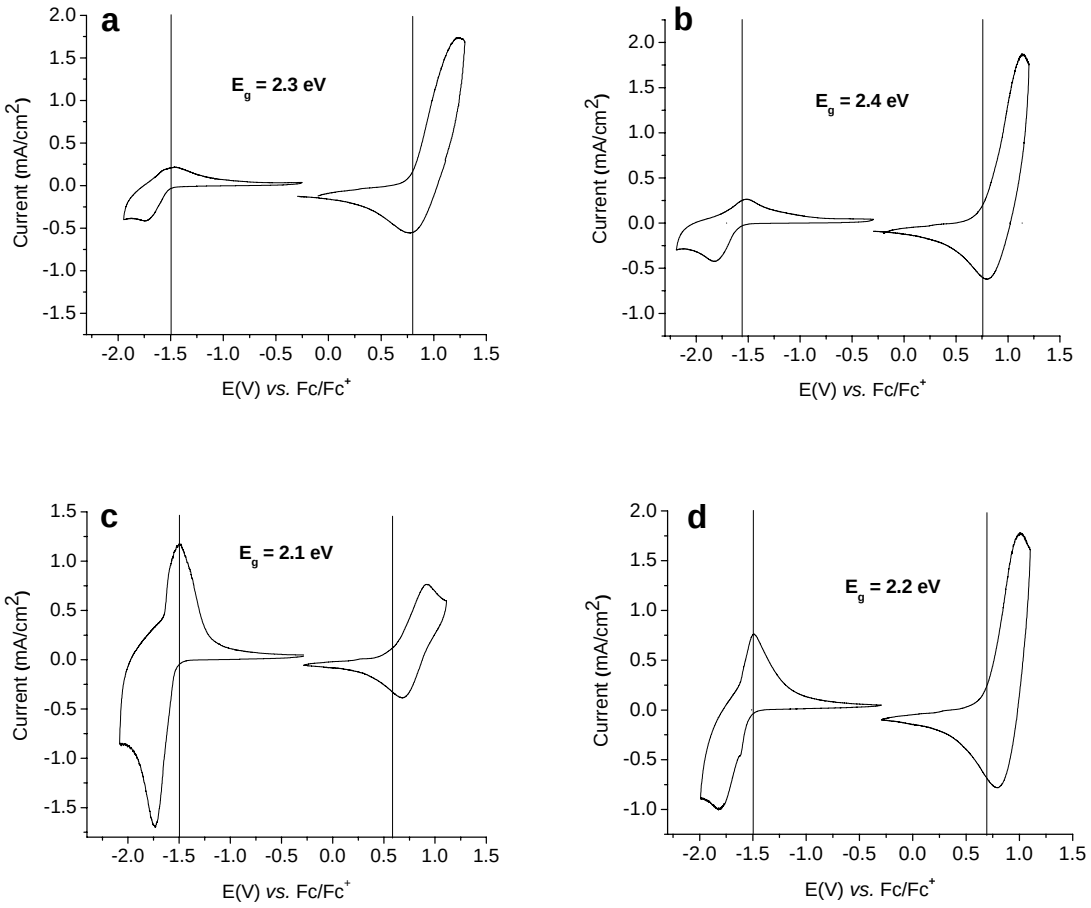

Figure 4-12. Cyclic voltammetry of ProDOT-cyanovinylene polymers. (a) PProDOT-$OEtHex_2$:CNPV-DDO (b) PProDOT-$OHex_2$:CNPV-DDO (c) PProDOT-$OHex_2$:CNPV-MEH, (d) PProDOT-$OHex_2$:CNPV-MDMO. Measurements were performed on a 0.02 cm^2 Pt button working electrode in 0.1 M $TBAPF_6$/ACN with a Pt foil counter electrode and a silver wire pseudo reference electrode calibrated vs Fc/Fc$^+$.

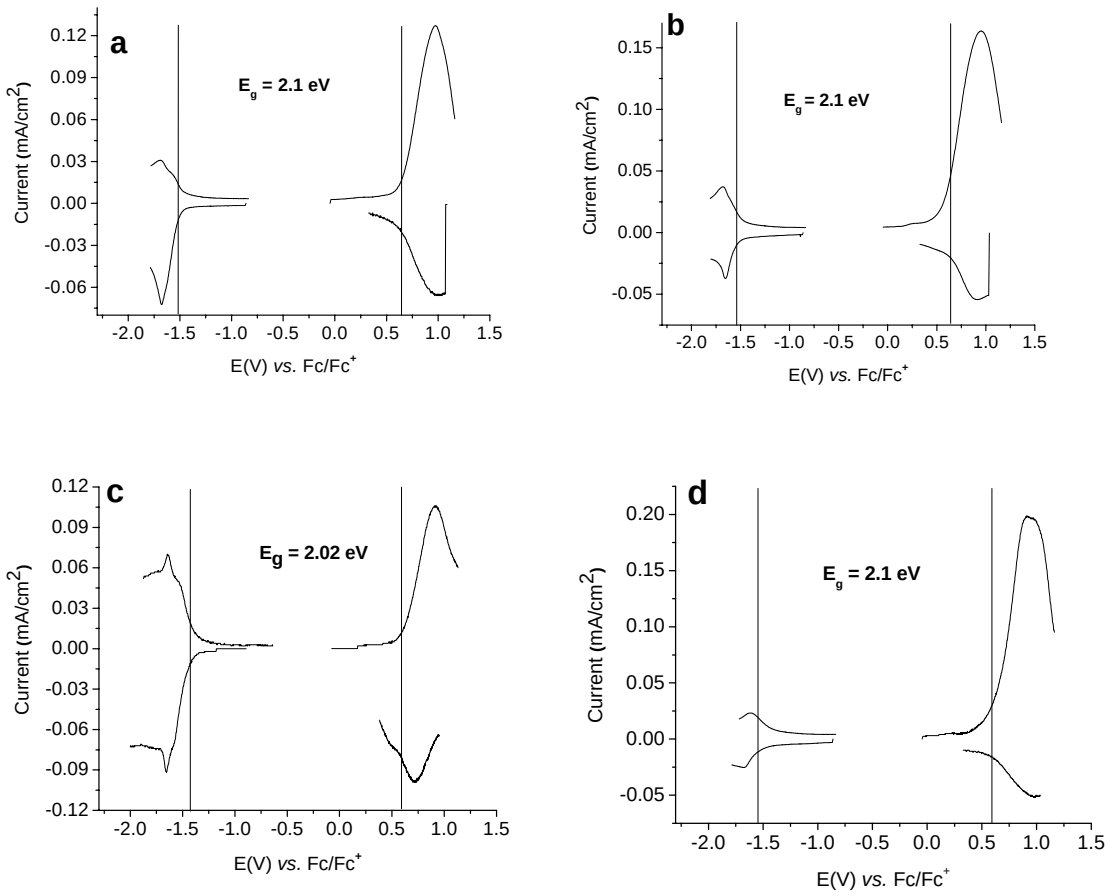

Figure 4-13. Differential pulse voltammetry of ProDOT-cyanovinylene polymers. (a) PProDOT-OEtHex$_2$:CNPV-DDO (b) PProDOT-OHex$_2$:CNPV-DDO (c) PProDOT-OHex$_2$:CNPV-MEH, (d) PProDOT-OHex$_2$:CNPV-MDMO. Measurements were performed on a 0.02 cm^2 Pt button working electrode in 0.1 M TBAPF$_6$/ACN with a Pt foil counter electrode and a silver wire pseudo reference electrode calibrated vs Fc/Fc$^+$.

Table 4-2. Summary of thin-film polymer electrochemistry, and HOMO and LUMO energies of the ProDOT:cyanovinylene polymers derived from the electrochemical results.

Polymer	$E_{onset,ox}$ CV (V)	HOMO CV (eV)	$E_{onset,red}$ CV (V)	LUMO CV (eV)	$E_{onset,ox}$ DPV (V)	HOMO DPV (eV)	$E_{onset,red}$ DPV (V)	LUMO DPV (eV)	$E_{g,opt}$ (eV)
PProDOT-OEtHex$_2$:CNPV-DDO	0.8	5.9	-1.5	3.6	0.6	5.7	-1.5	3.6	1.75
PProDOT-OHex$_2$:CNPV-DDO	0.8	5.9	-1.6	3.5	0.6	5.7	-1.5	3.6	1.70
PProDOT-OHex$_2$:CNPV-MEH	0.6	5.7	-1.5	3.6	0.6	5.7	-1.4	3.7	1.70
PProDOT-Hex$_2$:CNPV-MDMO	0.7	5.8	-1.5	3.6	0.6	5.7	-1.5	3.6	1.75

Spectroelectrochemical measurements were performed in order to define the optical band gaps of the polymers and observe their spectral response to doping. Homogeneous and high quality polymer films were produced by spray-casting polymer solutions (5 mg mL^{-1} in chloroform) onto ITO coated glass using an air brush at 12 psi. The spectral changes upon oxidation were recorded in 0.1 M TBAP/PC electrolyte as illustrated in Figure 4-14. In the neutral state, the polymers absorb across the entire visible region, exhibiting deep blue or purple (for PProDOT-$OHex_2$:CNPV-MDMO) colors, and optical band-gaps of 1.7-1.75 eV were calculated from the onset of the π-π* transition, right at the solar radiation maximum. These values are lower than the electrochemical values and such disagreements have been previously reported for cyanovinylene polymers.[18,43] It is important to note that for correlation to solar light absorption, and because CV and DPV measurements involve charge transfer by hopping and the diffusion of ions coming from the electrolyte into the polymer film, determination of the band gap for photovoltaic applications is best done using spectroscopic results. An error of about 0.3 eV was estimated for the band gaps determined by DPV, and an error of about 0.4-0.5 eV was estimated for the band gaps determined by CV due to the more poorly defined onsets of oxidation and reduction.

The polymer films were progressively oxidized by applying increasing positive potentials in 50 mV steps. Near the onset potential for oxidation, the π-π* transition of the neutral state started to decrease in intensity and lower energy charge carrier associated peaks started to grow in the near-IR region changing the film color to a transmissive light gray. It is interesting to note that these electrochromic properties are comparable to PEDOT which is most generally studied from electrochemically formed films, or from films prepared by casting/spin coating of PEDOT-

PSS. At the same time, these organic soluble and processed polymers are more stable in their neutral forms allowing easy handling.

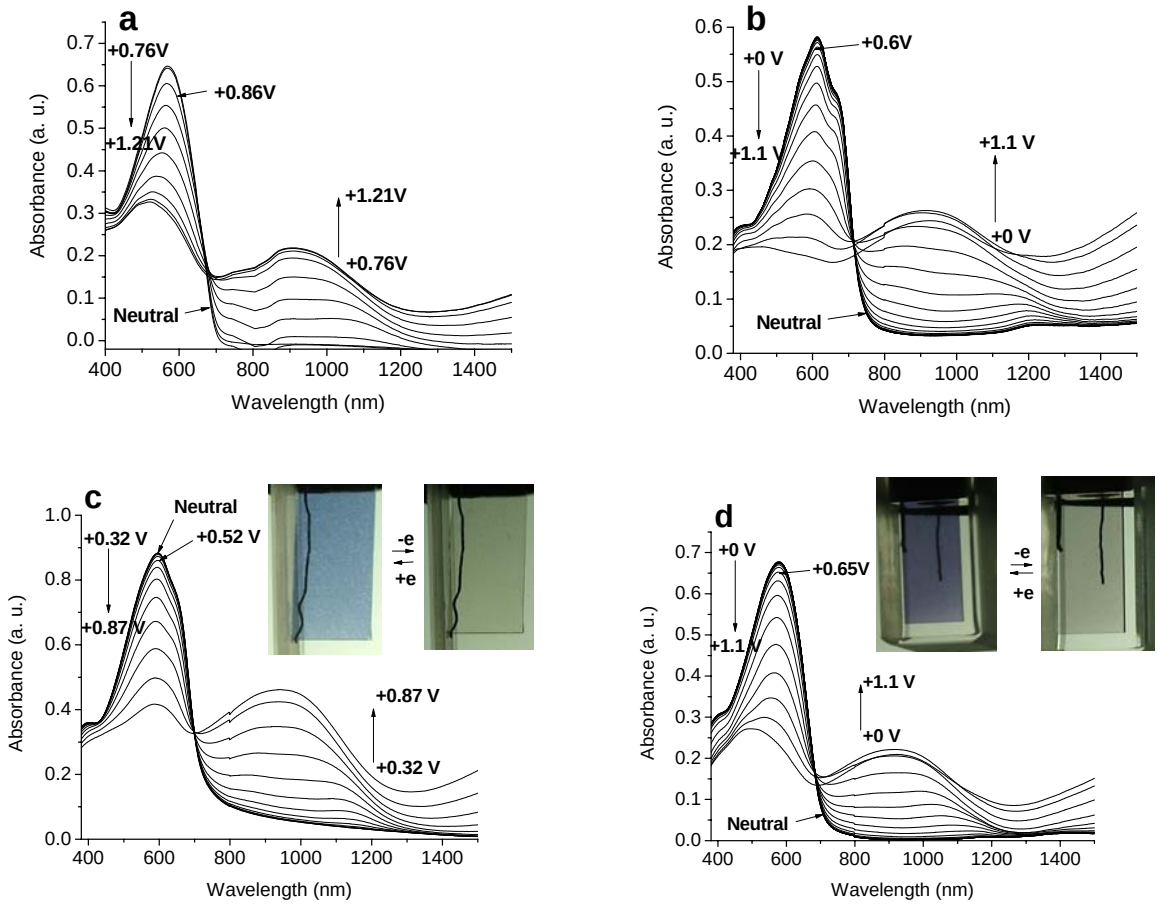

Figure 4-14. Oxidative spectroelectrochemistry of ProDOT:cyanovinylene polymers. (a) PProDOT-OEtHex$_2$:CNPV-DDO, (b) PProDOT-OHex$_2$:CNPV-DDO, (c) PProDOT-OHex$_2$:CNPV-MEH, (d) PProDOT-OHex$_2$:CNPV-MDMO. Polymer films were spray-cast from chloroform solution on ITO coated glass. All potentials are reported vs Fc/Fc^+. The supporting electrolyte consisted of 0.1 M TBAP/PC. The potential was increased in 50 mV steps.

The spectral changes were also recorded upon reduction in 0.1 M $TBAPF_6$/ACN electrolyte as illustrated in Figure 4-15. As for the CV and DPV measurements, these studies have been performed in an oxygen and water free environment. The polymer films were progressively reduced by applying increasing negative potentials in 100 mV steps. As the

potentials reach the onset of reduction observed by electrochemistry (for instance between -1.5 V and -1.6 V for PProDOT-OHex$_2$:CNPV-MEH), the π-π* transition of the neutral state decreases in intensity and lower energy charge carrier associated peaks evolve in the near-IR region changing the film color to transmissive light gray, as was also observed for the oxidation process. No data is recorded between 860 nm and 890 nm because the detectors used with the fiber optic spectrophotometer in this experiment do not cover this wavelength range.

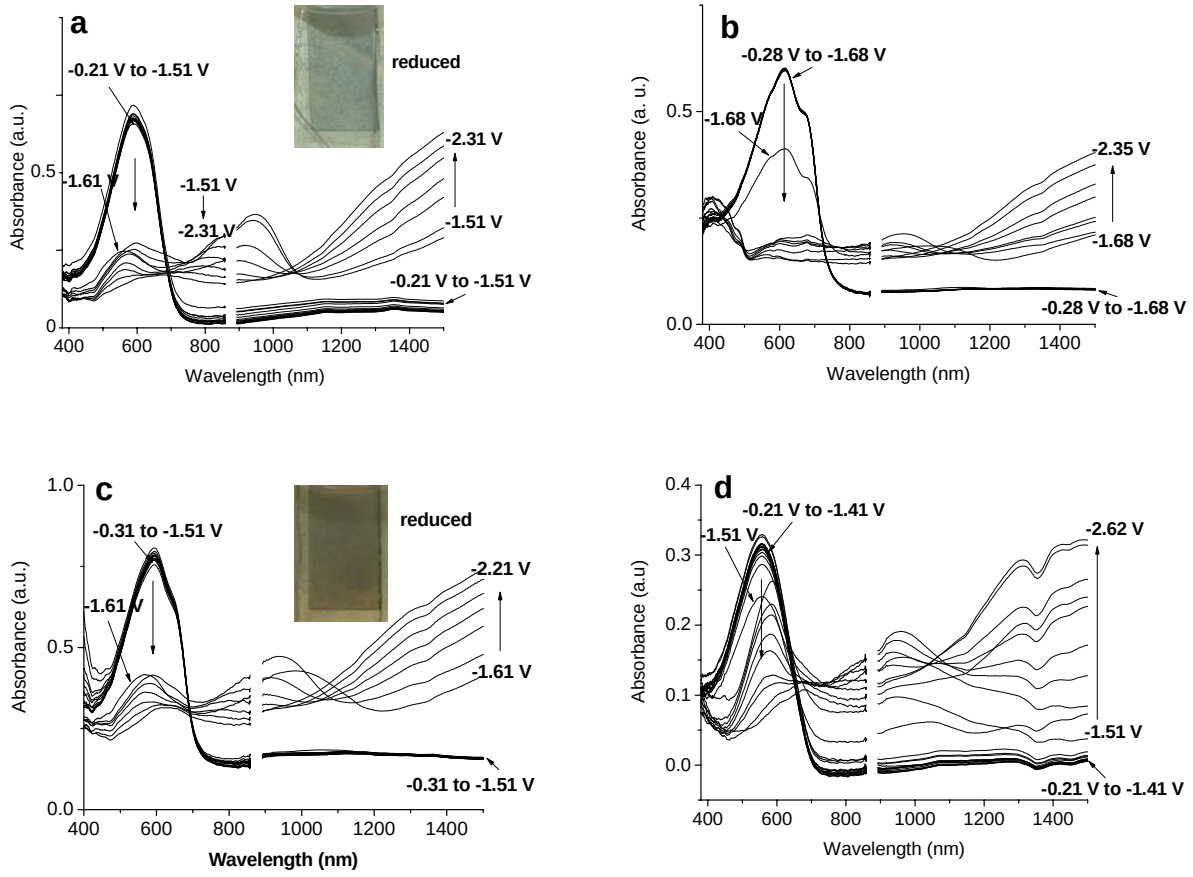

Figure 4-15. Reductive spectroelectrochemistry of ProDOT:cyanovinylene polymers. (a) PProDOT-OEtHex$_2$:CNPV-DDO, (b) PProDOT-OHex$_2$:CNPV-DDO, (c) PProDOT-OHex$_2$:CNPV-MEH, (d) PProDOT-OHex$_2$:CNPV-MDMO. Polymer films were spray-cast from chloroform solution on ITO coated glass. All potentials are reported vs Fc/Fc$^+$. The supporting electrolyte consisted of 0.1 M TBAPF$_6$/ACN. The potential was increased in 0.1 V steps. No data is shown between 860 nm and 890 nm as the detectors do not cover this wavelength range.

4.5 Colorimetry

Polymer films were deposited on ITO by spray-casting from 5 mg mL^{-1} chloroform solutions and were analyzed by in-situ colorimetric analysis using 0.1 M TBAP/PC as the supporting electrolyte. The relative luminance was measured as the polymers were progressively oxidized. Optical changes again occur once the potentials reach the electrochemical onsets of oxidation as illustrated in Figure 4-16. For instance, the onset of oxidation measured by CV for PProDOT-OEtHex$_2$:CNPV-DDO is at 0.8 V (Table 4-2) and the relative luminance starts increasing around this value. In the neutral state, the polymer films are quite opaque and colored, with a relative luminance varying between 27 and 37 %. In the fully oxidized state, the films become highly transmissive, with luminance values ranging from 65 to 82%, and a relative luminance change up to 50 % was observed for PProDOT-OHex$_2$:CNPV-MEH, which is useful for electrochromic applications. The L*a*b* values of the colors were also determined to allow color matching and the results are summarized in Table 4-3 along with the corresponding colors in the neutral and oxidized states.

Table 4-3. Colorimetric results for the neutral and oxidized ProDOT:cyanovinylene polymers.

Polymer film	Charge State	E(V)	L	a	b	Observed color
PProDOT-OEtHex$_2$:CNPV-DDO	N	0.65	58	1	-35	blue
PProDOT-OEtHex$_2$:CNPV-DDO	O	1.15	84	3	2	gray
PProDOT-OHex$_2$:CNPV-DDO	N	0.45	67	-4	-22	blue
PProDOT-OHex$_2$:CNPV-DDO	O	1.15	85	2	2	gray
PProDOT-OHex$_2$:CNPV-MEH	N	0.45	63	4	-28	blue
PProDOT-OHex$_2$:CNPV-MEH	O	1.15	90	0	5	gray
PProDOT-OHex$_2$:CNPV-MDMO	N	0.45	64	8	-18	purple
PProDOT-OHex$_2$:CNPV-MDMO	O	1.15	83	1	1	gray

Note: N = neutral, O = oxidized.

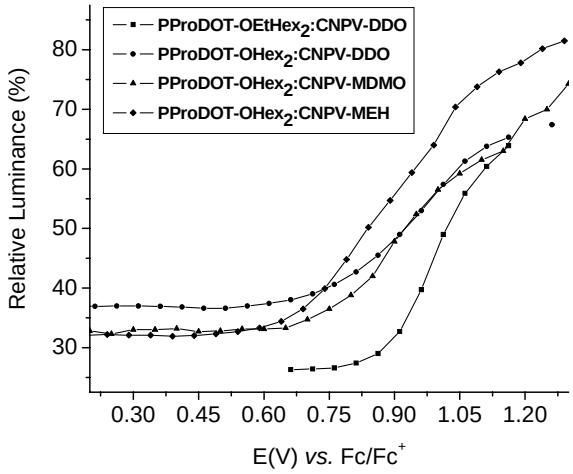

Figure 4-16. Relative luminance (%) as a function of applied potential for every ProDOT:cyanovinylene polymer. Polymer films were spray-cast from chloroform solution on ITO coated glass (5 mg mL^{-1}). The supporting electrolyte consisted of 0.1 M TBAP/PC.

4.6 Application in Devices

4.6.1 Polymer Light-Emitting Diodes*

As was shown in Figure 4-9c, the polymers exhibit a red fluorescence in toluene. The thin-film photoluminescence (PL) spectrum shown in Figure 4-17 for PProDOT-$OHex_2$:CNPV-MEH has a similar shape to the solution photoluminescence, although it is red-shifted due to a more organized conformation expected in the solid state. To evaluate the polymer's potential utility in LEDs, devices were prepared with the following architecture: ITO/PEDOT-PSS (40 nm)/ PProDOT-$OHex_2$:CNPV-MEH (50 nm)/Ca (5 nm)/Al (200 nm). As illustrated by the dotted line spectrum in Figure 4-17, the device exhibits a broad emission in the red and near-infra-red region dominated by a peak at λ_{max} = 704 nm. The bright red color observed is illustrated by the photograph in Figure 4-17. The electroluminescence (EL) spectrum is similar to the PL spectrum

* (Devices prepared by Dr. J. Mwaura)

of the solid film (Figure 4-17), indicating that the EL results from a singlet π,π* exciton with the same structure as that produced by photoexcitation. Figure 4-18 shows the device characteristics, especially a turn-on voltage of 4 V and an EL intensity which increases with voltage up to 10 V. We note that the radiance decreases at higher voltages possibly due to device breakdown. At 10 V, the device emits its highest luminance at ~ 77 μW cm^{-2} sr (526 cd m^{-2}) and current density of 1556 mA cm^{-2}. Unfortunately, the external electron-to-photon quantum efficiency was determined to be low and it has been concluded that the polymer is not likely effective for development in LED applications.

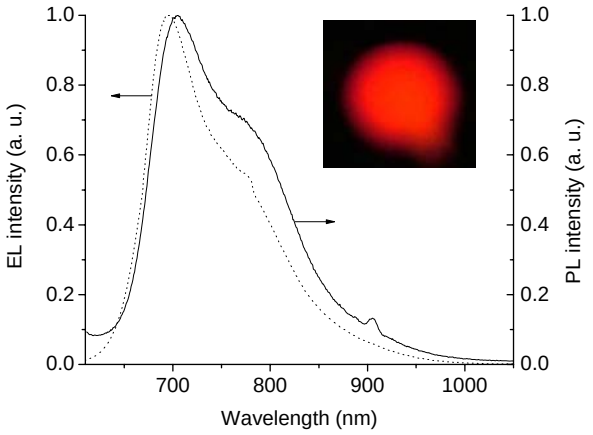

Figure 4-17. Normalized photoluminescence emission spectrum of PProDOT-$OHex_2$:CNPV-MEH in thin-film (solid line) superimposed with normalized electroluminescence spectrum and accompanying photograph of an ITO/PEDOT-PSS/PProDOT-$OHex_2$:CNPV-MEH/Ca/Al device (dotted line).

4.6.2 Photovoltaic Devices*

It was previously reported that the PProDOT-Hex_2:CNPPV analogue of our polymers can transfer electrons to PCBM upon photoexcitation.[43,58] This conclusion was based on PL quenching experiments showing that 95% of the PL was quenched in thin films blends with

* (Devices prepared by Dr. Y.-G. Kim).

PCBM, and on IPCE measurements of PProDOT-Hex_2:CNPPV/PCBM solar cells which indicate that the polymer is the major contributor to the photocurrent in the device.

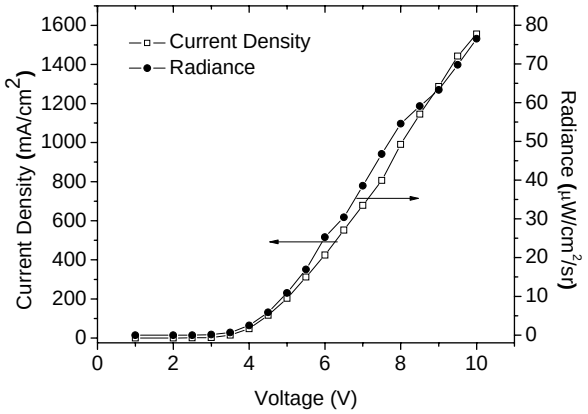

Figure 4-18. LED properties of an ITO/PEDOT-PSS/PProDOT-$OHex_2$:CNPV-MEH/Ca/Al device. Effect of applied voltage on current density (□) and radiance (●).

We prepared bulk heterojunction solar cells using the PProDOT-R_2:CNPV polymers as the electron donors and PCBM as the electron acceptor (device structure ITO/PEDOT-PSS/PProDOT-R_2:CNPV/PCBM/LiF/Al). Blends containing 1:4 (w/w) of each polymer with PCBM were spin-coated from dichlorobenzene solutions and the photoactive layer thickness was kept between 30 and 40 nm. Thicker photoactive layers led to drops in photocurrent density and fill factor, a phenomenon which is attributed to an increase in the series resistance. Figure 4-19 shows the i-V characteristics of the PProDOT-$OHex_2$:CNPV-MEH based device under AM 1.5 illumination for a calibrated solar simulator with an intensity of 100 mW cm^{-2}. The photovoltaic results obtained for the other polymers are summarized in Table 4-4. PProDOT-$OHex_2$:CNPV-MEH exhibited the best performance, with a power conversion efficiency (η) of about 0.4%, an open circuit voltage (V_{oc}) of 0.76 V, a short circuit current (I_{sc}) of 1.5 mA.cm^{-2} and a fill factor (FF) of 36%. According to the results summarized in the Table, there is a ~ 0.1-0.27% efficiency range for the other polymers which have lower molecular weights (vide ante). This observation

suggests that higher molecular weight materials are likely to enhance the photoinduced current densities in the PCBM solar cells. Independent device fabrication and measurements were conducted in both University of Florida (UF) and University of California (UCLA) laboratories for PProDOT-OEtHex$_2$:CNPV-DDO/PCBM. Very similar power conversion efficiencies of 0.27% vs 0.26% were achieved, supporting the reproducibility of the results.

Incident photon to current efficiency measurements (IPCE) match the polymer absorption spectra near the absorption maximum of the polymers, indicating that the polymers are effective photoexcited electron donors that contribute mainly to the photocurrent in the device. However, the IPCE values are quite low for all the polymers, between 6-8% in the 500 - 590 nm region and below 2% above 680 nm as illustrated in Figure 4-19b for the PProDOT-OHex$_2$:CNPV-MEH/PCBM device.

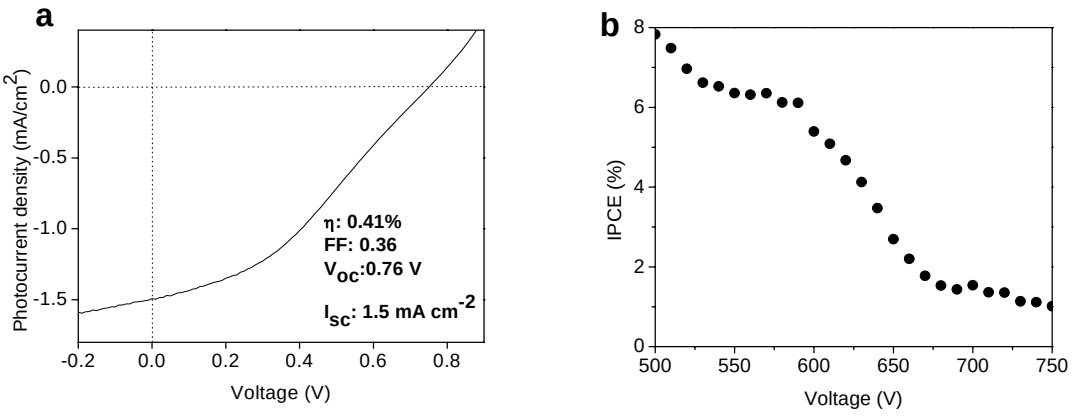

Figure 4-19. Photovoltaic results for a device made of a 1/4 blend (w/w) of PProDOT-OHex$_2$:CNPV-MEH/PCBM. (a) Current voltage characteristic under AM1.5 conditions (100 mW cm^{-2}). (b) IPCE of the device.

Several parameters are suspected to be responsible for the low efficiencies, and disorder is one of them. Disorder in a polymer inhibits hole mobility, which is believed to be the bottleneck for the short circuit current. In addition, when hole mobility is significantly lower than that of the

electron mobility in copolymer/PCBM blends, severe space charge effects lead to a poor fill factor. While our light absorption and energy level alignment are nearly optimal, reduced transport properties dominate and limit the device performance. Improving carrier mobility in these polymers is of primary importance for device enhancement. As seen before, initial studies on the ordering properties of the polymers have shown that only PProDOT-OEtHex$_2$:CNPV-DDO exhibits semicrystalline properties. It would be of great interest to study the effect of thermal annealing on the charge mobility and photovoltaic performance of this material. This was accomplished for example for thin-films of P3HT and has allowed making great improvements in charge mobility and photovoltaic efficiencies.[73-75]

Table 4-4. Summarized characteristics of ProDOT:cyanovinylene polymer/PCBM based solar cells.

Polymers	η (%)	FF	V_{oc} (V)	I_{sc} (mA/cm^2)	PAL thickness (nm)
PProDOT-OEtHex$_2$:CNPV-DDO	0.27	0.39	0.65	1.05	30
PProDOT-OHex$_2$:CNPV-DDO	0.1	0.34	0.58	0.5	37
PProDOT-OHex$_2$:CNPV-MEH	0.36	0.37	0.73	1.32	38
PProDOT-OHex$_2$:CNPV-MDMO	0.13	0.28	0.72	0.66	38

Note: Averaged values for 3 pixels for each polymer.

4.7 Summary and Perspective

This chapter gives an outlook on how small structural changes on a polymer backbone can affect the solubility, optical, and device properties of a material. PProDOT-Hex$_2$:CNPPV was initially targeted by the Reynolds group and utilized as a derivative of interest for electrochromics and photovoltaics. Working around its backbone structure and length, we were able to make progress towards improving film quality and photovoltaic properties. The replacement of the alkyl substituents by alkoxy substituents improved solubility without affecting the electronic properties. The highest molecular weight material was more efficient in enhancing the photoinduced current densities. The replacement of the linear substituents by

branches did not have a significant influence on the solubility. However, it significantly induced disorder and backbone twisting in solution especially in the polymers containing unsymmetrically substituted phenylene rings, shifting the absorption maxima of the polymer solutions to the blue region. DSC studies have shown that only PProDOT-OEtHex$_2$:CNPV-DDO is semicrystalline, and consequently that the disorder induced by the branched substituents on the phenylene rings is found in the solid state as well, and will affect intermolecular charge transport. It would be of great interest to study the influence of thermal annealing on the extent of ordering and on the photovoltaic performance of PProDOT-OEtHex$_2$:CNPV-DDO. As was observed for PProDOT-Hex$_2$:CNPPV, the polymers exhibit appealing electrochromic properties, switching between blue/purple colors in the neutral state and highly transmissive light gray colors in the reduced and oxidized states. These electrochromic properties, along with the improved film forming ability, make these materials of great interest for electrochromic applications involving large and flexible surfaces.

4.8 Experimental

Methoxy-4-(2-ethylhexyloxy)benzene.[145] *p*-Methoxyphenol (9.98 g, 8.05×10^{-2} mol) was dissolved in ethanol (200 mL) in a 500 mL three necked round bottom flask equipped with a condenser, under nitrogen. A solution of potassium hydroxide (5.01 g, 8.95×10^{-2} mol) in ethanol (50 mL) was slowly added and the solution was stirred at room temperature for 1 h. Then a solution of 2-ethylhexyl bromide (18.67 g, 9.67×10^{-2} mol) was added slowly and the mixture was stirred at 50°C overnight. After allowing the reaction to cool to ambient temperature, the solution was poured into a solution of sodium hydroxide (10%) and extracted with chloroform. The organic layer was dried over $MgSO_4$ and after filtration through a Büchner funnel the solvent was evaporated. The crude product was purified by column chromatography on silica gel using CH_2Cl_2:hexanes (1:2) and 12.17 g (64%) of product as a clear oil were collected. ^{1}H-NMR

($CDCl_3$): δ 6.84 (s, 4H), 3.80 (d, 2H), 3.70 (s, 3H), 1.71 (m, 1H), 1.27-1.53 (m, 8H), 0.93 (m, 6H). ^{13}C-NMR ($CDCl_3$): δ 153.87, 115.68, 114.85, 71.49, 55.99, 39.71, 30.77, 29.32, 24.10, 23.29, 14.30, 11.33. HRMS: calcd for $C_{15}H_{24}O_2$: 236.1776. Found: 236.1775. Anal. Calcd for $C_{15}H_{24}O_2$: C, 76.23; H, 10.24; Found: C, 79.97, H, 10.58.

1-(3,7-Dimethyloctyloxy)-4-methoxybenzene.[139] 1-(3,7-Dimethyloctyloxy)-4-methoxy-benzene was synthesized following the same procedure as for compound methoxy-4-(2-ethylhexyloxy)benzene using *p*-methoxyphenol (14.00 g, 1.13×10^{-1} mol), ethanol (250 mL), a solution of KOH (6.96 g, 1.24×10^{-1} mol) in ethanol (50 mL) and 3,7-dimethyloctylbromide (29.97 g, 1.36×10^{-1} mol). The crude product was purified by column chromatography on silica gel using CH_2Cl_2:hexanes (1:3) and 14.58 g (49%) of product as a clear oil were collected. ^{1}H-NMR ($CDCl_3$): δ 6.80 (s, 4H), 3.95 (t, 2H), 3.78 (s, 3H), 1.80 (m, 1H), 1.40-1.72 (m, 5H), 1.32 (m, 2H), 1.18 (m, 2H), 0.94 (d, 3H), 0.88 (d, 6H). HRMS: calcd for $C_{17}H_{28}O_2$: 264.2089. Found: 264.2096.

1,4-Bis(bromomethyl)-2,5-bis(dodecyloxy)benzene.[43] To a solution consisting of 33% HBr in acetic acid (30 mL) and glacial acetic acid (110 mL), 1,4-bis(dodecyloxy)benzene (13.80 g, 3.10×10^{-2} mol) and paraformaldehyde (2.80 g, 9.30×10^{-2} mol) were quickly added. The white slurry was heated to 70-75°C, resulting in the dissolution of all solids. The mixture was stirred at that temperature for 2 h, during which time a precipitate formed. The solution was cooled to 0°C, poured into cold water and extracted with chloroform. The organic layer was washed with Brine and dried over sodium sulfate. After filtration through a Büchner filter, the solvent was evaporated and a white solid was collected. After recrystallization in hexanes:methylene chloride (1:1), 10.23 g (53%) of pure product were obtained [mp = 93-95°C (lit.[146] mp = 93-94°C)]. ^{1}H-NMR ($CDCl_3$): δ 6.86 (s, 1H), 4.53 (s, 2H), 3.99 (s, 2H), 1.82 (m,

2H), 1.50 (m, 2H), 1.27 (m, 16H), 0.89 (t, 3H). ^{13}C-NMR ($CDCl_3$): δ 150.91, 127.79, 114.93, 69.28, 32.14, 29.87, 29.86, 29.82, 29.58, 28.94, 26.31, 22.91, 14.33. HRMS: calcd for $C_{32}H_{56}Br_2O_2$: 630.2647. Found: 630.2651. Anal. Calcd for $C_{32}H_{56}$ Br_2O_2: C, 60.76; H, 8.92; Found: C, 61.11, H, 9.13.

2,5-Bis(bromomethyl)-1-methoxy-4-[(2-ethylhexyl)oxy]benzene.[13] 2,5-Bis(bromomethyl)-1-methoxy-4-[(2-ethylhexyl)oxy]benzene was synthesized using the same procedure as for 1,4-bis(bromomethyl)-2,5-bis(dodecyloxy)benzene using 33% HBr in glacial acetic acid (60 mL), glacial acetic acid (180 mL), 1-methoxy-4-ethylhexyloxyphenylene (12.00 g, 5.08×10^{-2} mol) and paraformaldehyde (4.59 g, 1.53×10^{-1}mol). The crude product was collected as a brown solid and purified by column chromatography on silica gel, using methylene chloride:hexanes (1:5) for the elution, followed by recrystallization in hexanes. 3.60 g (17%) of white solid were obtained [mp = 80-82°C (lit.[138] mp = 81-82°C)]. ^{1}H-NMR ($CDCl_3$): δ 6.88 (s, 1H), 6.87 (s, 1H), 4.54 (s, 4H), 3.89 (d, 2H), 3.87 (s, 3H), 1.77 (m, 1H), 1.40-1.58 (m, 4H), 1.30-1.40 (m, 4H), 0.95 (m, 6H). ^{13}C-NMR ($CDCl_3$): δ 151.18, 127.53, 127.68, 114.50, 113.98, 71.14, 56.44, 39.81, 30.84, 29.33, 28.92, 28.86, 24.23, 23.27, 14.32, 11.47. HRMS: calcd for $C_{17}H_{26}Br_2O_2$: 420.0300. Found: 420.0306. Anal. Calcd for $C_{17}H_{26}Br_2O_2$: C, 48.36; H, 6.21; Found: C, 48.63, H, 6.32.

2,5-Bis(chloromethyl)-1-(3,7-dimethyloxy)-4-methoxybenzene.[139] 1-(3,7-Dimethyloctyloxy)-4-methoxybenzene (14.58 g, 55.20×10^{-2} mol) and paraformaldehyde (4.56 g, 1.52×10^{-1} mol), were put into a 500 mL three necked round bottom flask equipped with a condenser and an addition funnel, under nitrogen. After addition of 37% HCl (25 mL, 12M, 3.00×10^{-1} mol), acetic anhydride (56.38 g, 5.52×10^{-1} mol) was added dropwise at such a rate that the internal temperature did not exceed 70°C. After being stirred for 4.5 h at 70°C, the mixture was cooled to

room temperature. Then it was admixed with a cold saturated sodium acetate solution (50 mL) followed by a dropwise addition of 25% NaOH (36 mL). The mixture was heated to 52°C and subsequently cooled in an ice bath while stirring. The cream colored solid was filtered off, washed with water and dissolved in hexanes (100 mL). After extraction with deionized water, the organic phase was dried over $MgSO_4$, filtered through a Büchner filter and the solvent was evaporated. The crude product was purified by column chromatography on silica gel, using CH_2Cl_2:hexanes (1:4) for the elution, followed by recrystalllization in CH_2Cl_2:ethanol (1:3). 10 g (50%) of white solid were collected [mp = 57-58°C]. ^{1}H-NMR ($CDCl_3$): δ 6.94 (s, 1H), 6.93 (s, 1H), 4.65 (s, 2H), 4.64 (s, 2H), 4.02 (m, 2H), 3.87 (s, 3H), 1.84 (m, 1H), 1,7 (m, 1H), 1.48-1.78 (m, 4H), 1.1-1.40 (m, 4H), 0.96 (d, 3H), 0.88 (d, 6H). ^{13}C-NMR ($CDCl_3$): δ 151.24, 150.90, 127.33, 127.01, 114.59, 113.52, 67.65, 56.48, 41.53, 39.43, 37.46, 36.50, 30.04, 28.20, 24.90, 22.92, 22.82, 19.92. HRMS: calcd for $C_{19}H_{30}Cl_2O_2$: 360.1623. Found: 360.1621. Anal. Calcd for $C_{19}H_{30}Cl_2O_2$: C, 63.15; H, 8.37; Found: C, 63.45, H, 8.48.

1,4-Bis(chloromethyl)-5-(2-ethylhexyloxy)-2-methoxybenzene.[137] 1,4-bis(chloromethyl)-5-(2-ethylhexyloxy)-2-methoxybenzene was synthesized using the same procedure as for 2,5-bis(chloromethyl)-1-(3,7-dimethyloxy)-4-methoxybenzene using 1-methoxy-4-ethylhexyloxy-phenylene (33.00 g, 1.40×10^{-1} mol), paraformaldehyde (11.53 g, 3.84×10^{-1} mol), 37% HCl (63 mL, 12 M, 7.69×10^{-1} mol) and acetic anhydride (142.72 g, 1.40 mol). After recrystallization of the crude product with hexanes, 27.80 g (60%) of white solid were obtained. ^{1}H-NMR ($CDCl_3$): δ 6.94 (s, 1H), 6.92 (s, 1H), 4.64 (s, 4H), 3.88 (d, 2H), 3.87 (s, 3H), 1.75 (m, 1H), 1.40 -1.60 (m, 4H), 1.30-1.40 (m, 4H), 0.88-1.00 (m, 6H).

1,4-Bis(cyanomethyl)-2,5-bis(dodecyloxy)benzene (1a).[43] Sodium cyanide (1.94 g, 3.95 $\times 10^{-2}$ mol, 2.5 equiv.) and 1,4-bis(bromomethyl)-2,5-bis(dodecyloxy)benzene (10.00 g, 1.58 ×

10^{-2} mol) were dissolved in anhydrous DMF (250 mL) under nitrogen and the solution was heated to 110°C. The reaction was stirred for three days, during which time the reaction turned dark orange. The mixture was cooled to room temperature and poured into cold water (750 mL) containing 0.5 M of sodium hydroxide. The precipitate was filtered through a Büchner funnel, collected, and dissolved in chloroform. The chloroform solution was then extracted with deionized water; the organic layer collected and dried over $MgSO_4$. After solvent evaporation, a brown oil was obtained and purified by column chromatography on silica (1:1 hexanes and methylene chloride) followed by recrystallization from ethanol and chloroform (2:3) to give 5.32 g (64%) of the product as a slightly yellow solid [mp: 100-101°C (lit.[43] mp = 98-100°C)]. ^{1}H-NMR ($CDCl_3$): δ 6.92 (s, 1H), 3.98 (t, 2H), 3.71 (s, 2H), 1.80 (p, 2H), 1.43 (m, 2H), 1.28 (m, 16H), 0.89 (t, 3H). ^{13}C-NMR ($CDCl_3$): δ 150.25, 119.31, 118.06, 112.85, 69.24, 32.14, 29.88, 29.85, 29.82, 29.79, 29.59, 29.57, 29.47, 26.28, 22.91, 18.87, 14.34. IR (KBr cm^{-1}) 2916, 2849, 2245, 1513, 1464, 1426, 1393, 1340, 1262, 1222, 1143, 1070, 1043, 999, 963, 923, 872, 846, 801, 759, 721. HRMS: calcd for $C_{34}H_{56}N_2O_2$: 524.4342. Found: 524.4324. Anal. Calcd for $C_{34}H_{56}N_2O_2$: C, 77.81; H, 10.76; N, 5.34. Found: C, 77.62, H, 10.97; N, 5.06.

2,5-Bis(cyanomethyl)-1-methoxy-4-[(2-ethylhexyl)oxy]benzene (1b).[137] Same procedure as for the synthesis of 1,4-bis(cyanomethyl)-2,5-bis(dodecyloxy)benzene using sodium cyanide (8.71×10^{-1} g, 1.78×10^{-2} mol, 2.5 equiv.), 2,5-bis(bromomethyl)-1-methoxy-4-[(2-ethylhexyl)oxy]benzene (3.00 g, 7.11×10^{-3} mol) and anhydrous DMF (125 mL). The crude product was purified by column chromatography on silica (1:5 hexanes and methylene chloride) followed by recrystallization from hexanes to give 0.97 g (44%) of slightly yellow solid [mp: 80-82°C (lit.[137] mp = 91°C)]. ^{1}H-NMR ($CDCl_3$): δ 6.94 (s, 1H), 6.93 (s, 1H), 3.88 (d, 2H), 3.86 (s, 3H), 3.71 (s, 4H), 1.75 (m, 1H), 1.30-1.60 (m, 8H), 0.94 (m, 6H). IR (KBr cm^{-1}) 3054, 2959,

2933, 2874, 2248, 1513, 1466, 1421, 1406, 1318, 1231, 1195, 1187, 1107, 1036, 983, 915, 882, 844, 759. HRMS: calcd for $C_{19}H_{26}N_2O_2$: 314.1994. Found: 314.1994. Anal. Calcd for $C_{19}H_{26}N_2O_2$: C, 72.58; H, 8.33; N, 8.91. Found: C, 72.70, H, 8.40; N, 8.81.

Or same procedure as for the synthesis of 1,4-bis(cyanomethyl)-2,5-bis(dodecyl-oxy)benzene using sodium cyanide (10.23 g, 2.10×10^{-1} mol), 2,5-bis(chloromethyl)-1-methoxy-4-[(2-ethylhexyl)oxy]benzene (27.80 g, 8.35×10^{-2} mol) and anhydrous DMF (500 mL). Reaction stirred at 110°C for two days. After the workup, the crude product was purified by column chromatography on silica gel using methylene chloride/hexanes (5/1) for the elution and 12.00 g (46%) of slightly yellow solid were obtained. ^{1}H-NMR ($CDCl_3$): δ 6.94 (s, 1H), 6.93 (s, 1H), 3.88 (d, 2H), 3.86 (s, 3H), 3.71 (s, 4H), 1.75 (m, 1H), 1.30-1.60 (m, 8H), 0.94 (m, 6H). HRMS: calcd for $C_{19}H_{26}N_2O_2$: 314.1994. Found: 314.1967. Anal. Calcd for $C_{19}H_{26}N_2O_2$: C, 72.58; H, 8.33; N, 8.91. Found: C, 72.84, H, 8.75; N, 8.76.

1,4-Bis(cyanomethyl)-2-(3,7-dimethyloxy)-5-methoxybenzene (1c).[147] Same procedure as for the synthesis of 1,4-bis(cyanomethyl)-2,5-bis(dodecyloxy)benzene using sodium cyanide (4.00 g, 8.16×10^{-2} mol, 4.5 equiv.), 1,4-bischloromethyl-2-(3,7-dimethyloxy)-5-methoxy-benzene (6.54 g, 1.81×10^{-2} mol) and anhydrous DMF (250 mL). The crude product was purified by column chromatography on silica (hexanes and dichloromethane (1:4)) followed by recrystallization from hexanes to give 1.70 g (27 %) of slightly yellow solid [mp: 81-82˚C]. ^{1}H-NMR ($CDCl_3$): δ 6.93 (s, 2H), 4.02 (t, 2H), 3.86 (s, 3H), 3.71 (s, 4H), 1.84 (m, 1H), 1.50-1.70 (m, 5H), 1.10-1.40 (m, 4H), 0.96 (d, 3H), 0.88 (d, 6H). ^{13}C-NMR ($CDCl_3$): δ 150.72, 150.40, 119.36, 119.22, 118.0, 112.89, 112.0, 67.57, 56.34, 39.44, 37.49, 36.42, 30.12, 28.20, 24.9, 22.92, 22.82, 19.90, 18.88, 18.34. IR (KBr cm^{-1}) 3054, 2953, 2927, 2870, 2248, 1517, 1467, 1422, 1407, 1317, 1231, 1188, 1155, 1030, 975, 916, 882, 760, 734. HRMS: calcd for

$C_{21}H_{30}N_2O_2$: 342.2313. Found: 342.2307. Anal. Calcd for $C_{21}H_{30}N_2O_2$: C, 73.65; H, 8.83; N, 8.18. Found: C, 73.87, H, 8.88; N, 8.04.

3,3-Bis(bromomethyl)-3,4-dihydro-2*H*-thieno[3,4-*b*][1,4]-dioxepine [ProDOT($CH_2Br)_2$].[34] 3,4-Dimethoxythiophene (11.40 g, 6.61 × 10^{-2} mol), 2,2-bis(bromomethyl)-1,3-propanediol (42.52 g, 1.62 × 10^{-1} mol) and *p*-toluene-sulfonic acid (1.51 g, 7.92 × 10^{-3} mol) were dissolved in toluene (300 mL) in a 500 mL three-necked round bottom flask equipped with a Soxhlet condenser containing type 4 Å molecular sieves. The clear solution was refluxed for 24 h during which time the color turned green. Then it was cooled to room temperature, poured into deionized water and extracted with toluene. The organic layer was washed with brine and dried over $MgSO_4$. After filtration through a Büchner filter and solvent evaporation, a green solid was collected. The solid was purified by column chromatography on silica gel using CH_2Cl_2:hexanes (1:4) for the elution yielding 19.95 g (74%) of pure product. ^{1}H-NMR ($CDCl_3$): δ 6.51 (s, 1H), 4.11 (s, 2H), 3.62 (s, 2H). ^{13}C-NMR ($CDCl_3$): δ 148.86, 105.97, 74.36, 46.4, 34.62. Anal. Calcd for $C_9H_{10}Br_2O_2S$: C, 31.60; H, 2.95. Found: C, 31.59, H, 2.82.

3,3-Bis(hexyloxy)-3,4-dihydro-2*H*-thieno-[3,4-*b*][1,4]dioxepine [ProDOT($CH_2OC_6H_{13})_2$]. 1-Hexanol was refluxed overnight over magnesium turnings and distilled under reduced pressure (bp: 156°C at 760 mmHg). A 1 L 3 neck round bottom flask equipped with a condenser, filled with anhydrous DMF (400 mL), 1-hexanol (17.90 g, 1.76 × 10^{-1} mol) and sodium hydride (8.45 g, 3.52 × 10^{-1} mol) was heated overnight at 110°C. ProDOT($CH_2Br)_2$ (18.00 g, 52.63 × 10^{-2} mol) was added, and the reaction continued at 110°C for another 24 h, during which time the color turned brown. After completion, the solution was cooled to room temperature, deionized water was added, and the mixture extracted with diethyl

ether. The ether layer was washed with brine and dried over $MgSO_4$. After filtration through a Büchner funnel, the solvent was evaporated, and a brown oil was collected. The crude product was purified by column chromatography on silica using methylene chloride as elution solvent to give 14.00 g (69%) of the product as a slightly yellow oil. ^{1}H-NMR ($CDCl_3$): δ 6.45 (s, 1H), 4.02 (s, 2H), 3.49 (s, 2H), 3.41 (t, 2H), 1.54 (p, 2H), 1.29 (m, 6H), 0.90 (t, 3H). ^{13}C-NMR ($CDCl_3$): δ 149.93, 105.27, 73.97, 71.96, 69.79, 47.92, 31.88, 29.71, 26.02, 22.84, 14.27. HRMS: calcd for $C_{21}H_{36}O_4S$: 384.2334. Found: 384.2322.

3,3-Bis(2-ethylhexyloxymethyl)-3,4-dihydro-2*H*-thieno-[3,4-*b*][1,4]dioxepine [ProDOT($CH_2OEtHex)_2$].[34] 2-Ethyl-1-hexanol dried over calcium hydride for 2 h and distilled under reduced pressure (bp: 183-185°C at 760 mmHg). ProDOT($CH_2OEtHex)_2$ was synthesized according to the same procedure used for the synthesis of ProDOT($CH_2OC_6H_{13})_2$ with 2-ethyl-1-hexanol (2.85 g, 2.19×10^{-2} mol), sodium hydride (1.76 g, 60% in oil dispersion, 4.38×10^{-2} mol, 6 equiv.), anhydrous DMF (125 mL) and ProDOT($CH_2Br)_2$ (2.50 g, 7.30×10^{-2} mol). The crude product was purified by column chromatography on silica using methylene chloride as elution solvent to give 2.97 g (99%) of the pure product as a slightly yellow oil. ^{1}H-NMR ($CDCl_3$): δ 6.44 (s, 1H), 4.01 (s, 2H), 3.47 (s, 2H), 3.30 (s, 2H), 3.28 (d, 2H), 1.49 (m, 1H), 1.20-1.40 (m, 8H), 0.80-0.93 (m, 6H). ^{13}C-NMR ($CDCl_3$): δ 149.93, 105.14, 74.55, 74.01, 70.08, 48.11, 39.84, 30.90, 29.36, 24.23, 23.31, 14.32, 11.37. HRMS: calcd for $C_{25}H_{44}O_4S$: 440.2960. Found: 440.2968. Anal. Calcd for $C_{25}H_{44}O_4S$: C, 68.14; H, 10.06. Found: C, 71.19, H, 11.01.

3,3-Bis(hexyloxy)-3,4-dihydro-2*H*-thieno-[3,4-*b*][1,4]dioxepine-6,8-dicarbaldehyde [ProDOT-($CH_2OC_6H_{13})_2$-$(CHO)_2$] (2a). ProDOT($CH_2OC_6H_{13})_2$ (1.37 g, 3.98×10^{-3} mol) was dissolved in dry THF (40 mL) under nitrogen purge, and the solution was cooled to -78°C. *n*-Butyllithium (2.3 equiv., 9.15×10^{-3} mol) was added via syringe, and the solution warmed to 0°C

for 30 min and then cooled back to -78°C. Anhydrous DMF (1.5×10^{-2} mol, 3.8 equiv.) was added rapidly via syringe, and the solution warmed to room temperature and stirred for 1 hour. The solution was then poured into 3 M HCl and extracted with methylene chloride. The organic layer was washed with saturated $NaHCO_3$ and dried with $MgSO_4$. After filtration through a Büchner funnel, the solvent was evaporated, and a brown oil collected. The crude product was purified by column chromatography on silica using ethyl acetate/hexanes (1/3) yielding 0.817 g (51%) of product as a yellow oil. ^{1}H-NMR ($CDCl_3$): δ 9.98 (s, 1H), 4.19 (s, 2H), 3.46 (s, 2H), 3.37 (t, 2H), 1.56 (p, 2H), 1.23 (m, 6H), 0.82 (t, 3H). ^{13}C-NMR ($CDCl_3$): δ 182.22, 155.04, 128.21, 74.91, 72.07, 69.54, 47.78, 31.83, 29.65, 26.01, 22.84, 14.26. IR (KBr cm^{-1}) 3317, 2931, 2859, 2734, 2660, 1667, 1559, 1489, 1466, 1436, 1376, 1306, 1249, 1194, 1103, 1065, 925, 833, 760, 727, 694, 552. HRMS: calcd for $C_{23}H_{36}O_6S$: 440.2233. Found: 440.2236. Anal. Calcd for $C_{23}H_{36}O_6S$: C, 62.70; H, 8.24. Found: C, 63.06, H, 8.51.

3,3-Bis(2-ethylhexyloxymethyl)-3,4-dihydro-2*H*-thieno-[3,4-*b*][1,4]dioxepine-6,8-dicarbaldehyde [ProDOT-($CH_2OEtHex)_2$-$(CHO)_2$] (2b). Same procedure as for ProDOT-($CH_2OC_6H_{13})_2$-$(CHO)_2$ using ProDOT($CH_2OEtHex)_2$ (2.4 g, 5.44×10^{-3} mol), dry THF (40 mL), *n*-BuLi (2.3 equiv., 12.53×10^{-3} mol), dry DMF (3.7 equiv., 20.13×10^{-3} mol). Most of the impurities were removed from the crude product by column chromatography on silica (1:1, methylene chloride/hexanes); the product was then pushed out of the column with methylene chloride, decolorized with decolorizing carbon, and the rest of the impurities were removed by a second column chromatography on silica (1:2, ethyl acetate: hexanes) to yield 2.0 g (74%) of product as a yellow oil. ^{1}H-NMR ($CDCl_3$): δ 10.06 (s, 2H), 4.27 (s, 4H), 3.53 (s, 4H), 3.33 (d, 4H), 1.2-1.57 (m, 18H), 0.90 (m, 12H). ^{13}C-NMR ($CDCl_3$): δ 182.20, 155.04, 128.13, 74.99, 74.60, 47.92, 339.79, 30.84, 29.31, 24.2, 23.28, 14.31, 11.35. IR (KBr cm^{-1}) 3318, 2958, 2928,

2859, 2734, 2661, 1666, 1559, 1489, 1460, 1436, 1376, 1307, 1248, 1193, 1103, 1064, 917, 833, 760, 728, 694, 552. HRMS: calcd for $C_{27}H_{44}O_6S$: 496.2859. Found: 496.2859. Anal. Calcd for $C_{27}H_{44}O_6S$: C, 65.29; H, 8.93. Found: C, 65.47, H, 9.20.

PProDOT-OEtHex$_2$:CNPV-DDO. ProDOT-$(CH_2OEtHex)_2$-$(CHO)_2$ (0.5 g, 1×10^{-3} mol) and 1,4-bis(cyanomethyl)-2,5-bis(dodecyloxy)benzene (0.525 g, 1×10^{-3} mol) were dissolved in a mixture of dry THF (42 mL) and freshly distilled *t*-butanol (42 mL). Then, potassium *t*-butoxide (0.224 g, 2×10^{-3} mol) was added, and the solution heated to 70°C for 2 h. The color darkened progressively from yellow to blue to black. The solution was then cooled to room temperature and poured into ice cold methanol (600 mL) acidified with 1 mL of acetic acid. The resulting precipitate was isolated by filtration into a Soxhlet thimble and Soxhlet extracted for 48 h with methanol, 24 h with chloroform. The solvent was evaporated from the chloroform fraction and a blue solid collected (0.60 g, 61%). ^{1}H-NMR ($CDCl_3$, ppm): δ = 8.73 (b, 1H), 6.92 (b, 1H), 3.80-4.60 (bm, 6H), 3.20-3.80 (bm, 8H), 1.95 (b, 4H), 1.00-1.70 (bm, 34H), 0.92 (bm, 15H). IR (KBr cm^{-1}) 2958, 2924, 2854, 2205, 1640, 1574, 1512, 1475, 1448, 1378, 1282, 1181, 1142, 1069, 1026, 920, 861, 802. GPC analysis: M_n = 10,300, M_w = 14,800, PDI = 1.43. Anal. Calcd: C, 74.35; H, 10.06; N, 2.80; S, 3.20. Found: C, 64.87; H, 10.63; N, 2.11; S, 2.87.

PProDOT-OHex$_2$:CNPV-DDO. Same procedure as for the synthesis of PProDOT-OEtHex$_2$:CNPV-DDO using ProDOT-$(CH_2OC_6H_{13})_2$-$(CHO)_2$ (0.427 g, 9.7×10^{-4} mol), 1,4-bis(cyanomethyl)-2,5-bis(dodecyloxy)benzene (0.509 g, 9.7×10^{-4} mol), dry THF (39 mL), *t*-butanol (39 mL) and potassium *t*-butoxide (220 mg, 1.96×10^{-3} mol). During the polymerization, the solution color changed from yellow to black with a purple tint. After purification by Soxhlet extraction as above, 0.66 g (77%) of blue solid were collected. ^{1}H-NMR ($CDCl_3$, ppm): δ = 8.70 (b, 1H), 6.90 (b, 1H), 3.80-4.70 (bm, 6H), 3.20-3.70 (bm, 8H), 1.93 (b, 2H), 1.00-1.70 (bm,

34H), 0.89 (bm, 9H). IR (KBr cm^{-1}) 2961, 2923, 2853, 2204, 1653, 1573, 1512, 1476, 1448, 1382, 1260, 1092, 1074, 1020, 862, 800, 706. GPC analysis: M_n = 13,100, M_w = 17,500, PDI = 1.34. Anal. Calcd: C, 73.68; H, 9.81; N, 2.96; S, 3.39. Found: C, 51.56; H, 9.56; N, 1.40; S, 1.74.

PProDOT-OHex$_2$:CNPV-MEH. Same procedure as for the synthesis of PProDOT-OEtHex$_2$:CNPV-DDO using ProDOT-$(CH_2OC_6H_{13})_2$-$(CHO)_2$ (0.41 g, 9.3×10^{-4} mol), 2,5-bis(cyanomethyl)-1-methoxy-4-[(2-ethylhexyl)oxy]benzene (0.32 g, 9.3×10^{-4} mol), THF (35 mL), *t*-butanol (35 mL) and potassium *t*-butoxide (210 mg, 1.88×10^{-3} mol). During the polymerization, the solution color changed from yellow to black. After purification by Soxhlet extraction as above, 0.286 g (41%) of purple solid were collected. ^{1}H-NMR ($CDCl_3$, ppm): δ = 8.10-8.40 (b, 2H), 6.80-6.90 (b, 2H), 3.95-4.40 (bm, 9H), 3.45-3.95 (bm, 8H), 1.10-1.70 (bm, 25H), 0.89 (bm, 12H). IR (KBr cm^{-1}) 2955, 2925, 2858, 2205, 1647, 1578, 1505, 1476, 1445, 1378, 1281, 1261, 1217, 1100, 1067, 918, 868, 801. GPC analysis: M_n = 8,700, M_w = 11,400, PDI = 1.31. Anal. Calcd: C, 70.26; H, 8.50; N, 3.81; S, 4.36. Found: C, 54.10; H, 7.60; N, 2.30; S, 3.04.

PProDOT-OHex$_2$:CNPV-MDMO. Same procedure as for the synthesis of PProDOT-OEtHex$_2$:CNPV-DDO using ProDOT-$(CH_2OC_6H_{13})_2$-$(CHO)_2$ (0.45 g, 1.02×10^{-3} mol), 1,4-bis(cyanomethyl)-2-(3,7-dimethyloxy)-5-methoxybenzene (0.321 g, 1.02×10^{-3} mol), THF (35 mL), *t*-butanol (35 mL) and potassium *t*-butoxide (230 mg, 2.05×10^{-3} mol). During the polymerization, the solution color changed from yellow to black with a purple tint. After purification by Soxhlet extraction as above, 0.33 g (45%) of purple solid were collected. ^{1}H-NMR ($CDCl_3$, ppm): δ = 8.10-8.40 (b, 2H), 6.90 (b, 2H), 3.90-4.45 (bm, 9H), 3.45-3.90 (bm, 8H), 1.20-1.88 (bm, 26H), 0.90 (bm, 12H). IR (KBr cm^{-1}) 2959, 2920, 2851, 2204, 1720, 1646, 1573, 1506, 1476, 1446, 1415, 1261, 1095, 1068, 1025, 862, 801. GPC analysis: M_n = 23,700,

M_w = 31,100, PDI = 1.31. Anal. Calcd: C, 70.83; H, 8.72; N, 3.67; S, 4.20. Found: C, 62.44; H, 8.14; N, 2.97; S, 3.33.

CHAPTER 5
POLYPROPYLENEDIOXYTHIOPHENE POLYELECTROLYTES

5.1 Introduction

Incorporation of anionic or cationic functionality into a conjugated polymer yields a material that possesses the beneficial properties of a conjugated polymer along with solubility in polar solvents and possibly water.[148] It also allows the polymer to be complexed with other polymers of the opposite charge,[149] and consequently allows the building of multilayer films by the layer-by-layer thin-film processing technique.[150,151] This technique is an environmentally friendly method producing highly uniform multilayer films, with reproducible and controlled thicknesses and morphologies. Conjugated polyelectrolytes (CPEs) are of particular interest in solution-processed multilayer PLED devices. In such systems it is important to separate different functions such as charge injection, charge transport, and light emission. The multilayer deposition of conjugated polymers processed from organic solutions, and capable of accomplishing these functions, is difficult to achieve because of dissolution and mixing of the subsequently deposited layers. Polymers which have an incompatible solubility with the emissive material can circumvent that problem.[152-154] The most famous example is PEDOT-Poly(styrene sulfonate) (PEDOT-PSS) which is processed from water and successfully used as a hole transport layer in multilayer PLEDs.[155] The interest in CPEs for organic photovoltaic devices is more recent than for LEDs, and one of the most relevant examples would be the layer-by-layer fabrication of photovoltaic cells based on the poly(phenylene ethynylene) anionic electron donors and water-soluble cationic fullerene derivatives acceptors.[156] Fluorescent CPEs which exhibit very high sensitivity to oppositely charged molecular quenchers find also application in sensors.[157-160]

A broad range of CPEs has been reported in the literature, with most of them belonging to the families of poly(*para*-phenylene)s (PPPs), poly(phenylene vinylene)s (PPVs), or poly(phenylene ethynylene)s (PPEs).[148] Researchers have worked around the backbone of these polymers and introduced a variety of ionic side chains carrying sulfonates (SO_3^-), carboxylates (CO_2^-), phosphonates (PO_3^-) and ammoniums (NR_3^+). This allowed access to absorption maxima varying between about 215 nm[161] and 484 nm[162] and emission maxima varying between 408 nm[163] and 593 nm in polar solvents.[157] However higher wavelength regions have been more difficult to reach and to circumvent that problem more complicated structures and syntheses leading to narrower band gap CPEs are currently being investigated, with the ultimate goal of discovering a red-emitting water soluble conjugated polymer.[164] In order to shift the spectroscopic properties to the red region, we decided to investigate CPEs based on PProDOTs, which usually have solution absorptions centered in the 500-600 nm region and emissions centered in the 600-700 nm region.[34,165,166]

The synthesis of PProDOTs soluble in polar solvents has recently been investigated by the Reynolds group with the design of PProDOTs with polar functional groups such as oligoethers, ethers, alcohols, and esters.[165] However no cationic or anionic substituted PProDOTs have been reported as yet. In our quest for more red-shifted conjugated polyelectrolytes, we decided to synthesize homopolymers of amino-functionalized ProDOTs which can be fully characterized and then quaternized to the ammonium salt after a post-polymerization treatment. The structures of the targeted polymers are displayed in Figure 5-1. Alkoxy chains end-capped with tertiary amines were used for the substitution. These chains were chosen with reasonable lengths to induce solubility in organic solvents for polymer characterization, while not hindering the solubility in polar or aqueous systems after the post-polymerization treatment.

One of the designated polymers, poly[3,3'-(3,4-dihydro-2*H*-thieno[3,4-*b*][1,4]dioxepine-3,3-diyl)bis(methylene)bis(oxy)bis(*N*,*N*,*N*-trimethylpropan-1-aminium)] (PProDOT-NMe_3^+), carries amines substituted with methyl groups (Figure 5-1a). The other designated polymer, poly[*N*,*N*'-(2,2'-(3,4-dihydro-2*H*-thieno[3,4-*b*][1,4]dioxepine-3,3-diyl)bis(methylene)bis(oxy)bis(ethane-2,1-diyl))bis(*N*-isopropyl-*N*-methylpropan-2-aminium)] (PProDOT-$NMe(Isop)_2^+$), carries amines with disorder inducing isopropyl groups and exhibits a more branched and bulky appearance (Figure 5-1b): it was chosen to enhance the solubility in organic solvents.

The synthesis of the amino-substituted ProDOT monomers is described in section 5.2. The synthesis and macromolecular characterization of the neutral polymers are detailed in section 5.3. Sections 5.4 and 5.5 cover the redox, spectroelectrochemical, and electrochromic properties of these materials. Finally, the post-polymerization ionization of the polymers and their properties are developed in section 5.6.

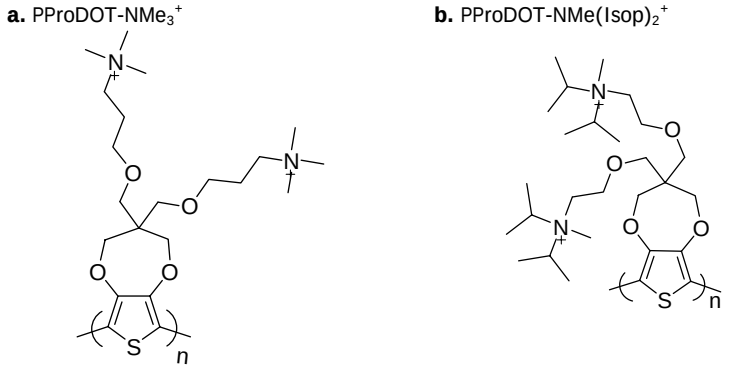

Figure 5-1. Structures of investigated amino-functionalized PProDOTs.

5.2 Monomer Synthesis and Characterization

The amino-substituted ProDOT monomers were synthesized by nucleophilic substitution of commercially available amino-alcohols (dimethylamino-1-propanol and 2-(diisopropylamino)ethanol) on the key ProDOT($CH_2Br)_2$ molecule in the presence of sodium hydride as illustrated in Figure 5-2. The monomers were particularly difficult to purify due to the

presence of the highly polar amine groups which tend to stick on neutral silica gel and make the separation from the monosubstituted products difficult. For these stubborn amines, elution had to be accomplished with 10 percent in volume of ammonium hydroxide (14.8 *N*) in a mixture of methanol and CH_2Cl_2 (making sure to not use more than 10 percent of methanol in order to not dissolve the silica gel), and in the case of ProDOT-NMe_2 basic alumina had to be used instead of silica gel. Due to these purification difficulties, the pure monomers were obtained in low yields (*ca.* 20-30 %). The monomers were characterized by ^{1}H-NMR, ^{13}C-NMR, elemental analysis, HRMS, and UV-Vis spectroscopy. They absorb in the UV, with absorption maxima in chloroform at 239 nm and 238 nm for PProDOT-NMe_2 and ProDOT-$NIsop_2$ respectively. The varying side chains do not lead to any observable differences in the monomer's optical properties.

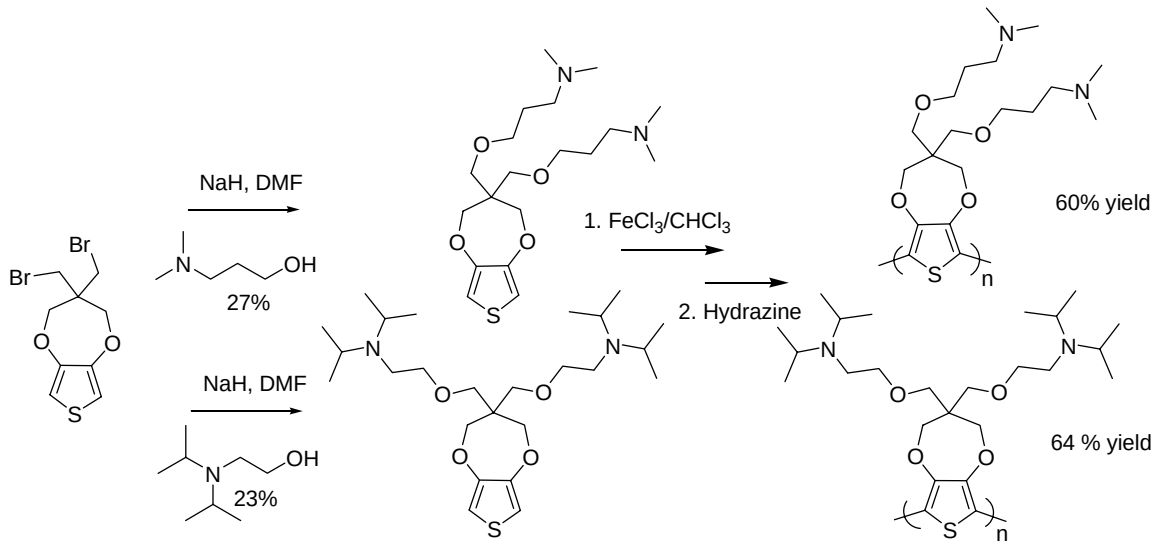

Figure 5-2. Synthesis of amino-substituted ProDOT monomers and polymers.

5.3 Polymer Synthesis and Characterization

The purification issues and low yields precluded extensive chemistry on the amino-substituted ProDOT unit and particularly the preparation of the dibromo-derivative for polymerization via GriM. Consequently, the polymerization of the amino-substituted ProDOT

monomers was accomplished by oxidative coupling using $FeCl_3$ as the oxidant as illustrated in Figure 5-2. The oxidized polymers were washed 4-5 times with methanol to remove the ferric impurities. The neutral polymers were obtained after dedoping with hydrazine monohydrate. Further purification was accomplished either by extraction with deionized water or Soxhlet extraction with methanol. Finally, the polymers were dissolved by Soxhlet extraction with chloroform, and isolated by solvent evaporation. Approximately one third of the polymer samples, probably high molecular weight material, was insoluble during chloroform extraction and was not further characterized. The isolated polymers are bright red solids, which once dried strongly aggregate and are difficult to re-dissolve. PProDOT-NMe_2 exhibits limited solubility in THF (~ 70-80%) and chloroform (~ 60%), while PProDOT-$NIsop_2$ is almost fully soluble in chloroform (~ 90%) and partially soluble in THF (~ 70-80%). The extent of solubility was estimated by dissolving a known amount of polymer in a certain solvent, then filtering the polymer solution with 45 μm filters, and finally weighting the amount of polymer recovered after filtration and solvent evaporation. PProDOT-$NIsop_2$ has a higher degree of solubility due to the presence of more disorder inducing branches which gives rise to less aggregation. Neither polymer is soluble in toluene and acidic solutions (pH = 1-2).

The polymers ^{1}H-NMR spectra showed broad signals and the signals of the ProDOT proton end-group peaks essentially disappeared as expected with the polymerizations which proceeded to a substantial degree (assuming the polymerization to be terminated by protons). This is illustrated in Figure 5-3 with the comparison between the ^{1}H-NMR spectra of ProDOT-$NIsop_2$ and PProDOT-$NIsop_2$. The signal of the monomer ProDOT protons, observed at 6.45 ppm in Figure 5-3a, disappeared in the polymer spectrum (Figure 5-3b), and a small new peak was observed at 6.19 ppm for PProDOT-$N(Isop)_2$, which is attributed to the polymer proton end-

groups. Looking at the integration of these peaks and making an assumption that each chain is terminated on both ends by hydrogen atoms, this suggests an average degree of polymerization of about 27. However this value is an upper limit as there are likely other chain ends such as chlorines (vide post). For PProDOT-NMe_2 no oligomeric or polymeric proton end-groups could be detected.

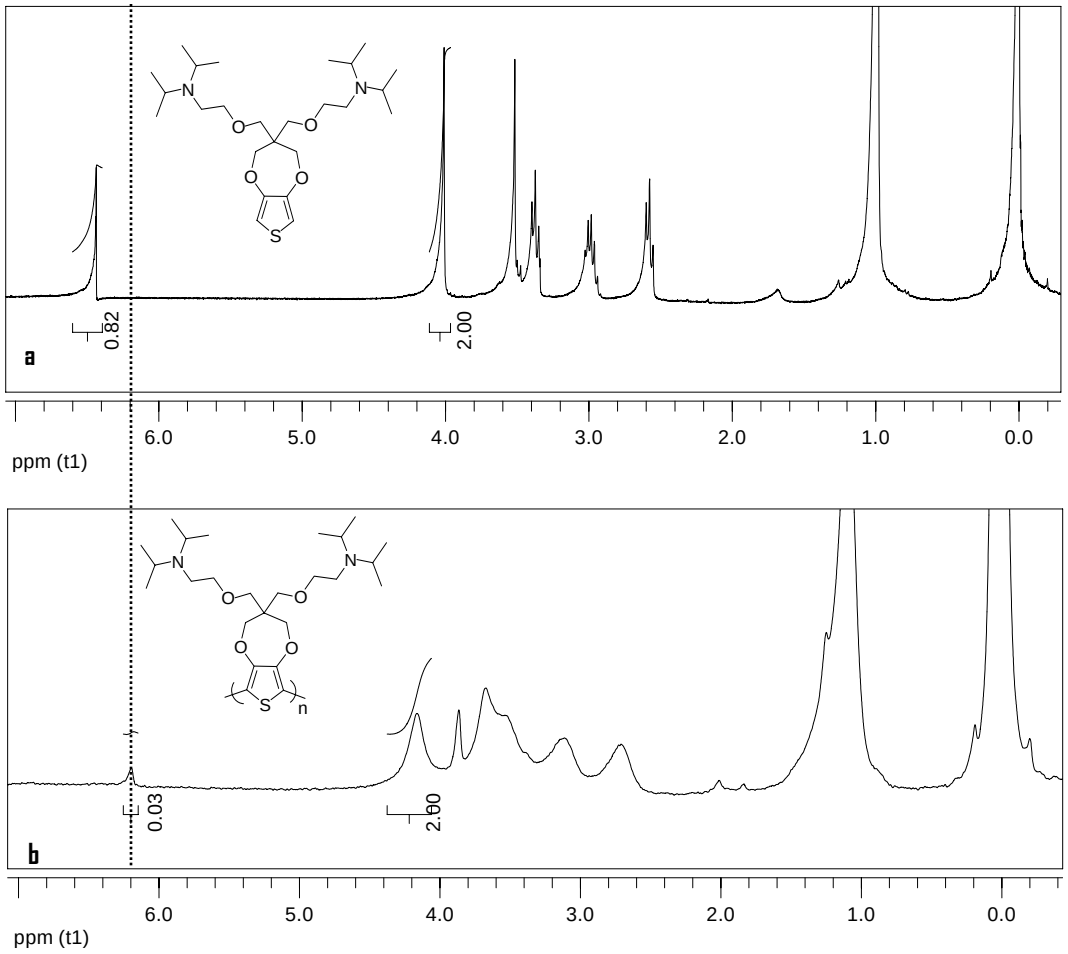

Figure 5-3. ^{1}H-NMR spectra. (a) ^{1}H-NMR spectrum of ProDOT-$NIsop_2$; (b) ^{1}H-NMR spectrum of PProDOT-$NIsop_2$.

It was not possible to estimate the polymers molecular weights by GPC (unsuccessful attempts were done in THF and chloroform, at room temperature and at elevated temperature (40°C)). Even PProDOT-$NIsop_2$ which is soluble in chloroform did not give any signal by GPC. The polymer solubility in these solvent and temperature conditions is probably too poor and the

polymers get stuck onto the GPC column. This is surprising since the molecular weights of a variety of amino-functionalized conjugated polymers have been estimated by GPC.[167-169] In the examples where the instrumental details were specified, it even appeared that the GPC columns were the same as the ones used here.

The polymers elemental analyses showed relatively large amounts of iron and chlorine trapped inside the polymers, especially in the case of PProDOT-NIsop$_2$. The analysis of PProDOT-NMe$_2$ showed the presence of one iron per 36 sulfurs, and of one chlorine per 10 sulfurs, and the analysis of PProDOT-NIsop$_2$ showed the presence of one iron per 13 sulfurs, and of one chlorine per 2 sulfurs. This is probably due to the highly aggregated morphology of the polymers which prevented efficient washing of these impurities. It is interesting to note that PProDOT-NMe$_2$ was washed both with deionized water and methanol, whereas PProDOT-NIsop$_2$ was only washed with methanol. Consequently there is also a possibility that water allowed a more efficient washing of the ferric impurities. This will be verified in the near-future on a scale-up polymerization of PProDOT-NIsop$_2$. It should be noted that the carbon analyses were somewhat lower than expected. This might be explained by the fact that highly aromatic polymers are difficult to fully combust and some carbonization may have occurred during the measurements.

As structure proof, the polymers were characterized by MALDI mass spectrometry using a dithranol matrix. The spacing between the peaks corresponds to ~384 amu for PProDOT-NMe$_2$, and ~469 amu for PProDOT-NIsop$_2$, which correlates well with the calculated molecular weight of the repeat unit of the polymer. Poorly soluble polymers pose particular challenges to analysis by MALDI because they do not readily form the mixed polymer/matrix crystals. In the case of PProDOT-NMe$_2$, the MALDI measurements were probably affected by the limited solubility of

the polymer because they showed poor peak resolution and intensity as illustrated in Figure 5-4 (each "peak" is a cluster of peaks that have similar masses). For this reason it was not possible to identify the end-group peaks. In the MALDI spectrum of PProDOT-NIsop$_2$ displayed in Figure 5-5, it seems that the masses of the main series match better with oligomers having chlorine end-groups than oligomers having hydrogen end-groups. For example, if we take the oligomer series with *m/z* at 3,821, we get *m/z* of about 3,819 after removal of two hydrogens and *m/z* of about 3,750 after removal of two chlorines. It corresponds to 8.1 repeat units in the first case (hydrogen end-groups) and to exactly 8 repeat units in the second case (chlorine end-groups). This could be an explanation for the high level of chlorine atoms observed in the polymer's elemental analysis. Since only one reference[170] could be found reporting such a phenomenon, a deeper investigation will be accomplished on a new sample of PProDOT-NIsop$_2$ thoroughly washed with a methanol solution containing 1,10-phenanthroline. Phenanthroline has the ability to form chelates with iron and is often used to remove ferric impurities from polymers. Meanwhile, the mechanism involving chlorine ions, resulting from the reduction of Fe(III) to Fe(II) upon polymer oxidation, has been speculated and is displayed in Figure 5-6. The observation of "peaks" (or clusters) up to *m/z* 7,000 (18 repeat units) for PProDOT-NMe$_2$, and up to *m/z* 4,760 (10 repeat units) for PProDOT-NIsop$_2$ in the MALDI results proves that the materials are at least oligomers.

The thermal stability of the polymers (previously dried under vacuum for a few days) was studied by thermogravimetric analysis (TGA) in a nitrogen atmosphere using a 20°C min^{-1} temperature ramp from 50°C to 900°C (Figure 5-7). The polymer degradation seemed to occur in two steps, the first one being the thermal degradation of the amino chains (from ~ 280°C up to ~ 380°C for PProDOT-NIsop$_2$, and from ~ 210°C up to ~ 265°C for PProDOT-NMe$_2$), and the

second one being the backbone degradation (from ~ 380°C to 900° C for PProDOT-NIsop$_2$ and from ~ 265°C to 650° C for PProDOT-NMe$_2$). At 900°C less than 12% of materials remained.

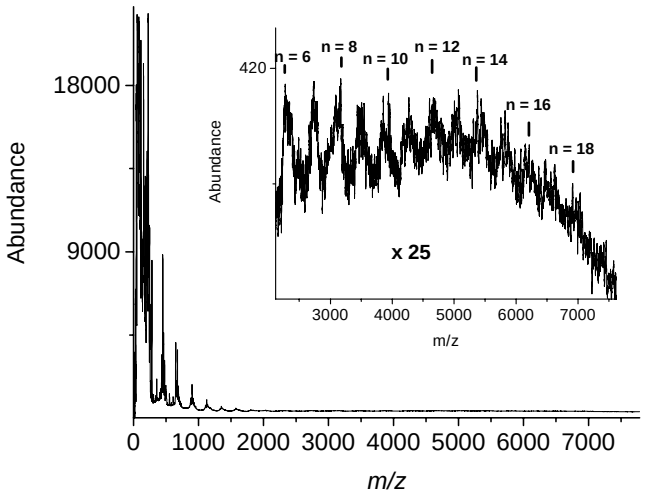

Figure 5-4. MALDI-MS of PProDOT-NMe$_2$. Dithranol was used as the matrix and the peaks up to *m/z* 2000 are dithranol matrix clusters.

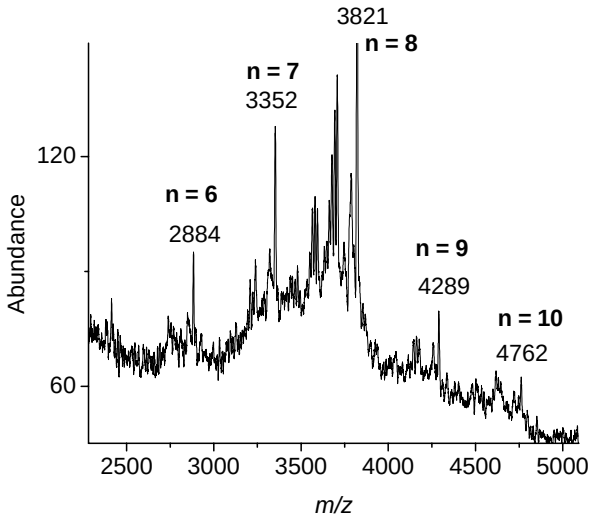

Figure 5-5. MALDI MS of PProDOT-NIsop$_2$. Dithranol was used as the matrix. The peaks up to *m/z* 2000 are not displayed since they were hidden by dithranol matrix clusters.

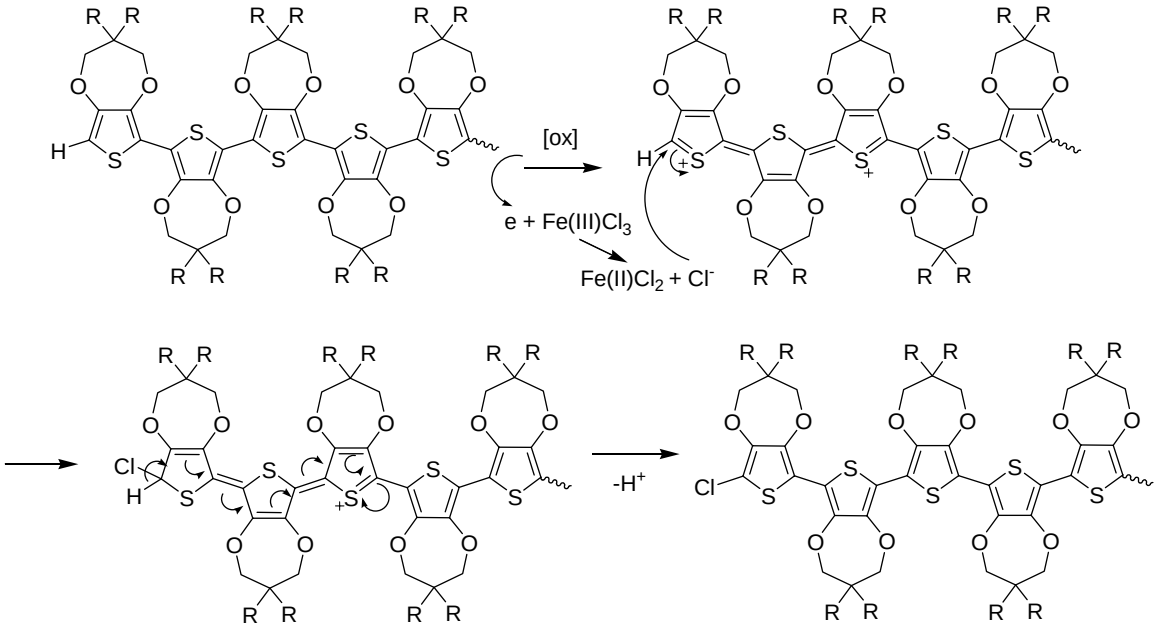

Figure 5-6. Speculated mechanism of the chlorine termination of PProDOT-NIsop$_2$ growing chains.

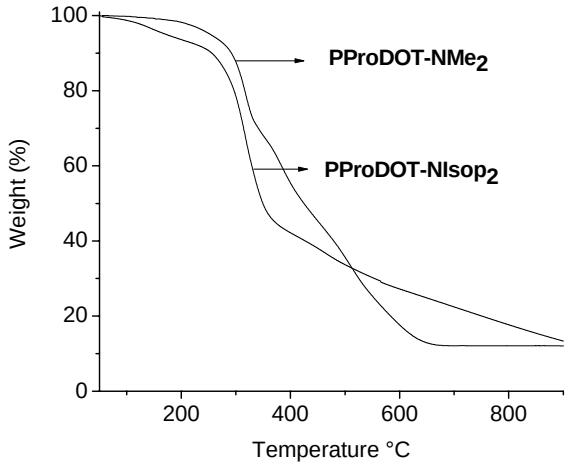

Figure 5-7. Thermogravimetric analysis of the amino-functionalized PProDOTs in a nitrogen atmosphere.

Figures 5-8a and 5-8b show the UV-Vis absorption and photoluminescence of the polymers in chloroform. They absorb over a broad spectral range (*ca.* 450-620 nm) and their solutions are purple-pink. The absorption maximum (λ_{abs}) of PProDOT-NIsop$_2$ is a little bit blue-shifted (525 nm) compared to the absorption maximum of PProDOT-NMe$_2$ (536 nm) due to the

increased degree of branching which creates more disorder and decreases the conjugation length. The polymers emit in the red and near-IR region with an emission maximum (λ_{em}) at 616 nm for PProDOT-NMe_2, and at 618 nm for PProDOT-$NIsop_2$. The UV-Vis absorption and photoluminescence behavior of the polymers is comparable to what was observed for the previously reported ester-substituted PProDOT family, with for instance an average 20 repeat units sample of PProDOT($CH_2OC(O)C_6H_{13})_2$ (molecular weight estimated by GPC) exhibiting a λ_{abs} of 535 nm and a λ_{em} of 604 nm in toluene.[165] The fluorescence quantum yields were evaluated at 19% for PProDOT-NMe_2 and 21 % for PProDOT-$NIsop_2$ (Cresyl violet perchlorate standard; $\Phi = 0.54$).[171] The polymer solutions were filtered through 0.45 μm filters prior to the fluorescence measurements, in order to remove the small amounts of non-solubilized aggregates which could hinder the fluorescence. It is also worth noting that the presence of iron impurities might have affected the PL efficiencies.

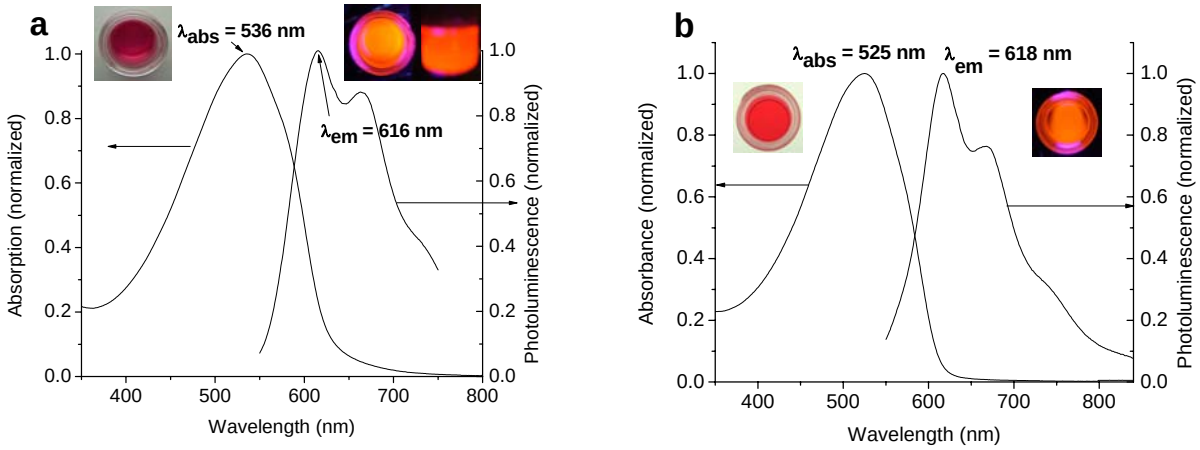

Figure 5-8. UV-vis absorption and photoluminescence spectra of neutral amino-functionalized PProDOTs. (a) PProDOT-NMe_2 in chloroform, (b) PProDOT-$NIsop_2$ in chloroform. In each spectrum, the left photograph represents the color of the solution under visible light and the right photograph represents the photoluminescence of the solution irradiated by UV-light.

5.4 Polymer Spectroelectrochemistry and Electrochemistry

Thin-films (~ 150 nm thick) of the amino-substituted ProDOT polymers were spray-cast from chloroform solutions (3-5 mg mL^{-1}) onto ITO coated glass electrodes, and studied by spectroelectrochemistry as illustrated in Figures 5-9a and 5-9b. The polymer films are pink-purple in the neutral state with PProDOT-NMe_2 exhibiting an absorption maximum at 547 nm, whereas PProDOT-$NIsop_2$ exhibits an absorption maximum at 538 nm. Band-gaps of ~ 1.9 for PProDOT-$NIsop_2$ and ~ 2.0 eV for PProDOT-NMe_2 were determined from the onset of the π to π^* transition in the neutral spectra. The spectral changes upon oxidation were recorded in 0.1 M TBAP/PC, with the potential being stepped from -0.3 V to +0.8 V every 0.05 V for PProDOT-NMe_2, and from -0.38 V to +0.92 V every 0.05 V for PProDOT-$NIsop_2$. The onsets of oxidation occur at about -0.05 V for PProDOT-NMe_2 and -0.03 V for PProDOT-$NIsop_2$. As the oxidation goes, the π-π^* transition of the neutral state disappears and polaron and bipolaron transitions appear in the 600-1500 nm region changing the films to a highly transmissive clear appearance. Such behavior is typical of PProDOTs and is one of the reasons why PProDOTs are so interesting for electrochemical applications.[34,165] Similar color changes (from red to clear) have also been reported for poly(3,4-ethylenedioxypyrrole)s (PEDOPs).[172] It is important to specify that the color switching was only reversible for about 2-3 cycles, the polymer falling of the electrode with further redox cycling.

The polymers were deposited by drop-casting on Pt button electrodes and their redox properties were recorded by CV and DPV, in 0.1 M TBAP in PC. The dedoping of the oxidized polymer was difficult to observe because the oxidized polymer dissolved in the electrolyte solution, and after only one cycle the signal almost completely disappeared. This phenomenon had been observed on ester- and alcohol-substituted PProDOTs;[165] changing the solvent used for

the electrolyte preparation did not solve the problem (unsuccessful attempts were done using ACN, benzonitrile, and water), neither did the replacement of the Pt button electrode by a gold electrode. DPV measurements done on thinner films were more sensitive and allowed capturing the reduction potential of the oxidized polymers as shown in Figures 5-10a and 5-10b. It is important to note that the oxidation and reduction potentials observed by DPV are not accurate since no redox cycling could be performed, previous to recording the data, for breaking in the polymer film. The onset of oxidation of PProDOT-NMe_2 is found around -0.07 V, which matches quite well with the onset of oxidation observed by spectroelectrochemistry, and an $E_{1/2}$ value of 0.13 V has been determined by DPV. An onset of oxidation of ~ 0.08 V and an $E_{1/2}$ of 0.35 V have been determined by DPV for PProDOT-$NIsop_2$. This $E_{1/2}$ value is quite bigger than the value found for PProDOT-NMe_2 and the difference might be explained by the bulkier chains on PProDOT-$NIsop_2$ which inhibit the fast movement of counter ions. However no definitive conclusion will be given since we do not know to what extent these values can be trusted, as explained before. The solubility of the polymers in the oxidized state does not make these materials good candidates for absorptive/transmissive electrochromism.

5.5 Colorimetry

Thin-films of the amino-substituted PProDOTs were deposited on ITO by spray-casting from 5 mg mL^{-1} chloroform solutions and were analyzed by in-situ colorimetric analysis. The relative luminance was measured as the neutral polymers were progressively oxidized and the luminance changes confirmed the positioning of the onsets of oxidation observed by spectroelectrochemistry. It should be noted that in correlation with the electrochemical results this would not be reversible. As illustrated in Figure 5-11a for PProDOT-NMe_2, oxidation started at -0.05 V, and there was a luminance change of ~ 35% in the small -0.05 V – 0.1 V potential

window. A luminance change of ~ 25% was observed for PProDOT-NIsop$_2$ between the onset of oxidation at ~ 0.02 V and 0.20 V (Figure 5-11b).

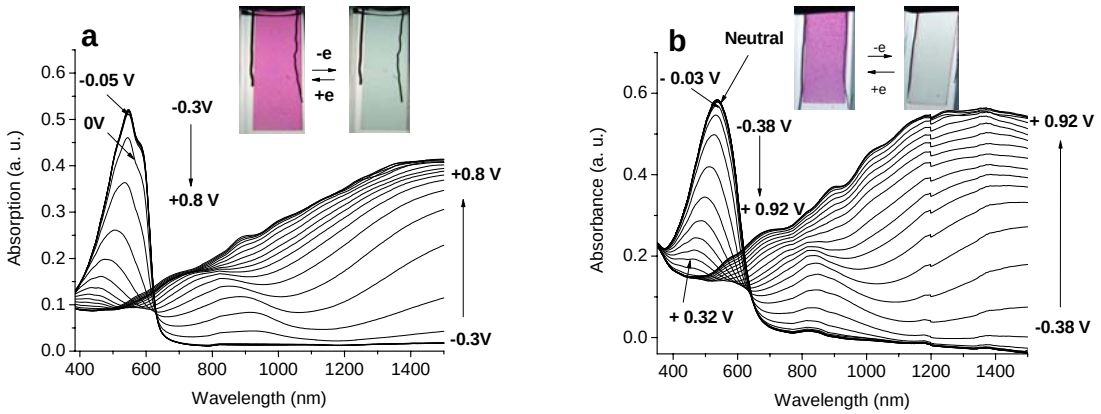

Figure 5-9. Spectroelectrochemisty of thin-films of the neutral amino-functionalized PProDOTs. (a) PProDOT-NMe$_2$ and (b) PProDOT-NIsop$_2$. The polymer films were prepared by spray-casting chloroform solutions of the polymers (3-5 mg mL^{-1}) onto ITO coated glass. The spectral changes were recorded in 0.1 M TBAP/PC and all potentials are reported vs Fc/Fc$^+$. The potential was increased in 50 mV steps. The photographs represent the film colors in the neutral state (left) and after oxidation (right).

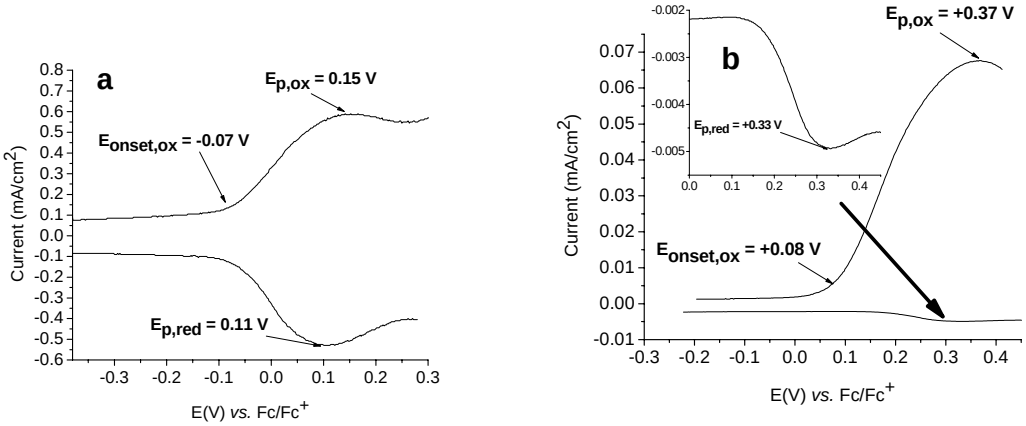

Figure 5-10. Differential pulse voltammetry of amino-substituted PProDOTs. (a) DPV of PProDOT-NMe$_2$, (b) DPV of PProDOT-NIsop$_2$. Measurements were performed on a 0.02 cm^2 Pt button working electrode in 0.1 M TBAP/PC with a Pt foil counter electrode and a silver wire pseudo reference electrode calibrated vs Fc/Fc$^+$.

The L*a*b* values of the colors were also determined to allow color matching. For PProDOT-NMe_2 in the neutral purple-pink state L = 66, a = 34, b = -15, and in the fully oxidized transparent state L = 87, a = -4 and b = -4. For PProDOT-$NIsop_2$ in the neutral violet state L = 72, a = 27, b = -7, and in the fully oxidized transparent state L = 88, a = 2, and b = 2.

The available color states were also tracked using the *xy* chromaticity diagrams shown in Figures 5-12a and 5-12b. Note that for clarity, these chromaticity diagrams are a 10 x magnification of the region of interest of the full *xy* chromaticity diagram displayed in Chapter 2. As the potential was increased and the polymers were doped the *y* coordinate increased and the *x* coordinate decreased after being stable during the beginning of oxidation. The abrupt color changes which occurred between -0.05 V and 0.10 V for PProDOT-NMe_2 and between 0.02 V and 0.20 V for PProDOT-$NIsop_2$, and which were observed on the luminance spectra in Figures 5-11a and 5-11b, can also be clearly seen on the xy chromaticity diagram by a large change in the *xy* coordinates between these potentials.

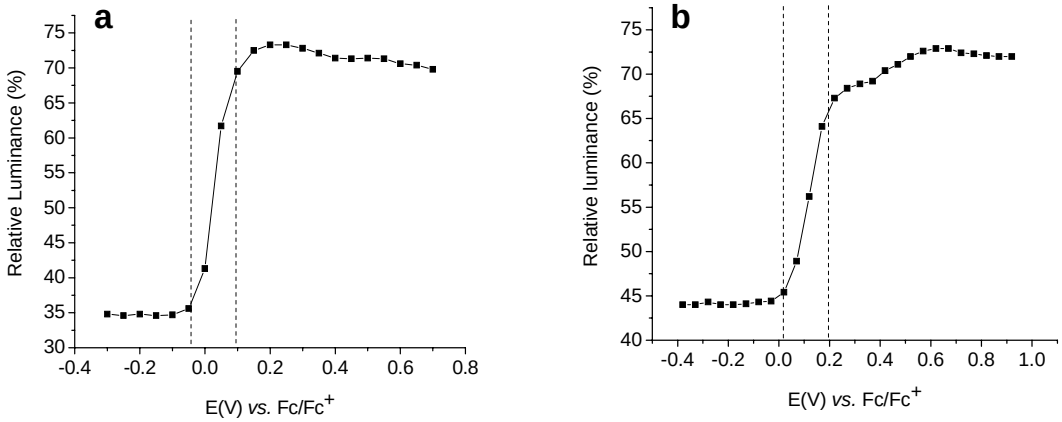

Figure 5-11. Relative luminance (%) versus applied potential for amino-substituted PProDOTs. (a) for PProDOT-NMe_2 and (b) for PProDOT-$NIsop_2$. The films were prepared by spray-casting chloroform solutions of the polymers (5 mg mL^{-1}) onto ITO. The measurements were performed in 0.1 M TBAP/PC and are reported vs. Fc/Fc^+. The potential was increased in 50 mV steps.

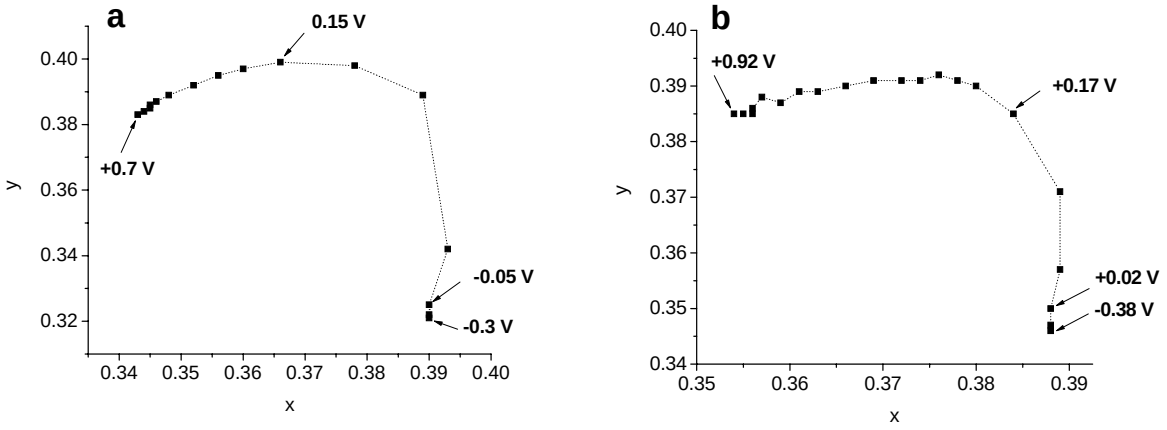

Figure 5-12. CIE 1931 *xy* chromaticity diagram of amino-substituted PProDOTs. Circles linked by a dotted line represent the color track for thin films of (a) PProDOT-NMe_2 and (b) PProDOT-$NIsop_2$ which go from pink-violet colors to clear. All potentials are reported vs Fc/Fc^+. The potential was increased in 50 mV steps.

5.6 Quaternization of the Amino-substituted PProDOTs

The ionisation of PProDOT-NMe_2 and PProDOT-$NIsop_2$ was accomplished by reaction of the tertiary amines with the iodomethane methylating agent as previously reported for polymers substituted with amines (Figure 5-13).[167,173] The quaternization was run at room temperature for 2 days in THF or $CHCl_3$. The ionic polymers are violet solids which are both well solvated in polar aprotic solvents such as dimethylsulfoxide (DMSO) and also *N*,*N*-dimethylformamide (DMF). The polymers were exposed to a variety of other solvents at room temperature to evaluate their solubility properties and the results are summarized in Table 5-1. PProDOT-NMe_3^+ is interestingly moderately soluble in water. The higher degree of branching of PProDOT-$NIsop_2$ allowed better solubility, and easier manipulation and characterization of the neutral polymer, but as opposed to PProDOT-NMe_3^+, the hydrocarbon chains are too large to allow solubility of the quaternized derivative in water.

It was not possible to give a detailed ^{1}H-NMR description (peak position and integration) of the polymers since most of the peaks were overlapped by a broad water peak which shows up at 3.33 ppm in DMSO. However, the effective removal of the excess of methyl iodide was confirmed by the disappearance of the MeI ^{1}H-NMR peak at 2.21 ppm. The presence of a singlet at 3.09 ppm in the ^{1}H-NMR spectrum of PProDOT-NMe(Isop)$_2^+$ proved that a certain amount of MeI effectively reacted with the amines. Iodine elemental analysis provides one method of determining the quaternization efficiency of the reaction between the neutral polymers and MeI. The N/I ratio determined by elemental analysis indicates quaternization of approximately 91% of the available amine sites of PProDOT-NMe$_3^+$, and of about 98% of the available amine sites of PProDOT-NMe(Isop)$_2^+$.

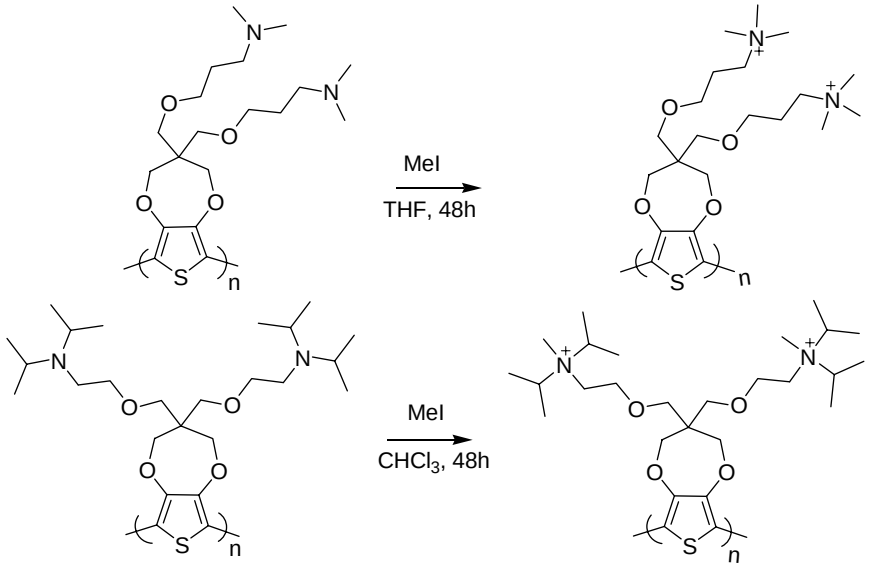

Figure 5-13. Quaternization of amino-substituted PProDOTs using MeI.

Table 5-1. Solubility of ionic amino-substituted PProDOTs in various solvents at room temperature.

Polymer	DMSO	water	methanol	ethanol	acetone	acetonitrile	$CHCl_3$	DMF
PProDOT-NMe$_3^+$	xxxx	xxx	x	0	0	0	0	xxx
PProDOT-NMe(Isop)$_2^+$	xxxx	0	xx	x	0	xx	x	xxx

0 = insoluble; x = very slightly soluble; xx = slightly soluble; xxx = moderately soluble; xxxx = very soluble.

Figures 5-14a and 5-15a show the UV-Vis absorption and photoluminescence of PProDOT-NMe_3^+ and PProDOT-$NMe(Isop)_2^+$ in DMSO respectively. The solutions are pink-purple, as illustrated by the photographs, with absorption maxima at 540 nm for PProDOT-NMe_3^+ and 542 nm for PProDOT-$NMe(Isop)_2^+$. These values are red-shifted (4-17 nm) compared to their corresponding neutral precursor polymers. This phenomenon has been observed in similar polyelectrolytes and is due to the polyelectrolyte which has a more rigid chain conformation than the corresponding neutral precursors.[168] The polyelectrolyte tends to optimize hydrophobic interactions between adjacent polymer chains by increasing the π-π stacking, and at the same time allows the polar amine groups to fully extend into the polar solvent. As stated previously, PProDOT-NMe_3^+ is moderatly soluble in water (Table 5-1). The UV-Vis absorption spectrum in water shown in Figure 5-14b overlaps quite well the spectrum recorded in DMSO with just a small blue-shift of λ_{abs} (9 nm) probably due to a solvatochromic effect. The effect of water on the increased degree of aggregation compared to DMSO will be discussed in the fluorescence section below (vide post). The higher degree of solubility of PProDOT-$NMe(Isop)_2^+$ in DMSO compared to methanol is clearly seen by comparing the UV-Vis absorption spectra of the polymer in these two systems. There is a 23 nm red-shift of the absorption maximum in methanol compared to DMSO, as well as a more defined fine structure with a shoulder at 617 nm (Figure 5-15b), and the solution has a more violet appearance as seen in the photograph in Figure 5-15. These observations are suggestive of a more aggregated structure imposing more π-stacking and an increased π-conjugation.[174]

The polymers emit a bright orange-red color in DMSO, with emission maxima at 612 nm for PProDOT-NMe_3^+ and 615 nm for PProDOT-$NMe(Isop)_2^+$ (see photographs in Figures 5-14a and 5-15a). PProDOT-NMe_3^+ and PProDOT-$NMe(Isop)_2^+$ exhibit fluorescence quantum

efficiencies of 16 and 11% respectively in DMSO (Cresyl violet perchlorate standard; Φ = 0.54).[171] As a consequence of the lower degree of solubility in water and of a more aggregated state, the fluorescence quantum efficiencies of PProDOT-NMe_3^+ dropped to 1.5% in water. These values are encouraging since the most red-shifted CPEs reported prior to this work (λ_{em} = 592-603 nm in methanol and 630-634 nm in water) exhibit fluorescence quantum efficiencies which do not exceed 3% in methanol and 0.06% in water.[164]

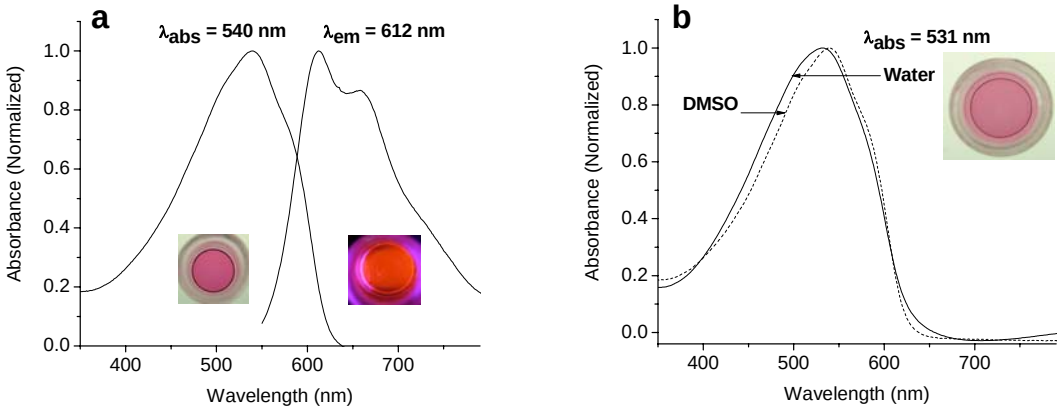

Figure 5-14. Solution spectroscopy for PProDOT-NMe_3^+. (a) UV-Vis absorption and photoluminescence of PProDOT-NMe_3^+ in DMSO; left photograph: color of the solution under visible light; right photograph: photoluminescence of the solution irradiated by UV-light; (b) UV-Vis absorption of PProDOT-NMe_3^+ in DMSO and deionized water; photograph: color of the water solution under visible light.

5.7 Summary and Perspective

For the first time, conjugated polyelectrolytes of the PProDOT family have been designed. These polymers feature cationic (R–N^+–R) side groups and were prepared by post-polymerization quaternization of alkoxyamine sites along the ProDOT polymer backbone. This methodology was expected to facilitate the molecular weight characterization of the polyelectrolytes, but unfortunately, due to solubility limitations of the neutral precursors of the

polymers in organic solvents, we were not able to take advantage of it and to estimate the molecular weights by GPC.

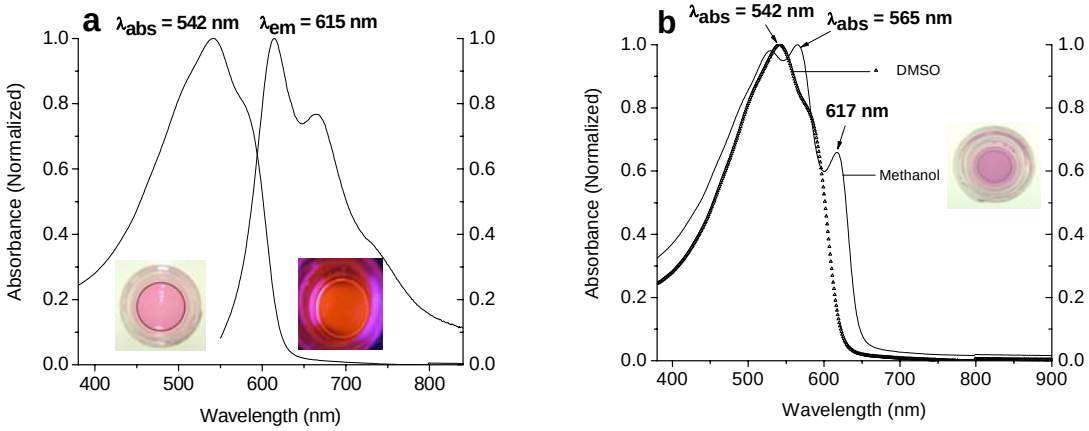

Figure 5-15. Solution spectroscopy for PProDOT-NMe(Isop)$_2^+$. (a) UV-Vis absorption and photoluminescence of PProDOT-NMe(Isop)$_2^+$ in DMSO; left photograph: color of the solution under visible light; right photograph: photoluminescence of the solution irradiated by UV-light. (b) UV-Vis absorption of PProDOT-NMe(Isop)$_2^+$ in DMSO and methanol; photograph: color of the methanol solution under visible light.

The neutral precursors of the polymers were prepared by ferric chloride oxidative polymerization. They exhibit good film properties by spray-casting, and cathodically switch between purple colors in the neutral state and a highly transmissive clear oxidized state. However, as was observed for previously reported polar PProDOTs, the oxidized forms of the films dissolved in water, acetonitrile, or propylene carbonate, making the neutral polymers poor candidates for electrochromic applications, but interesting for applications necessitating the processing of the conducting form in an environmentally friendly solvent.

The polymers in their ionic forms can be added to the extremely small list of reported red-shifted polyelectrolytes and are presently the most fluorescent of them.[164] They are well solvated in DMSO, PProDOT-NMe$_3^+$ also exhibits moderate solubility in water, and PProDOT-

$NMe(Isop)_2^+$ is partially soluble in methanol. The CPEs exhibit relatively good fluorescence efficiencies in DMSO, but the fluorescence quenching, which occurs in methanol or water upon aggregation, suggests that the fluorescence from the polymers in the films will be probably strongly quenched. A new door has been opened for multilayer optoelectronic devices, and studies of the application of these materials in devices are now needed.

5.8 Experimental

3,3'-(3,4-Dihydro-2*H*-thieno[3,4-*b*][1,4]dioxepine-3,3-diyl)bis(methylene)bis(oxy)bis-(*N*,*N*-dimethylpropan-1-amine) [ProDOT-NMe_2]. 3-Dimethylamino-1-propanol was refluxed overnight over magnesium turnings and then distilled under reduced pressure. 3-Dimethylamino-1-propanol (4.51 g, 4.38×10^{-2} mol) and sodium hydride (2.10 g, 8.76×10^{-2} mol, 60% dispersion in oil) were dissolved in anhydrous DMF (80 mL) and the mixture was heated at 110°C for 24 h under nitrogen. ProDOT($CH_2Br)_2$ (5.00 g, 1.46×10^{-2} mol) was added and the solution stirred at 110°C for an extra 24 h. The brown solution was cooled to room temperature, poured into deionized water and the mixture was extracted with diethyl ether. The organic layer was washed with Brine and dried over $MgSO_4$. After filtration through a Büchner filter, the solvent was evaporated and the crude product was collected as a brown oil. The product was purified by column chromatography on basic alumina using one volume of methanol/NH_4OH (10/1) dissolved in 10 volumes of CH_2Cl_2 for the elution, yielding 1.55 g (27%) of the pure product as a yellow oil. ^{1}H-NMR ($CDCl_3$): δ 6.45 (s, 1H), 4.01 (s, 2H), 3.49 (s, 2H), 3.46 (t, 2H), 2.32 (t, 2H), 2.22 (s, 6H), 1.73 (m, 2H). ^{13}C-NMR ($CDCl_3$): δ 149.89, 105.32, 73.88, 70.08, 69.87, 56.89, 47.93, 45.77, 28.14. HRMS: calcd for $C_{19}H_{34}N_2O_4S$: 386.2239. Found: 386.2258. Anal. Calcd for $C_{19}H_{34}N_2O_4S$: C, 59.04; H, 8.87; N, 7.25. Found: C, 58.66, H, 9.42, N, 7.23.

N,N'-(2,2'-(3,4-dihydro-2*H*-thieno[3,4-*b*][1,4]dioxepine-3,3-diyl)bis(methylene)bis (oxy)bis(ethane-2,1-diyl))bis(*N*-isopropylpropan-2-amine) [ProDOT-$NIsop_2$]. 2-(Diisopro-

pylamino)ethanol was refluxed overnight over magnesium turnings and then distilled under reduced pressure. 2-(Diisopropylamino)ethanol (11.89 g, 8.18×10^{-2} mol) and sodium hydride (3.93 g, 1.64×10^{-1} mol, 60% dispersion in oil) were dissolved in anhydrous DMF (200 mL) and the mixture was heated at 110°C for 24 h under nitrogen. ProDOT($CH_2Br)_2$ (7.00 g, 2.04×10^{-2} mol) was added and the solution stirred at 110°C for an extra 72 h. The brown solution was cooled to room temperature, poured into deionized water and the mixture was extracted with diethyl ether. The organic layer was washed with Brine and dried over $MgSO_4$. After filtration through a Büchner filter, the solvent was evaporated and the crude product was collected as a brown oil. The product was purified by column chromatography on silica gel using one volume of methanol/NH_4OH (10/1) dissolved in 30 volumes of CH_2Cl_2 for the elution, yielding 2.17 g (23%) of the pure product as a yellow oil. ^{1}H-NMR ($CDCl_3$): δ 6.45 (s, 1H), 4.02 (s, 2H), 3.50 (s, 2H), 3.38 (t, 2H), 3.01 (m, 2H), 2.58 (t, 2H), 1.01 (d, 12H). ^{13}C-NMR ($CDCl_3$): δ 149.86, 105.22, 73.86, 73.63, 70.20, 49.59, 47.99, 44.91, 20.97. HRMS: calcd for $C_{25}H_{46}N_2O_4S$: 470.3178. Found: 470.3149. Anal. Calcd for $C_{25}H_{46}N_2O_4S$: C, 63.79; H, 9.85; N, 5.95. Found: C, 63.13, H, 10.32, N, 5.96.

PProDOT-NMe$_2$. ProDOT-NMe_2 (0.55 g, 1.42×10^{-3} mol) was dissolved in dry $CHCl_3$ (20 mL) and a slurry of $FeCl_3$ (1.15 g, 7.10×10^{-3} mol) in chloroform (20 mL) was added by small portions over a 2 h period. A black gum formed rapidly in the yellow-brown solution. After 5 h, the solution was poured into a beaker of methanol (500 mL). The black precipitate formed was filtered through a Soxhlet thimble, washed a couple of times with methanol (200 mL total), and then stirred for 15 h with excess hydrazine monohydrate (10 mL) in chloroform (200 mL). The polymer dissolved and the solution color turned purple-pink. This chloroform solution was extracted with deionized water to remove the maximum of iron impurities. Then, the organic

layer was collected, the solvent was evaporated and the red solid obtained was put in a Soxhlet thimble and Soxhlet extracted for 24 h with chloroform. A lot of insoluble polymer was left in the Soxhlet thimble. The solvent was evaporated from the chloroform fraction and a red solid was collected and dried under a nitrogen flow (0.33 g, 60%). ^{1}H-NMR ($CDCl_3$, ppm): δ = 4.16 (b, 2H), 3.63 (b, 2H), 3.50 (b, 2H), 2.34 (b, 2H), 2.23 (b, 6H), 1.72 (b, 2H). Anal. Calcd for $C_{19}H_{34}N_2O_4S$: C, 59.04; H, 8.87; N, 7.25; O, 16.56; S, 8.30. Found: C, 49.32; H, 8.30; N, 5.05; S, 5.03; Cl, 0.55; Fe, 0.24.

PProDOT-NIsop$_2$. ProDOT-NIsop$_2$ (1.02 g, 2.16×10^{-3} mol) was dissolved in dry $CHCl_3$ (30 mL) and a slurry of $FeCl_3$ (1.75 g, 1.08×10^{-2} mol) in chloroform (30 mL) was added by small portions over a 2 h period. A black gum formed rapidly in the yellow-brown solution. After 5 h, the solution was poured into a beaker of methanol (500 mL). The black precipitate was filtered through a Soxhlet thimble, washed with methanol a couple of time (200 mL total), and then stirred for 15 h with excess hydrazine monohydrate (10 mL) in chloroform (400 mL). The polymer dissolved and the solution color turned purple-red. The solvent was evaporated and a red solid collected and transferred into a beaker of methanol (400 mL). The precipitate formed was filtered through a Soxhlet thimble, purified via Soxhlet extraction for 15 h with methanol, and extracted for 24 h with chloroform. A lot of insoluble polymer was left in the Soxhlet thimble. The solvent was evaporated from the chloroform fraction and a red solid was collected and dried under a nitrogen flow (0.65 g, 64%). ^{1}H-NMR ($CDCl_3$, ppm): δ = 6.19 (b, 0.03H), 4.3-4.1 (b, 2H), 3.9-3.3 (bm, 4H), 3.3-3.0 (b, 2H), 2.9-2.6 (b, 2H), 1.3-1.0 (b, 12H). Anal. Calcd for $C_{25}H_{46}N_2O_4S$: C, 63.79; H, 9.85; N, 5.95; S, 6.81. Found: C, 55.86, H, 8.39, N, 5.27; S, 6.58; Cl, 4.54; Fe, 0.85.

General Quaternization Procedure. The amino-substituted PProDOTs were dissolved in THF or $CHCl_3$, and the solutions were stirred with methyl iodide for 2 days at room temperature under nitrogen. Starting from the moment where MeI was added, the red polymer solutions turned more and more violet due to the formation of a precipitate. Then the solvent was evaporated and the polymers were precipitated in acetone, collected on 0.45 μm filter papers, washed thoroughly with acetone and dried under vacuum, yielding violet solids.

PProDOT-NMe_3^+. Use of PProDOT-NMe_2 (4.50×10^{-2} g), THF (30 mL) and MeI (1mL). ^{1}H-NMR (DMSO, ppm): δ = 3.0-3.6 (bm, 17H), 1.9-2.1 (b, 2H). Anal. Calcd for $C_{19}H_{34}N_2O_4S$•2.0 CH_3I: C, 37.62; H, 6.01; N, 4.18; S, 4.78; I, 37.86. Found: C, 33.96; H, 5.98; N, 2.64; S, 3.40; I, 23.53; Cl, 0.64.

PProDOT-$NMe(Isop)_2^+$. Use of PProDOT-$NIsop_2$ (4.00×10^{-2} g), $CHCl_3$ (15 mL) and MeI (2 mL). ^{1}H-NMR (DMSO, ppm): δ = 3.1-3.5 (bm, 10H), 3.09 (s, 3H), 1.3 (b, 12H). Anal. Calcd for $C_{25}H_{46}N_2O_4S$•2.0 CH_3I: C, 42.98; H, 6.95; N, 3.71; S, 4.25; I, 33.64. Found: C, 35.77, H, 7.10, N, 1.92; S, 2.19; Cl, 1.01; I, 15.29.

CHAPTER 6
SUMMARY

The work assembled in this dissertation gives a broad overview of the variety of properties that conjugated polymers can offer to the field of optoelectronic devices, such as light emission, light absorption, and thermally-, electrically- or solvent-induced chromism. The various characterizations accomplished on the thienylene polymer families studied here, show that each conjugated polymer family has the potential of being used in multiple applications, and that research on a selected family is consequently truly interdisciplinary. This work also makes it evident how the synthetic flexibility and easy derivatization of conjugated polymers can be used as a tool for manipulating the band gaps, the optical and electronic properties, as well as the solubility, for building optoelectronic materials with various properties.

Chapter 3 described the quest for a wide band gap polymer of the thienylene-phenylene polymer family, being organo-soluble and processable, and which could be synthesized in high bulk yields. Looking at the literature on thiophene-dialkoxybenzene (PBT-$B(OR)_2$) and EDOT-dialkoxybenzene (PBEDOT-$B(OR)_2$) derivatives raised the potential of these molecules for electrochromics, or as hole transporting materials for photovoltaics, but also suggested the need for further synthetic improvements. The polymerization of derivatives having solubilizing alkoxy-substituents was revisited, and the synthetic versatility of the molecules allowed diverse polymerization methods to be attempted (Yamamoto coupling, GriM, and solid state polymerization). However they failed to give high molecular weights or highly processable materials, due to the low solubility properties of the growing molecules. This problem was overcome by designing a new member, PBProDOT-Hex_2-$B(OC_{12}H_{25})_2$, which contains a dihexyl-functionalized ProDOT as the thienylene ring. The functionalized ProDOT ring introduced electron donating properties similar to EDOT, as well as an increased degree of

solubility. It allowed formation of a low oxidation potential material, which could be spray-cast onto large and flexible surfaces. This material cathodically switches between a neutral orange state and a transparent oxidized state, which is of great interest for electrochromic display and smart window applications.

The major focus of Chapter 4 was the optimization of the processability of the recently reported narrow band gap PProDOT-Hex_2:CNPPV. Preliminary work had shown that this polymer exhibits nearly optimal light absorption properties and energy level alignment for use in photovoltaics with the electron acceptor PCBM, and is also an excellent electrochromic material. Replacing the hexyl side chains of the ProDOT ring by linear or branched alkoxy substituents improved the solubility in organic solvents and film quality as a consequence. It also introduced an increased degree of disorder as observed by the blue-shift of the absorption spectra. Unsymmetrical and branched substitution of the phenylene ring did not bring further solubility improvement, but important optical changes were observed, probably created by a change in the polymer conformation or interaction with the adjacent chains. Photovoltaic power conversion efficiencies of 0.4% were attained with this type of molecule, as opposed to the 0.6% attained with the higher band gap and semicrystalline PBT-$B(OR)_2$ family synthesized by Yamamoto coupling and studied in Chapter 3. It appeared that even if the electronic properties were more favorable for absorbing photons, and even if homogeneous films could be prepared due to the improved solubility, the device performance was limited by the higher degree of disorder of these molecules. More attention needs to be directed towards improving the transport properties in this type of materials. As of now it seems that the best application of these molecules would be in electrochromics. Indeed, similarly to PEDOT, they switched from neutral blue or purple

colors to transparent films in the oxidized state with the extra advantages of being stable in the neutral state and spray-coatable.

In Chapter 5, attention was turned to making a new type of conjugated polyelectrolyte from amino-substituted PProDOTs. The design of the two ProDOT monomers studied here had to be thought through carefully in order for the neutral polymers to be soluble in organic solvents for easy characterization, and for their ionic forms to be soluble in polar and aqueous solvents. The selected amino-substituted PProDOTs derivatives were synthesized via ferric chloride oxidative polymerization, and their ionization was carried out by post-polymerization quaternization of the amine groups. The neutral derivatives exhibited partial solubility in organic solvents, which hindered their complete characterization, suggesting the need for further side chain manipulation. The polymers in their ionic forms were well solvated in DMSO and are presently the most fluorescent red-shifted polyelectrolytes ever reported. However, further structural adjustments need to be accomplished in order to induce a high degree of solubility in water. This project was consequently partially successful and is very promising for future research on PProDOT polyelectrolytes.

APPENDIX A
CRYSTALLOGRAPHIC INFORMATION FOR COMPOUNDS

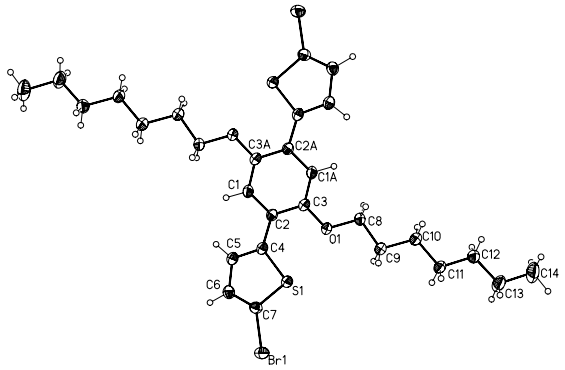

Figure A-1. Numbering system for Br_2-BT-B(OC_7H_{15})$_2$ crystal structure.

Table A-1. Crystal data and structure refinement for Br_2-BT-B(OC_7H_{15})$_2$.

Identification code	eg01	
Empirical formula	$C_{28}H_{36}Br_2O_2S_2$	
Formula weight	628.51	
Temperature	173(2) K	
Wavelength	0.71073 Å	
Crystal system	Monoclinic	
Space group	C2/c	
Unit cell dimensions	a = 30.2887(18) Å	α= 90°
	b = 5.7902(3) Å	β= 114.9510(10)°
	c = 17.7458(10) Å	γ = 90°
Volume	2821.7(3) Å^3	
Z	4	
Density (calculated)	1.479 Mg/m^3	
Absorption coefficient	3.044 mm^{-1}	
F(000)	1288	
Crystal size	0.32 x 0.15 x 0.08 mm^3	
Theta range for data collection	2.33 to 27.50°	
Index ranges	-34≤h≤39, -6≤k≤7, -22≤l≤20	
Reflections collected	8743	
Independent reflections	3172 [R(int) = 0.0394]	
Completeness to theta = 27.50°	97.7 %	

Absorption correction	Integration
Max. and min. transmission	0.8025 and 0.5065
Refinement method	Full-matrix least-squares on F^2
Data / restraints / parameters	3172 / 0 / 154
Goodness-of-fit on F^2	1.025
Final R indices [I>2sigma(I)]	R1 = 0.0243, wR2 = 0.0640 [2643]
R indices (all data)	R1 = 0.0321, wR2 = 0.0668
Largest diff. peak and hole	0.409 and -0.295 e.$Å^{-3}$

$R1 = \sum(||F_o| - |F_c||) / \sum|F_o|$

$wR2 = [\sum[w(F_o^2 - F_c^2)^2] / \sum[w(F_o^2)^2]]^{1/2}$

$S = [\sum[w(F_o^2 - F_c^2)^2] / (n-p)]^{1/2}$

$w= 1/[\sigma^2(F_o^2)+(m*p)^2+n*p]$, $p = [\max(F_o^2,0)+ 2* F_c^2]/3$, m & n are constants.

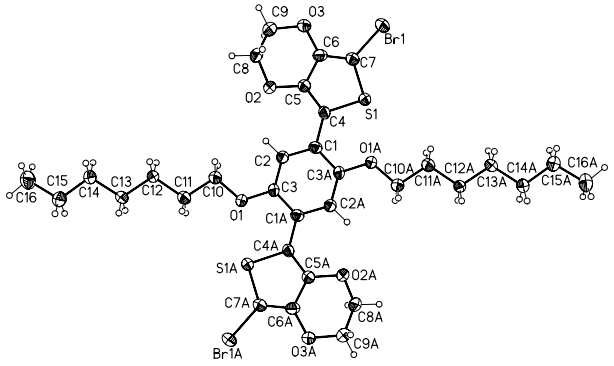

Figure A-2. Numbering system for Br_2-BEDOT-$B(OC_7H_{15})_2$ crystal structure.

Table A-2. Crystal data and structure refinement for Br_2-BEDOT-$B(OC_7H_{15})_2$.

Identification code	eg02	
Empirical formula	$C_{32}H_{40}Br_2O_6S_2$	
Formula weight	744.58	
Temperature	173(2) K	
Wavelength	0.71073 Å	
Crystal system	Monoclinic	
Space group	P2(1)/n	
Unit cell dimensions	a = 12.8685(8) Å	α= 90°
	b = 7.5486(4) Å	β= 99.761(2)°

	c = 17.0305(10) Å γ = 90°
Volume	1630.38(16) $Å^3$
Z	2
Density (calculated)	1.517 Mg/m^3
Absorption coefficient	2.656 mm^{-1}
F(000)	764
Crystal size	0.22 x 0.20 x 0.04 mm^3
Theta range for data collection	1.84 to 27.99°
Index ranges	-16≤h≤15, -6≤k≤9, -18≤l≤22
Reflections collected	10309
Independent reflections	3767 [R(int) = 0.0400]
Completeness to theta = 27.99°	95.9 %
Absorption correction	Integration
Max. and min. transmission	0.8933 and 0.5734
Refinement method	Full-matrix least-squares on F^2
Data / restraints / parameters	3767 / 0 / 190
Goodness-of-fit on F^2	1.036
Final R indices [I>2sigma(I)]	R1 = 0.0311, wR2 = 0.0821 [2897]
R indices (all data)	R1 = 0.0440, wR2 = 0.0854
Largest diff. peak and hole	0.596 and -0.512 $e.Å^{-3}$

$R1 = \sum(||F_o| - |F_c||) / \sum|F_o|$

$wR2 = [\sum[w(F_o^2 - F_c^2)^2] / \sum[w(F_o^2)^2]]^{1/2}$

$S = [\sum[w(F_o^2 - F_c^2)^2] / (n-p)]^{1/2}$

$w= 1/[\sigma^2(F_o^2)+(m*p)^2+n*p]$, $p = [\max(F_o^2,0)+ 2* F_c^2]/3$, m & n are constants.

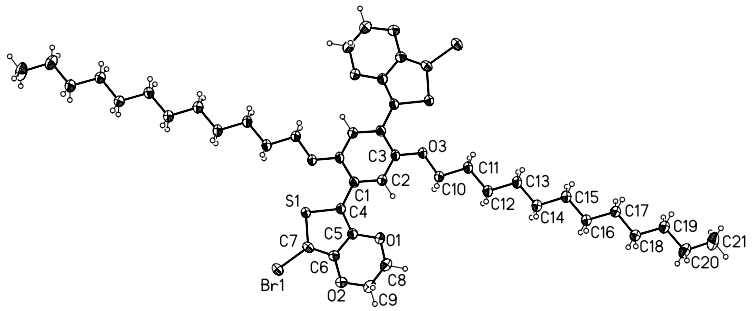

Figure A-3. Numbering system for Br_2-BEDOT-$B(OC_{12}H_{25})_2$ crystal structure.

Table A-3. Crystal data and structure refinement for Br_2-BEDOT-B($OC_{12}H_{25}$)$_2$.

Identification code	eg03	
Empirical formula	$C_{42}H_{60}Br_2O_6S_2$	
Formula weight	884.84	
Temperature	173(2) K	
Wavelength	0.71073 Å	
Crystal system	Monoclinic	
Space group	C2/c	
Unit cell dimensions	a = 30.0350(18) Å	α= 90°
	b = 7.7635(5) Å	β= 102.441(2)°
	c = 18.8621(11) Å	γ = 90°
Volume	4294.9(5) $Å^3$	
Z	4	
Density (calculated)	1.368 Mg/m^3	
Absorption coefficient	2.028 mm^{-1}	
F(000)	1848	
Crystal size	0.51 x 0.13 x 0.05 mm^3	
Theta range for data collection	2.21 to 27.49°	
Index ranges	-38≤h≤38, -10≤k≤9, -24≤l≤19	
Reflections collected	13547	
Independent reflections	4871 [R(int) = 0.0470]	
Completeness to theta = 27.49°	98.7 %	
Absorption correction	Integration	
Max. and min. transmission	0.8974 and 0.5235	
Refinement method	Full-matrix least-squares on F^2	
Data / restraints / parameters	4871 / 0 / 235	
Goodness-of-fit on F^2	1.017	
Final R indices [I>2sigma(I)]	R1 = 0.0339, wR2 = 0.0864 [3598]	
R indices (all data)	R1 = 0.0495, wR2 = 0.0899	
Largest diff. peak and hole	0.780 and -0.677 e.$Å^{-3}$	

$R1 = \sum(||F_o| - |F_c||) / \sum|F_o|$

$wR2 = [\sum[w(F_o^2 - F_c^2)^2] / \sum[w(F_o^2)^2]]^{1/2}$

$S = [\sum[w(F_o^2 - F_c^2)^2] / (n-p)]^{1/2}$

$w= 1/[\sigma^2(F_o^2)+(m*p)^2+n*p]$, $p = [\max(F_o^2,0)+ 2* F_c^2]/3$, m & n are constants.

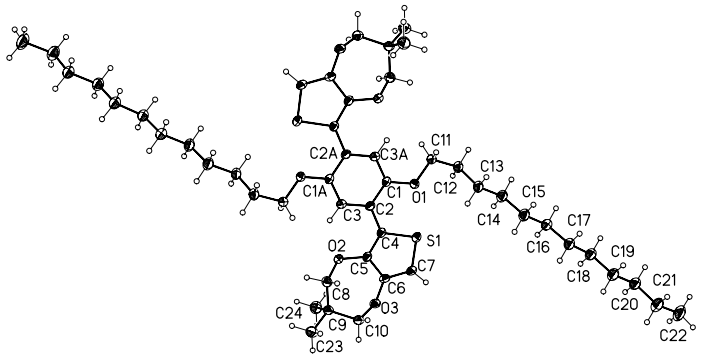

Figure A-4. Numbering system for BProDOT-Me_2-B($OC_{12}H_{25}$)$_2$ crystal structure.

Table A-4. Crystal data and structure refinement for BProDOT-Me_2-B($OC_{12}H_{25}$)$_2$.

Identification code	eg04	
Empirical formula	$C_{48}H_{74}O_6S_2$	
Formula weight	811.19	
Temperature	173(2) K	
Wavelength	0.71073 Å	
Crystal system	Triclinic	
Space group	P-1	
Unit cell dimensions	a = 5.6233(11) Å	α= 72.237(4)°
	b = 11.932(2) Å	β= 86.101(4)°
	c = 18.465(4) Å	γ = 77.433(4)°
Volume	1151.6(4) Å^3	
Z	1	
Density (calculated)	1.170 Mg/m^3	
Absorption coefficient	0.161 mm^{-1}	
F(000)	442	
Crystal size	0.23 x 0.11 x 0.07 mm^3	
Theta range for data collection	1.85 to 27.49°	
Index ranges	-7≤h≤6, -9≤k≤13, -15≤l≤23	
Reflections collected	4305	
Independent reflections	3679 [R(int) = 0.0433]	
Completeness to theta = 27.49°	69.3 %	
Absorption correction	Integration	
Max. and min. transmission	0.9914 and 0.9739	

Refinement method	Full-matrix least-squares on F^2
Data / restraints / parameters	3679 / 0 / 253
Goodness-of-fit on F^2	1.032
Final R indices [I>2sigma(I)]	R1 = 0.0469, wR2 = 0.1158 [2881]
R indices (all data)	R1 = 0.0647, wR2 = 0.1290
Largest diff. peak and hole	0.204 and -0.255 e.Å^{-3}

$R1 = \sum(||F_o| - |F_c||) / \sum|F_o|$

$wR2 = [\sum[w(F_o^2 - F_c^2)^2] / \sum[w(F_o^2)^2]]^{1/2}$

$S = [\sum[w(F_o^2 - F_c^2)^2] / (n-p)]^{1/2}$

$w= 1/[\sigma^2(F_o^2)+(m*p)^2+n*p]$, $p = [\max(F_o^2,0)+ 2* F_c^2]/3$, m & n are constants.

APPENDIX B
GEL PERMEATION CHROMATOGRAMS OF POLYMERS

UNIVERSITY OF FLORIDA George and Josephine Butler Polymer Laboratory

Reported by User: System Project Name: RTGPC0405

SAMPLE INFORMATION

Sample Name:	EG_102405_PProHx2BOC12	Acquired By:	System
Sample Type:	Broad Unknown	Date Acquired:	10/24/2005 7:07:44 PM
Vial:	8	Acq. Method Set:	Summer 2004_2
Injection #:	1	Date Processed:	10/26/2005 11:27:51 AM
Injection Volume:	10.00 ul	Processing Method:	Fall 2005
Run Time:	19.0 Minutes	Channel Name:	Wvln Ch1
Sample Set Name:		Proc. Chnl. Descr.:	PDA 482.2 nm

Auto-Scaled Chromatogram

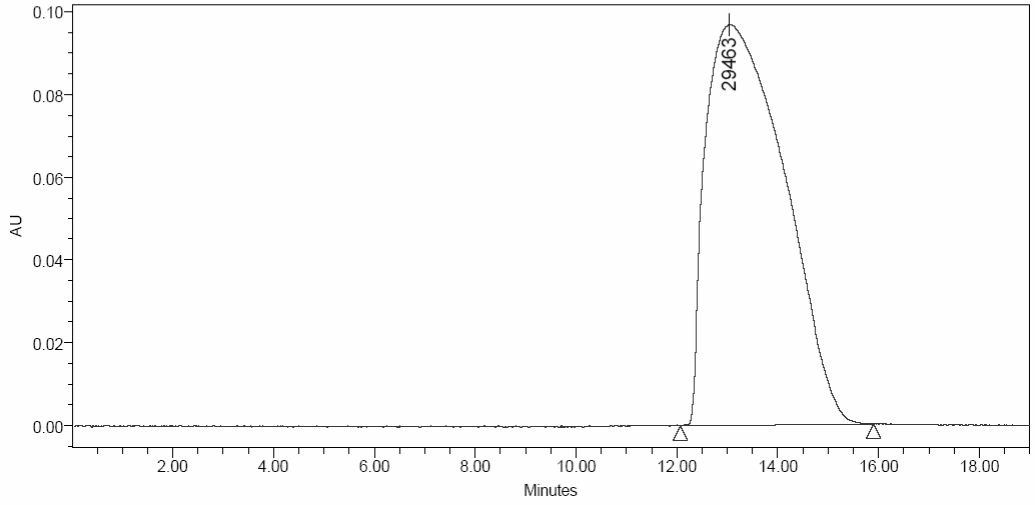

GPC Results

	Dist Name	Mn	Mw	Mv	MP	Mz	Mz+1	Polydispersity	K	alpha
1		14603	22987		29463	31187	37397	1.574101		

Report Method: Butler Report Printed 7:10:44 PM 1/13/2006 Page: 1 of 3

Figure B-1. Gel permeation chromatogram of PBProDOT-Hex_2-$B(OC_{12}H_{25})_2$.

UNIVERSITY OF FLORIDA

George and Josephine Butler Polymer Laboratory

Reported by User: System

Project Name: RTGPC0405

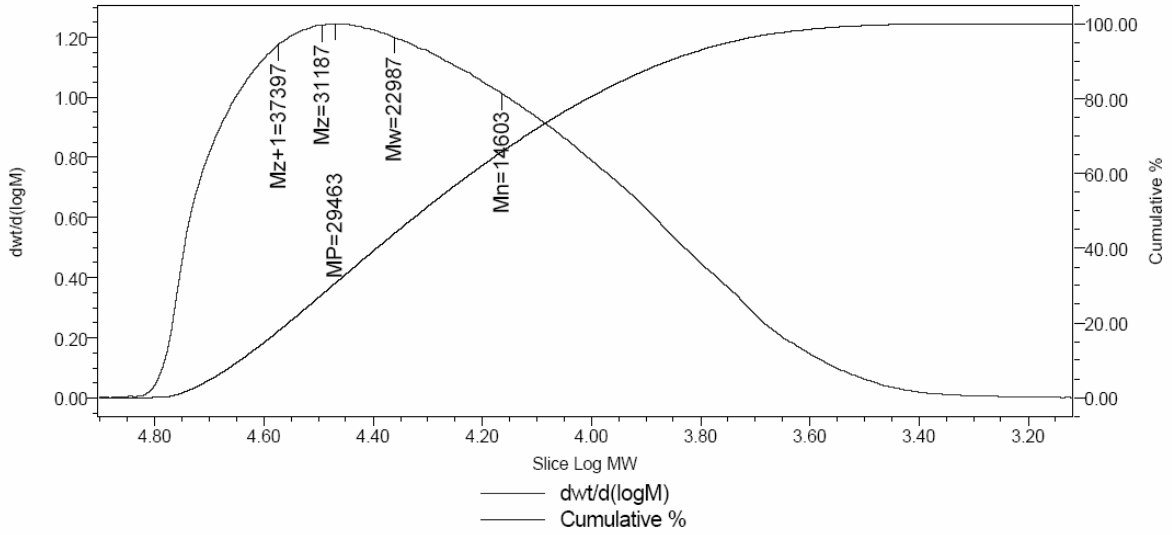

Mp: 29463 Name: C8-calibrate-test

	RT	Mol Wt	Log Mol Wt	Area	Cumulative %	dwt/d(logM)	Outside Vo-Vt
1	12.176	71716	4.855618	783	0.009	0.000000	No
2	12.286	64074	4.806684	7509	0.057	0.002200	No
3	12.395	57265	4.757888	100654	0.912	0.002946	No
4	12.505	51192	4.709202	291379	3.974	0.000680	No
5	12.614	45772	4.660604	446416	8.317	0.002130	No
6	12.724	40932	4.612067	531278	13.429	0.003853	No
7	12.833	36607	4.563566	585515	19.036	0.004923	No
8	12.943	32740	4.515077	617808	24.937	0.004582	No
9	13.052	29280	4.466575	632808	30.959	0.007012	No
10	13.162	26184	4.418034	633442	36.976	0.005108	No
11	13.271	23411	4.369429	624184	42.897	0.006817	No
12	13.381	20928	4.320736	608834	48.671	0.011718	No
13	13.490	18704	4.271929	589739	54.264	0.020650	No
14	13.600	16710	4.222984	568715	59.646	0.037136	No
15	13.710	14924	4.173875	544352	64.788	0.062520	No
16	13.819	13322	4.124577	516212	69.671	0.104329	No
17	13.929	11887	4.075066	486067	74.264	0.159015	No
18	14.038	10600	4.025316	452974	78.543	0.235938	No
19	14.148	9447	3.975302	416503	82.468	0.338518	No
20	14.257	8414	3.925000	377818	86.026	0.468949	No
21	14.367	7488	3.874383	334605	89.177	0.611303	No

Figure B-1. Continued.

UNIVERSITY OF FLORIDA

George and Josephine Butler Polymer Laboratory

Reported by User: System Project Name: RTGPC0405

Mp: 29463 Name: C8-calibrate-test

	RT	Mol Wt	Log Mol Wt	Area	Cumulative %	dwt/d(logM)	Outside Vo-Vt
22	14.476	6659	3.823428	287286	91.864	0.744630	No
23	14.586	5917	3.772109	241028	94.116	0.862300	No
24	14.695	5253	3.720401	195594	95.947	0.961765	No
25	14.805	4659	3.668279	148582	97.309	1.047096	No
26	14.914	4128	3.615719	107542	98.299	1.117780	No
27	15.024	3653	3.562694	75575	98.992	1.185838	No
28	15.133	3230	3.509180	49680	99.444	1.242392	No
29	15.243	2852	3.455153	29804	99.709	1.297945	No
30	15.352	2515	3.400586	15826	99.849	1.348212	No
31	15.462	2215	3.345455	8225	99.917	1.396269	No
32	15.571	1949	3.289735	4512	99.955	1.441509	No
33	15.681	1712	3.233402	2628	99.980	1.482889	No
34	15.790	1501	3.176429	1816	99.992	1.523721	No
35	15.900	1315	3.118791	1880	100.002	1.559550	No

GPC Calibration Plot

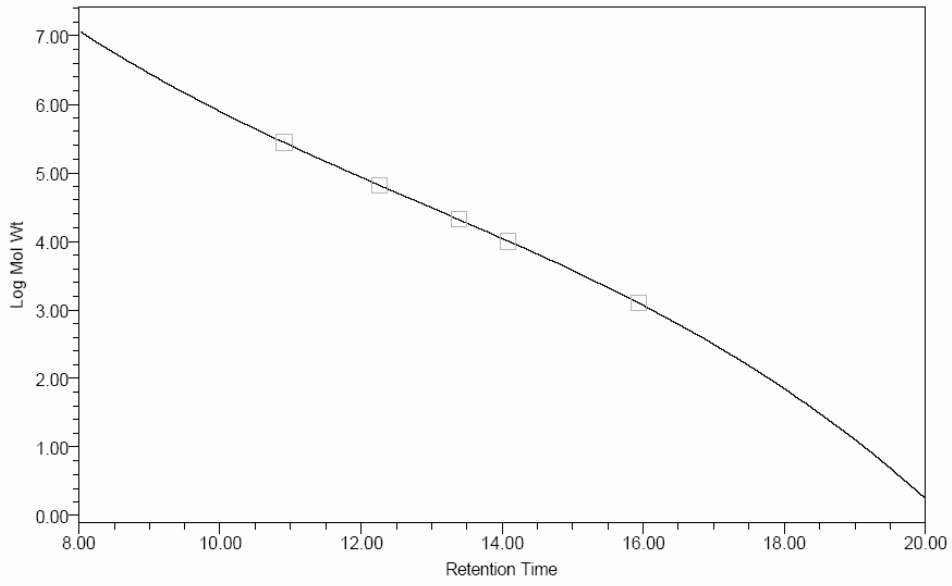

Report Method: Butler Report Printed 7:10:44 PM 1/13/2006 Page: 3 of 3

Figure B-1. Continued.

LIST OF REFERENCES

1. Chiang, C. K.; Fincher, C. R.; Park, Y. W.; Heeger, A. J.; Shirakawa, H.; Louis, E. J.; Gau, S. C.; MacDiarmid, A. G. *Phys. Rev. Lett.* **1977**, *39*, 1098-1101.

2. Heeger, A. J. *Reviews of Modern Physics* **2001**, *73*, 681-700.

3. Burroughes, J. H.; Bradley, D. D. C.; Brown, A. R.; Marks, R. N.; Mackay K.; Friend, R. H.; Burns, P. L.; Holmes, A. B.; *Nature* **1990**, *347*, 539-541.

4. Moliton, A.; Hiorns, R. C. *Polym. Int.* **2004**, *53*, 1397-1412.

5. Peierls R. E. Quantum Theory of Solids; Oxford University Press: London, 1955.

6. Kertesz, M.; Choi, C. H.; Yang, S. *Chem. Rev.* **2005**, *105*, 3448-3481.

7. Salzner, U. *Curr. Org. Chem.*, **2004**, *8*, 569-590.

8. Menon, R.; Yoon, C. O.; Moses, D.; Heeger, A. J. Metal-Insulator Transition in Doped Conducting Polymers. In *Handbook of Conducting Polymers*; 2nd Ed.; Stockheim, T. A.; Elsenbaumer, R. L.; Reynolds, J. R., Eds. Marcel Dekker: New York, 1998; Chapter 2.

9. Chance, R. R.; Brédas, J. L.; Silbey, R. *Phys. Rev. B* **1984**, *29*, 4491-4495.

10. Brédas, J. L.; Street, G. B. *Acc. Chem. Res.* **1985**, *18*, 309-315.

11. Roncali, J. *Chem. Rev*. **1997**, *97*, 173-205.

12. Winder, C.; Matt, G.; Hummelen, J. C.; Janssen, R. A. J.; Sariciftci, N. S. ; Brabec, C. J. *Thin Film Solids* **2002**, *403-404*, 373-379.

13. van Mullekom, H. A. M.; Vekemans, J. A. J. M.; Havinga, E. E.; Meijer, E. W. *Mater. Sci. Eng.* **2001**, *32*, 1-40.

14. Brédas, J. L. *J. Chem. Phys.* **1985**, *82*, 3808-3811.

15. Brédas, J. L.; Heeger, A. J.; Wudl, F. *J. Chem. Phys.* **1986**, *85*, 4673-4678.

16. Havinga, E. E.; Hoeve, W.; Wynberg, H. *Polym. Bull.* **1992**, *29*, 119-126.

17. Thomas, C. A.; Zong, K.; Abboud, K. A.; Steel, P. J.; Reynolds, J. R. *J. Am. Chem. Soc.* **2004**, *126*, 16440-16450.

18. Thompson, B. C.; Kim, Y.-G.; McCarley, T. D.; Reynolds, J. R. *J. Am. Chem. Soc.* **2006**, *128*, 12714-12725.

19. Brédas, J. L.; Street, G. B.; Thémans, B.; André, J. M.; *J. Chem. Phys.* **1985**, *83*, 1323-1329.

20. Kim, J. *Pure Appl. Chem.* **2002**, *74*, 2031-2044.

21. Gustafsson-Carlberg, J. C.; Inganäs, O.; Andersson, M. R.; Booth, C.; Azens, A.; Granqvist, C. G. *Electrochim. Acta*, **1995**, *40*, 2233-2235.

22. Ruiz, J. P.; Dharia, J. R.; Reynolds, J. R.; Buckley, L. J. *Macromolecules* **1992**, *25*, 849-860.

23. Irvin, J. A. A. Low oxidation potential electroactive polymers. Ph.D. Thesis, University of Florida, Gainesville, FL, 1998.

24. Sotzing, G. A.; Reynolds, J. R.; Steel, P. J. *Chem. Mater.* **1996**, *8*, 882-889.

25. Sankaran, B.; Reynolds, J. R. *Macromolecules* **1997**, *30*, 2582-2588.

26. Tourillon, G. Polythiophene and its Derivatives. In *Handbook of Conducting Polymers*. Skotheim, T. A., Ed.; Marcel Dekker: New York and Basel, 1986, volume 1, Chapter 9.

27. Pavlishchuk, V. V.; Addison, A. W. *Inorg. Chim. Acta* **2000**, *298*, 97-102.

28. Groenendaal, L. B.; Zotti, G.; Aubert, P.-H.; Waybright, S. M.; Reynolds, J. R. *Adv. Mater.* **2003**, *15*, 855-877.

29. McCullough, R. D.; Ewbank, P. C. Regioregular, Head-to-Tail Coupled Poly(3-alkylthiophene) and Its Derivatives. In *Handbook of Conducting Polymers*; 2nd Ed. Stockheim, T. A.; Elsenbaumer, R. L.; Reynolds, J. R., Eds.; Marcel Dekker: New York, 1998, Chapter 9.

30. Sentein, C.; Mouanda, B.; Rosilio, A.; Rosilio, C. *Synth. Met.* **1996**, *83*, 27-37.

31. Chen, T. A.; Rieke, R. D. *Synth. Met.* **1993**, *60*, 175-177.

32. (a) McCullough, R. D.; Lowe, R. D. *J. Chem. Soc., Chem. Commun.* **1992**, 70-72. (b) McCullough, R. D.; Lowe, R. D.; Jayaraman, M.; Anderson, D. L. *J. Org. Chem.* **1993**, *58*, 904-912. (c) Loewe, R. S.; Khersonsky, S. M.; McCullough, R. D. *Adv. Mater.* **1999**, *11*, 250-253.

33. Wu, C.-G.; Lin, Y.-C.; Wu, C.-E.; Huang, P.-H. *Polymer* **2005**, *46*, 3748-3757.

34. Reeves, B. D.; Grenier, C. R. G.; Argun, A. A.; Cirpan, A.; McCarley, T. D.; Reynolds J. R. *Macromolecules* **2004**, *37*, 7559-7569.

35. (a) Sheina, E. E.; Liu, J.; Iovu, M. C.; Laird, D. W.; McCullough, R. D. *Macromolecules* **2004**, *37*, 3526-3528. (b) Iovu, M. C.; Sheina, E. E.; Gil, R. R.; McCullough, R. D. *Macromolecules* **2005**, *38*, 8649-8656.

36. Wang, F.; Wilson, M. S.; Rauh, R. D.; Schottland, P.; Thompson, B. C.; Reynolds, J. R. *Macromolecules* **2000**, *33*, 2083-2091.

37. Zhang, Z.-B.; Fujiki, M.; Tang, H.-Z.; Motonaga, M.; Torimitsu, K. *Macromolecules* **2002**, *35*, 1988-1990.

38. Yamamoto, T.; Wakabayashi, S.; Osakada, K. *J. Organomet. Chem.*, **1992**, *428*, 223-237.

39. (a) Shiraishi, K.; Kanbara, T.; Yamamoto, T.; Groenendaal, L. B. *Polymer*, **2001**, *42*, 7229-7232. (b) Asawapirom, U.; Scherf, U. *Macromol. Rapid. Commun.* **2001**, *22*, 746-749.

40. Yamamoto, T.; Ito, T.; Kubota, K. *Chem. Lett.*, **1988**, 153-154.

41. Meng, H.; Perepichka, D. F.; Bendikov, M.; Wudl, F.; Pan, G. Z.; Yu, W.; Dong, W.; Brown, S. *J. Am. Chem. Soc.* **2003**, *125*, 15151-15162.

42. Boucard, V.; Adès, D.; Siove, A.; Romero, D.; Schaer, M.; Zuppiroli, L. *Macromolecules* **1999**, *32*, 4729-4731.

43. Thompson, B. C. Variable band gap poly(3,4-alkylenedioxythiophene)-based polymers for photovoltaic and electrochromic applications. Ph.D. Thesis, University of Florida, Gainesville, FL, 2005.

44. Cervini, R.; Holmes, A. B.; Moratti, S. C. ; Köhler, A. ; Friend, R. H. *Synth. Met.* **1996**, *76*, 169-171.

45. Roncali, J. Advances in the Molecular Design of Functional Conjugated Polymers. In *Handbook of Conducting Polymers*; 2nd Ed. Stockheim, T. A.; Elsenbaumer, R. L.; Reynolds, J. R., Eds.; Marcel Dekker: New York, 1998, Chapter 12.

46. Irvin, J. A.; Reynolds, J. R. *Polymer* **1998**, *39*, 2339-2347.

47. Groenendaal, L. B.; Jonas, F.; Freitag, D.; Pielartzik, H.; Reynolds, J. R. *Adv. Mater.* **2000**, *12*, 481-494.

48. Kirchmeyer, S.; Reuter, K. *J. Mater. Chem.* **2005**, *15*, 2077-2088.

49. Roncali, J.; Blanchard, P.; Frère, P. *J. Mater. Chem.* **2005**, *15*, 1589-1610.

50. Child, A. D.; Sankaran, B.; Larmat, F.; Reynolds, J. R. *Macromolecules* **1995**, *28*, 6571-6578.

51. Bhattacharya, A.; De, A. *J. Macromol. Sci. Rev. Macromol. Chem. Phys.* **1999**, *C39*, 17-56.

52. Kumar, A.; Welsh, D. M.; Morvant, M. C.; Piroux, F.; Abboud, K. A.; Reynolds, J. R. *Chem. Mater.* **1998**, *10*, 896-902.

53. Welsh, D. M.; Kloeppner, L. J.; Madrigal, L.; Pinto, M. R.; Thompson, B. C.; Schanze, K. S.; Abboud, K. A.; Powell, D.; Reynolds, J. R. *Macromolecules* **2002**, *35*, 6517-6525.

54. Mishra, S. P.; Krishnamoorthy, K.; Sahoo, R.; Kumar, A. *J. Polym. Sci.: Part A: Polym. Chem.* **2005**, *43*, 419-428.

55. Mishra, S. P.; Sahoo, R.; Ambade, A. V.; Contractor, A. Q.; Kumar, A. *J. Mater. Chem*. **2004**, *14*, 1896-1900.

56. Perepichka, I. F.; Roquet, S.; Leriche, P. ; Raimundo, J.-M. ; Frère, P. ; Roncali, J. *Chem. Eur. J.* **2006**, *12*, 2960-2966.

57. Grenier, C. R. G.; Pisula, W.; Joncheray, T. J.; Müllen, K.; Reynolds, J. R. *Angew. Chem. Int. Ed.* In press.

58. Thompson, B. C.; Kim, Y.-G.; Reynolds, J. R. *Macromolecules* **2005**, *38*, 5359-5362.

59. Taranekar, P.; Abdulbaki, M.; Krishnamoorti, R.; Phanichphant, S.; Waenkaew, P.; Patton, D.; Fulghum, T.; Advincula, R. *Macromolecules* **2006**, *39*, 3848-3854.

60. Yang, J. S.; Swager, T. M. *J. Am. Chem. Soc.* **1998**, *120*, 5321-5322.

61. Nguyen, T.-Q.; Schwartz, B. J. *J. Chem. Phys.* **2002**, *116*, 8198-8208.

62. Sonmez, G.; *Chem. Commun.* **2005**, 5251-5259.

63. Pei, Q.; Zuccarello, G.; Ahlskog, M.; Inganäs, O. *Polymer* **1994**, *35*, 1347.

64. Thompson, B. C.; Schottland, P.; Zong, K.; Reynolds, J. R. *Chem. Mater.* **2000**, *12*, 1563-1571.

65. Schwendeman, I.; Hickman, R.; Sönmez, G.; Schottland, P.; Zong, K.; Welsh, D. M.; Reynolds, J. R. *Chem. Mater.* **2002**, *14*, 3118-3122.

66. Sönmez, G.; Shen, C. K. F.; Rubin, Y.; Wudl, F. *Angew. Chem. Int. Ed.* **2004**, *43*, 1498-1502.

67. Coakley, K. M.; McGehee, M. D. *Chem. Mater.* **2004**, *16*, 4533-4542.

68. Winder, C.; Sariciftci, N. S. *J. Mater. Chem.* **2004**, *14*, 1077-1086.

69. Mozer, A. J.; Sariciftci, N. S. *C. R. Chimie* **2006**, *9*, 568-577.

70. Brabec, C. J.; Zerza, G.; Cerullo, G.; De Silvestri, S.; Luzzati, S. ; Hummelen, J. C. ; Sariciftci, S. *Chem. Phys. Lett.*, **2001**, *340*, 232-236.

71. Padinger, F.; Rittberger, R. S.; Sariciftci, N. S. *Adv. Funct. Mater.* **2003**, *13*, 85-88.

72. Montanari, I.; Nogueira, A. F.; Nelson, J. ; Durrant, J. R. ; Winder, C. ; Loi, M. A. ; Sariciftci, N. S. ; Brabec, C. *Appl. Phys. Lett.* **2002**, *81*, 3001-3003.

73. Ma, W.; Yang, C.; Gong, X.; Lee, K.; Heeger, A. J. *Adv. Funct. Mater.* **2005**, *15*, 1617-1622.

74. Reyes-Reyes, M.; Kim, K.; Carroll, D. L. *Appl. Phys. Lett.* **2005**, *87*, 083506.

75. Li, G.; Shrotriya, V.; Huang, J.; Yao, Y.; Moriarty, T.; Emery, K.; Yang, Y. *Nat. Mater.* **2005**, *4*, 864-868.

76. Alem, S.; de Bettignies, R.; Nunzi, J.-M. *Appl. Phys. Lett.* **2004**, *84*, 2178-2180.

77. Padinger, F.; Fromherz, T. *Appl. Phys. Lett.* **2001**, *78*, 841-843.

78. de Leeuw, D. M.; Simenon, M. J. J.; Brown, A. R. ; Einerhand, R. E. F. *Synth. Met.* **1997**, *87*, 53-59.

79. Bard, A. J.; Faulkner, L. R. Electrochemical Methods: Fundamentals and Applications, 2nd Ed.; Wiley: New York, 2001.

80. Meskers, S. C. J.; Hübner, J.; Oestreich, M.; Bässler, H. *J. Phys. Chem. B* **2001**, *105*, 9139-9149.

81. Kim, Y.; Cook, S.; Tuladhar, S. M.; Choulis, S. A.; Nelson, J.; Durrant, J. R.; Bradley, D. D. C.; Giles, M.; McCulloch, I.; Ha, C.-S.; Ree, M. *Nature Materials* **2006**, *5*, 197-203.

82. Hou, J. ; Tan, Z. ; Yan, Y. ; He, Y. ; Yang, C.; Li, Y. *J. Am. Chem. Soc.* **2006**, *128*, 4911-4916.

83. Thomas, C. A. Donor-acceptor methods for band gap reduction in conjugated polymers: the role of electron rich donor heterocycles. Ph.D. Thesis, University of Florida, Gainesville, FL, 2002.

84. Welsh, D. M. High contrast and three-color electrochromic polymers. Ph.D. Thesis, University of Florida, Gainesville, FL, 2001.

85. Gaupp, C. L. Structure-property relationships of electrochromic 3,4-alkylenedioxyheterocycle-based polymers and copolymers. Ph.D. Thesis, University of Florida, Gainesville, FL, 2002.

86. Gritzner, G.; Kuta, G. J. *Pure Appl. Chem.* **1984**, *56*, 461-466.

87. Brett, C. M. A.; Brett, A. M. O. Electrochemistry, Principles, Methods, and Applications; Oxford University: Oxford, 1993.

88. Rieger, P. H. Electrochemistry; Prentice-Hall: Englewood Cliffs, New Jersey, 1987.

89. Lévesque, I. ; Leclerc, M. *Chem. Mater.* **1996**, *8*, 2843-2849.

90. Garreau, S. ; Leclerc, M. ; Errien, N. ; Louarn, G. *Macromolecules* **2003**, *36*, 692-697.

91. Bouachrine, M. ; Lère-Porte, J.-P. ; Moreau, J. J. E. ; Serein-Spirau, F. ; Torreilles, C. *J. Mater. Chem.* **2000**, *2*, 263-268.

92. Politis, J. K. ; Somoza, F. B. ; Kampf, J. W.; Curtis, M. D.; Ronda, L. G. ; Martin, D. C. *Chem. Mater.* **1999**, *11*, 2274-2284.

93. Dufresne, G.; Bouchard, J.; Belletête, M.; Durocher, G.; Leclerc, M. *Macromolecules* **2000**, *33*, 8252-8257.

94. Bernier, S.; Garreau, S.; Béra-Abérem, M.; Gravel, C.; Leclerc, M. *J. Am. Chem. Soc.* **2002**, *124*, 12463-12468.

95. Greenham, N. C.; Samuel, I. D. W.; Hayes, G. R.; Phillips, R. T.; Kessener, Y. A. R. R.; Moratti, S. C.; Holmes A. B.; Friend R. H. *Chem. Phys. Lett.* **1995**, *241*, 89-96.

96. Pålsson, L.-O.; Monkman, A. P. *Adv. Mater.* **2002**, *14*, 757-758.

97. Williams, A. T. R.; Winfield, S. A.; Miller, J. N. *Analyst*, **1983**, *108*, 1067-1071.

98. Eaton, D. F. *Pure & Appl. Chem.* **1988**, *60*, 1107-1114.

99. Du, H.; Fuh, R. A.; Li, J.; Corkan, A.; Lindsey, J. S. *Photochem. Photobiol.* **1998**, *68*, 141-142.

100. Reynolds, G. A.; Drexhage, K. H. *Optics Commun.* **1975**, *13*, 222-225.

101. Magde, D.; Brannon, J. H.; Cremers, T. L.; Olmsted, J. *J. Phys. Chem.* **1979**, *83*, 696-699.

102. Thompson, B. C.; Schottland, P.; Sönmez, G.; Reynolds, J. R. *Synth. Met.* **2001**, *119*, 333-334.

103. Tada, K.; Onoda, M.; Yoshino, K. *J. Phys. D: Appl. Phys.* **1997**, *30*, 2063-2068.

104. Pei, J.; Yu, W.-L.; Ni, J.; Lai, Y.-H.; Huang, W.; Heeger, A. J. *Macromolecules* **2001**, *34*, 7241-7248.

105. Irvin, J. A.; Piroux, F.; Morvant, M. C.; Robertshaw, V. L.; Angerhofer, A.; Reynolds, J. R. *Synth. Met.* **1999**, *102*, 965-966.

106. Bao, Z.; Chan, W.; Yu, L. *Chem. Mater.* **1993**, *5*, 2-3.

107. Pelter A.; Jenkins I.; Jones D. E. *Tetrahedron* **1997**, *53*, 10357-10400.

108. Bouachrine, M.; Bouzakraoui, S.; Hamidi, M.; Ayachi, S.; Alimi K.; Lère-Porte J.-P.; Moreau J. *Syn. Met.* **2004**, *145*, 237-243.

109. Mushrush, M.; Facchetti A.; Lefenfeld, M.; Katz H. E.; Marks T. J. *J. Am. Chem. Soc.* **2003**, *125*, 9414-9423.

110. Xu M.-H.; Zhang H.-C.; Pu L. *Macromolecules* **2003**, *36*, 2689-2694.

111. Reynolds, J. R.; Ruiz, J. P.; Child, A. D.; Marynick, D. S.; Nayak, K. *Macromolecules* **1991**, *24*, 678-687.

112. Brédas, J. L.; Calbert, J. P.; da Silva Filho, D. A.; Cornil, J. *Proc. Natl. Acad. Sci.* **2002**, *99*, 5804-5809.

113. Beljonne, D.; Cornil, J.; Sirringhaus, H.; Brown, P. J.; Shkunov, M.; Friend, R. H.; Brédas, J.-L. *Adv. Funct. Mater.* **2001**, *11*, 229-234.

114. Mitchell. R. H.; Lai, Y.-H.; Williams, R. V. *J. Org. Chem.* **1979**, *44*, 4733-4735.

115. Cao, J.; Kampf, J. W.; Curtis, M. D. *Chem. Mater.* **2003**, *15*, 404-411.

116. Ertas, E.; Ozturk, T. *Tetrahedron Lett.* **2004**, *45*, 3405-3407.

117. DuBois, C. J. Donor-acceptor methods for band gap control in conjugated polymers. Ph.D. Thesis, University of Florida, Gainesville, FL, 2003.

118. Dai, C.; Fu, G. C. *J. Am. Chem. Soc.* **2001**, *123*, 2719-2724.

119. Thompson, B. C.; Schottland, P.; Sonmez, G.; Reynolds, J. R. *Synth. Met.* **2001**, *119*, 333-334.

120. Leclerc, M.; Dufresne, G.; Blondin, P.; Bouchard, J ; Belletête, M.; Durocher, G. *Synth. Met.* **2001**, *119*, 45-48.

121. (a) Perzon, E.; Wang, X.; Admassie, S.; Inganäs, O.; Andersson, M. R. *Polymer* **2006**, *47*, 4261-4268. (b) Lee, S. K.; Cho, N. S.; Kwak, J. H.; Lim, K. S.; Shim, H.-K.; Hwang, D.-H.; Brabec, C. J. *Thin Solid Films* **2006**, *511*, 157-162. (c) Wienk, M. M.; Struijk, M. P.; Janssen, R. A. J. *Chem. Phys. Lett.* **2006**, *422*, 488-491. (d) Xia, Y.; Luo, J.; Deng, X.; Li, X.; Li, D.; Zhu, X.; Yang, W.; Cao, Y. *Macromol. Chem. Phys.* **2006**, *207*, 511-520. (e) Yang, R.; Tian, R.; Yan, J.; Zhang, Y.; Yang, J.; Hou, Q.; Yang, W.; Zhang, C.; Cao, Y. *Macromolecules* **2005**, *38*, 244-253.

122. Pratt, J. R.; Pinkerton, F. H.; Thames, S. F. *J. Organomet. Chem.* **1972**, *38*, 29-36.

123. Gronowitz, S. *Acta Chem. Scand.* **1959**, *13*, 1045-1046.

124. Goldoni, F.; Langeveld-Voss, B. M. W.; Meijer, E. W. *Synth. Comm.* **1998**, *28*, 2237-2244.

125. Overberger, C. G.; Lal, J. *J. Am. Chem. Soc.* **1951**, *73*, 2956-2957.

126. Welsh, D. M.; Kumar, A.; Meijer, E. W.; Reynolds, J. R. *Adv. Mater.* **1999**, *11*, 1379-1382.

127. Yang, R.; Tian, R.; Yan, J.; Zhang, Y.; Yang, J.; Hou, Q.; Yang, W.; Zhang, C.; Cao, Y. *Macromolecules* **2005**, *38,* 244-253.

128. Zhang, F.; Perzon, E.; Wang, X.; Mammo, W.; Andersson, M. R.; Inganäs, O. *Adv. Funct. Mater.* **2005**, *15*, 745-750.

129. Xia, Y.; Luo, J.; Deng, X.; Li, X.; Li, D.; Zhu, X.; Yang, W.; Cao, Y. *Macromol. Chem. Phys.* **2006**, *207*, 511-520.

130. Wienk, M. M.; Turbiez, M. G. R.; Struijk, M. P.; Fonrodona, M.; Janssen, R. A. J. *Appl. Phys. Lett.* **2006**, *88*, 153511.

131. Arbizzani, C.; Catellani, M.; Mastragostino, M.; Mingazzini, C. *Electrochim. Acta*, **1995**, *40*, 1871-1876.

132. Arbizzani, C.; Cerroni, M. G.; Mastragostino, M. *Sol. Energy Mater. Sol. Cells* **1999**, *56*, 205-211.

133. Du Bois, C. J. Jr.; Larmat, F.; Irvin, D. J.; Reynolds, J. R. *Synth. Met.*, **2001**, *119*, 321-322.

134. Salzner, U. *Synth. Met.* **2001**, *119*, 215-216.

135. Huang, H.; He, Q.; Lin, H.; Bai, F.; Cao, Y. *Thin Solid Films*, **2005**, *477*, 7-13.

136. Cacialli, F.; Wilson, J. S.; Michels, J. J.; Daniel, C.; Silva, C.; Friend, R. H.; Severin, N.; Samori, P.; Rabe, J. P.; O'Connell, M. J.; Taylor, P. N.; Anderson, H. L. *Nature Materials* **2002**, *1*, 160–164.

137. Li, X.-C.; Liu, Y.; Liu, M. S. ; Jen, A. K.-Y. *Chem. Mater.* **1999**, *11*, 1568-1575.

138. Neef, C. J.; Ferraris, J. P. *Macromolecules* **2000**, *33*, 2311-2314.

139. Roex, H.; Adriaensens, P.; Vanderzande, D.; Gelan, J. *Macromolecules* **2003**, *36*, 5613-5622.

140. Kricheldorf, H. R.; Schwartz, G. *Macromol. Rapid Commun.* **2003**, *24*, 359-381.

141. Kricheldorf, H. R.; Fritsch, D.; Vakhtangishvili, L.; Schwartz, G. *Macromol. Chem. Phys.* **2005**, *206*, 2239-2247.

142. Montaudo, G.; Montaudo, M. S.; Puglisi, C.; Samperi, F. *Rapid Commun. Mass Spectrom.* **1995**, *9*, 453-460.

143. Axelsson, J.; Scrivener, E.; Haddleton, D. M.; Derrick, P. J. *Macromolecules* **1996**, *29*, 8875-8882.

144. Schriemer, D. C.; Li, L. *Anal. Chem.* **1997**, *69*, 4169-4175.

145. Cho, N. S.; Hwang, D. H.; Shim, H. K.; Kim, J. C., *Int. Pat.*, WO 03/016430A1.

146. Saito, H.; Ukai, S.; Iwatsuki, S.; Itoh, T.; Kubo, M. *Macromolecules* **1995**, *28*, 8363-8367.

147. Wagner, P.; Aubert, P. H.; Lutsen, L.; Vanderzande, D. *Electrochem. Commun.* **2002**, *4*, 912-916.

148. Pinto, M. R.; Schanze, K. S. *Synthesis* **2002**, *9*, 1293-1309.

149. Baur, J. W.; Kim, S.; Balanda, P. B.; Reynolds, J. R.; Rubner, M. F. *Adv. Mater.* **1998**, *10*, 1452-1455.

150. Decher, G.; Hong, J. D.; Schmitt, J.; *Thin Solid Films* **1992**, *210/211*, 831-835.

151. Decher, G. *Science* **1997**, *277*, 1232-1237.

152. Kim, S.; Jackiw, J.; Robinson, E.; Schanze, K. S.; Reynolds, J. R.; Baur, J.; Rubner, M. F.; Boils, D. *Macromolecules* **1998**, *31*, 964-974.

153. Ma, W.; Iyer, P., K.; Gong, X.; Liu, B.; Moses, D.; Bazan, G. C.; Heeger, A. J. *Adv. Mater.* **2005**, *17*, 274-277.

154. Shi, W.; Fan, S.; Huang, F.; Yang, W.; Liu, R.; Cao, Y. *J. Mater. Chem.* **2006**, *16*, 2387-2394.

155. Brown, T. M.; Kim, J. S.; Friend, R. H.; Cacialli, F.; Daik, R.; Feast, W. J. *Appl. Phys. Lett.* **1999**, *75*, 1679-1681.

156. Mwaura, J. K.; Pinto, M. R.; Witker, D.; Ananthakrishnan, N.; Schanze, K. S.; Reynolds, J. R. *Langmuir* **2005**, *21*, 10119-10126.

157. Wang, D.; Gong, X.; Heeger, P. S.; Rininsland, F.; Bazan, G. C.; Heeger, A. J. *Proc. Natl. Acad. Sci.* **2002**, *99*, 49-53.

158. Pinto, M. R.; Schanze, K. S. *Proc. Nat. Acad. Sci.* **2004**, *101*, 7505-7510.

159. Achyuthan, K. E.; Bergstedt, T. S.; Chen, L.; Jones, R. M.; Kumaraswamy, S.; Kushon, S. A.; Ley, K. D.; Lu, L.; McBranch, D.; Mukundan, H.; Rininsland, F.; Shi, X.; Xia, W.; Whitten, D. G. *J. Mater. Chem.* **2005**, *15*, 2648-2656.

160. Herland, A.; Nilsson, K. P. R.; Olsson, J. D. M.; Hammarström, P.; Konradsson, P.; Inganäs, O. *J. Am. Chem. Soc.* **2005**, *127*, 2317-2323.

161. Taylor, P. N.; O'Connell, M. J.; McNeill, L. A.; Hall, M. J.; Aplin, R. T.; Anderson, H. L. *Angew. Chem. Int. Ed.* **2000**, *39*, 3456-3460.

162. Peng, Z.; Xu, B.; Zhang, J.; Pan, Y. *Chem. Commun.* **1999**, 1855-1856.

163. Harrison, B. S.; Ramey, M. B.; Reynolds, J. R.; Schanze, K. S. *J. Am. Chem. Soc.* **2000**, *122*, 8561.

164. Zhao, X.; Pinto, M. R.; Hardison, L. M.; Mwaura, J.; Müller, J.; Jiang, H.; Witker, D.; Kleiman, V. D.; Reynolds, J. R.; Schanze, K. S. *Macromolecules* **2006**, *39*, 6355-6366.

165. Reeves, B. D. Processable disubstituted poly(propylenedioxythiophenes). Ph.D. Thesis, University of Florida, Gainesville, FL, 2005.

166. Welsh, D. M.; Kloeppner, L. J.; Madrigal, L.; Pinto, M. R.; Thompson, B. C.; Schanze, K. S.; Abboud, K. A.; Powell, D.; Reynolds, J. R. *Macromolecules* **2002**, *35*, 6517-6525.

167. Ramey, M. B.; Hiller, J.'A.; Rubner, M. F.; Tan, C.; Schanze, K. S.; Reynolds, J. R. *Macromolecules* **2005**, *38*, 234-243.

168. Huang, F.; Hou, L.; Shen, H.; Yang, R.; Hou, Q.; Cao, Y. *J. Polym. Sci. Part A: Polym. Chem.* **2006**, *44*, 2521-2532.

169. Liu, B.; Yu, W.-L.; Lai, Y.-H. ; Huang, W. *Chem. Commun.* **2000**, 551-552.

170. McCarley, T. D.; Noble, C. O. IV; Dubois, C. J. Jr.; McCarley, R. L. *Macromolecules* **2001**, *34*, 7999-8004.

171. Magde, D.; Brannon, J. H.; Cremers, T. L.; Olmsted, J. *J. Phys. Chem.* **1979**, *83*, 696-699.

172. Gaupp, C. L.; Zong, K.; Schottland, P. ; Thompson, B. C.; Thomas, C. A.; Reynolds, J. R. *Macromolecules* **2000**, *33*, 1132-1133.

173. Wanli, M.; Iyer, P. K.; Gong, X.; Liu, B.; Moses, D.; Bazan, G.; Heeger, A. J. *Adv. Mater.* **2005**, *17*, 274-277.

174. Tan, C.; Pinto, M. R.; Schanze, K. S. *Chem. Commun.* **2002**, 446-447.

BIOGRAPHICAL SKETCH

Emilie M. Galand was born in Lille, France, in 1980. After high school she pursued two-year intensive undergraduate studies in chemistry, physics, and maths at the Graduate School of Chemistry of Lille (ENSCL), France, giving access to Elite French Graduate Schools of Chemistry. At the end of that program, she joined in August of 2000 the Graduate School of Chemistry and Physics of Bordeaux (ENSCPB), France, to complete her undergraduate studies. She accomplished two years of that 3-year program in Bordeaux, and then for the last year she decided to study at the University of Florida, USA, in order to gain international experience. At the end of that year (June 2003), she obtained her master's diploma from ENSCPB (Engineer degree in chemistry and physics). She stayed in Florida for another three and a half years to pursue a Ph.D. in the area of electroactive polymers under the supervision of Prof. John R. Reynolds.